Development of new chemical tools to study the cannabinoid receptor type 2

Paus, L.V. de

Development of New Chemical Tools to Study the Cannabinoid Receptor Type 2

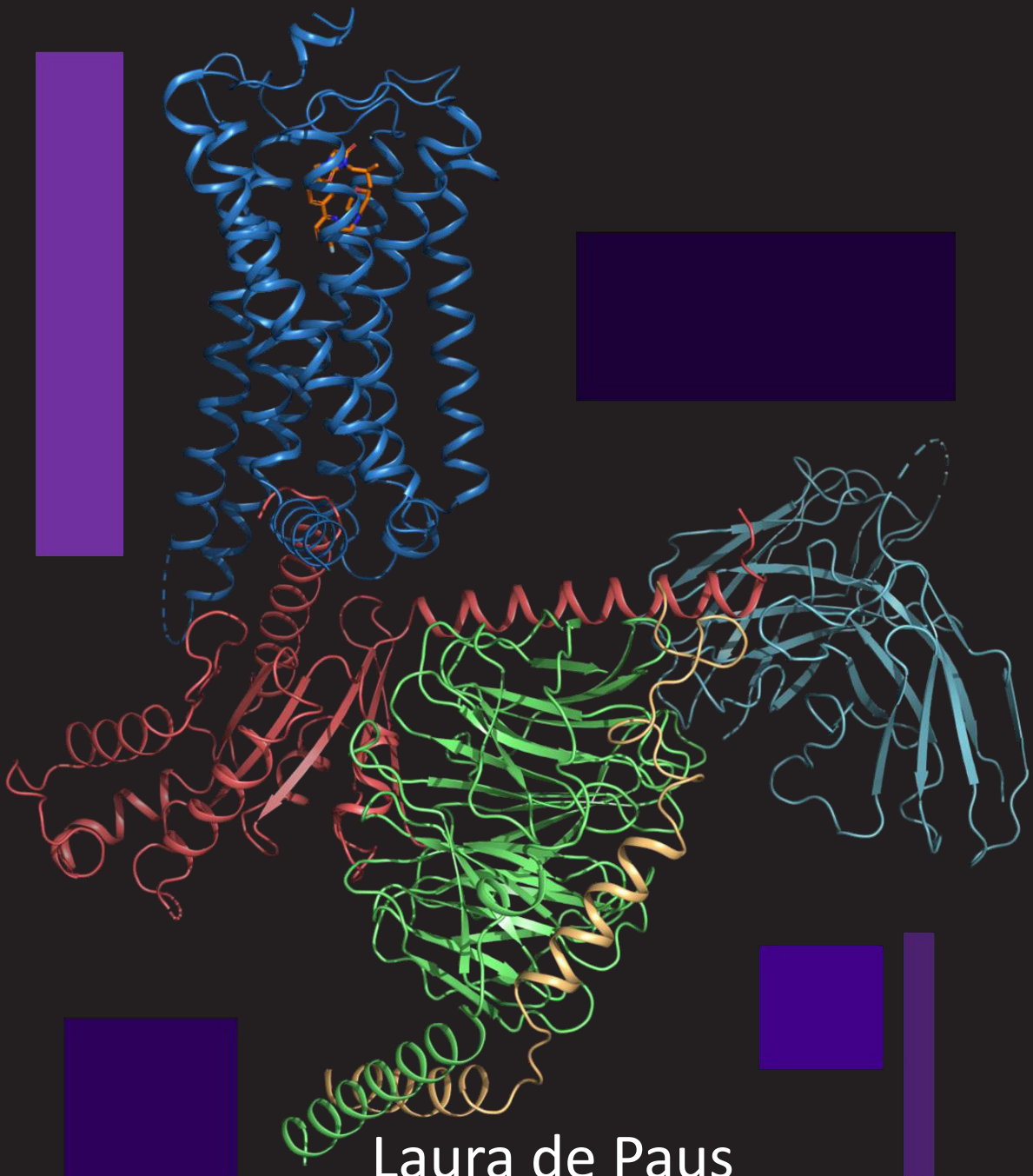

Laura de Paus

Development of New Chemical Tools to Study the Cannabinoid Receptor Type 2

Proefschrift

ter verkrijging van

de graad van doctor aan de Universiteit Leiden,

op gezag van rector magnificus prof.dr.ir. H. Bijl,

volgens besluit van het college voor promoties

te verdedigen op woensdag 22 mei 2024

klokke 13:45 uur

door

Laura de Paus

geboren te Leiden, Nederland

in 1994

Promotores:

Prof.dr. M. van der Stelt

Prof.dr. L.H. Heitman

Co-promotor:

Dr. R.J.B.H.N. van den Berg

Promotiecommissie:

Prof.dr. M. Ubbink

Prof.dr. S.I. van Kasteren

Dr. M.P. Baggelaar (Universiteit Utrecht)

Dr. M. Mulder (LUMC)

Prof.dr. G.J.P. van Westen

Printed by: ProefschriftMaken | Proefschriftmaken.nl

Cover Design: Cryo-EM structure of LEI-102 bound to CB_2 receptor (PDB: 8GUT) rendered with Open Source PyMOL v.2.5.

Table of Content

Chapter 1

General Introduction

General Introduction

Cannabinoid Receptors

The endocannabinoid system (ECS) is a collection of lipid transmitters that bind receptors to elicit cellular responses, as well as the enzymes involved in their synthesis and catabolism.[1] The system is involved in a plethora of physiological processes, including cognitive and immune responses, as well as the psychoactive effects of *cannabis sativa*.[2]

The two main receptors in the ECS are cannabinoid receptor type 1 (CB_1R) and cannabinoid receptor type 2 (CB_2R). Though there are some other receptors, such as GPR55, that are also targeted by endocannabinoid-like compounds, their role in the ECS is much less understood.[3] The cannabinoid receptors are class A G protein-coupled receptors (GPCRs), which rely on dynamic changes in their structure to relay the binding of an extracellular ligand to an internal signal.[4] As their name implies, they convey the main portion of their signalling through the recruitment of G proteins. Various G proteins exist, generally consisting of an α and βγ subunit.[5] CBRs recruit $G_{i/o}$ proteins for their signalling, although CB_1R has also been shown to recruit $G_{q/11}$ proteins in astrocytes.[6]

CB_1R and CB_2R have some similarities in their mode of action. Both inhibit adenylyl cyclase, promote PI3K, MAPK, ceramide production and gene transcription. While CB_1R is also adept in modulation of voltage-gated calcium channels (VDCCs) and G protein inwardly-rectifying potassium channels (GIRKs), CB_2R is a very poor modulator of these channels.[7] Additional differences lie in their cell type distribution, leading to different effects. For example, the specific neuronal distribution of CB_1R leads to the psychoactive effects of cannabinoids, while CB_2R does not elicit such responses.[7]

The best studied endogenous ligands of CB_1R and CB_2R are anandamide (AEA, Figure 1.1) and 2-arachidonoylglycerol (2-AG), though many more have been postulated, including noladin ether, *N*-arachidonoyldopamine (NADA), and docosatetraenylethanolamide (DEA).[1] Δ^9-Tetrahydrocannabinol (THC) is considered the primary phytocannabinoid in *cannabis sativa* and similarly binds to both CB_1R or CB_2R.[8,9]

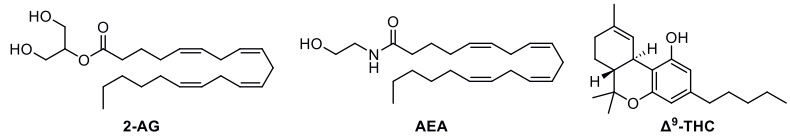

Figure 1.1 The chemical structures of the major two endocannabinoids (2-AG and AEA) that act as ligands on CB_1R and CB_2R, as well as the structure of the primary constituent of cannabis, Δ^9-THC.

CB_1R was first cloned in 1990; which proved that cannabinoids act by interaction with a specific receptor to elicit central nervous system (CNS) effects, rather than through membrane disruption.[10] CB_1R is the most abundantly expressed GPCR in the brain.[11] It has been found in high levels in the basal ganglia, cerebellum, prefrontal cortex, hippocampus, nucleus accumbens, hypothalamus, paraventricular nucleus and the central amygdala, mainly in the terminals of neurons and glial cells.[12,13] Here it plays a role in many neurological processes, including appetite, learning and memory, anxiety, depression and addiction. Consequently, CB_1R is reported to play a role in many neurological disorders, such as stroke, multiple sclerosis, epilepsy and neurodegenerative diseases.[14–17] CB_1R expression is not restricted to the nervous system, as it is also present in peripheral tissues including the muscles, liver, pancreas, GI tract and fat tissue.[18] The peripheral roles of CB_1R include nociception, inflammation,

energy metabolism, functioning of the gastrointestinal tract and the musculoskeletal system, intraocular pressure, cardiovascular, glandular and reproductive functioning and cancer.[13,19,20]

CB_2R is thought to be exclusively expressed in cells and organs of the immune system, including spleen, tonsils, thymus and lymphocytes[21], where its major role is the regulation of (neuro)inflammatory processes. During inflammation CB_2R inhibits cytokine production, lowers antigen presentation, and modulates microglia M1/M2 differentiation.[22–24] Disruption of the inflammation modulation of CB_2R may play a role in various autoimmune and neurodegenerative diseases, such as Alzheimer's, Parkinson's, Huntington's, dementia and others.[25] The presence and activity of CB_2R in neurons is highly debated.[26]

The Structure of CB_1R and CB_2R

CB_1R and CB_2R share a sequence homology of 44%, which is increased to 68% in the transmembrane domain.[2728] They exhibit the general features of the Class A GPCRs. The receptors both consist of seven transmembrane helices (TMH), three intracellular (IC) and extracellular (EC) loops, an extracellular N-terminus and intracellular C-terminus which includes a short helix (Hx8).[29] The ligand binding site is located in the interior of the seven (TMH) bundle. The biggest difference between CB_1R and CB_2R is the ECL2. The ECL2 from CB_1R is much longer and can dip into the binding pocket in the inactive state.[30–32] The shorter ECL2 of CB_2R acts more like a lid on the binding pocket in active and inactive CB_2R, akin to active CB_1R.[33]

The first 3D structure of a GPCR was elucidated in 2000 with X-ray crystallography, which was rhodopsin.[34] The first CB_1R crystal structure was elucidated in 2016, in complex with antagonist AM6538 (Figure 1.2A).[31] The receptor required several modifications to increase stability and limit flexibility during the crystallization process. The protein was crystallized in a lipidic cubic phase with additional cholesterol to mimic the CB_1R membrane environment.[31] In 2019 the same group was able to crystallize CB_2R to elucidate the 3D protein structure (Figure 1.2B). By using the antagonist AM10257 and similar modifications as for CB_1R, they were able to form a stable complex.[33]

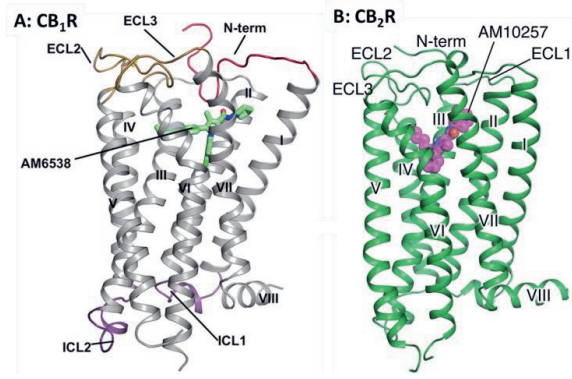

Figure 1.2 Structure of the Cannabinoid Receptors. (A) A side view of CB_1R (grey) in complex with antagonist AM6538 (light green). The N-terminus is shown in red, while the extracellular loops are shown in brown and the intracellular loops in purple. (B) A side view of CB_2R (green) in complex with antagonist AM10257 (purple). Picture adopted from Hua *et al.* Cell (2016)[31] and Hua *et al.* Cell (2019).[33]

Since then, several other CBR crystal structures with other ligands have been published.[35–39] Of note, the crystal structures are limited to the inactive state as they are all bound to antagonists. Information about the respective active states of the receptors was obtained using cryogenic electron microscopy (Cryo-EM). This new technique does not rely on X-ray scattering from very uniform protein crystals, but

rather uses electrons to visualize the surface of frozen protein particles. Cryo-EM does not require the growth of crystals, which can take months up to years to find the right receptor constructs and crystallization conditions. Instead the proteins are frozen at liquid nitrogen or helium temperatures. Thereupon a surge of structures obtained from cryo-EM has been observed in the RCSB database. In 2017 the first Cryo-EM structure of a GPCR, calcitonin[40], was published, followed in 2019 by the first Cryo-EM structure of an active state CB_1R in complex with both the G protein and an agonist (Figure 1.3A).[41] One year later, a CB_2R-G protein in complex with agonist WIN55,212-2 (Figure 1.3B) was published.[42]

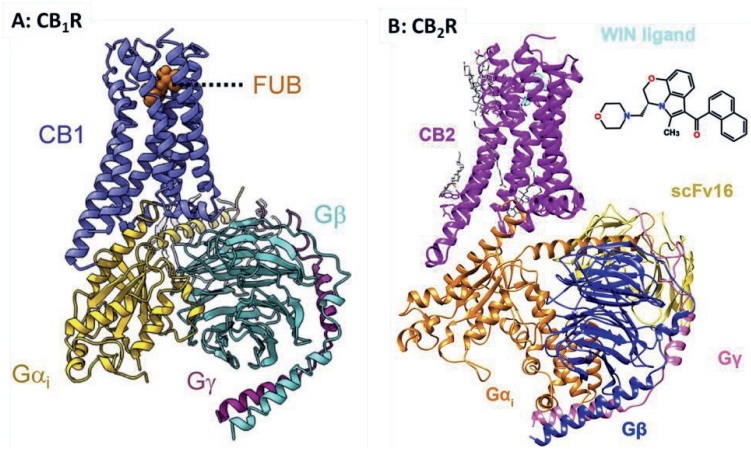

Figure 1.3 The three-dimensional protein structures of the CBR-G protein complexes bound to an agonist, obtained through cryo-EM. (A) Side view of CB_1R (blue) with agonist MDMB-Fubinaca (orange) and $G_{\alpha i}$, G_β and G_γ (yellow, cyan and purple respectively). (B) Side view of CB_2R (magenta) with agonist WIN55,212-2 (cyan), $G_{\alpha i}$, G_β and G_γ (orange, blue and pink respectively) and scFv16 (gold; additive to stabilize complex). Pictures adopted from Kumar K, Cell (2019) and Xing C, Cell (2020).[41,42]

When comparing active and inactive structures, both CB_1R and CB_2R feature an outward movement of TM6 upon activation, as well as movement of $Y^{7.53}$ (Ballesteros-Weinstein numbering in superscript) towards TM5. There are additional changes in conformation that are specific to either CB_1R or CB_2R, and may explain ligand selectivity and their differences in signalling.[43] In CB_1R the N-terminus moves away from the orthosteric binding site upon activation, while the position of the N-terminus in CB_2R does not move substantially between the inactive and active state. Furthermore, the TM1 in the CB_1R is positioned more outward in the antagonist bound structure than in the agonist complex. Again CB_2R shows no significant movement of TM1. The best known difference is probably the (twin-)toggle switch. In CB_1R $W356^{6.48}$ and $F200^{3.36}$ form a twin-toggle switch, where $F200^{3.36}$ locks $W356^{6.48}$ into the inactive state until an agonist disrupts the pi-bond, leading to a translational change for both residues.[43] In CB_2R only $W258^{6.48}$ acts as a toggle, and no transitional change is observed. Instead, $W258^{6.48}$ undergoes a 64° clockwise rotational change and $F117^{3.36}$ has a small 10° counter clockwise rotation upon CB_2R activation.[42] Note that these observations were made by comparison of the inactive receptor states and the G protein bound active receptor states. There may be differences in activation mechanism for β-arrestin bound active states.[43] The three-dimensional protein structures showed the difference between the agonist binding pocket of CB_1R an CB_2R is minimal, and it remains unclear how selective CB_2R agonists selectively activate CB_2R.[44]

CBR Therapeutics

Starting from the chemical structure of the psychoactive CB_1R/CB_2R agonist tetrahydrocannabinol (Δ^9-THC) isolated from *Cannabis Sativa*, many small molecules have been designed that have affinity for CB_1R and/or CB_2R. The first generation were THC-derived classical cannabinoids such as L-759,656, CP-55,940, JWH-133 and HU210 (Figure 1.4). Many of these were non-selective or only moderately selective for CB_2R over CB_1R. A next generation included analogues of natural products (*e.g.* hexahydrocannabinol) and endocannabinoid derivatives (*e.g.* AM356).[45,46] The pool of small molecules was then expanded to include compounds with a wide variety of scaffolds and chemical groups (*e.g.* JWH-018, WIN55,212-2, APD371).[47,48]

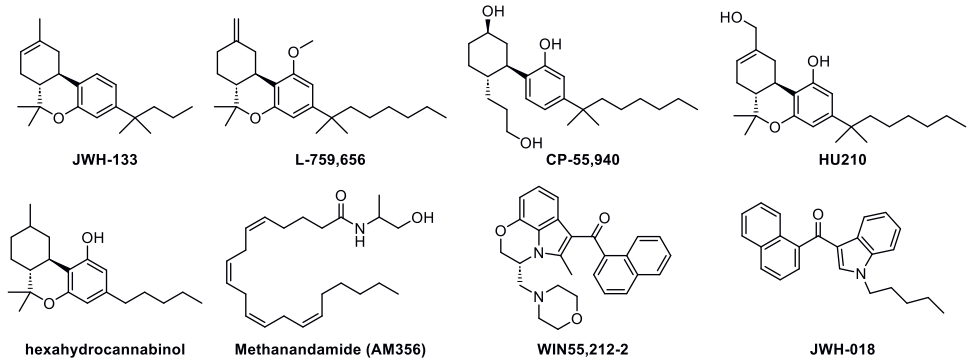

Figure 1.4 The chemical structures of several classical and non-classical CB_2R agonists.

CB_2R as Therapeutic Target

CB_2R plays an important role in immunoregulation, but does not induce the psychoactive effects that plagues CB_1R activation. It has been shown that CB_2R is upregulated under several pathological conditions.[49] Inflammation is reduced by CB_2R as it modulates macrophages to adopt the anti-inflammatory M2 subtype.[50] As such, CB_2R therapeutics could be beneficial for arthritis[51], cardiovascular[52] and inflammatory bowel disease[53], fibrosis[54], inflammation-induced pain[55] and neurodegenerative diseases.[56] Similarly to CB_1R, it also shows beneficial effects in other peripheral areas including skeletal and metabolic disorders[57,58], and cancer.[59]

CB_2R ligands will require high selectivity over CB_1R to avoid side effects, but when achieved will have therapeutic potential.[60] An advantage is that CB_2R agonists promote similar analgesic effects as CB_1R agonists, yet do not create tolerance over time, physical dependence or autonomic withdrawal.[61] While no selective CB_2R ligand has yet reached the market, many are currently under evaluation in animal studies and clinical trials.[62] AM1241 (Figure 1.5) was one of the first compounds used to investigate the analgesic properties of CB_2R agonists. However, AM1241 did not reach clinical trials due to its engagement with an endogenous opioid receptor, low efficacy and complex molecular pharmacology which differed for each enantiomer.[63] Cannabinor (PRS-211,375) was introduced in phase I and II clinical trials after beneficial anti-nociceptive effects in osteoarthritis in rat models. However, the promising pre-clinical results could not be replicated in humans.[64] GW842166 from GlaxoSmithKline showed the same problem with translation to humans.[60] S-777469 completed a Phase II clinical trial for atopic dermatitis in 2009, but no follow-up clinical research has been reported or planned since.[65–67] Lenabasum (HU239) was shown to have anti-inflammatory effects in a Phase II clinical trial, and has been given the FDA Orphan drug designation for treatment of diabetes mellitus.[68] It is currently in consideration as treatment for cystic fibrosis[69], Systemic Lupus Erythematosus[70], and Dermatomyositis[71], though it showed no significant effect in Phase III trials for Diffuse Cutaneous

Systemic Sclerosis.[72] HU308 is a synthetic cannabinoid with 440-fold selectivity for CB_2R over CB_1R, and was used as a case study to show anti-inflammatory and analgesic properties stemmed from CB_2R activation by showing absence of CNS-side effects in mouse models.[73] However, its lipophilic structure resulted in poor solubility, which prevented success in clinical trials.[74] In contrast, APD371 is one of the most polar CB_2R-selective agonists, which gives it excellent pharmacokinetics, peripheral restriction and oral availability.[60] It showed promising results in a Phase 2a trial for gastrointestinal pain in Crohn's disease, though a Phase 2b trial did not reach its primary endpoint.[75–77] Similarly Vicasinabin (RG-7774) was pulled by Roche after a Phase 2 trial in diabetic retinopathy showed underwhelming efficacy.[78]

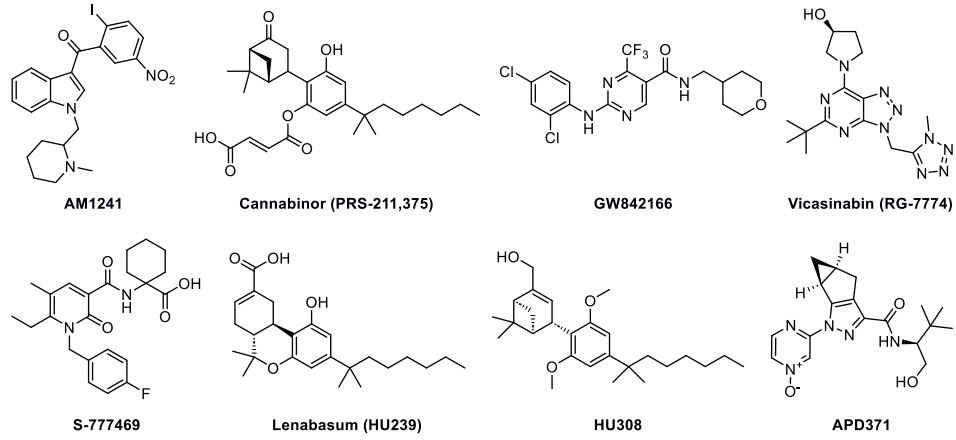

Figure 1.5 The chemical structures of several CB_2R agonists that have previously participated in clinical trials or have a clinical trial ongoing.

CB_1R as Therapeutic Target

Despite the wide distribution of CB_1R, its role in many pathologies makes it a popular target. Indeed, together with the serotonin receptor 2A it is the joined most popular target for CNS diseases in current preclinical studies.[62] Nonetheless, the development of drugs targeting CB_1R is difficult due to the numerous roles of CB_1R in a variety of peripheral and central nervous system processes, as well as the difficulty of observing neuropathologic symptoms. Additionally, targeting CB_1R can result in undesirable effects such as addiction, anxiety and psychoactive effects that limit its possibilities as a therapeutic target.[14] Regardless, many beneficial effects have been noted for CB_1R agonists. Foremost, both synthetic analogues of THC and cannabis extracts have been approved for treatment of neuropathic pain.[79] Furthermore, CB_1R agonists have been suggested as potential treatment of post-traumatic stress disorder (PTSD) due to the memory impairment effect.[80] Other avenues currently under investigation include their ability to reduce anxiety[81] and depressive tendencies[82], as an anticonvulsant for epilepsy[83] and to ensure neuroprotection during cerebral ischemia events.[84] Additionally, the effect of CB_1R agonists in neurodegenerative diseases such as Alzheimer's, Huntington's[85], and Parkinson's[86] is being investigated. CB_1R antagonists have had a set-back with the withdrawal of the first antagonist Rimonabant from therapeutic use due to CNS-mediated psychological side effects.[87] Nevertheless a new generation of peripherally restricted antagonists is showing promise in treatment of obesity, several forms of tissue fibrosis and improvement of cardiometabolic profile while preventing neurological side effects.[88,89]

Strategies to Limit Side Effects

As mentioned above, CB_1R and CB_2R have a plethora of roles in different systems and diseases. Many promising drug candidates fail in clinical trials because tissue exposure/selectivity is not considered

during development.[90] Therefore several strategies have been devised to limit side effects while preserving the therapeutic effect, such as allosteric modulation, functional selectivity and controlled delivery through localized delivery or activation, or target-directing modification.

Allosteric Modulation

Allosteric modulators work differently from orthosteric ligands in the sense that they do not bind in the same binding pocket as the endogenous ligand, and thus result in a non-competitive mode of action. As such, positive allosteric modulators (PAM) can enhance the response of CB_2R to endogenous ligand binding, while negative allosteric modulators (NAM) decrease the response.[91] The idea is that exacerbation of the signal rather than creating a *de novo* signal retains the native signalling pattern of the receptor. Additionally, allosteric binding sites are not conserved and may provide selectivity between highly homologous subtypes (which is relevant for CB_1R and CB_2R).[92] An example of CB_2R PAM is Ec2la (C-2)[93], while PSNCBAM-1 is a CB_1R NAM (Figure 1.6).[94]

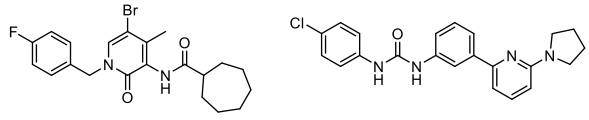

Ec2la (C-2) (PAM) **PSNCBAM-1**

Figure 1.6 An Example of a CB_2R positive allosteric modulator (Ec2la (C-2) and a CB_1R negative allosteric modulator (PSNCBAM-1).

Functional Selectivity

Like many GPCRs, CB_2R conveys its signals through both G protein activation and β-arrestin recruitment. However, not all agonists activate these two signalling pathway equally well. Some ligands are functionally selective, *i.e.* they do not result in equal signal strength via the G protein or β-arrestin. Certain synthetic agonists may initiate only a slight activation of G protein signalling, while a significant amount of β-arrestin is recruited upon agonist binding, or *vice versa*. Endocannabinoids can also show bias, *e.g.* 2-AG has significant bias for the β-arrestin pathway on CB_2R.[74] Contrarily, Δ^9-THC shows prominent G protein activation but barely any β-arrestin recruitment.[74] A functionally selective drug may perhaps discriminate between beneficial and adverse effects, thus minimizing side effects without compromise on the therapeutic effect.[95] Interestingly, HU308 is a balanced agonist on human CB_2R, but does show bias towards G protein activation on mouse CB_2R.[74] This further highlights the difficulties of developing CB_2R agonists as there are high interspecies differences that may account for the high failure rate of ligands in clinical trials after promising results in animal models.

Controlled delivery

Through controlled delivery accumulation of drugs in healthy tissue can be minimized through control over the transport of the drug. Nanocarriers can optimize drug administration, site-specific accumulation and (timed) drug release due to their (tuneable) physicochemical surface properties. Additionally, capsulation of the drug avoids off-target toxicity and prevents premature enzymatic breakdown.[96] Liposomes, micelles and polymeric nanoparticles have been proposed as possible nanocarriers.[97] Currently no nanocarriers with CBR (ant)agonists have yet reached clinical trial,[98] however, there are some promising applications. For example, recently the capsulation of CB_2R agonist β-caryophyllene (BCP) was described with a polymer of ethylene glycol (PEG) which allowed for administation through the intranasal route, circumventing the first-pass metabolism.[99] Additionally, a protein-based nanoparticle for cannabidiol (PNP-CBD) was designed to improve water solubility and increase CB_2R targeting.[100] For CB_1R efficient liver-targeting was shown with a ((poly(lactic-co-glycolic

acid)) (PLGA) encapsulated rimonabant nanoparticle.[101] There are currently over 90 marketed nanoformulations (non-CBR) and such an application is also being investigated for the CBRs.[102]

Peripheral restriction is also a form of controlled delivery.[103] By altering the physicochemical properties, such as topological polar surface area (tPSA) and H bonding capacity of known compounds[103], the blood brain barrier (BBB) penetration can be limited, preventing neurological side effects.

Phototherapy may also be considered controlled delivery. The inactive compound only activates with the light source, thus only activating receptors at the location with the light.[101,104] While this has not yet been translated to therapeutic CBR drugs, for research purposes a photoswitchable Δ^9-tetrahydrocannabinol (*azo*-THC) has been designed[105], as well as a 'caged' 2-AG with photoactivated release.[106]

A new type of controlled delivery instead looks at the drugs cellular distribution. In 2013 it became evident that immune cells have CB_2Rs present both on the plasma membrane and intracellularly.[107] This intracellular fraction of (active) CB_2R is present in the endoplasmic reticulum (ER) and endolysosomes.[108–110] The different roles of extracellular and intracellular CB_2R have yet to be determined. Nevertheless, evidence of a functional role for internal CB_2R is the time delay in CB_2R-dependent Ca^{2+}-response observed when administering CB_2R agonists extracellularly via bath application versus microinjection.[109] (a.k.a. the agonist first had to internalize when applied extracellularly.) Similarly CB_1R is distributed to both the plasma membrane and intracellularly in mitochondria[111] and lysosomes.[112,113]

Neutral Antagonism

Decrease of CB_1R activity by Rimonabant and other inverse agonists has been shown to lead to side effects of anxiety, depression and sometimes suicidal behaviour.[114] Hence, neutral antagonists for CB_1R have been in focus recently, for example in relation to substance abuse disorder (SAD) and weight loss.[115] In theory, neutral antagonism can limit side effects, when these are the result of decreased basal or constitutive activity of the receptor. For example, CB_1R antagonist AM4113 (Figure 1.7) showed great results in preclinical mice studies for SAD without inducing depression like behaviour, however, its poor oral availability and outcome of a recent study that did show anxiety-like behaviour do not make it the best candidate.[116,117] AM6527 does show promise with increased oral availability.[116] PIMSR is a neutral antagonist based on Rimonabant that exhibits the same depression of cocaine self-administration in mice, but without the detrimental effects.[114] Current results are promising, but, more research will need to be done on these types of drug candidates. Of note, whether CBRs are constitutionally active or are activated by a constitutive agonist tone, *i.e.* constitutive endocannabinoid levels, is difficult to determine.[118] Moreover, constitutive activity of receptors *in vitro* may be an artefact of the overexpression systems used, which could result in an inverse agonist *in vitro* behaving as a neutral antagonist *in vivo*.[119] This is an important consideration when pursuing neutral antagonists in drug discovery.

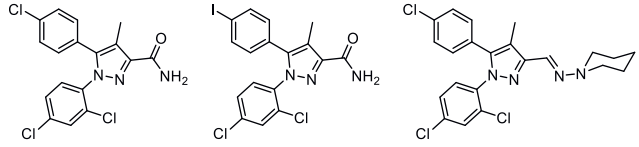

Figure 1.7 Chemical structures of several CB_1R neutral antagonists currently in development.

The Current Tools for CBR Research: Small Molecules

To determine target validation, CB_2R engagement and mode of action, tools are needed.[120,121] Small molecules can be turned into probes by introducing the right chemical groups. Probes can serve as a tool to image ligand-protein interaction and early identify potential problems such as off-target engagement. Many early drugs failed in clinical trials because it was not ascertained if the ligand had sufficient access to the target site and exhibited actual target engagement prior to entry.[120]

Positron Emission Tomography (PET) probes can image proteins and identify variations in activity and distribution with a radioisotope. They are widely used in medical imaging. However, drawbacks are short lifetime, exposure to radiation and nanomolar affinity requirements and possibility of false-positives.[122,123] The first CBR PET tracer was based on THC: [^{18}F]-Δ^8-THC (Figure 1.8), but it proved unstable and was unable to show specific binding *in vivo*.[124] [^{11}C]NE40 was used in human subjects to perform *in vivo* PET imaging, but CB_2R proved a bad biomarker for Alzheimer's Disease.[125] Many other designed PET tracers were abandoned due to high non-specific binding.[126] A recent CB_2R specific PET tracer is [^{18}F]RoSMA-18-d_6, which has nanomolar affinity and has successfully mapped CB_2R in nonhuman primates.[127,128]

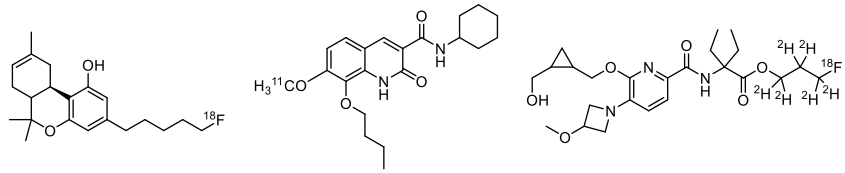

Figure 1.8 The chemical structures of several CBR PET tracers.

Fluorescence Resonance Energy Transfer (FRET) is a way to detect target engagement through a fluorescent signal that is only given when an acceptor and donor on the ligand and protein are in close proximity. However, it requires modification of the protein which may affect its structure and activity and cannot be used *in vivo*.[129] Likewise, many fluorescent small molecule probes have also been used for biological imaging. They are more accessible and stable than radioligands, do not require protein modification such as FRET, and are applicable in a wide range of biochemical assays. Introduction of a spacer chain minimizes the effect of the bulk of the fluorescent group on the scaffold's affinity for the target protein.[130] Cy5 and AF647 are commonly used due to their high quantum yield and stability under many conditions. Fluorescent probes are especially useful to image ligand-target interactions.[131,132] A Chromenopyrazole-Cy5 probe (Figure 1.9) has been shown to have moderately high affinity (hCB_2R pK_i = 7.38 ± 0.05, Table 1.1) with over 100-fold selectivity over hCB_1R.[133] Near-infrared fluorophores are popular due to their low interference with autobio-fluorescence and minimal damage to the cell during irradiation.[134,135] NIR760-mbc94 was designed and shown to effectively image tumours in murine models in a CB_2R selective manner.[136] Instead of direct ligand-fluorophore probes, sometimes two-step probes are utilized. HU210 was tagged with a biotin group, and was able to show CB_2R in microglial cells when streptavidin-AlexaFluor488 was added.[137] However, the two-step labelling and additional step to block endogenous biotin makes these probes unsuitable for staining and flow cytometry.[138] Other reported fluorescent CB_2R probes include *azo*-HU308-3, HU210-AF488, Naphthyridine-BODIPY630/650, RO6852763-SiR, HU308/AM841-chimera-NBD, HU308-AttoThio12, N-adamantyl-4-oxo-1,4-dihydroquinoline-3-carboxamide-4-DMAP, LEI-121 and more.[138–145]

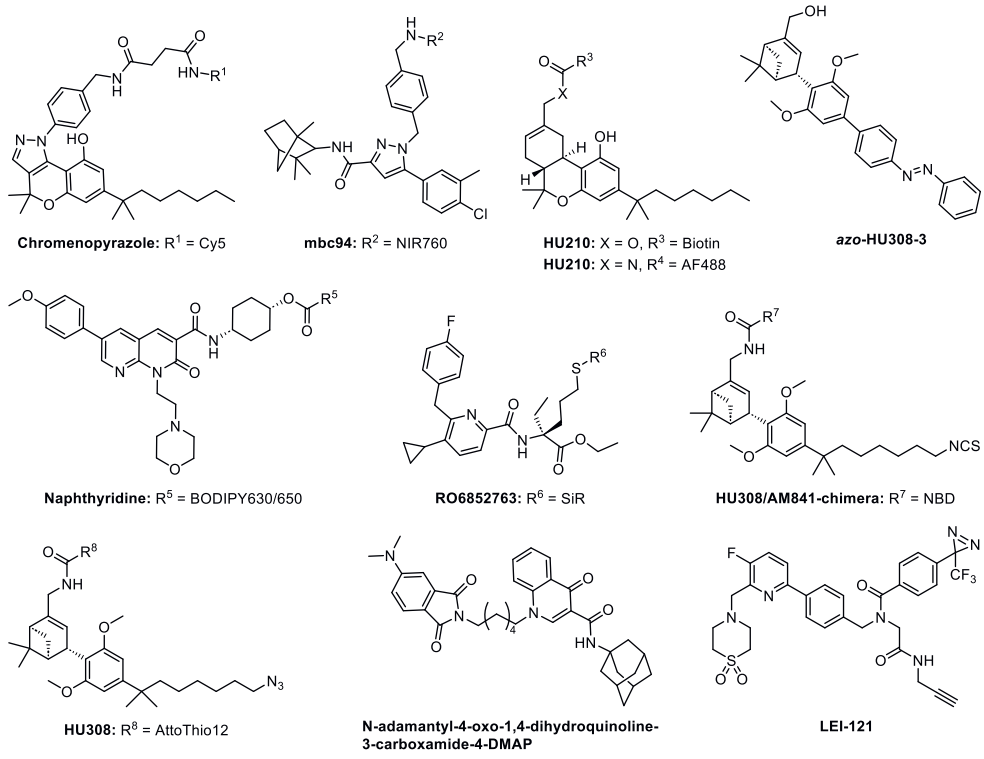

Figure 1.9 Chemical structures of reported fluorescent CB_2R probes.

Table 1.1 Reported fluorescent CB_2R probes.[146]

Name	CB_1R (pK_i ± SEM)	CB_2R (pK_i ± SEM)	Functionality
Chromenopyrazole-Cy5[133]	5.26 ± 0.11	7.38 ± 0.05	Inverse agonist
NIR760-mbc94[136]	N.R.	K_d = 26.9 ± 3.7 nM	N.R.
HU210-biotin[137]	8.62 ± 0.11	8.80 ± 0.11	N.R.
Azo-HU308-3[139]	N.R.	N.R.	Agonist
HU210-AF488[138]	7.57 ± 0.06	6.10 ± 0.11	Agonist
Naphthyridine-BODIPY630/650[140]	< 5	6.33 ± 0.02	Agonist
RO6852763-SiR[141]	6.94	7.21	Agonist
HU308/AM841-chimera-NBD[142]	5	8.38	N.R.
HU308-AttoThio12[143]	5.97	8.33	(Partial) agonist
N-adamantyl-4-oxo-1,4-dihydroquinoline-3-carboxamide-4-DMAP[144]	< 5	6.89	N.R.
LEI-121[145]	< 5	7.2 ± 0.4	Partial Agonist
N.R. not reported.			

Bifunctional, covalent probes can extent the applicability of the probes as they are no longer in a tenuous equilibrium where changes in environment can disengage the probe from the target. Electrophilic probes and photoaffinity probes first engage the target with high affinity through non-covalent means, after which an activatable group reacts with the protein to form a covalent bond. Electrophilic probes do this through an electrophilic group such as isothiocyanate (NCS), but are limited to reacting with nucleophilic amino acids.[147] Photoactivatable probes contain an inert group such as

diazirine that forms a reactive species upon irradiation with light, and this reactive species can insert into any bond nearby.[148] A bifunctional probe can then use a reporter tag (such as a radioisotope of fluorophore) to image the desired trait. Leiden University previously reported on the first bifunctional photoaffinity probe LEI-121 with a high selectivity for CB_2R in 2018.[145]

A new highly selective CB_2R agonist enters the stage

In 2011 LEI-101 (Figure 1.10) with its 5-fluoropyridin-2-yl-benzyl-imidazolidine-2,4-dione scaffold was reported to be an orally available, peripherally restricted, high affinity, selective CB_2R agonist.[149] It doesn't induce central nervous system (CNS) -mediated effects and protects against cisplatin induced damage.[150] LEI-101 derivatives were used to substantiate the drug-target residence time model, where compounds with increased residence time showed higher functional potency.[151] With this in mind, the improved CB_2R agonist LEI-102 was recently reported.[44]

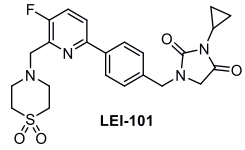

Figure 1.10 The chemical structure of LEI-101, the first in the 5-fluoropyridin-2-yl-benzyl-imidazolidine-2,4-dione series of compounds.

Thesis Outline

The endocannabinoid receptors CB_1R and CB_2R are involved in a plethora of processes, and consequently are involved in many pathological conditions. Their wide distribution makes the CBRs both an interesting therapeutic target and hard to study. Additional chemical tools are required to study and understand the function and mechanism of CB_1R and CB_2R. This thesis describes the development of several such tools to improve our insight in the (pathological) roles of the receptors in order to develop novel and improved therapeutics. **Chapter 2** describes the evaluation of three-dimensional ligand-CB_2R complexes made and analysed with Cryo-EM. Hotspots that potentially generate selectivity between CB_1R and CB_2R are evaluated with point-mutations *in vitro*. **Chapter 3** describes the development of the first tools, two-step bifunctional probes based on LEI-121 and LEI-102. Because two-step probes are not compatible with every assay, the toolbox is expanded with a one-step fluorescent probe. **Chapter 4** describes the design of a CB_2R fluorescent probe using the ligand-CB_2R complex from **Chapter 2**, and consequent synthesis. Switching to CB_1R, **Chapter 5** describes the design of CB_1R ligands with negatively charged phosphonium groups that are potentially selective for $mtCB_1R$. The thesis is concluded with a summary and outlook in **Chapter 6**.

References

1. Battista N, Tommaso M Di, Bari M, Maccarrone M. The endocannabinoid system: An overview. *Front Behav Neurosci*. 2012;6(FEBRUARY 2012):1-7. doi:10.3389/fnbeh.2012.00009

2. Aizpurua-Olaizola O, Elezgarai I, Rico-Barrio I, Zarandona I, Etxebarria N, Usobiaga A. Targeting the endocannabinoid system: future therapeutic strategies. *Drug Discov Today*. 2017;22(1):105-110. doi:10.1016/j.drudis.2016.08.005

3. Tudurí E, López M, Diéguez C, Nadal A, Nogueiras R. GPR55 and the regulation of glucose homeostasis. *Int J Biochem Cell Biol*. 2017;88:204-207. doi:10.1016/j.biocel.2017.04.010

4. Latorraca NR, Venkatakrishnan AJ, Dror RO. GPCR Dynamics: Structures in Motion. *Chem Rev*. 2017;117(1):139-155. doi:10.1021/acs.chemrev.6b00177

5. Neves SR, Ram PT, Iyengar R. G Protein Pathways. *Science (80-)*. 2002;296(5573):1636-1639. doi:10.1126/science.1071550

6. Noriega-Prieto JA, Kofuji P, Araque A. Endocannabinoid signaling in synaptic function. *Glia*. 2023;71(1):36-43. doi:10.1002/glia.24256

7. Atwood BK, MacKie K. CB 2: A cannabinoid receptor with an identity crisis. *Br J Pharmacol*. 2010;160(3):467-479. doi:10.1111/j.1476-5381.2010.00729.x

8. Costa B. On the Pharmacological Properties of Δ9-Tetrahydrocannabinol (THC). *Chem Biodivers*. 2007;4(8):1664-1677. doi:10.1002/cbdv.200790146

9. Gertsch J, Pertwee RG, Di Marzo V. Phytocannabinoids beyond the Cannabis plant - do they exist? *Br J Pharmacol*. 2010;160(3):523-529. doi:10.1111/j.1476-5381.2010.00745.x

10. Matsuda LA, Lolait SJ, Brownstein MJ, Young AC, Bonner TI. Structure of a cannabinoid receptor and functional expression of the cloned cDNA. *Nature*. 1990;346(6284):561-564. doi:10.1038/346561a0

11. Tsou K, Brown S, Sañudo-Peña M., Mackie K, Walker J. Immunohistochemical distribution of cannabinoid CB1 receptors in the rat central nervous system. *Neuroscience*. 1998;83(2):393-411. doi:10.1016/S0306-4522(97)00436-3

12. Howlett AC, Bidaut-Russell M, Devane WA, Melvin LS, Johnson MR, Herkenham M. The cannabinoid receptor: biochemical, anatomical and behavioral characterization. *Trends Neurosci*. 1990;13(10):420-423. doi:10.1016/0166-2236(90)90124-S

13. Navarrete F, García-Gutiérrez MS, Jurado-Barba R, et al. Endocannabinoid System Components as Potential Biomarkers in Psychiatry. *Front Psychiatry*. 2020;11(April):1-30. doi:10.3389/fpsyt.2020.00315

14. Pacher P, Bátkai S, Kunos G. The endocannabinoid system as an emerging target of pharmacotherapy. *Pharmacol Rev*. 2006;58(3):389-462. doi:10.1124/pr.58.3.2

15. Kano M, Ohno-Shosaku T, Hashimotodani Y, Uchigashima M, Watanabe M. Endocannabinoid-mediated control of synaptic transmission. *Physiol Rev*. 2009;89(1):309-380. doi:10.1152/physrev.00019.2008

16. Di Marzo V, Stella N, Zimmer A. Endocannabinoid signalling and the deteriorating brain. *Nat Rev Neurosci*. 2015;16(1):30-42. doi:10.1038/nrn3876

17. Iversen L. Cannabis and the brain. *Brain*. 2003;126(Pt 6):1252-1270. doi:10.1093/brain/awg143

18. O'Sullivan SE, Yates AS, Porter RK. The Peripheral Cannabinoid Receptor Type 1 (CB1) as a

Molecular Target for Modulating Body Weight in Man. *Molecules*. 2021;26(20):6178. doi:10.3390/molecules26206178

19. Zou S, Kumar U. Cannabinoid receptors and the endocannabinoid system: Signaling and function in the central nervous system. *Int J Mol Sci*. 2018;19(3). doi:10.3390/ijms19030833

20. Maccarrone M, Bab I, Bíró T, et al. Endocannabinoid signaling at the periphery: 50 years after THC. *Trends Pharmacol Sci*. 2015;36(5):277-296. doi:10.1016/j.tips.2015.02.008

21. Galiegue S, Mary S, Marchand J, et al. Expression of Central and Peripheral Cannabinoid Receptors in Human Immune Tissues and Leukocyte Subpopulations. *Eur J Biochem*. 1995;232(1):54-61. doi:10.1111/j.1432-1033.1995.tb20780.x

22. Mecha M, Feliú A, Carrillo-Salinas FJ, et al. Endocannabinoids drive the acquisition of an alternative phenotype in microglia. *Brain Behav Immun*. 2015;49:233-245. doi:10.1016/j.bbi.2015.06.002

23. Contino M, Capparelli E, Colabufo NA, Bush AI. Editorial: The CB2 Cannabinoid System: A New Strategy in Neurodegenerative Disorder and Neuroinflammation. *Front Neurosci*. 2017;11. doi:10.3389/fnins.2017.00196

24. Argenziano M, Tortora C, Bellini G, Di Paola A, Punzo F, Rossi F. The endocannabinoid system in pediatric inflammatory and immune diseases. *Int J Mol Sci*. 2019;20(23). doi:10.3390/ijms20235875

25. Vuic B, Milos T, Tudor L, et al. Cannabinoid CB2 Receptors in Neurodegenerative Proteinopathies: New Insights and Therapeutic Potential. *Biomedicines*. 2022;10(12). doi:10.3390/biomedicines10123000

26. Manzanares J, Cabañero D, Puente N, García-Gutiérrez MS, Grandes P, Maldonado R. Role of the endocannabinoid system in drug addiction. *Biochem Pharmacol*. 2018;157:108-121. doi:10.1016/j.bcp.2018.09.013

27. Fernández-Ruiz J, Romero J, Velasco G, Tolón RM, Ramos JA, Guzmán M. Cannabinoid CB2 receptor: a new target for controlling neural cell survival? *Trends Pharmacol Sci*. 2007;28(1):39-45. doi:10.1016/j.tips.2006.11.001

28. Munro S, Thomas KL, Abu-Shaar M. Molecular characterization of a peripheral receptor for cannabinoids. *Nature*. 1993;365(6441):61-65. doi:10.1038/365061a0

29. Al-Zoubi, Morales, Reggio. Structural Insights into CB1 Receptor Biased Signaling. *Int J Mol Sci*. 2019;20(8):1837. doi:10.3390/ijms20081837

30. Shao Z, Yin J, Chapman K, et al. High-resolution crystal structure of the human CB1 cannabinoid receptor. *Nature*. 2016;540(7634):602-606. doi:10.1038/nature20613

31. Hua T, Vemuri K, Pu M, et al. Crystal Structure of the Human Cannabinoid Receptor CB1. *Cell*. 2016;167(3):750-762.e14. doi:10.1016/j.cell.2016.10.004

32. Ramesh K, Rosenbaum DM. Molecular basis for ligand modulation of the cannabinoid CB 1 receptor. *Br J Pharmacol*. 2022;179(14):3487-3495. doi:10.1111/bph.15627

33. Li X, Hua T, Vemuri K, et al. Crystal Structure of the Human Cannabinoid Receptor CB2. *Cell*. 2019;176(3):459-467.e13. doi:10.1016/j.cell.2018.12.011

34. García-Nafría J, Tate CG. Structure determination of GPCRs: Cryo-EM compared with X-ray crystallography. *Biochem Soc Trans*. 2021;49(5):2345-2355. doi:10.1042/BST20210431

35. Hua T, Li X, Wu L, et al. Activation and Signaling Mechanism Revealed by Cannabinoid Receptor-

Gi Complex Structures. *Cell*. 2020;180(4):655-665.e18. doi:10.1016/j.cell.2020.01.008

36. Shao Z, Yin J, Chapman K, et al. High-resolution crystal structure of the human CB1 cannabinoid receptor. *Nature*. 2016;540(7634):602-606. doi:10.1038/nature20613

37. Hua T, Vemuri K, Nikas SP, et al. Crystal structures of agonist-bound human cannabinoid receptor CB1. *Nature*. 2017;547(7664):468-471. doi:10.1038/nature23272

38. Shao Z, Yan W, Chapman K, et al. Structure of an allosteric modulator bound to the CB1 cannabinoid receptor. *Nat Chem Biol*. 2019;15(12):1199-1205. doi:10.1038/s41589-019-0387-2

39. Wang X, Liu D, Shen L, et al. A Genetically Encoded F-19 NMR Probe Reveals the Allosteric Modulation Mechanism of Cannabinoid Receptor 1. *J Am Chem Soc*. 2021;143(40):16320-16325. doi:10.1021/jacs.1c06847

40. Liang Y-L, Khoshouei M, Radjainia M, et al. Phase-plate cryo-EM structure of a class B GPCR–G-protein complex. *Nature*. 2017;546(7656):118-123. doi:10.1038/nature22327

41. Krishna Kumar K, Shalev-Benami M, Robertson MJ, et al. Structure of a Signaling Cannabinoid Receptor 1-G Protein Complex. *Cell*. 2019;176(3):448-458.e12. doi:10.1016/j.cell.2018.11.040

42. Xing C, Zhuang Y, Xu T-H, et al. Cryo-EM Structure of the Human Cannabinoid Receptor CB2-Gi Signaling Complex. *Cell*. 2020;180(4):645-654.e13. doi:10.1016/j.cell.2020.01.007

43. Dutta S, Shukla D. Distinct Activation Mechanisms Regulate Subtype Selectivity of Cannabinoid Receptors. *bioRxiv*. January 2022:2022.09.27.509760. doi:10.1101/2022.09.27.509760

44. Li X, Chang H, Bouma J, et al. Structural basis of selective cannabinoid CB2 receptor activation. *Nat Commun*. 2023;14(1):1447. doi:10.1038/s41467-023-37112-9

45. Lee YR, Xia L. Efficient one-pot synthetic approaches for cannabinoid analogues and their application to biologically interesting (−)-hexahydrocannabinol and (+)-hexahydrocannabinol. *Tetrahedron Lett*. 2008;49(20):3283-3287. doi:10.1016/j.tetlet.2008.03.075

46. Abadji V, Lin S, Taha G, et al. (R)-Methanandamide: A Chiral Novel Anandamide Possessing Higher Potency and Metabolic Stability. *J Med Chem*. 1994;37(12):1889-1893. doi:10.1021/jm00038a020

47. Le Boisselier R, Alexandre J, Lelong-Boulouard V, Debruyne D. Focus on cannabinoids and synthetic cannabinoids. *Clin Pharmacol Ther*. 2017;101(2):220-229. doi:10.1002/cpt.563

48. Lauckner JE, Hille B, Mackie K. The cannabinoid agonist WIN55,212-2 increases intracellular calcium via CB 1 receptor coupling to G q/11 G proteins. *Proc Natl Acad Sci*. 2005;102(52):19144-19149. doi:10.1073/pnas.0509588102

49. Magham SV, Thaggikuppe krishnamurthy P, Shaji N, Mani L, Balasubramanian S. Cannabinoid receptor 2 selective agonists and Alzheimer's disease: An insight into the therapeutic potentials. *J Neurosci Res*. 2021;99(11):2888-2905. doi:10.1002/jnr.24933

50. Vuic B, Milos T, Tudor L, et al. Cannabinoid CB2 Receptors in Neurodegenerative Proteinopathies: New Insights and Therapeutic Potential. *Biomedicines*. 2022;10(12):3000. doi:10.3390/biomedicines10123000

51. Bai J, Ge G, Wang Y, et al. A selective CB2 agonist protects against the inflammatory response and joint destruction in collagen-induced arthritis mice. *Biomed Pharmacother*. 2019;116:109025. doi:10.1016/j.biopha.2019.109025

52. Fulmer ML, Thewke DP. The Endocannabinoid System and Heart Disease: The Role of Cannabinoid Receptor Type 2. *Cardiovasc Hematol Disord Targets*. 2018;18(1):34-51.

doi:10.2174/1871529X18666180206161457

53. Tartakover Matalon S, Ringel Y, Konikoff F, Drucker L, Pery S, Naftali T. Cannabinoid receptor 2 agonist promotes parameters implicated in mucosal healing in patients with inflammatory bowel disease. *United Eur Gastroenterol J*. 2020;8(3):271-283. doi:10.1177/2050640619889773

54. Hashiesh HM, Sheikh A, Meeran MN, et al. [beta]-Caryophyllene, a dietary CB2 receptor selective cannabinoid mitigates myocardial fibrosis in a mice model of diabetic cardiomyopathy. *Endocr Abstr*. May 2022. doi:10.1530/endoabs.81.OC1.4

55. Moura CV, dos Santos R, Duarte L, Galdino G. Cannabinoid CB 2 receptors and spinal microglia are implicated in tingenone-mediated antinociception in mice. *Asian Pac J Trop Biomed*. 2021;11(4):141. doi:10.4103/2221-1691.310200

56. Alberti TB, Coelho DS, Maraschin M. β-Caryophyllene nanoparticles design and development: Controlled drug delivery of cannabinoid CB2 agonist as a strategic tool towards neurodegeneration. *Mater Sci Eng C*. 2021;121(December 2020):111824. doi:10.1016/j.msec.2020.111824

57. Hu S-J, Cheng G, Zhou H, et al. Identification of Novel Cannabinoid CB2 Receptor Agonists from Botanical Compounds and Preliminary Evaluation of Their Anti-Osteoporotic Effects. *Molecules*. 2022;27(3):702. doi:10.3390/molecules27030702

58. Kumawat VS, Kaur G. Therapeutic potential of cannabinoid receptor 2 in the treatment of diabetes mellitus and its complications. *Eur J Pharmacol*. 2019;862:172628. doi:10.1016/j.ejphar.2019.172628

59. Tsoukalas NG, Giaginis C, Alexandrou P, et al. 1995P Clinical significance of cannabinoid receptor CB2 expression in non-small cell lung cancer (NSCLC). *Ann Oncol*. 2020;31:S1115. doi:10.1016/j.annonc.2020.08.1301

60. Whiting ZM, Yin J, de la Harpe SM, Vernall AJ, Grimsey NL. Developing the Cannabinoid Receptor 2 (CB2) pharmacopoeia: past, present, and future. *Trends Pharmacol Sci*. 2022;43(9):754-771. doi:10.1016/j.tips.2022.06.010

61. Deng L, Guindon J, Cornett BL, Makriyannis A, Mackie K, Hohmann AG. Chronic Cannabinoid Receptor 2 Activation Reverses Paclitaxel Neuropathy Without Tolerance or Cannabinoid Receptor 1–Dependent Withdrawal. *Biol Psychiatry*. 2015;77(5):475-487. doi:10.1016/j.biopsych.2014.04.009

62. GlobalData Healthcare. Cannabinoids receptors: popular preclinical target but banned in 137 countries. Pharmaceutical Technology. https://www.pharmaceutical-technology.com/comment/cannabinoids-receptors/. Published 2022. Accessed February 17, 2023.

63. Dhopeshwarkar A, Mackie K. CB 2 Cannabinoid Receptors as a Therapeutic Target—What Does the Future Hold? *Mol Pharmacol*. 2014;86(4):430-437. doi:10.1124/mol.114.094649

64. Leleu-Chavain N, Body-Malapel M, Spencer J, Chavatte P, Desreumaux P, Millet R. Recent Advances in the Development of Selective CB2 Agonists as Promising Anti-Inflammatory Agents. *Curr Med Chem*. 2012;19(21):3457-3474. doi:10.2174/092986712801323207

65. Haruna T, Soga M, Morioka Y, et al. S-777469, a Novel Cannabinoid Type 2 Receptor Agonist, Suppresses Itch-Associated Scratching Behavior in Rodents through Inhibition of Itch Signal Transmission. *Pharmacology*. 2015;95(1-2):95-103. doi:10.1159/000371890

66. Shionogi Inc. A Randomized, Double-Blind Study to Evaluate the Safety and Efficacy of 2 Doses

of S-777469 in Patients With Atopic Dermatitis. ClinicalTrials.gov. https://clinicaltrials.gov/ct2/show/NCT00703573?term=S-777469&draw=2&rank=1. Accessed March 1, 2023.

67. Tarawneh AH, Pandey P, Al-Momani LA, et al. 1,2,3-Triazole derivatives as highly selective cannabinoid receptor type 2 (CB2) agonists. *Arab J Chem*. 2022;15(1):103545. doi:10.1016/j.arabjc.2021.103545

68. Corbus Pharmaceutical. Corbus Pharmaceuticals Receives FDA Orphan Drug Designation for Lenabasum for the Treatment of Dermatomyositis. https://www.corbuspharma.com/press-releases/detail/276/corbus-pharmaceuticals-receives-fda-orphan-drug-designation. Published 2018. Accessed March 1, 2023.

69. Corbus Pharmaceuticals Inc. Trial to Evaluate Efficacy and Safety of Lenabasum in Cystic Fibrosis. ClinicalTrials.gov. https://clinicaltrials.gov/ct2/show/study/NCT03451045?term=Lenabasum&draw=2&rank=1. Published 2023. Accessed March 1, 2023.

70. Corbus Pharmaceuticals Inc. JBT-101 in Systemic Lupus Erythematosus (SLE). ClinicalTrials.gov. https://clinicaltrials.gov/ct2/show/NCT03093402?term=Lenabasum&draw=2&rank=6. Published 2022. Accessed March 1, 2023.

71. Corbus Pharmaceuticals Inc. Trial to Evaluate Efficacy and Safety of Lenabasum in Dermatomyositis (DETERMINE). ClinicalTrials.gov. https://clinicaltrials.gov/ct2/show/NCT03813160?term=Lenabasum&draw=2&rank=3. Published 2022. Accessed March 1, 2023.

72. Spiera R, Kuwana M, Khanna D, et al. OP0171 PHASE 3 TRIAL OF LENABASUM, A CB2 AGONIST, FOR THE TREATMENT OF DIFFUSE CUTANEOUS SYSTEMIC SCLEROSIS (DCSSC). *Ann Rheum Dis*. 2021;80(Suppl 1):102-103. doi:10.1136/annrheumdis-2021-eular.1795

73. Hanuš L, Breuer A, Tchilibon S, et al. HU-308: A specific agonist for CB 2 , a peripheral cannabinoid receptor. *Proc Natl Acad Sci*. 1999;96(25):14228-14233. doi:10.1073/pnas.96.25.14228

74. Soethoudt M, Grether U, Fingerle J, et al. Cannabinoid CB2 receptor ligand profiling reveals biased signalling and off-target activity. *Nat Commun*. 2017;8(1):13958. doi:10.1038/ncomms13958

75. Arena Pharmaceuticals. Tolerability, Pharmacokinetics, and Efficacy of APD371 in Participants With Crohn's Disease Experiencing Abdominal Pain. ClinicalTrials.gov. https://clinicaltrials.gov/ct2/show/NCT03155945. Published 2021. Accessed March 1, 2023.

76. Chang L, Cash BD, Lembo A, et al. Efficacy and safety of olorinab, a full agonist of the cannabinoid receptor 2, for the treatment of abdominal pain in patients with irritable bowel syndrome: Results from a phase 2b randomized placebo-controlled trial (<scp>CAPTIVATE</scp>). *Neurogastroenterol Motil*. February 2023. doi:10.1111/nmo.14539

77. Jones C, Turner S, Ruckle J, Liu Q, Christopher R, Klassen P. Safety, tolerability, and pharmacokinetics of APD371, a highly selective CB 2 agonist, in healthy adults. *J Pain*. 2018;19(3):S82. doi:10.1016/j.jpain.2017.12.200

78. Manalac T. Roche Cuts Pipeline as COVID, Currency Headwinds Impact Q3 Results. BioSpace. https://www.biospace.com/article/roche-cuts-pipeline-as-covid-19-headwinds-batter-q3-sales/. Published 2023. Accessed October 24, 2023.

79. Woodhams SG, Chapman V, Finn DP, Hohmann AG, Neugebauer V. The cannabinoid system and pain. *Neuropharmacology*. 2017;124:105-120. doi:10.1016/j.neuropharm.2017.06.015

80. Sbarski B, Akirav I. Cannabinoids as therapeutics for PTSD. *Pharmacol Ther*. 2020;211:107551. doi:10.1016/j.pharmthera.2020.107551

81. Haller J, Varga B, Ledent C, Freund TF. CB1 cannabinoid receptors mediate anxiolytic effects: convergent genetic and pharmacological evidence with CB1-specific agents. *Behav Pharmacol*. 2004;15(4):299-304. doi:10.1097/01.fbp.0000135704.56422.40

82. Hill MN, Carrier EJ, McLaughlin RJ, et al. Regional alterations in the endocannabinoid system in an animal model of depression: effects of concurrent antidepressant treatment. *J Neurochem*. 2008;106(6):2322-2336. doi:10.1111/j.1471-4159.2008.05567.x

83. Wallace MJ, Wiley JL, Martin BR, DeLorenzo RJ. Assessment of the role of CB1 receptors in cannabinoid anticonvulsant effects. *Eur J Pharmacol*. 2001;428(1):51-57. doi:10.1016/S0014-2999(01)01243-2

84. Hayakawa K, Mishima K, Nozako M, et al. Δ9-tetrahydrocannabinol (Δ9-THC) prevents cerebral infarction via hypothalamic-independent hypothermia. *Life Sci*. 2007;80(16):1466-1471. doi:10.1016/j.lfs.2007.01.014

85. Glass M, Faull RLM, Dragunow M. Loss of cannabinoid receptors in the substantia nigra in huntington's disease. *Neuroscience*. 1993;56(3):523-527. doi:10.1016/0306-4522(93)90352-G

86. Leo LM, Abood ME. Cb1 cannabinoid receptor signaling and biased signaling. *Molecules*. 2021;26(17):1-22. doi:10.3390/molecules26175413

87. Cinar R, Iyer MR, Kunos G. The therapeutic potential of second and third generation CB1R antagonists. *Pharmacol Ther*. 2020;208:107477. doi:10.1016/j.pharmthera.2020.107477

88. Maccarrone M, Bab I, Bíró T, et al. Endocannabinoid signaling at the periphery: 50 years after THC. *Trends Pharmacol Sci*. 2015;36(5):277-296. doi:10.1016/j.tips.2015.02.008

89. Tam J, Cinar R, Liu J, et al. Peripheral Cannabinoid-1 Receptor Inverse Agonism Reduces Obesity by Reversing Leptin Resistance. *Cell Metab*. 2012;16(2):167-179. doi:10.1016/j.cmet.2012.07.002

90. Sun D, Gao W, Hu H, Zhou S. Why 90% of clinical drug development fails and how to improve it? *Acta Pharm Sin B*. 2022;12(7):3049-3062. doi:10.1016/j.apsb.2022.02.002

91. Morales P, Jagerovic N. Novel approaches and current challenges with targeting the endocannabinoid system. *Expert Opin Drug Discov*. 2020;15(8):917-930. doi:10.1080/17460441.2020.1752178

92. Mielnik CA, Lam VM, Ross RA. CB1 allosteric modulators and their therapeutic potential in CNS disorders. *Prog Neuro-Psychopharmacology Biol Psychiatry*. 2021;106:110163. doi:10.1016/j.pnpbp.2020.110163

93. Gado F, Di Cesare Mannelli L, Lucarini E, et al. Identification of the First Synthetic Allosteric Modulator of the CB 2 Receptors and Evidence of Its Efficacy for Neuropathic Pain Relief. *J Med Chem*. 2019;62(1):276-287. doi:10.1021/acs.jmedchem.8b00368

94. Morales P, Goya P, Jagerovic N, Hernandez-Folgado L. Allosteric Modulators of the CB 1 Cannabinoid Receptor: A Structural Update Review. *Cannabis Cannabinoid Res*. 2016;1(1):22-30. doi:10.1089/can.2015.0005

95. Fowler CJ. The endocannabinoid system – current implications for drug development. *J Intern Med*. 2021;290(1):2-26. doi:10.1111/joim.13229

96. El-Hammadi MM, Small-Howard AL, Fernández-Arévalo M, Martín-Banderas L. Development of

enhanced drug delivery vehicles for three cannabis-based terpenes using poly(lactic-co-glycolic acid) based nanoparticles. *Ind Crops Prod*. 2021;164:113345. doi:10.1016/j.indcrop.2021.113345

97. Natarajan J V., Nugraha C, Ng XW, Venkatraman S. Sustained-release from nanocarriers: a review. *J Control Release*. 2014;193:122-138. doi:10.1016/j.jconrel.2014.05.029

98. Bobo D, Robinson KJ, Islam J, Thurecht KJ, Corrie SR. Nanoparticle-Based Medicines: A Review of FDA-Approved Materials and Clinical Trials to Date. *Pharm Res*. 2016;33(10):2373-2387. doi:10.1007/s11095-016-1958-5

99. Alberti TB, Coelho DS, Maraschin M. β-Caryophyllene nanoparticles design and development: Controlled drug delivery of cannabinoid CB2 agonist as a strategic tool towards neurodegeneration. *Mater Sci Eng C*. 2021;121:111824. doi:10.1016/j.msec.2020.111824

100. Moniruzzaman M, Rewatkar P, Begun J, Popat A. P037 Enhancing the efficacy of cannabidiol using protein nanoparticles to treat inflammatory bowel disease. *J Crohn's Colitis*. 2023;17(Supplement_1):i204-i205. doi:10.1093/ecco-jcc/jjac190.0167

101. Hirsch S, Hinden L, Naim MB-D, et al. Hepatic targeting of the centrally active cannabinoid 1 receptor (CB1R) blocker rimonabant via PLGA nanoparticles for treating fatty liver disease and diabetes. *J Control Release*. 2023;353:254-269. doi:10.1016/j.jconrel.2022.11.040

102. Jia Y, Jiang Y, He Y, et al. Approved Nanomedicine against Diseases. *Pharmaceutics*. 2023;15(3). doi:10.3390/pharmaceutics15030774

103. Cinar R, Iyer MR, Kunos G. The therapeutic potential of second and third generation CB1R antagonists. *Pharmacol Ther*. 2020;208:107477. doi:10.1016/j.pharmthera.2020.107477

104. Wang H, Zhang H, Xiang Y, Pan W, Li N, Tang B. An efficient strategy for cancer therapy using a tumor- and lysosome-targeted organic photothermal agent. *Nanoscale*. 2021;13(19):8790-8794. doi:10.1039/D1NR01547H

105. Westphal M V., Schafroth MA, Sarott RC, et al. Synthesis of Photoswitchable Δ 9 -Tetrahydrocannabinol Derivatives Enables Optical Control of Cannabinoid Receptor 1 Signaling. *J Am Chem Soc*. 2017;139(50):18206-18212. doi:10.1021/jacs.7b06456

106. Laguerre A, Hauke S, Qiu J, Kelly MJ, Schultz C. Photorelease of 2-Arachidonoylglycerol in Live Cells. *J Am Chem Soc*. 2019;141(42):16544-16547. doi:10.1021/jacs.9b05978

107. Castaneda JT, Harui A, Kiertscher SM, Roth JD, Roth MD. Differential Expression of Intracellular and Extracellular CB2 Cannabinoid Receptor Protein by Human Peripheral Blood Leukocytes. *J Neuroimmune Pharmacol*. 2013;8(1):323-332. doi:10.1007/s11481-012-9430-8

108. Castaneda JT, Harui A, Roth MD. Regulation of Cell Surface CB2 Receptor during Human B Cell Activation and Differentiation. *J Neuroimmune Pharmacol*. 2017;12(3):544-554. doi:10.1007/s11481-017-9744-7

109. Brailoiu GC, Deliu E, Marcu J, et al. Differential activation of intracellular versus plasmalemmal CB2 Cannabinoid receptors. *Biochemistry*. 2014;53(30):4990-4999. doi:10.1021/bi500632a

110. Schuchman EH, Ledesma MD, Simonaro CM. New paradigms for the treatment of lysosomal storage diseases: targeting the endocannabinoid system as a therapeutic strategy. *Orphanet J Rare Dis*. 2021;16(1):151. doi:10.1186/s13023-021-01779-4

111. Xing L, Lyu J-Y, Yang Y, et al. pH-Responsive de-PEGylated nanoparticles based on triphenylphosphine–quercetin self-assemblies for mitochondria-targeted cancer therapy. *Chem Commun*. 2017;53(62):8790-8793. doi:10.1039/C7CC04058J

112. Maniganda S, Sankar V, Nair JB, Raghu KG, Maiti KK. A lysosome-targeted drug delivery system based on sorbitol backbone towards efficient cancer therapy. *Org Biomol Chem*. 2014;12(34):6564-6569. doi:10.1039/C4OB01153H

113. Wang L, Xiao Y, Tian W, Deng L. Activatable Rotor for Quantifying Lysosomal Viscosity in Living Cells. *J Am Chem Soc*. 2013;135(8):2903-2906. doi:10.1021/ja311688g

114. Galaj E, Xi Z-X. Potential of Cannabinoid Receptor Ligands as Treatment for Substance Use Disorders. *CNS Drugs*. 2019;33(10):1001-1030. doi:10.1007/s40263-019-00664-w

115. Seltzman HH, Maitra R, Bortoff K, et al. Metabolic Profiling of CB1 Neutral Antagonists. In: ; 2017:199-215. doi:10.1016/bs.mie.2017.06.025

116. Sink KS, Vemuri VK, Wood J, Makriyannis A, Salamone JD. Oral bioavailability of the novel cannabinoid CB1 antagonist AM6527: Effects on food-reinforced behavior and comparisons with AM4113. *Pharmacol Biochem Behav*. 2009;91(3):303-306. doi:10.1016/j.pbb.2008.07.013

117. Jarbe T, Lemay B, Olszewska T, Vemuri V, Wood J, Makryannis A. Intrinsic effects of AM4113, a putative neutral CB1 receptor selective antagonist, on open-field behaviors in rats. *Pharmacol Biochem Behav*. 2008;91(1):84-90. doi:10.1016/j.pbb.2008.06.014

118. Fong TM. Constitutive Activity in Cannabinoid Receptors. In: ; 2014:121-133. doi:10.1016/B978-0-12-417197-8.00004-3

119. Khilnani G, Khilnani A. Inverse agonism and its therapeutic significance. *Indian J Pharmacol*. 2011;43(5):492. doi:10.4103/0253-7613.84947

120. Bunnage ME, Chekler ELP, Jones LH. Target validation using chemical probes. *Nat Chem Biol*. 2013;9(4):195-199. doi:10.1038/nchembio.1197

121. Simon GM, Niphakis MJ, Cravatt BF. Determining target engagement in living systems. *Nat Chem Biol*. 2013;9(4):200-205. doi:10.1038/nchembio.1211

122. Matthews PM, Rabiner EA, Passchier J, Gunn RN. Positron emission tomography molecular imaging for drug development. *Br J Clin Pharmacol*. 2012;73(2):175-186. doi:10.1111/j.1365-2125.2011.04085.x

123. Evens N, M. Bormans G. Non-Invasive Imaging of the Type 2 Cannabinoid Receptor, Focus on Positron Emission Tomography. *Curr Top Med Chem*. 2010;10(15):1527-1543. doi:10.2174/156802610793176819

124. Charalambous A, Marciniak G, Shiue C-Y, et al. PET studies in the primate brain and biodistribution in mice using (−)-5′-18F-Δ8-THC. *Pharmacol Biochem Behav*. 1991;40(3):503-507. doi:10.1016/0091-3057(91)90354-5

125. Ahmad R, Postnov A, Bormans G, Versijpt J, Vandenbulcke M, Van Laere K. Decreased in vivo availability of the cannabinoid type 2 receptor in Alzheimer's disease. *Eur J Nucl Med Mol Imaging*. 2016;43(12):2219-2227. doi:10.1007/s00259-016-3457-7

126. Hou L, Rong J, Haider A, et al. Positron Emission Tomography Imaging of the Endocannabinoid System: Opportunities and Challenges in Radiotracer Development. *J Med Chem*. 2021;64(1):123-149. doi:10.1021/acs.jmedchem.0c01459

127. Haider A, Gobbi L, Kretz J, et al. Identification and Preclinical Development of a 2,5,6-Trisubstituted Fluorinated Pyridine Derivative as a Radioligand for the Positron Emission Tomography Imaging of Cannabinoid Type 2 Receptors. *J Med Chem*. 2020;63(18):10287-10306. doi:10.1021/acs.jmedchem.0c00778

128. Haider A, Wang L, Gobbi L, et al. Evaluation of [18 F]RoSMA-18-d 6 as a CB2 PET Radioligand in Nonhuman Primates. *ACS Chem Neurosci*. 2023;14(20):3752-3760. doi:10.1021/acschemneuro.3c00222

129. Schürmann M, Janning P, Ziegler S, Waldmann H. Small-Molecule Target Engagement in Cells. *Cell Chem Biol*. 2016;23(4):435-441. doi:10.1016/j.chembiol.2016.03.008

130. Stoddart LA, Kilpatrick LE, Briddon SJ, Hill SJ. Probing the pharmacology of G protein-coupled receptors with fluorescent ligands. *Neuropharmacology*. 2015;98:48-57. doi:10.1016/j.neuropharm.2015.04.033

131. Wu Y, Zhang B, Xu H, et al. The chronological evolution of fluorescent GPCR probes for bioimaging. *Coord Chem Rev*. 2023;480:215040. doi:10.1016/j.ccr.2023.215040

132. Karlsson JKG, Laude A, Hall MJ, Harriman A. Photo-isomerization of the Cyanine Dye Alexa-Fluor 647 (AF-647) in the Context of dSTORM Super-Resolution Microscopy. *Chem – A Eur J*. 2019;25(65):14983-14998. doi:10.1002/chem.201904117

133. Singh S, Oyagawa CRMM, Macdonald C, Grimsey NL, Glass M, Vernall AJ. Chromenopyrazole-based High Affinity, Selective Fluorescent Ligands for Cannabinoid Type 2 Receptor. *ACS Med Chem Lett*. 2019;10(2):209-214. doi:10.1021/acsmedchemlett.8b00597

134. Luo S, Zhang E, Su Y, Cheng T, Shi C. A review of NIR dyes in cancer targeting and imaging. *Biomaterials*. 2011;32(29):7127-7138. doi:10.1016/j.biomaterials.2011.06.024

135. Briddon SJ, Kellam B, Hill SJ. Design and Use of Fluorescent Ligands to Study Ligand–Receptor Interactions in Single Living Cells. In: ; 2011:211-236. doi:10.1007/978-1-61779-126-0_11

136. Zhang S, Shao P, Bai M. In Vivo Type 2 Cannabinoid Receptor-Targeted Tumor Optical Imaging Using a Near Infrared Fluorescent Probe. *Bioconjug Chem*. 2013;24(11):1907-1916. doi:10.1021/bc400328m

137. Martín-Couce L, Martín-Fontecha M, Palomares Ó, et al. Chemical Probes for the Recognition of Cannabinoid Receptors in Native Systems. *Angew Chemie Int Ed*. 2012;51(28):6896-6899. doi:10.1002/anie.201200467

138. Martín-Fontecha M, Angelina A, Rückert B, et al. A Fluorescent Probe to Unravel Functional Features of Cannabinoid Receptor CB 1 in Human Blood and Tonsil Immune System Cells. *Bioconjug Chem*. 2018;29(2):382-389. doi:10.1021/acs.bioconjchem.7b00680

139. Sarott RC, Viray AEG, Pfaff P, et al. Optical Control of Cannabinoid Receptor 2-Mediated Ca 2+ Release Enabled by Synthesis of Photoswitchable Probes. *J Am Chem Soc*. 2021;143(2):736-743. doi:10.1021/jacs.0c08926

140. Cooper AG, Oyagawa CRM, Manning JJ, et al. Development of selective, fluorescent cannabinoid type 2 receptor ligands based on a 1,8-naphthyridin-2-(1 H)-one-3-carboxamide scaffold. *Medchemcomm*. 2018;9(12):2055-2067. doi:10.1039/C8MD00448J

141. Gazzi, Thais, Brennecke B, et al. Drug Derived Fluorescent Probes for the Specific Visualization of Cannabinoid Type 2 Receptor - A Toolbox Approach. *ChemRxiv*. 2019. doi:10.26434/chemrxiv.10283027.v1

142. Westphal M V., Sarott RC, Zirwes EA, et al. Highly Selective, Amine-Derived Cannabinoid Receptor 2 Probes. *Chem – A Eur J*. 2020;26(6):1380-1387. doi:10.1002/chem.201904584

143. Sarott RC, Westphal M V., Pfaff P, et al. Development of High-Specificity Fluorescent Probes to Enable Cannabinoid Type 2 Receptor Studies in Living Cells. *J Am Chem Soc*. 2020;142(40):16953-16964. doi:10.1021/jacs.0c05587

144. Spinelli F, Giampietro R, Stefanachi A, et al. Design and synthesis of fluorescent ligands for the detection of cannabinoid type 2 receptor (CB2R). *Eur J Med Chem*. 2020;188:112037. doi:10.1016/j.ejmech.2020.112037

145. Soethoudt M, Stolze SC, Westphal M V., et al. Selective Photoaffinity Probe That Enables Assessment of Cannabinoid CB 2 Receptor Expression and Ligand Engagement in Human Cells. *J Am Chem Soc*. 2018;140(19):6067-6075. doi:10.1021/jacs.7b11281

146. Hamilton AJ, Payne AD, Mocerino M, Gunosewoyo H. Imaging Cannabinoid Receptors: A Brief Collection of Covalent and Fluorescent Probes for CB. *Aust J Chem*. 2021;74(6):416-432. doi:10.1071/CH21007

147. Kulkarni PM, Kulkarni AR, Korde A, et al. Novel Electrophilic and Photoaffinity Covalent Probes for Mapping the Cannabinoid 1 Receptor Allosteric Site(s). *J Med Chem*. 2016;59(1):44-60. doi:10.1021/acs.jmedchem.5b01303

148. Smith E, Collins I. Photoaffinity labeling in target- and binding-site identification. *Future Med Chem*. 2015;7(2):159-183. doi:10.4155/fmc.14.152

149. van der Stelt M, Cals J, Broeders-Josten S, et al. Discovery and Optimization of 1-(4-(Pyridin-2-yl)benzyl)imidazolidine-2,4-dione Derivatives As a Novel Class of Selective Cannabinoid CB2 Receptor Agonists. *J Med Chem*. 2011;54(20):7350-7362. doi:10.1021/jm200916p

150. Mukhopadhyay P, Baggelaar M, Erdelyi K, et al. The novel, orally available and peripherally restricted selective cannabinoid CB 2 receptor agonist LEI-101 prevents cisplatin-induced nephrotoxicity. *Br J Pharmacol*. 2016;173(3):446-458. doi:10.1111/bph.13338

151. Soethoudt M, Hoorens MWH, Doelman W, Martella A, van der Stelt M, Heitman LH. Structure-kinetic relationship studies of cannabinoid CB 2 receptor agonists reveal substituent-specific lipophilic effects on residence time. *Biochem Pharmacol*. 2018;152:129-142. doi:10.1016/j.bcp.2018.03.018

Chapter 2

Structural Basis of Selective Cannabinoid CB_2 Receptor Activation

Published as: Li X, Chang H, Bouma J, et al. Structural basis of selective cannabinoid CB2 receptor activation. Nat Commun. 2023;14(1):1447. doi:10.1038/s41467-023-37112-9

Structural Basis of Selective Cannabinoid CB_2 Receptor Activation

Introduction

Preparations of the plant *Cannabis sativa* have been used for centuries in the treatment of various diseases, including cancer and neuropathic pain.[1] The synthetic version of its psychoactive constituent, Δ^9-tetrahydrocannabinol (THC, Figure 2.1), is in FDA approved drugs Marinol® or Syndros® (dronabinol). The extracted version of THC is one of the active constituents of oromucosal spray Sativex® (nabiximols). These drugs are primarily used for the treatment of chemotherapy-induced nausea, enhancement of appetite in cachexic AIDS-patients, and to alleviate the spasticity and pain associated with multiple scleroses.[2–6] However, THC-based therapies are associated with clinically undesired psychotropic and cardiovascular adverse effects and challenging pharmacokinetic properties due to their high lipophilicity that may limit their therapeutic efficacy.[7–10]

THC exerts its therapeutic effects mostly via the G protein-coupled receptors (GPCRs) cannabinoid CB_1 and CB_2 receptors (CB_1R and CB_2R), which have 68% sequence identity in their seven transmembrane (TM) domains.[11] Both receptors are activated by the endogenous signaling lipids anandamide (AEA) and 2-arachidonoylglycerol (2-AG) (Figure 2.1), the two main endocannabinoids. The CB_1R, which is the most abundantly expressed GPCR in the central nervous system (CNS) is responsible for the psychotropic side effects of THC.[12–14] It plays a role in memory, learning, neurogenesis, neuronal migration, and synaptogenesis. Furthermore, its presence in many organ tissues belies more non-neurological functions.[15] The CB_2R is mainly found on the cells of the immune system and is upregulated under pathophysiological conditions.[16,17] Its activation in general is associated with anti-inflammatory responses in tissue injury of the liver, heart, kidney, colon, and brain as determined in various preclinical models.[18–22] Based on preclinical studies it is thought that selective CB_2R agonists may retain and exceed certain therapeutic properties of THC without inducing psychotropic side effects.[23]

Various academic and industrial groups have developed selective CB_2R ligands.[24] HU308 (Figure 2.1) was the first selective CB_2R agonist to be reported that displayed anti-inflammatory and analgesic properties in mouse models without inducing CNS-side effects.[18] However, poor physico-chemical properties (*e.g.* low solubility, high lipophilicity) of HU308, which has a calculated logarithm of octanol-water partition coefficient (cLogP) of 8.0[25], and its analogs prevented the successful clinical translation of this class of cannabinoid-based drugs.

A next generation of CB_2R ligands was developed with improved drug-like properties. For instance, Olorinab® (APD371, Figure 2.1) is the most polar CB_2R agonist reported to date with a cLogP of -0.4.[26] A phase 2a small-scale safety and tolerability trial in 14 patients with chronic abdominal pain associated with Crohn's disease showed mild-to-moderate adverse events and an improvement in abdominal pain scores.[27] Pyridinylbenzylimidazolidine-2,4-dione derivatives were previously disclosed as selective CB_2R agonists and their affinity studied, along with target binding kinetics and potency as a function of their lipophilicity, which resulted in the discovery of the orally available and peripherally restricted selective CB_2R agonist LEI-101 (Figure 2.1).[28–30] It is intriguing that the CB_2R binding pocket tolerates a wide array of ligands with very different scaffolds and hydrophobicity. For example, HU308 has a 2-billion-fold higher lipophilicity than APD371. Despite the tremendous progress in the field of CB_2R drug discovery, there is still a poor molecular understanding on how these CB_2R agonists selectively activate CB_2R over CB_1R.

Recently, three-dimensional structures of the CB_1R and CB_2R have been elucidated in both the active and inactive states by crystallography or cryo-electron microscopy (cryo-EM) and the binding modes of

diverse ligands and their activation mechanism were reported.[31–35] Remarkably, those structures revealed that CB_1R and CB_2R possess a highly similar, lipophilic orthosteric agonist binding pocket, which makes it challenging to explain the selective activation of CB_2R. To date, no structural studies with selective CB_2R agonists have been reported that could aid in understanding the molecular basis of CB_2R selectivity.

Here, LEI-102 is introduced as a novel, potent and selective CB_2R agonist with excellent physico-chemical and biological properties. LEI-102 was used in conjunction with CB_2R selective agonists APD371 and HU308, and non-selective agonist CP-55,940 to investigate the activation mechanism of CB_2R. This study combined ligand-target binding kinetics, site-directed mutagenesis, and cryo-EM methods. It was found that CB_2R has a distinct activation mechanism compared to CB_1R. Additionally, the physico-chemical properties of the ligands was found to influence their entry pathway into the receptor. Highly lipophilic ligands, such as HU308 and the endocannabinoids, may reach the binding pocket through the membrane, whereas more polar ligands, such as LEI-102, APD371 and CP-55,940, enter the receptor via an alternative route. Furthermore, it was shown that the favorable physico-chemical properties of LEI-102 and CB_2R selectivity underscore its promising *in vivo* efficacy via oral administration in a chemotherapy-induced nephropathy model without inducing CNS-mediated side effects. Together, these studies enhance the current insights of how certain physico-chemical properties of ligands translate to *in vivo* activity and changes their engagement to GPCRs.

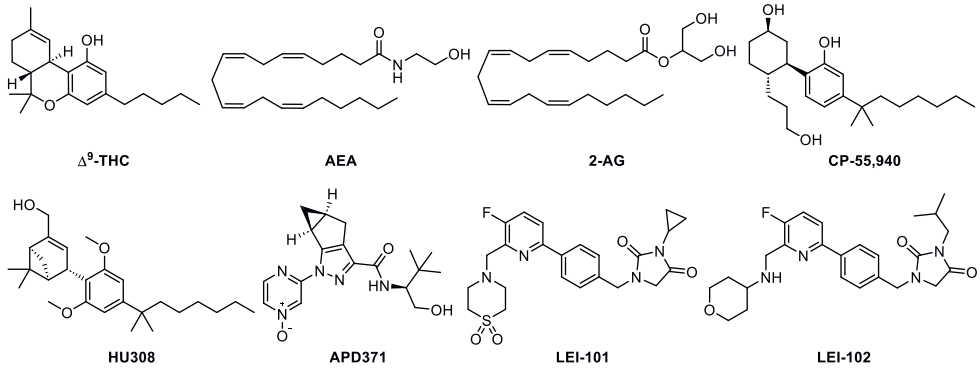

Figure 2.1 The chemical structures of the main constituent of Cannabis sativa Δ^9-tetrahydrocannabinol (THC), and the two major endocannabinoids anandamide (AEA) and 2-arachidonoylglycerol (2-AG), as well as of non-selective CBR agonist CP-55,940 and CB_2R agonists HU308, APD371, LEI-101 and LEI-102.

Results

LEI-102 as a high affinity and potent CB_2R--selective agonist

To obtain a novel CB_2R agonist with beneficial physico-chemical properties, LEI-102, a pyridinylbenzylimidazolidine-2,4-dione derivative, was designed and synthesized (Scheme 2.1). LEI-102 combined an isobutyl substituent on the imidazolidine with an aminotetrahydropyran to replace the cyclopropyl and thiomorpholine 1,1-dioxide in LEI-101, respectively.[30]

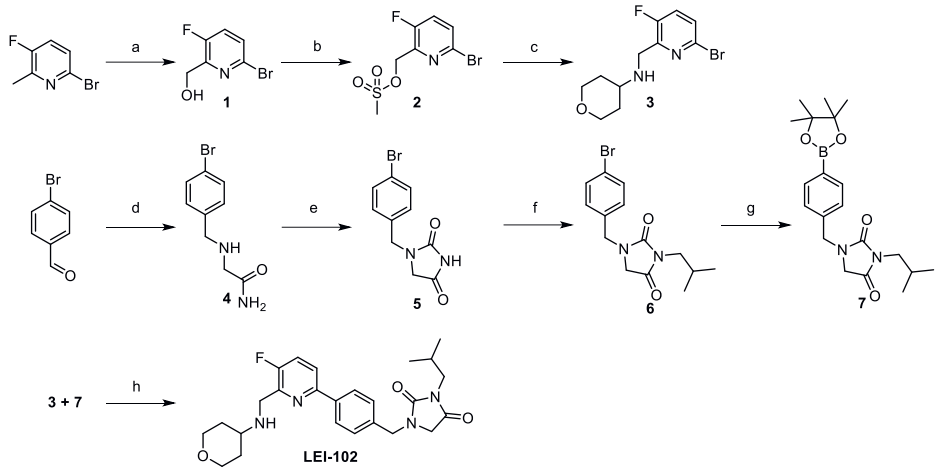

Scheme 2.1 Synthetic route of LEI-102. Reagents and conditions: a) Step 1: *m*-CPBA (1.8 eq), 0 °C-RT, DCM, 4 days; Step 2: TFAA (2.2 eq), 55 °C, 3 h; Step 3: K_2CO_3 (2.4 eq), THF:MeOH (20:1), 17 h, 35% (three steps); b) Et_3N (2.3 eq), MsCl (1.7 eq), THF, 0 °C-RT, 1 h, 75%; c) K_2CO_3 (2.2 eq), tetrahydro-2H-pyran-4-amine (1.3 eq), ACN, 50 °C, 3 h, 67%; d) Step 1: 2-aminoacetamide hydrochloride (1.0 eq), NaOH (1.1 eq), MeOH:H_2O (5:1), RT, 18 h; Step 2: $NaBH_4$ (2.1 eq), 18 h, 91% (two steps); e) CDI (2.1 eq), DMAP (2.1 eq), ACN, 60 °C, 70 h, 37%; f) K_2CO_3 (3.0 eq), 1-bromo-2-methylpropane (2.0 eq), DMF, RT, 20 h, 88%; g) KOAc (4.4 eq), bis(pinacolato)diboron (1.5 eq), Pd(dppf)Cl_2 (0.06 eq), DMF, 75 °C, 20 h; h) **3** (1.0 eq), **7** (1.5 eq), K_2CO_3 (6.0 eq), $Pd(PPh_3)_4$ (0.1 eq), toluene:EtOH (4:1), 75 °C, 18 h, 45% (two steps).

LEI-102 has a cLogP of 2.1 as calculated by ChemDraw 19.0 (Table 2.1). The inhibitory constant (pK_i), potency (pEC_{50}) and intrinsic activity (E_{max}) of LEI-102 were determined in [^{3}H]-RO6957022 displacement assays on stably expressing CB_2R membranes and [^{35}S]GTPγS G protein activation assays using HEK293T membranes transiently expressing recombinant hCB_2R or hCB_1R, respectively (Table 2.2). APD371, HU308, CP-55,940 and the endocannabinoids AEA and 2-AG were also explored. LEI-102 had a high binding affinity for CB_2R (pKi = 8.0 ± 0.1) and was more potent than the selective CB_2R agonists APD371 and HU308. LEI-102 did not bind CB_1R, thereby showing at least 1000-fold selectivity (Table 2.5). In G protein activation assays, LEI-102 activated the receptor as a partial agonist (E_{max} 76 ± 1 %) with a pEC_{50} value of 6.9 ± 0.2 (Table 2.2).

Table 2.1 Physico-chemical properties of the investigated ligands.

Compound	CLogP	SLogP	TPSA (Å)	MW (g/mol)	Num RotatableBonds	NumHBD	NumHBA
Δ^9-THC	7.24	5.74	29.5	314.5	4	1	2
2-AG	6.89	5.03	66.8	378.6	17	2	4
AEA	6.18	5.24	49.3	347.5	16	2	2
CP-55,940	5.82	5.66	60.7	376.6	10	3	3
HU308	8.00	6.63	38.7	414.6	10	1	3
APD371	-0.35	0.70	107.0	357.4	4	2	6
LEI-102	2.07	3.58	74.8	454.5	8	1	5
LEI-101[30]	0.89	-	90.4	472.5	6	0	6

All values calculated using RDKit KNIME nodes version 4.5.0.v202207051536, apart from CLogP which was calculated using ChemDraw 19.0. For LEI-101 all values were calculated with Chemdraw 22.2.0.

Table 2.2 Functional Activity, Affinity and Kinetic Parameters of Synthetic Agonists and Endocannabinoids on hCB_2R.

Compound	pEC_{50}[a]	E_{max} (%)[b]	pK_i (K_i, nM)[c]	k_{on} ($M^{-1}s^{-1}$)[d]	ET (s)[e]	k_{off} (s^{-1})[f]	RTD (min)[g]	K_D (nM)[h]
LEI-101[30,i]	6.6 ± 0.2	65 ± 8	6.51 ± 0.1 (309.0)	$(3.0 \pm 1.1) \times 10^4$	33.3 ± 8.91	$(2.1 \pm 0.5) \times 10^{-3}$	8.8 ± 1.6	76 ± 10
LEI-102	6.9 ± 0.2	76 ± 1	8.0 ± 0.1 (9.7)	$(6.3 \pm 1.1) \times 10^4$	16.0 ± 2.82	$(1.0 \pm 0.2) \times 10^{-3}$	16 ± 3.3	16.5
APD371	7.9 ± 0.1	134 ± 12	7.5 ± 0.1 (35.3)	$(2.5 \pm 0.4) \times 10^4$	40.1 ± 5.90	$(3.7 \pm 0.5) \times 10^{-4}$	45 ± 6.6	14.9
HU308	7.1 ± 0.2	91 ± 8	7.0 ± 0.1 (92.4)	$(7.0 \pm 2.3) \times 10^3$	143 ± 47.9	$(2.3 \pm 0.4) \times 10^{-4}$	71 ± 11	33.7
CP-55,940	8.5 ± 0.3	98 ± 4	8.9 ± 0.1 (1.4)	$(1.8 \pm 0.4) \times 10^6$	0.57 ± 0.13	$(5.2 \pm 0.9) \times 10^{-4}$	32 ± 5.5	0.3
AEA	6.3 ± 0.2	60 ± 5	6.3 ± 0.1 (484.5)	$(6.6 \pm 0.5) \times 10^3$	152 ± 10.4	$(2.4 \pm 0.1) \times 10^{-3}$	6.8 ± 0.4	371.7
2-AG	5.9 ± 0.1	93 ± 22	7.0 ± 0.1 (97.3)	$(5.3 \pm 1.0) \times 10^4$	18.8 ± 3.61	$(2.3 \pm 0.3) \times 10^{-3}$	7.4 ± 1.0	42.7

[a, b] Potency (pEC_{50}) and efficacy (E_{max}) values were obtained from [^{35}S]GTPγS assays on HEK293T membranes transiently expressing CB_2R WT. The percentage maximum effect (E_{max} in %) was calculated compared to CP-55,940. [c, d, f] Binding affinities (pK_i), association (k_{on}) and dissociation (k_{off}) rate constants were determined in [^{3}H]-RO6957022 binding assays on CHOK1_hCB_2R_bgal membranes at 10 °C. [e] Engagement time (ET) of the compound to the receptor at 1 μM agonist was determined by $ET = 1/(k_{on} \cdot 1 \times 10^{-6})$ and is expressed in seconds (s), whereas k_{on} is expressed in $M^{-1}s^{-1}$. [g] Residence time (RTD) was determined by $RTD = 1/(60 \cdot k_{off})$ and is expressed in min, whereas k_{off} is expressed in s^{-1}. [h] Kinetic K_D values, defined by $K_D = k_{off}/k_{on}$. Values represent the mean ± SEM of at least three independent experiments performed in duplicate. [i]LEI-101 data was obtained from literature and values were measured on CHO_K1_hCB_2R_bgal membranes.

Distinct target binding kinetic profiles of CB_2R agonists

For the quantification of the ligand-target binding kinetic parameters of the agonists, displacement and competition association assays with [^{3}H]-RO6957022 were performed on CHO membranes stably over-expressing hCB_2R_bgal (Table 2.1). The equilibrium K_i and kinetic K_D values were well correlated, validating the competition association assay. The determined dissociation rate constants (k_{off}) of all agonists was converted into Residence Time Distribution (RTD). LEI-102 had an RTD of 16 min, which was around half that of APD371 (45 min) and CP-55,940 (32 min), whereas HU308 had the longest RTD at the receptor of 71 min (Table 2.1). Endocannabinoids 2-AG and AEA had the shortest RTD, both approximately 7 min. The association rate constants (k_{on}) varied greatly between the different agonists, ranking from fast to slow engagement CP-55,940 > LEI-102 > 2-AG > APD371 > HU308 = AEA. The calculated engagement time (ET) to CB_2 at 1 µM of each agonist further emphasized that CP-55,940 arrived at CB_2R within one second, whereas APD371, LEI-102 and 2-AG needed between 16 and 40 s to reach the CB_2R binding site. Interestingly, HU308 and AEA took 143 and 152 s to bind CB_2R, respectively. Due to the distinct target-binding kinetic profiles found for the four synthetic CB_2R agonists the choice was made to elucidate their binding poses in CB_2R with cryo-EM.

Overall similar structural comparison of CB_2R-G_i in complex with different agonists

To obtain the stable complex sample of CB_2R-G_i bound with LEI-102, APD371, HU308, or CP-55,940, a similar procedure was used as for the complex preparation previously described for AM12033-CB_2R-G_i (PDB: 6KPF). Single particle analysis of the cryo-EM samples yielded a normal global map for CB_2R-LEI-102-G_i-scFv16, CB_2R-APD371-G_i-scFv16, CB_2R-HU308-G_i-scFv16 and CB_2R-CP-55,940-G_i-scFv16, complex, at 2.9 Å, 3.0 Å, 3.0 Å and 2.9 Å, respectively (Figure 2.2). The ligand, receptor and G protein in the isolated complex were clearly visible in the cryo-EM maps (Figure 2.2). The overall structures of the four complexes were comparable, with root mean square deviation (RMSD) of the Cα atoms of the receptors are around 0.35 Å. The ligand binding interfaces of the four CB_2R and G_i complexes were similar to each other, and to those of the previous AM12033-CB_2R-G_i or WIN55212-2-CB_2R-G_i complex structures.

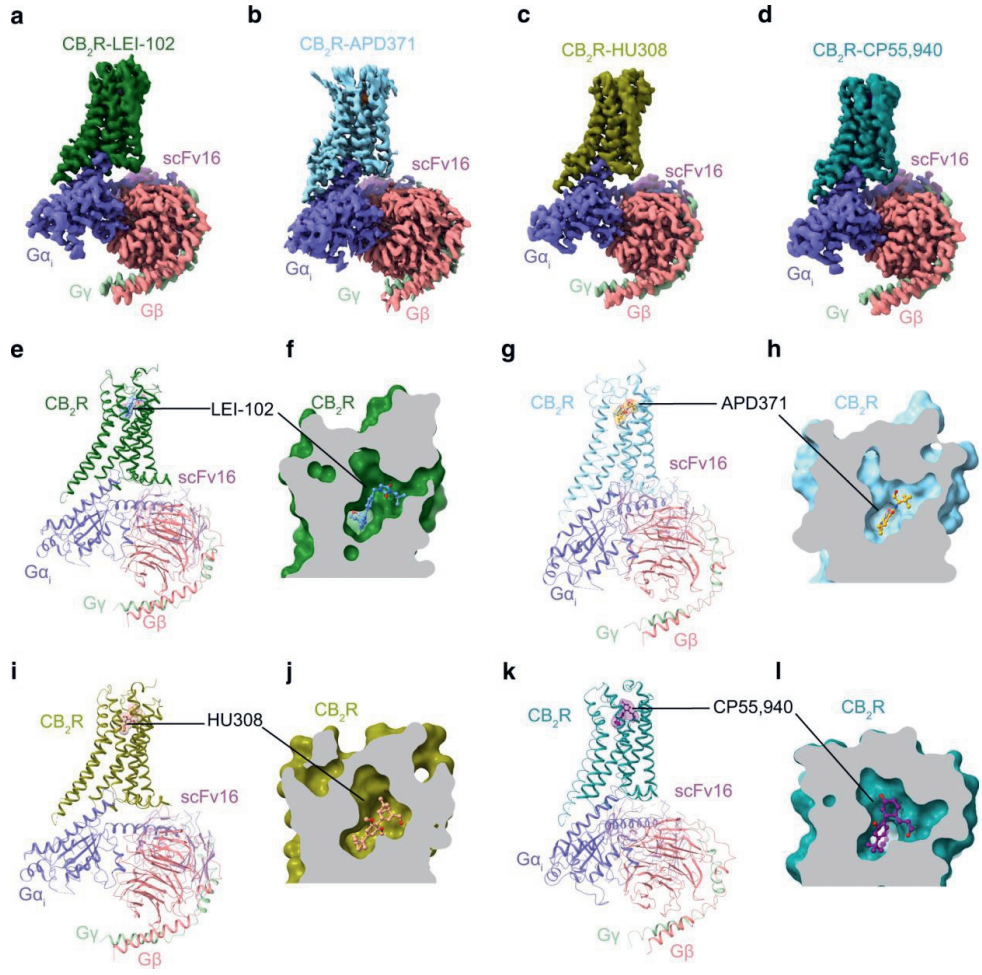

Figure 2.2 Cryo-EM structures of CB_2R-G_i complexes (A-D) Cryo-EM density maps of (A) LEI-102 (Dark green), (B) APD371 (Sky blue), (C) HU308 (Olive) and (D) CP-55,940 (Teal) bound CB_2R in complex with $G_{\alpha i}$ (Slate), Gβ (Salmon), Gγ (Pale green), scFv16 (Violet purple). (E-L) Overall structures of CB_2R-G_i complexes and enlarged view of orthosteric pocket of (F) LEI-102, (H) APD371, (J) HU308 and (L) CP-55,940 using the same color codes as (A-D), with agonists shown as Cornflower blue (LEI-102), Orange (APD371), Dark salmon (HU308) and Purple (CP-55,940) sticks, respectively.

The binding mode of LEI-102 in CB_2R

A clear electron density in the orthosteric ligand binding pocket in the LEI-102-CB_2R-G_i complex resulted in the unambiguously defined binding pose of LEI-102. LEI-102 predominantly interacted with the residues in the binding pocket via hydrophobic interactions (Figure 2.3A). The isobutyl substituent of LEI-102 showed interactions with residues $S90^{2.60}$ (Ballesteros-Weinstein numbering in superscript), $F106^{3.25}$, $K109^{3.28}$, and $I110^{3.29}$ in CB_2R. The imidazolidine-2,4-dione forms π-π interaction with $F94^{2.64}$ and showed further hydrophobic interactions with $F106^{3.25}$ and $P184^{ECL2}$. The benzyl formed an aromatic interaction with $F183^{ECL2}$, and hydrophobic interactions with $F87^{2.57}$ and $S285^{7.39}$. The phenyl ring in the core of LEI-102 formed a cation π interaction with $F183^{ECL2}$ and T-shaped π-π interaction with $F281^{7.35}$. The pyridine had hydrophobic contacts with $F117^{3.36}$ and $W258^{6.48}$. The aminotetrahydropyran sidechain protruded into the long channel and formed hydrophobic interactions with residues $I110^{3.29}$,

$T114^{3.33}$, $I186^{ECL2}$, $Y190^{5.39}$, $L191^{5.40}$, $W194^{5.43}$ and $M265^{6.55}$. Additionally, a hydrogen bond was formed with $T114^{3.33}$ (Figure 2.3A).

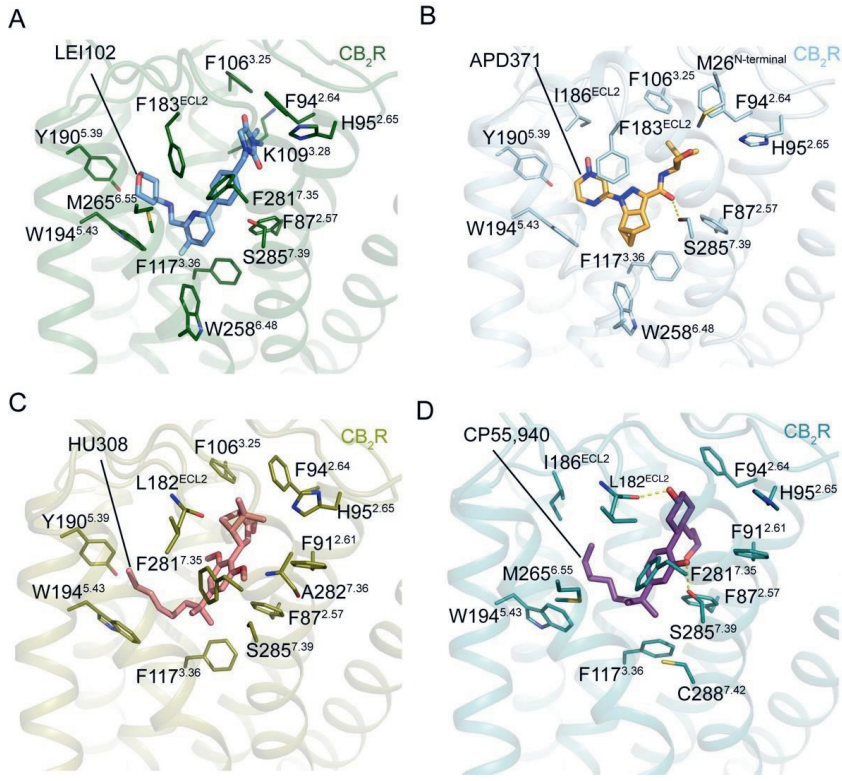

Figure 2.3 Key interactions between CB_2R structure and agonists (A-D) Key residues involved in (A) LEI-102 (cornflower blue) with CB_2R-G_i (dark green), (B) APD371 (orange) with CB_2R-G_i (sky blue), (C) HU308 (dark salmon) with CB_2R-G_i (olive) and (D) CP-55,940 (purple) with CB_2R-G_i (teal) binding in the complex structures. The amino acids involved interactions are showing sticks, hydrogen bonds are highlighted with yellow dashed lines.

The binding mode of APD371 in CB_2R

APD371 mainly formed hydrophobic and aromatic interactions with residues from ECL2, TM2, TM3, TM5, TM6 and TM7 (Figure 2.3B). The carbonyl group of APD371 formed a putative hydrogen bond with $S285^{7.39}$ and a hydrophobic interaction with $F87^{2.57}$. The pyrazole and pyrazine cores of APD371 formed aromatic interaction with $F183^{ECL2}$. Furthermore, the pyrazine core formed hydrophobic contacts with $T114^{3.33}$, $I186^{ECL2}$, $L191^{5.40}$ and $W194^{5.43}$. The (*S*)-1-hydroxy-3,3-dimethylbutyl head formed hydrophobic contacts with residues $M26^{N\text{-terminus}}$, $S90^{2.60}$, $F94^{2.64}$, $F106^{3.25}$, $I110^{3.29}$ and $V113^{3.32}$. The cyclopropyl group formed hydrophobic contacts with $F117^{3.36}$, $W194^{5.43}$, $W258^{6.48}$ and $V261^{6.51}$.

The binding mode of HU308 in CB_2R

The interactions between HU308 and CB_2R were hydrophobic, including residues from ECL2, TM2, TM3, TM5, TM6 and TM7 (Figure 2.3C). The phenyl of 2,6-dimethoxyphenyl core formed hydrophobic interactions with $F87^{2.57}$, $F183^{ECL2}$ and $S285^{7.39}$, the C2-methoxy formed hydrophobic contacts with $A282^{7.36}$ and $S285^{7.39}$, and the C6-methoxy formed hydrophobic contacts with $I110^{3.29}$, $V113^{3.32}$ and $T114^{3.33}$, respectively. The dimethylheptyl chain of HU308 extended into the long channel and formed hydrophobic interactions with residues from ECL2 ($F183^{ECL2}$), TM3 ($T114^{3.33}$, $F117^{3.36}$), TM5 ($W194^{5.43}$). The 1,1-dimethyl formed hydrophobic interactions with residues $F87^{2.57}$, $F117^{3.36}$, $F281^{7.35}$ and $S285^{7.39}$.

The bicyclic head of HU308 formed hydrophobic interactions with M26$^{N\text{-terminus}}$, F106$^{3.25}$, I110$^{3.29}$, S90$^{2.60}$, F94$^{2.64}$, P184^{ECL2} and the 2-methanol formed a hydrophobic interaction with F94$^{2.64}$.

The binding mode of CP-55,940 in CB_2R

CP-55,940 adopted an L-shape conformation in the orthosteric binding pocket (Figure 2.3D). The cyclohexanol group formed hydrophobic interactions with F94$^{2.64}$, L182^{ECL2}, F183^{ECL2}, and P184^{ECL2}. The hydroxyl group established a hydrogen bond with L182^{ECL2} and the hydroxypropyl formed hydrophobic contacts with F87$^{2.57}$, S90$^{2.60}$, F91$^{2.61}$, I110$^{3.29}$, and V113$^{3.32}$. The phenol core formed hydrophobic interactions with F87$^{2.57}$, F183^{ECL2}, F281$^{7.35}$ and S285$^{7.39}$, and its hydroxyl additionally formed a hydrogen bond with S285$^{7.39}$. The dimethyl formed hydrophobic interactions with F183^{ECL2}, F281$^{7.35}$, M265$^{6.55}$, F87$^{2.57}$, F117$^{3.36}$ and C288$^{7.42}$. The dimethylheptyl alkyl chain of CP-55,940 extended into the long channel and formed hydrophobic interactions with residues I110$^{3.29}$, F183^{ECL2}, I186^{ECL2}, W194$^{5.43}$, T114$^{3.33}$ and F117$^{3.36}$.

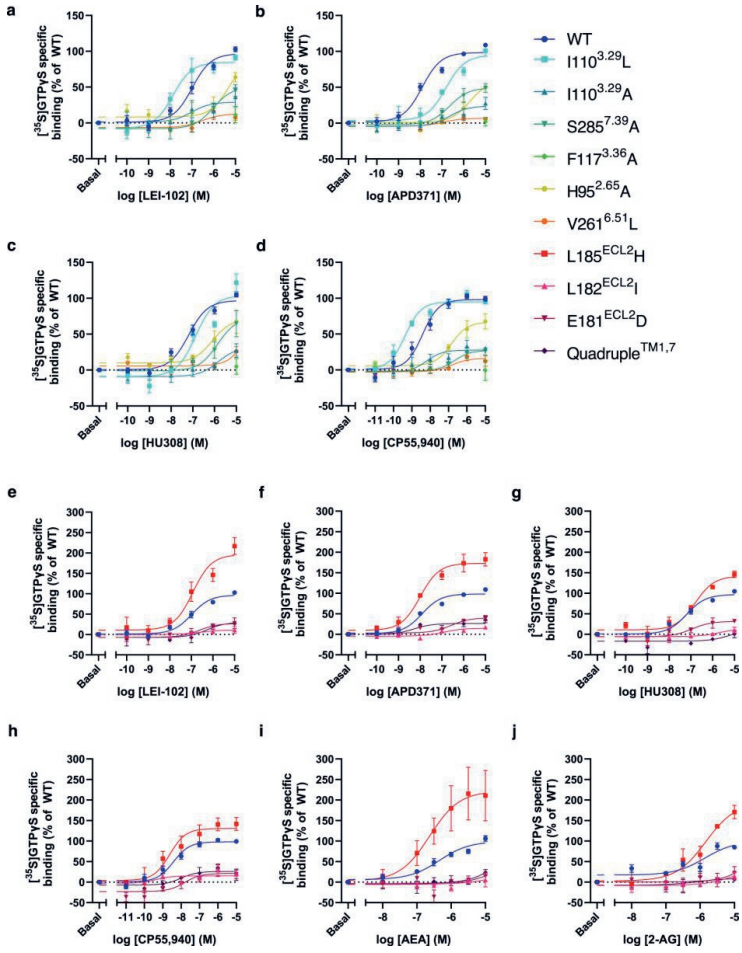

Figure 2.4 Characterization of G Protein activation of wild type (WT) and mutant CB_2R by synthetic agonists and endocannabinoids. (A-D) Dose-response curves for G protein activation of WT and mutants that are located in the CB_2R binding pocket by (A) LEI-102, (B) APD371, (C) HU308 and (D) CP-55,940. (E-J) Dose response curves for G protein activation of WT and mutants that are proposed to be involved in ligand entry of CB_2R via either the ECL2 or membrane access by (E) LEI-102, (F) APD371, (G) HU308, (H) CP-55,940, (I) AEA and (J) 2-AG. (A-J) The maximum activation level of WT CB_2R was set

to 100% while the basal levels were set to 0%. Data are presented as mean ± SEM of at least three individual experiments performed in duplicate.

LEI-102 and APD371 require $H95^{2.65}$ for G protein activation in CB_2R

To study the mechanism of CB_2R activation, five residues in the binding pocket were further characterized based on the complex structures (Figure 2.3). Six CB_2R mutants were created, *i.e.* four residues ($S285^{7.39}$, $H95^{2.65}$, $I110^{3.29}$ and $F117^{3.36}$) were replaced by alanine, as these are conserved between CB_2R and CB_1R, and two others ($I110^{3.29}$, $V261^{6.51}$) were substituted by the CB_1R reciprocal residue leucine. All mutants were sufficiently expressed at the cell surface as determined with an ELISA (Figure 2.5, Table 2.3). To characterize the binding mechanisms of LEI-102, APD371, HU308 and CP-55,940, their responses were investigated by [^{3}H]CP-55,940 displacement and [^{35}S]GTPγS binding assays. Of note, in the [^{3}H]CP-55,940 displacement assay, only the CB_2R-$I110^{3.29}$L mutant showed a sufficient binding window (data not shown). This prevented the affinity determination of the four agonists on other mutant receptors. Five mutant receptors, except CB_2R-$F117^{3.36}$A, were still active in the [^{35}S]GTPγS functional assay for study of the receptor activation mechanism (Figure 2.4A-D, Table 2.4). All four synthetic agonists were unable to activate CB_2R-$F117^{3.36}$A, which indicated an important role of this residue in the activation of CB_2R.

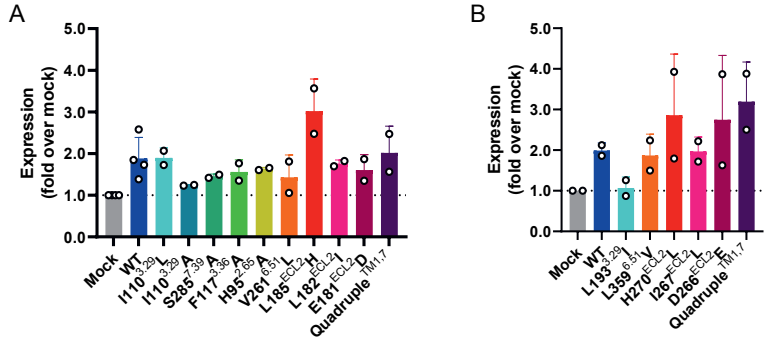

Figure 2.5 Cell Surface Receptor Expression. Receptor expression as determined by ELISA for (A) CB_2R and (B) CB_1R wild type (WT) and mutants. Data are expressed as mean ± SD of at least two experiments performed in quintuplicate.

Table 2.3 Cell surface expression levels of cannabinoid receptor constructs in ELISA.

	CB_2R	Expression (fold over Mock)	CB_1R	Expression (fold over Mock)
	WT	1.9 ± 0.5	WT	2.0 ± 0.2
Binding pocket	$I110^{3.29}L$	1.9 ± 0.2	$L193^{3.29}I$	1.1 ± 0.3
	$I110^{3.29}A$	1.2 ± 0.0	$L193^{3.29}A$	n.d.
	$S285^{7.39}A$	1.5 ± 0.1	$S383^{7.39}A$	n.d.
	$F117^{3.36}A$	1.6 ± 0.3	$F200^{3.36}A$	n.d.
	$H95^{2.65}A$	1.6 ± 0.0	$H178^{2.65}A$	n.d.
	$V261^{6.51}L$	1.4 ± 0.5	$L359^{6.51}V$	1.9 ± 0.5
Ligand entry	$L185^{ECL2}H$	3.0 ± 0.8	$H270^{ECL2}L$	2.9 ± 1.5
	$L182^{ECL2}I$	1.8 ± 0.1	$I267^{ECL2}L$	2.0 ± 0.4
	$E181^{ECL2}D$	1.6 ± 0.4	$D266^{ECL2}E$	2.7 ± 1.6
	$Quadruple^{TM1,7}$	2.0 ± 0.6	$Quadruple^{TM1,7}$	3.2 ± 1.0

Mutations are shown in the numbering of the cannabinoid CB2 (CB2R) or CB1 receptor (CB1R) amino acid sequence as well as the Ballesteros and Weinstein GPCR numbering system. Data are presented as fold over mock (empty pcDNA3.1 vector) and are mean ± SD of at least two individual experiments performed in quintuplicate. n.d. is not determined.

Table 2.4 The Affinity and Potency of the Agonists on the CB_2R mutants.

CB_2R	LEI-102		CP-55,940		HU308		APD371	
Construct	**pK_i**	**pEC_{50}**	**pK_i**	**pEC_{50}**	**pK_i**	**pEC_{50}**	**pK_i**	**pEC_{50}**
WT	7.5 ± 0.1	6.9 ± 0.2	9.2 ± 0.2	8.5 ± 0.3	7.8 ± 0.2	7.1 ± 0.2	8.0 ± 0.0	7.9 ± 0.1
$I110^{3.29}L$	7.9 ± 0.0	7.8 ± 0.1**	9.1 ± 0.1	9.4 ± 0.2	7.3 ± 0.1	6.7 ± 0.4	7.1 ± 0.0***	6.7 ± 0.3
$I110^{3.29}A$	n.d.	7.0 ± 0.6	n.d.	8.7 ± 0.4	n.d.	6.4 ± 0.5	n.d.	6.6 ± 0.6
$S285^{7.39}A$	n.d.	6.3 ± 0.3	n.d.	6.7 ± 0.1**	n.d.	5.9 ± 0.1***	n.d.	6.5 ± 0.3
$F117^{3.36}A$	n.d.	n.d.	n.d.	n.d.	n.d.	n.d.	n.d.	n.d.
$H95^{2.65}A$	n.d.	<5	n.d.	6.9 ± 0.2**	n.d.	6.6 ± 0.6	n.d.	5.7 ± 0.2**
$V261^{6.51}L$	n.d.	6.4 ± 0.0	n.d.	<5	n.d.	<5	n.d.	6.9 ± 0.2*
$L185^{ECL2}H$	7.3 ± 0.1	6.9 ± 0.1	9.4 ± 0.1	8.9 ± 0.4	7.2 ± 0.0	6.8 ± 0.2	7.7 ± 0.1	8.0 ± 0.1
$L182^{ECL2}I$	n.d.	7.4 ± 0.8	n.d.	8.8 ± 0.8	n.d.	<5	n.d.	6.6 ± 0.4
$E181^{ECL2}D$	n.d.	6.9 ± 0.6	n.d.	7.9 ± 0.5	n.d.	7.0 ± 0.7	n.d.	6.9 ± 0.6
$Quadruple^{TM1,7}$	6.8 ± 0.2	6.2 ± 0.2	9.2 ± 0.1	8.1 ± 0.2	7.1 ± 0.4	n.d.	6.7 ± 0.3	8.4 ± 0.1

Mutants that gave no dpm window could not have their potency determined (n.d. not determined). Mutations are shown in the numbering of the cannabinoid receptor 2 amino acid sequence as well as the Ballesteros and Weinstein GPCR numbering system. pEC_{50} <5 was reported when the curve fit was not finished. Values are presented as the mean ± SEM of at least three independent experiments performed in duplicate. One-way Welch ANOVA with Dunnett's T3 posthoc test or Welch's t-test was used to analyze differences in pEC_{50} and E_{max} values compared to WT (*p < 0.05, ** p < 0.01, *** p < 0.001).

Table 2.5 The Affinity and Potency of the Agonists on the CB_1R mutants.

CB_1R	LEI-102		CP-55,940		HU308		APD371	
Construct	**Displacement (%)**	**Potency (fold over basal)**	**pK_i**	**Potency (fold over basal)**	**Displacement (%)**	**Potency (fold over basal)**	**Displacement (%)**	**Potency (fold over basal)**
WT	6 ± 7	1.0 ± 0.1	8.2 ± 0.0	1.2 ± 0.1	17 ± 7	0.8 ± 0.0	-19 ± 17	1.0 ± 0.0
$L359^{6.51}V$	41 ± 10	1.1 ± 0.1	8.3 ± 0.1	1.4 ± 0.2	25 ± 6	0.9 ± 0.1	18 ± 9	1.1 ± 0.1
$H270^{ECL2}L$	46 ± 3	1.2 ± 0.0	8.3 ± 0.1	1.6 ± 0.1	47 ± 5	1.2 ± 0.1*	8 ± 3	1.1 ± 0.0
$I267^{ECL2}L$	-7 ± 19	1.0 ± 0.0	8.4 ± 0.1	1.0 ± 0.0	25 ± 3	0.8 ± 0.0	-24 ± 17	0.9 ± 0.0
$D266^{ECL2}E$	34 ± 5	1.1 ± 0.1	8.4 ± 0.1	1.4 ± 0.1	38 ± 10	0.8 ± 0.1	12 ± 7	0.9 ± 0.1
$Quadruple^{TM1,7}$	-13 ± 22	1.2 ± 0.1	8.0 ± 0.2	1.8 ± 0.1*	26 ± 10	0.9 ± 0.0	0 ± 25	1.1 ± 0.0

Affinity is expressed as pK_i for CP-55,940, but as displacement (receptor occupancy by agonist at 10 μM) for the CB_2R-selective agonists. The Potency is displayed as fold over basal (with basal the endogenous activity of the mutant). Mutations are shown in the numbering of the cannabinoid receptor 2 amino acid sequence as well as the Ballesteros and Weinstein GPCR numbering system. pEC_{50} <5 was reported when the curve fit was not finished. Values are presented as the mean ± SEM of at least three independent experiments performed in duplicate. One-way Welch ANOVA with Dunnett's T3 posthoc test or Welch's t-test was used to analyze differences in pEC_{50} and E_{max} values compared to WT (*p < 0.05, ** p < 0.01).

The potency of LEI-102 was significantly increased at the CB_2R-$I110^{3.29}L$ mutant to a pEC_{50} value of 7.8 ± 0.1 in the G protein activation assay, while the binding affinity remained similar to wild type (WT) receptor (Figure 2.4A, Table 2.4). Three mutations CB_2R-$I110^{3.29}A$, CB_2R-$S285^{7.39}A$ and CB_2R-$V261^{6.51}L$ had no significant effect on the potency of LEI-102 in the functional assay. In contrast, the potency on mutant receptor CB_2R-$H95^{2.65}A$ was significantly reduced for LEI-102. No gain in binding affinity for the swap mutant in CB_1R-$L359^{6.51}V$ was found with LEI-102 (Table 2.5).

APD371 acted as a full CB_2R agonist with a pEC_{50} value of 7.9 ± 0.1 and a higher maximal activation compared to that of CP-55,940 in the functional assay (Table 2.2). Mutant receptor CB_2R-$I110^{3.29}L$ did not affect the G protein response of APD371 (Figure 2.4B, Table 2.4), while the binding affinity was significantly reduced to a pK_i of 7.1 ± 0.0 (Table 2.4). APD371 potency was not affected by mutant receptors CB_2R-$I110^{3.29}A$ or CB_2R-$S285^{7.39}A$. The responses of APD371 for CB_2R-$H95^{2.65}A$ and CB_2R-$V261^{6.51}L$ were significantly impacted with 158-fold and 10-fold drop in potency, respectively (Table 2.4).

It is apparent that CB_2R-$H95^{2.65}$ has a crucial role in G protein activation of CB_2R by LEI-102 and APD371. Additionally, LEI-102 activation was increased for the CB_2R-$I110^{3.29}L$ mutant, while APD371 activation relied on CB_2R-$V261^{6.51}$.

An important role for $S285^{7.39}$ and $V261^{6.51}$ in CB_2R activation by HU308 and CP-55,940

The potency and affinity of HU308 on CB_2R were not affected by the CB_2R-$I110^{3.29}L$ swap mutant (Figure 2.4C, Table 2.4). In addition, activation of mutant receptors CB_2R-$I110^{3.29}A$ and CB_2R-$H95^{2.65}A$ by HU308 was not affected with pEC_{50} values of 6.4 ± 0.5 and 6.6 ± 0.6, respectively. The maximum activation level of mutant receptor CB_2R-$S285^{7.39}A$ was unaffected compared to WT receptor, but a significant 15-fold loss in potency was observed. Lastly, CB_2R-$V261^{6.51}L$ had a significant loss of potency, *i.e.* more than 120-fold lower (Figure 2.4C, Table 2.4).

Similar to HU308, the potency of CP-55,940 on CB_2R was not affected by the CB_2R-$I110^{3.29}$ mutations compared to WT in the G protein activation assay, nor was its binding affinity for CB_2R-$I110^{3.29}L$ (Figure 2.4D, Table 2.4). In response to CP-55,940, mutant receptors CB_2R-$S285^{7.39}A$ and CB_2R-$V261^{6.51}L$ were significantly affected with decreased pEC_{50} values of 6.7 ± 0.1 and <5, respectively. Moreover, the potency of CP-55,940 was significantly affected on the CB_2R-$H95^{2.65}A$ with a 40-fold decrease compared to WT receptor (Figure 2.4D, Table 2.4). No gain in potency or affinity was observed for the swap mutant CB_1R-$L359^{6.51}V$ for either HU308 or CP-55,940 (Table 2.5).

Taken together, this showed that CB_2R-$S285^{7.39}$ and CB_2R-$V261^{6.51}$ were crucial for HU308 and CP-55,940 to activate the G protein at CB_2R, where CP-55,940 additionally required an interaction with CB_2R-$H95^{2.65}$.

Table 2.6 The Affinity and Potency of the Endocannabinoids on both CB_2R and CB_1R.

		AEA		2-AG	
CB_2R	**Construct**	**pK_i**	**pEC_{50}**	**pK_i**	**pEC_{50}**
	WT	6.2 ± 0.1	6.3 ± 0.2	5.8 ± 0.1	5.9 ± 0.1
	$L185^{ECL2}H$	6.3 ± 0.1	6.6 ± 0.0	6.4 ± 0.2	5.9 ± 0.2
	$L182^{ECL2}I$	n.d.	<5	n.d.	<5
	$E181^{ECL2}D$	n.d.	<5	n.d.	<5
	$Quadruple^{TM1,7}$	5.6 ± 0.3	<5	<5	<5

CB_1R	**Construct**	**pK_i**	**Potency (fold over basal)**	**pK_i**	**Potency (fold over basal)**
	WT	6.2 ± 0.1	1.2 ± 0.1	5.4 ± 0.2	1.3 ± 0.1

H270^{ECL2}L	6.1 ± 0.0	1.4 ± 0.1	5.0 ± 0.4	1.5 ± 0.1
I267^{ECL2}L	6.2 ± 0.1	1.0 ± 0.1	5.9 ± 0.2	1.1 ± 0.0
D266^{ECL2}E	6.4 ± 0.1	1.3 ± 0.1	5.7 ± 0.1	1.5 ± 0.2
Quadruple^{TM1,7}	6.3 ± 0.0	1.6 ± 0.1	5.2 ± 0.0	1.8 ± 0.1*

pEC_{50} <5 was reported when the curve fit was not finished. Values are presented as the mean ± SEM of at least three independent experiments performed in duplicate. One-way Welch ANOVA with Dunnett's T3 posthoc test or Welch's t-test was used to analyze differences in pEC_{50} and E_{max} values compared to WT (*p < 0.05, ** p < 0.01). n.d. not determined.

HU308 and endocannabinoids gain access via membrane entry

The ligand-target binding kinetics (Table 2.2) revealed that the highly lipophilic HU308 and anandamide had a very slow on-rate compared to the other ligands. It has been postulated that ligands of lipid receptors may gain access to the binding pocket via a membrane channel. Both potential ligand entry pathways, *i.e.* either via ECL2 or via a membrane channel between TM1 and TM7, were examined. To this end, four additional mutant receptors were created. Three residues in the ECL2 of CB_2R, which were different from CB_1R, were mutated towards the reciprocal CB_1R residues, i.e. CB_2R-L185^{ECL2}H, CB_2R-L182^{ECL2}I and CB_2R-E181^{ECL2}D. In the fourth mutant receptor, four residues in TM1 and TM7 that align the potential membrane channel in CB_2R were mutated to the reciprocal CB_1R residues and combined as a quadruple mutant, i.e. CB_2R-K279$^{7.33}$T, CB_2R-K33$^{1.32}$Q, CB_2R-V36$^{1.35}$I and CB_2R-C40$^{1.39}$S (termed "CB_2R-Quadruple^{TM1,7}"). Next, all four synthetic agonists and the two endocannabinoids were tested on these four CB_2R mutant receptors in [^{3}H]CP-55,940 and [^{35}S]GTPγS assays. Only CB_2R-L185^{ECL2}H and CB_2R-Quadruple^{TM1,7} were evaluated in the [^{3}H]CP-55,940 displacement assays due to insufficient binding window for the other two mutant receptors (data not shown). The binding affinities of the agonists were not affected for mutant receptors CB_2R-L185^{ECL2}H and CB_2R-Quadruple^{TM1,7} (Table 2.6. Interestingly, the potencies of LEI-102, APD371 and CP-55,940 in the functional assay were not significantly affected for any of the mutant receptors, whereas HU308 and the endocannabinoids were less potent on CB_2R-L182^{ECL2}I (Figure 2.4E-J, Tables 2.4 and 2.6). Additionally, the endocannabinoids showed a decreased potency on CB_2R-L181^{ECL2}D, but not on CB_2R-L185^{ECL2}H. Of note, HU308 and both endocannabinoids completely lost their ability to activate CB_2R in the CB_2R-Quadruple^{TM1,7} mutant, suggesting that this may be an important access point to the receptor binding pocket for these agonists (Figure 2.4G, I-J).

Discussion

Currently, several crystal and cryo-EM CBR structures have been resolved in which non-selective agonists adopt a nearly identical binding position in the orthosteric pocket, regardless of the receptor.[34–38] The results of the site-directed mutagenesis, ligand-target binding kinetics and cryo-EM studies were used to generate a better understanding of the binding and activation mechanism of CB_2R-selective agonists.

F117$^{3.36}$ has an important role in CB_2R activation that does not mimic F200$^{3.36}$ in CB_1R

The data revealed a crucial role for CB_2R-F117$^{3.36}$ as replacement by alanine resulted in a complete loss of G protein activation by all tested agonists (Figure 2.4A-D, Table 2.4). It has been shown that the CB_1R counterpart F200$^{3.36}$ plays an important regulatory role in activation as part of the "twin toggle switch" with CB_1R-W356$^{6.48}$.[39] In contrast, CB_2R-W258$^{6.48}$ has been described to be solely responsible for activation as a toggle switch without the help of CB_2R-F117$^{3.36}$ in structural studies, since the conformation of CB_2R-F117$^{3.36}$ in agonist-bound structures is comparable to the conformation in the antagonist-bound CB_2R structure as well as the CB_1R agonist-bound structures.[33,36] The mutational data supports this hypothesis, as the constitutive activity pattern observed by McAllister *et al.* for the reciprocal CB_1R-F200$^{3.36}$A, is not observed here. This excludes CB_2R-F117$^{3.36}$ from having a suppressive

function.[39] Together, this data provides strong support for a different, but important, role for F117$^{3.36}$ in CB_2R activation.

Potential polar network of H95$^{2.65}$ and S285$^{7.39}$ in CB_2R

In CB_1R, water-mediated interactions between CB_1R-H178$^{2.65}$, CB_1R-S383$^{7.39}$ and bound ligands have previously been shown with *in silico* modelling.[40,41] The importance of CB_1R-S383$^{7.39}$ for classical synthetic cannabinoids such as AM11542, AM841 and CP-55,940 was further emphasized in CB_1R-S383$^{7.39}$A mutants.[36] This is in line with the observation that removal or methylation of the phenolic OH on classical cannabinoids, such as in L-759656, JWH-133 and HU308, always affords selectivity over CB_1R.[18,42] Non-classical agonists, such as WIN55,212-2, do not form a hydrogen bond with CB_1R-S383$^{7.39}$ and consequently are not affected by an alanine mutation.[43] This translates to the observation that CP-55,940 and HU308 are more affected by the CB_2R-S285$^{7.39}$A mutation than LEI-102 and APD371 (Figure 2.4A-D, Table 2.4). The decrease in activation is at least 30-fold smaller for CB_2R than CB_1R.[36] The elucidated cryo-EM structures of the four agonists chosen in this study did not show direct interactions with CB_2R-H95$^{2.65}$, though its role in stabilizing the surrounding residues cannot be ruled out. The large effect seen on G protein activation of CB_2R-H95$^{2.65}$A by LEI-102, APD371 and CP-55,940 (Figure 2.4A-D, Table 2.4) must therefore stem from an indirect interaction, supporting the polar network hypothesis between CB_2R-H95$^{2.65}$ and CB_2R-S285$^{7.39}$ in CB_2R.

V261$^{6.51}$ as a potential selectivity hotspot for CB_2R over CB_1R

Residues at position 6.51 have previously been described to be involved in the binding sites of μ, δ, and κ opioid receptors, the dopamine D2 receptor and adenosine receptors, and could play a role in ligand binding selectivity between different subtypes.[44–46] The results show a reduction of G protein activation by APD371, HU308, and CP-55,940 with introduction of the bulkier CB_1R leucine in CB_2R-V261$^{6.51}$L. LEI-102 could still be accommodated in the binding pocket and was not affected (Figure 2.4A-D, Table 2.4). Additionally, in the swap mutant CB_1R-L359$^{5.61}$V partial recovery of [^{3}H]CP-55,940 replacement was found for CB_2R-selective agonists LEI-102, HU308 and APD371, albeit not significant (Table 2.5). This supports the role of this residue in selectivity of agonists in CB_2R.

The lowly-conserved ECL2 is a large effector of GPCR selectivity

The ECL2 has frequently been implicated to be important for GPCR activation and some GPCRs even use their ECL2 as a ligand to auto-activation.[47] There are distinct differences between the conformations of ECL2 in CB_1R and CB_2R. In antagonist-bound CB_1R crystal structures, the ECL2 dips into the binding pocket, interacting with the ligand and inducing the inactive conformation.[31,32] The inactive state of CB_2R, however, does not expand like CB_1R and instead the ECL2 acts more as a lid on the binding pocket in active and inactive CB_2R, akin to active CB_1R.[33] A key distinction seen in the CB_1R crystal structures with AM6538 and Taranabant, is the ionic lock formed by CB_1R-E100$^{N\text{-terminus}}$ (CB_2R-L17) and CB_1R-H270^{ECL2} (CB_2R-L185).[31,32] The results showed improved binding of [^{3}H]CP-55,940 for LEI-102 and HU308 with the CB_1R-H270^{ECL2}L mutation, while the non-selective agonists showed no change (Table 2.5). Through the loss of this ionic lock, selectivity over CB_1R is partially lost, showing that expulsion of ECL2 upon ligand entry may play an important role in selectivity.

An alternative entry pathway for lipophilic agonists via a membrane channel

In recent years, computational studies have suggested that lipophilic ligands for various GPCRs, such as the opsin receptor, sphingosine-1-phosphate receptor 1 ($S1P_1$) and cannabinoid receptors, might gain access to the binding pocket through lateral diffusion via a membrane channel between TM1 and TM7.[32,40,48–51] The membrane entry pathway was evaluated with a CB_2R quadruple mutant (K33$^{1.32}$Q, V36$^{1.35}$I, C40$^{1.39}$S and K279$^{7.33}$T), which showed a significant loss in potency and a corresponding decrease in affinity, albeit not significant, for HU308 and the endocannabinoids (Figure 2.4E-J, Table 2.4

and 2.6). These compounds are more lipophilic than LEI-102 and APD371, making them more suitable to traverse the membrane to enter between TM1 and TM7. Notably, HU308 and anandamide also showed a substantially longer ET in the kinetic assays compared to the other agonists (Table 2.2). This might suggest a possible relationship between slow association and membrane channel entry at the CB_2R. Likewise, for a peptide GPCR a trend in reduced association rate was found with increasing lipophilicity.[52] Alternatively, this is in contrast with the mechanism at the α2-adrenoceptor at which lipophilic compounds had a faster association rate.[53] This shows the diversity in drug-target binding kinetics as receptor-specific properties and thus the importance of investigating these mechanisms for individual receptors.[54]

The discovery of a membrane access channel for endocannabinoids on the CB_2R is also intriguing from a physiological perspective. Endocannabinoids are produced on demand and act as autocrine or paracrine effectors in the immune system regulating the migration of CB_2R-expressing immune cells.[17] The results suggest that endocannabinoids first have to travel through the plasma membrane via lateral diffusion to reach the receptor. This may suggest that the trafficking and cellular uptake of endocannabinoids could be regulated through extracellular or intracellular vesicles that merge with the plasma membrane. Regardless of the exact mechanism of endocannabinoid trafficking, the results provide experimental evidence of a membrane channel located between TM1 and TM7 in CB_2R that is used by the endocannabinoids to enter the receptor.

Conclusion

In silico and mutational studies on LEI-102 and five other CBR agonists have shown that physicochemical properties determine both pharmacokinetic properties of the ligand and their manner of engagement with the target. The ECL2 and CB_2R-V261$^{5.61}$ are hotspots for inducing selectivity over CB_1R, and CB_2R-F117$^{3.36}$ is vital for receptor activation. Additionally lipophilic ligands including the endocannabinoids may enter the binding pocket through a membrane entrance between TM1 and TM7. Altogether, these discovered molecular mechanisms for selective receptor engagement and activation can have implication for drug design and lipid signaling at GPCRs in general.

Experimental Section

Chemistry

General Remarks

All reagents and solvents were purchased from commercial sources and were of analytical grade (Sigma-Aldrich, BroadPharm®). Reagents and solvents were not further purified before use. All moisture sensitive reactions were performed under inert atmosphere. Solvents were dried using 4 Å molecular sieves prior to use when anhydrous conditions were required. Water used in reactions was always demineralized. Analytical Thin-layer Chromatography (TLC) was routinely performed to monitor the progression of a reaction and was conducted on Merck Silica gel 60 F254 plates. Reaction compounds on the TLC plates were visualized by UV irradiation (λ254) and/or spraying with potassium permanganate solution (K_2CO_3 (40 g), $KMnO_4$ (6 g), and H_2O (600 mL)), ninhydrin solution (ninhydrin (1.5 g), n-butanol (100 mL) and acetic acid (3.0 mL)) or molybdenum solution ($(NH_4)_6Mo_7O_{24}{\cdot}4H_2O$ (25 g/L) and $(NH_4)_4Ce(SO_4)_4{\cdot}2H_2O$ (10 g/L) in sulfuric acid (10%)) followed by heating as appropriate. Purification by flash column chromatography was performed using Screening Devices B.V. silica gel 60 (40-63 µm, pore diameter of 60 Å). Solutions were concentrated using a Heidolph laborata W8 4000 efficient rotary evaporator with a Laboport vacuum pump. Analytical purity was determined with Liquid Chromatography-Mass Spectrometry (LC-MS) using a Finnigan LCQ Advantage MAX apparatus with electrospray ionization (ESI), equipped with a Phenomenex Gemini 3 µm NX-C18 110Å column (50x4.6mm), measuring absorbance at 254 nm using a Waters 2998 PDA UV detector and the m/z ratio by using an Acquity Single Quad (Q1) detector. Injection was with the Finnigan Surveyor Autosampler

Plus and pumped through the column with the Finnigan Surveyor LC pump plus to be analyzed with the Finnigan Surveyor PDA plus detector. Samples were analyzed using eluent gradient 10% → 90% ACN in MilliQ water (+ 0.1% TFA (v/v)). For purification by mass guided preparative High-Performance Liquid Chromatography (Prep-HPLC) was performed on a Waters AutoPurification HPLC/MS apparatus with a Gemini prep column 5 µm 18C 110 Å (150x21.2mm), Waters 2767 Sample manager, Waters 2545 Binary gradient module, Waters SFO System fluidics organizer, Waters 515 HPLC pump M, Waters 515 HPLC pump L attached to a Waters SQ detector Acquity Ultra performance LC. A five column volume purification protocol was applied with the eluents A: 0.2% aq. TFA, B: ACN, flow 25 mL/min, with a minimum start gradients of 0% to maximum end gradient of 100% of B. ^{1}H, ^{13}C, ^{1}H-COSY and HSQC Nuclear Magnetic Resonance (NMR) spectra were recorded on a Bruker AV 300 (300/75 MHz), AV 400 (400/100 MHz) or AV 500 (500/125 MHz) spectrometer at ambient temperature using $CDCl_3$ as solvent. Chemical shifts (δ) are referenced in parts per million (ppm) with tetramethylsilane (TMS) or $CDCl_3$ resonance as the internal standard peak ($CDCl_3$/TMS, δ 0.00 for ^{1}H (TMS), δ 77.16 for ^{13}C ($CDCl_3$)). Multiplicity is reported as bs = broad singlet, s = singlet, d = doublet, bd = broad doublet, dd = doublet of doublet, t = triplet, q = quartet, p = quintet, m = multiplet. Coupling-constants (*J*) are reported in Hertz (Hz).

Synthesis of LEI-102

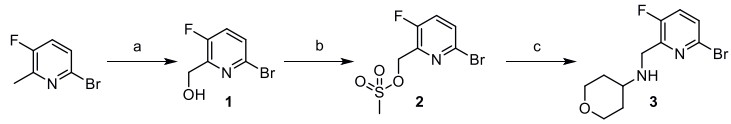

Scheme 2.2 Reagents and conditions: a) Step 1: *m*-CPBA (1.8 eq), 0 °C-RT, DCM, 4 days; Step 2: TFAA (2.2 eq), 55 °C, 3 h; Step 3: K_2CO_3 (2.4 eq), THF:MeOH (20:1), 17 h, 35% (three steps); b) Et_3N (2.3 eq), MsCl (1.7 eq), THF, 0 °C-RT, 1 h, 75%; c) K_2CO_3 (2.2 eq), tetrahydro-2H-pyran-4-amine (1.3 eq), ACN, 50 °C, 3 h, 67%.

(6-Bromo-3-fluoropyridin-2-yl)methanol (1): To a stirred and cooled (0 °C) mixture under inert atmosphere of 6-bromo-3-fluoro-2-methylpyridine (10.7 g, 56.3 mmol, 1 eq) in DCM (370 mL) was added portion-wise *m*-CPBA (23.6 g, 70-75%, 100 mmol, 1.8 eq). The reaction mixture was stirred at room temperature (RT) for 4 days. Sat. $NaHCO_3$ (aq) and sat. $Na_2S_2O_3$ (aq) was added (1:1, v/v) and the layers were separated. The aqueous layer was extracted thrice with DCM. The combined organic layer was dried ($MgSO_4$), filtered, and concentrated under reduced pressure. To the residue was added TFAA (17 mL, 122 mmol, 2.2 eq) at 0 °C. After 15 minutes the temperature was increased to 55 °C for 3 h. The mixture was concentrated under reduced pressure, redissolved in DCM and sat. Na_2CO_3 (aq) was added. The layers were separated and the organic layer was washed with sat. $NaHCO_3$ (aq). The solvent was evaporated and the crude was dissolved in THF:MeOH (20:1, v/v) and K_2CO_3 (18.2 g, 132 mmol, 2.3 eq) was added. After 17 h H_2O was added and the layers were separated. The aqueous layer was extracted thrice with EtOAc. The combined organic layer was dried ($MgSO_4$), filtered, and the solvent evaporated under reduced pressure. The crude product was purified with flash column chromatography (10-20% EtOAc in pentane) to yield a white solid (5.79 g, 19.7 mmol, 35%). ^{1}H-NMR (500 MHz, $CDCl_3$) δ 7.42 (ddt, *J* = 8.5, 3.5, 0.7 Hz, 1H), 7.29 (t, *J* = 8.5 Hz, 1H), 4.80 (d, *J* = 3.3 Hz, 2H). ^{13}C-NMR (126 MHz, $CDCl_3$) δ 156.10 (d, *J* = 256.2 Hz), 148.74 (d, *J* = 19.1 Hz), 135.01 (d, *J* = 2.9 Hz), 128.17 (d, *J* = 4.2 Hz), 126.09 (d, *J* = 19.8 Hz), 59.07.

(6-Bromo-3-fluoropyridin-2-yl)methyl methanesulfonate (2): To a cooled (0 °C) mixture of **1** (1.6 g, 7.8 mmol, 1 eq) and Et_3N (2.5 mL, 17.9 mmol, 2.3 eq) in dry THF (40 mL) was added dropwise MsCl (1.0 mL, 12.9 mmol, 1.7 eq). After stirring at RT for 1 h the solution was concentrated under reduced pressure. DCM and H_2O were added and the layers were separated. The aqueous layer was extracted thrice with DCM. The combined organic layer was washed with brine, dried ($MgSO_4$), filtered, and the

solvent evaporated under reduced pressure to yield a yellow solid (1.65 g, 5.8 mmol, 75%). ^{1}H-NMR (500 MHz, $CDCl_3$) δ 7.52 (dd, *J* = 8.6, 3.5 Hz, 1H), 7.37 (t, *J* = 8.5 Hz, 1H), 5.33 (d, *J* = 2.1 Hz, 2H), 3.13 (s, 3H). ^{13}C-NMR (126 MHz, $CDCl_3$) δ 157.82 (d, *J* = 261.3 Hz), 142.15 (d, *J* = 16.0 Hz), 130.74 (d, *J* = 4.4 Hz), 127.06 (d, *J* = 20.4 Hz), 65.50 (d, *J* = 1.6 Hz), 38.39.

***N*-((6-Bromo-3-fluoropyridin-2-yl)methyl)tetrahydro-2*H*-pyran-4-amine (3)**: A stirred suspension of **2** (1.49 g, 5.3 mmol, 1 eq), K_2CO_3 (1.6 g, 11.6 mmol, 2.2 eq) and tetrahydro-2*H*-pyran-4-amine (0.66 mL, 6.7 mmol, 1.3 eq) in acetonitrile (25 mL) was heated (50 °C) for 6 h, then stirred an additional 3 days at RT. After dilution with DCM and H_2O the layers were separated. The aqueous layer was extracted thrice with DCM. The combined organic layer was dried ($MgSO_4$), filtered, and the solution evaporated under reduced pressure. The crude product was purified with flash column chromatography (20-100% EtOAc in pentane) to yield a yellow oil (1.01 g, 3.5 mmol, 67%). ^{1}H-NMR (300 MHz, $CDCl_3$) δ 7.40 (dd, *J* = 8.6, 3.6 Hz, 1H), 7.35 – 7.26 (m, 1H), 4.08 – 3.95 (m, 4H), 3.42 (td, *J* = 11.6, 2.2 Hz, 2H), 2.74 (tt, *J* = 10.5, 4.1 Hz 1H), 1.89 (ddd, *J* = 12.7, 4.5, 2.3 Hz, 2H), 1.52 (dtd, *J* = 13.1, 11.0, 4.5 Hz, 2H). ^{13}C-NMR (75 MHz, $CDCl_3$) δ 157.12 (d, *J* = 255.9 Hz), 149.21 (d, *J* = 17.0 Hz), 127.83 (d, *J* = 4.2 Hz), 125.97 (d, *J* = 21.2 Hz), 66.76, 53.64, 44.90, 33.59.

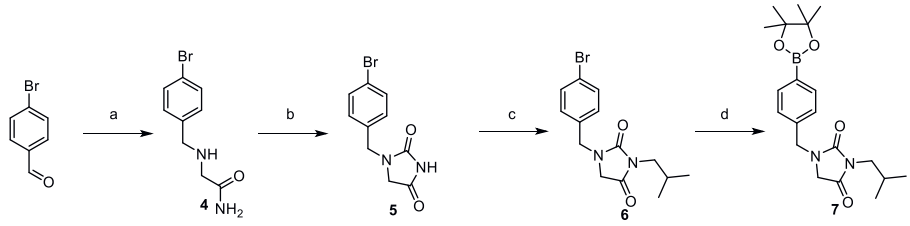

Scheme 2.3 Reagents and Conditions: a) Step 1: 2-aminoacetamide hydrochloride (1.0 eq), NaOH (1.1 eq), MeOH:H_2O (5:1), RT, 18 h; Step 2: $NaBH_4$ (2.1 eq), 18 h, 91% (two steps); b) CDI (2.1 eq), DMAP (2.1 eq), ACN, 60 °C, 70 h, 37%; c) K_2CO_3 (3.0 eq), 1-bromo-2-methylpropane (2.0 eq), DMF, RT, 20 h, 88%; d) KOAc (4.4 eq), bis(pinacolato)diboron (1.5 eq), Pd(dppf)Cl_2 (0.06 eq), DMF, 75 °C, 20 h.

2-((4-Bromobenzyl)amino)acetamide (4): To a stirred mixture of 4-bromobenzaldehyde (9.2 g (49.7 mmol, 1.1 eq) and 2-aminoacetamide hydrochloride (5.06 g, 45.8 mmol, 1.0 eq) in MeOH:H_2O (170 mL, 5:1, v/v) was added NaOH (2.06 g, 51.5 mmol, 1.1 eq). After stirring at RT overnight, $NaBH_4$ (3.6 g, 95.2 mmol, 2.1 eq) was added and the solution was stirred overnight at RT. The solution was acidified to pH 3 with 2 M HCl, then neutralized with sat. $NaHCO_3$ (aq). Methanol was evaporated under reduced pressure and the resulting slurry was filtered to yield a white solid (11.0 g, 45.2 mmol, 91%). ^{1}H-NMR (300 MHz, MeOD) δ 7.69 – 7.59 (m, 2H), 7.47 – 7.38 (m, 2H), 4.22 (s, 2H), 3.81 (s, 2H).

1-(4-Bromobenzyl)imidazolidine-2,4-dione (5): To stirred suspension of **4** (10.0 g, 40.1 mmol, 1.0 eq) in acetonitrile (300 mL) were added CDI (13.86 g, 85.5 mmol, 2.1 eq) and DMAP (10.2 g, 83.5 mmol, 2.1 eq). The mixture was heated (60 °C) under inert atmosphere for 70 h. 1 M HCl (aq, 250 mL) was added and the aqueous layer extracted thrice with EtOAc. The combined organic layer was washed with H_2O and brine, dried ($MgSO_4$), filtered, and the solvent evaporated under reduced pressure. The crude product was purified with flash column chromatography with dry loading over Celite (5-10% acetone in DCM) to yield a yellow solid (3.95 g, 14.7 mmol, 37%). ^{1}H-NMR (300 MHz, $CDCl_3$) δ 7.83 (bs, 1H), 7.56 – 7.45 (m, 2H), 7.20 – 7.10 (m, 2H), 4.49 (s, 2H), 3.79 (s, 2H). ^{13}C-NMR (75 MHz, $CDCl_3$) δ 132.41, 129.95, 77.58, 77.16, 76.74, 50.36, 46.01.

1-(4-Bromobenzyl)-3-isobutylimidazolidine-2,4-dione (6): To a stirred solution of **5** (2.00 g, 7.4 mmol, 1,0 eq) in anhydrous DMF (18 mL) were subsequently added K_2CO_3 (3.08 g, 22.3 mmol, 3,0 eq) and 1-bromo-2-methylpropane (1.62 mL, 14.9 mmol, 2,0 eq). After stirring at RT for 20 h, the mixture was

filtered and the filtrate diluted with diethyl ether and washed thrice with H_2O (3 x 50 mL). The combined organic layer was washed with brine, dried ($MgSO_4$), filtered, and concentrated under reduced pressure. The crude product was purified with flash column chromatography (10-40% EtOAc in pentane) to yield a white solid (2.12 g, 6.52 mmol, 88%). ^{1}H-NMR (300 MHz, $CDCl_3$) δ 7.47 (d, *J* = 8.3 Hz, 2H), 7.14 (d, *J* = 8.3 Hz, 2H), 4.52 (s, 2H), 3.74 (s, 2H), 3.33 (d, *J* = 7.4 Hz, 2H), 2.15 – 2.04 (m, 1H), 0.91 (d, *J* = 6.8 Hz, 6H). ^{13}C-NMR (75 MHz, $CDCl_3$) δ 169.57, 156.78, 134.41, 131.79, 129.48, 121.77, 60.01, 48.61, 45.98, 45.71, 28.57, 19.70. LCMS (LCQ Fleet, 10-90): t_r = 7.00 min, m/z: 325.17 $[M+H]^+$, 327.08 $[M+H]^+$ (Br).

3-Isobutyl-1-(4-(4,4,5,5-tetramethyl-1,3,2-dioxaborolan-2-yl)benzyl)imidazolidine-2,4-dione (7): A mixture of **6** (0.50 g, 1.54 mmol, 1 eq), KOAc (0.66 g, 6.76 mmol, 4.4 eq) and bis(pinacolato)diboron (0.59 g, 2.31 mmol, 1.5 eq) in DMF (10 mL) was sonicated for 15 min under argon flow. Subsequently, $Pd(dppf)Cl_2$ (0.07 g, 0.09 mmol, 0.06 eq) was added and the mixture was heated (75 °C) for 20 h. The mixture was cooled to RT, diluted with EtOAc (100 mL) and H_2O (10 mL) and the layers were separated. The aqueous layer was extracted thrice with EtOAc (3 × 20 mL). The combined organic layer was extracted with sat. $NaHCO_3$ (aq), H_2O and brine, dried ($MgSO_4$), filtered, and concentrated under reduced pressure. The crude product was co-evaporated with $CHCl_3$ and used in the next step without further purification.

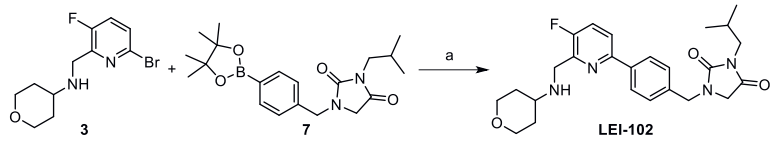

Scheme 2.4 Reagents and Conditions: a) **3** (1.0 eq), **7** (1.5 eq), K_2CO_3 (6.0 eq), $Pd(PPh_3)_4$ (0.1 eq), toluene:EtOH (4:1), 75 °C, 18 h, 45% (two steps).

1-(4-(5-Fluoro-6-(((tetrahydro-2H-pyran-4-yl)amino)methyl)pyridin-2-yl)benzyl)-3-isobutylimidazolidine-2,4-dione (LEI-102): To a degassed mixture of **3** (0.29 g, 1.0 mmol, 1,0 eq), **7** (0.56 g, ~1.5 mmol, crude) and K_2CO_3 (1.29 g, 6.0 mmol, 6,0 eq) in toluene:ethanol (10 mL, 4:1, v/v) was added under argon atmosphere $Pd(PPh_3)_4$ (0.18 g, 0.10 mmol, 0.1 eq). The resulting mixture was heated (75° for 18 h, then cooled to RT and filtered. The filtrate was diluted with EtOAc and washed with H_2O and brine, dried ($MgSO_4$), filtered, and concentrated under reduced pressure. The crude product was purified with flash column chromatography (0-20% MeOH in EtOAc) to yield a white solid (0.24 g, 0.53 mmol, 53%). Further purification with preparative HPLC resulted in a yield of 0.204 g (0.45 mmol, 45%). ^{1}H-NMR (400 MHz, CD_3CN) δ 8.05 (d, *J* = 8.3 Hz, 2H), 7.86 (dd, *J* = 8.7, 3.6 Hz, 1H), 7.61 (t, *J* = 9.0 Hz, 1H), 7.34 (d, *J* = 8.1 Hz, 2H), 4.53 (s, 2H), 4.45 (s, 2H), 3.93 (dd, *J* = 11.4, 4.4 Hz, 2H), 3.77 (s, 1H), 3.47 (tt, *J* = 11.8, 3.8 Hz, 2H), 3.30 (td, *J* = 11.9, 1.9 Hz, 2H), 3.24 (d, *J* = 7.3 Hz, 2H), 2.05 (bd, *J* = 13.3 Hz, 2H), 1.99 (dt, *J* = 13.2, 6.6 Hz, 1H), 1.83 (qd, *J* = 12.1, 4.5 Hz, 2H), 0.88 (d, *J* = 6.7 Hz, 6H). ^{13}C-NMR (100 MHz, CD_3CN) δ 171.54, 157.25 (d, *J* = 226.6 Hz), 156.12, 153.03 (d, *J* = 4.5 Hz), 140.51 (d, *J* = 16.1 Hz), 138.83, 137.70, 129.13, 128.22, 125.56 (d, *J* = 18.8 Hz), 122.81 (d, *J* = 4.3 Hz), 118.38, 66.55, 55.55, 50.30, 46.81 (d, *J* = 7.9 Hz), 42.95, 30.02, 28.32, 20.32. LCMS (LCQ Advantage, 10 90%): t_r = 5.32 min, m/z: 455.27 $[M+H]^+$, 908.93 $[2M+H]^+$. HRMS (ESI+) m/z: calcd. for $C_{25}H_{32}FN_4O_3$ [M+H], 455.245; found, 455.245.

Biology

General Remarks

Monoclonal M2 mouse anti-FLAG primary antibody (#F3165) was purchased from Sigma-Aldrich (Zwijndrecht, the Netherlands), while secondary goat anti-mouse HRP-conjugated antibody (#115-035-003) was bought from Jackson ImmunoResearch Laboratories (West Grove, PA, USA). Bicinchoninic acid

(BCA) ad BCA protein assay reagent was obtained from Pierce Chemical Company (Rockford, IL, USA). [^{3}H]-RO6957022 (specific activity 82.83 Ci mmol^{-1}) was custom synthesized at F. Hoffman-La Roche Ltd (Basel, Switzerland). [^{35}S]GTPγS (specific activity 1250 Ci mmol^{-1} #NEG030H250UC), [^{3}H]-CP-55,940 (specific activity 108.5 Ci mmol^{-1} #NET1051250UC) and GF/C filter plates (#6055690) were purchased from PerkinElmer (Waltham, MA, USA). CP-55,940 (#C1112), AM630 (#SML0327) and DL-dithiotreitol (DTT, #646563) were obtained from Sigma-Aldrich, HU308 (#H800010) was from LKT Laboratories (St. Paul, MN, USA), APD371 was provided by F. Hoffmann-La Roche Ltd, anandamide (AEA, #1339), 2-Arachidonylglycerol (2-AG, #1298) and phenylmethylsulfonyl fluoride (PMSF, #4486) were purchased from Tocris Bioscience (Bristol, UK) and GDP (#J61646) was from Thermo Fisher Scientific (Waltham, MA, USA). All buffers and solutions were prepared using Millipore water (deionized using a MilliQ A10 Biocel with a 0.22 µm filter) and analytical grade reagents and solvents. Buffers are prepared at room temperature (RT) and stored at 4 °C, unless stated otherwise.

Quantification and statistical analysis

All experimental data were analyzed using GraphPad Prism 9.0 (GraphPad Software Inc., San Diego, CA). All values obtained are means ± standard error of the mean (SEM) of at least three independent experiments performed in duplicate, unless stated otherwise.

From [^{3}H]-RO6957022 competition association assays, the k_{on} and k_{off} were determined by non-linear regression analysis, using the "kinetics of competitive binding" model as described by Motulsky and Mahan[55]:

$$K_a = k_1 \cdot [L] \cdot 10^{-9} + k_2$$

$$K_b = k_3 \cdot [I] \cdot 10^{-9} + k_4$$

$$S = \sqrt{(K_a - K_b)^2 + 4 \cdot k_1 \cdot k_3 \cdot [L] \cdot [I] \cdot 10^{-18}}$$

$$K_f = 0.5 \cdot (K_a + K_b + S)$$

$$K_s = 0.5 \cdot (K_a + K_b - S)$$

$$Q = \frac{Bmax \cdot k_1 \cdot [L] \cdot 10^{-9}}{K_f - K_s}$$

$$[Y] = Q \cdot \left(\frac{k_4 \cdot (K_f - K_s)}{K_f \cdot K_s} + \frac{k_4 - K_f}{K_f} \cdot \mathrm{e}^{(-K_f \cdot X)} - \frac{k_4 - K_s}{K_s} \cdot \mathrm{e}^{(-K_S \cdot X)} \right)$$

Where [L] is the radioligand concentration per experiment (~1.5 nM), I is the IC_{50} concentration of agonist (nM), X is the time (s), and Y is the specific binding of the radioligand (dpm). K_a and K_b are the observed association rate constants (k_{obs}) of the radioligand and the agonist of interest, respectively. k_1 and k_3 are the association rate constants (k_{on} in $M^{-1}s^{-1}$) of [^{3}H]-RO6957022 (determined per experiment) and the agonist of interest, respectively. Similarly, k_2 and k_4 are the dissociation rate constants (k_{off} in s^{-1}) of [^{3}H]-RO6957022 (experimentally determined at 4.3×10^{-4} s^{-1}, data not shown) and the agonist of interest, respectively. The engagement time (ET in seconds) of the agonists of interest was determined at 1 µM of agonist using the equation ET= $1/(k_{on} \cdot 1 \times 10^{-6})$. The residence time distribution (RTD in min) was calculated using the equation RTD=$1/(60 \cdot k_{off})$.[56] The association and dissociation rate constants were used to calculate the kinetic K_D using: $K_D = k_{off}/k_{on}$.

[^{35}S]GTPγS agonist responses on CB_2R constructs were baseline-corrected for the individual mutant's basal activity. The responses were normalized to the basal activity of the construct (0%) and top of the CP-55,940 (for WT responses only) or WT curve (for mutants, 100%). The potency (pEC_{50}) and efficacy (E_{max}) values were obtained by non-linear regression to a sigmoidal concentration-effect curve with a

Hill slope of 1 by using the "log(agonist) vs response (three parameters)" model. [^{35}S]GTPγS data from CB_1R constructs were expressed as fold over the mutant's basal activity to also quantify the effects of CB_2R selective agonists.

Displacement assays were baseline-corrected with NSB and normalized to this value (0%) and TB (100%). The equilibrium dissociation constants (K_D) of [^{3}H]-CP-55,940 on different mutants were calculated from homologous displacements by non-linear regression analysis, using the "one-site homologous" model. The half-maximal inhibitory concentrations (pIC_{50}) of the agonists in [^{3}H]-CP-55,940 and [^{3}H]-RO6957022 assays were obtained by non-linear regression analysis of the homologous and heterologous displacement curves and further converted into inhibitory constant pK_i using the Cheng-Prusoff equation.[57] In which the experimentally determined K_D for each construct was used for [^{3}H]-CP-55,940 assays or 0.78 nM for [^{3}H]-RO6957022 assays (data not shown).

Differences in pEC_{50}, E_{max}, pK_D and pK_i values for each mutant compared to WT were analyzed using a one-way Welch's ANOVA with Dunnett's T3 multiple comparisons test or an unpaired Student's t-test with Welch's correction. Significant differences are displayed as * $p < 0.05$; ** $p < 0.01$, *** $p < 0.001$ and **** $p < 0.0001$.

Cell Culture

Cells were cultured and prepared similar to previously described.[44] Spodoptera frugiperda (Sf9) cells were used for CB2R-Gi co-expression for cryo-EM studies. Sf9 cells were grown in ESF 921 medium (Expression systems) at 27 °C and 125 rpm. For transfections, human embryonic kidney 293 T (HEK293T; female, ATCC #CRL-3216) cells were grown as monolayers in culture medium i.e. Dulbecco's Modified Eagle's Medium (Sigma-Aldrich #6546), supplemented with 10% fetal calf serum (Sigma-Aldrich #F7524), 2 mM L-glutamine (Sigma-Aldrich #G8541), 100 IU/mL penicillin and 100 µg/mL streptomycin (Duchefa Biochemie #P0142 and #S0148) under a humidified atmosphere at 37 °C with 5% CO_2. Subculture was done twice a week at 80 – 90% confluence on 10 cm ø plates by trypsinization. CHO cells stably expressing hCB_2 (CHOK1_hCB_2R_bgal; PathHunter EA Parental Cell line, female, DiscoverX #93-0706C2) were cultured in Ham's F12 Nutrient Mixture (Sigma-Aldrich #4888) supplemented with 10% fetal calf serum, 2 mM L-glutamine, 100 IU/mL penicillin, 100 µg/mL streptomycin, 300 µg/mL hygromycin (Bio-Connect #ANT-HG-5) and 800 µg/mL G418 (Bio-Connect #SC-29065B) in a humidified atmosphere at 37 °C with 5% CO_2. Cells were subcultured twice a week when reaching 80 - 90% confluence on 10 or 15 cm ø plates by trypsinization.

Constructs and Expression of CB_2R and G_i heterotrimer

A N-BRIL fused WT human CB_2R construct was cloned into a modified pFastBac1 vector with an HA signal sequence at the N-terminus followed by a 10×His-tag and a FLAG-tag. Human $G_{\alpha i1}$ and $G_{\beta 1\gamma 2}$ subunits were cloned into pFastbac1 and pFastDual vector individually. The CB_2R and G_i heterotrimer were co-expressed in Sf9 insect cells using the Bac-to-Bac Baculovirus Expression System (Invitrogen). Sf9 cells were infected at a cell density of 2-2.5×10^6 cells/ml with three separate virus preparations for CB_2R, $G_{\alpha i1}$ and $G_{\beta 1\gamma 2}$ at a ratio of 1:2:2. The infected cells were cultured at 27 °C for 48 h before collection by centrifugation and the cell pellets were stored at -80 °C for future use.

Constructs, Expression and Purification of scFv16

Methods of complex expression and purification in the current study have been described previously.[34] The CB_2R and G_i heterotrimer were co-expressed in Sf9 insect cells using the Bac-to-Bac Baculovirus Expression System (Invitrogen). Cells were infected with three separate virus preparations for CB_2R, $G_{\alpha i1}$ and $G\beta_{1\gamma 2}$ at a ratio of 1:2:2 at a cell density of 2.5×10^6 cells/mL. After 48 h, the cell culture was collected by centrifugation and the cell pellets were stored at -80 °C until use. The cell pellets were thawed and lysed in the hypotonic buffer of 10 mM HEPES (pH 7.5), 10 mM $MgCl_2$, 20 mM KCl with EDTA-free

complete protease inhibitor cocktail tablets (Roche, #5056489001). The CB_2R-G_i complex was formed in membranes by addition of 25 µM agonist (LEI-102, APD371, HU308 and CP-55,940, respectively) and 2 units of apyrase (NEB, #M0398S) in the presence 500 µg scFv16. The lysate was incubated for overnight at 4 °C and discard the supernatant by centrifugation at 40,000 rpm for 30 min. Subsequently, the solubilization buffer containing 50 mM HEPES (pH 7.5), 100 mM NaCl, 0.75% (w/v) lauryl maltose neopentyl glycol (LMNG, Anatrace, #4216588), 0.15% (w/v) cholesterol hemisucinate (CHS, Sigma-Aldrich, #C6512) supplemented with 25 µM agonist and 2 units of apyrase (NEB) were added to solubilize complexes for 2 h at 4 °C. Insoluble material was removed by centrifugation at 40,000 rpm for 30 min and the supernatant was immobilized by batch binding to TALON IMAC resin (Clontech, #635507) including 20 mM imidazole over 6 h at 4 °C. Then, the resin was packed and washed with 15 column volumes (CVs) of washing buffer I containing 25 mM HEPES (pH 7.5), 100 mM NaCl, 10% (v/v) glycerol, 0.1% (w/v) LMNG, 0.02% (w/v) CHS, 30 mM imidazole and 20 µM agonist, and 15 CVs of washing buffer II containing 25 mM HEPES (pH 7.5), 100 mM NaCl, 10% (v/v) glycerol, 0.03% (w/v) LMNG, 0.006% (w/v) CHS, 50 mM imidazole and 20 µM agonist. After that, the protein was eluted using 3 CVs of elution buffer containing 25 mM HEPES (pH 7.5), 100 mM NaCl, 10% (v/v) glycerol, 0.01% (w/v) LMNG, 0.002% (w/v) CHS, 250 mM imidazole and 25 µM agonist. Finally, the complex was concentrated using the centrifugal filter with 100 KD molecular weight cutoff and loaded onto a Superdex200 10/300 GL column (GE Healthcare) with buffer containing 20 mM HEPES (pH 7.5), 100 mM NaCl, 0.00075% (w/v) LMNG, 0.00025% GDN (Anatrace, #GDN101), 0.0001% (w/v) CHS, 100 µM TCEP. The fractions consisting of purified CB_2-G_i complex were collected and concentrated to 0.8-1.0 mg/ml for electron microscopy experiments.

CB_2R-G_i-scFv16 Complex Formation and Purification

The cell pellets corresponding to 1 L CB_2R-G_i co-expression culture were thawed and lysed in the hypotonic buffer of 10 mM HEPES, pH7.5, 10 mM $MgCl_2$, 20 mM KCl with EDTA-free complete protease inhibitor cocktail tablets (Roche). The CB_2R-G_i complex was formed in membranes by addition of 20 µM agonist (LEI-102, APD371, HU308 or CP-55,940) and 2 units of apyrase (NEB) in the presence of 500 µg scFv16. The lysate was incubated overnight at 4 °C and the supernatant discarded after centrifugation at 40,000 rpm for 30 min. The complex was separated from the membranes in buffer containing 50 mM HEPES (pH 7.5), 100 mM NaCl, 0.75% (w/v) lauryl maltose neopentyl glycol (LMNG, Anatrace), 0.15% (w/v) cholesterol hemisucinate (CHS, Sigma-Aldrich), 20 µM agonist and 2 units of apyrase (NEB) at 4 °C for 2 h. The supernatant was isolated by ultracentrifugation, and then incubated with TALON IMAC resin (Clontech) and 20 mM imidazole over 6 h at 4 °C. The resin was washed with 15 column volumes of washing buffer I (25 mM HEPES (pH 7.5), 100 mM NaCl, 10% (v/v) glycerol, 0.1% (w/v) LMNG, 0.02% (w/v) CHS, 30 mM imidazole and 20 µM agonist) and 15 column volumes of washing buffer II (25 mM HEPES (pH 7.5), 100 mM NaCl, 10% (v/v) glycerol, 0.03% (w/v) LMNG, 0.006% (w/v) CHS, 50 mM imidazole and 20 µM agonist). The protein was eluted using 3 column volumes of elution buffer (25 mM HEPES (pH 7.5), 100 mM NaCl, 10% (v/v) glycerol, 0.01% (w/v) LMNG, 0.002% (w/v) CHS, 250 mM imidazole and 25 µM agonist). The purified CB_2R-G_i-scFv16 complex was concentrated, then injected onto a Superdex200 10/300 GL column (GE Healthcare) equilibrated in buffer (20 mM HEPES (pH 7.5), 100 mM NaCl, 0.00075% (w/v) LMNG, 0.00025% GDN, 0.0001% (w/v) CHS, 100 µM TCEP). The complex peak fractions were collected and concentrated individually to 0.8-1.0 mg/mL for electron microscopy experiments.

Cryo-EM grid Preparation and data collection

For cryo-EM grids preparation of the CB_2R-G_i complexes, 3 µL of the concentrated protein was loaded to a glow-discharged holey carbon grid (CryoMatrix Amorphous alloy film R1.2/1.3, 300 mesh), and subsequently were plunge-frozen in liquid ethane using a Vitrobot Mark IV (Thermo Fisher Scientific).

The chamber of Vitrobot was set to 100% humidity at 4 °C. The sample was blotted for 2.5 s with blot force 2. Cryo-EM images were collected on a Titan Krios microscope operated at 300 kV equipped with a Gatan Quantum energy filter, with a slit width of 20 eV, a Gatan K2 summit direct electron camera (Gatan). Images were taken at a dose rate of 8e-/Å2/s with a defocus range of -0.8 to -2.0 µm using SerialEM software[58] in EFTEM nanoprobe mode, with 50 µm C2 aperture, at a calibrated magnification of 130,000 corresponding to a magnified pixel size of 1.04 Å. The total exposure time was 8.1 s and 45 frames were recorded per micrograph.

Image Processing and 3D Reconstruction

The cryo-EM data processing was performed with CryoSPARC.[59] For CB_2R-$G_{\alpha i}$-scFv16-APD371/LEI-102/HU308/CP-55,940 dataset, a total of 7443, 5282, 7530 and 6473 movies were collected, respectively. For all datasets, patch motion correction was used for beam-induced motion correction. Contrast transfer function (CTF) parameters for each micrograph were determined by patch CTF estimation. Using Blob Picker in CryoSPARC to auto pick particles in the first 500 micrographs of CB_2R-$G_{\alpha i}$-scFv16-APD371 complex dataset and then 258347 particles were extracted to conduct 2D classification. 9277 particles in good 2D patterns were selected as templates to pick better particles. 5,239,870, 3,398,611, 4,653,294 and 3,595,875 particles extracted, respectively, in a 256 Å box were divided into three hundred two-dimensional (2D) class averages with a maximum alignment resolution of 6 Å. Then, 1,152,146, 762,471, 355,832 and 440,292 particles were selected from good 2D classification after two round 2D classification, individually. Following 2D classification, these particles were subjected for ab initio reconstruction into four classes. After heterogeneous refinement, homogeneous refinement, non-uniform refinement and local refinement of the best-looking dataset in CryoSPARC, the final map has an indicated global resolution of 3.08 Å, 2.98 Å, 2.97 Å and 2.84 Å at a Fourier shell correlation (FSC) of 0.143, respectively. Local resolution was determined using the Bsoft package with half maps as input maps.[60]

Model Building and Refinement

The CB_2R-AM12033 cryo-EM structure and G_i protein in CB_2R were used as the starting model for model refinement. The model was docked into the CB_2R-agonist-G_i-scFv16 EM density map using Chimera[61], followed by iterative manual adjustment and rebuilding in COOT[62] and phenix.real_space_refine in Phenix.[63] The model statistics were validates using MolProbity.[64] Structural figures were prepared in Chimera and PyMOL (http://www.pymol.org). The extent of any model overfitting during refinement was measured by refining the final model against one of the half-maps and by comparing the resulting map versus model FSC curves with the two half-maps and full model.

Generation of Mutants

The WT CB_1R and CB_2R genes were subcloned into vector pcDNA3.1 with an N-terminal HA signal peptide and FLAG-tag. Mutations were introduced by QuikChange PCR (as described by supplier).

Transfection

24 h prior to transfection, HEK293T cells were seeded on 10 cm ø plates to reach approximately 50% confluence at the start of transfection. The cells were transfected with 10 µg plasmid DNA of WT hCB_2R or hCB_1R receptor, or mutant receptor using the calcium phosphate precipitation method.[65] In short, a DNA-calcium mix was made containing 270 mM $CaCl_2$ and 10 µg plasmid DNA to which Hank's Balanced Salt Solution (HBSS; 280 mM NaCl, 10 mM KCl, 1.5 mM Na_2HPO_4 and 50 mM HEPES) was added in a 1:1 (v/v) ratio and mixed by aeration to create consistent calcium phosphate precipitates. For transfection, 1 mL DNA-calcium mix was added per 10 cm ø plate, followed by a 24/48 h incubation under a humidified atmosphere at 37 °C with 5% CO_2.

Enzyme-Linked Immunosorbent Assay (ELISA)

Receptor expression after transfection was measured with ELISA. A control was made by transfecting HEK293T cells transfected with an empty pcDNA3.1 vector. HEK293T cells were transfected 24 h prior to seeding. A clear, culture-treated 96-wells plate was treated with 100 µL/well 0.1 mg/mL poly-D-lysine for 30 min. after which the wells were washed twice with 200 µL/well PBS and the plate air-dried for 1 h. Cells were detached by incubation for 15 min. at 37 °C with 1.5 mL warm PBS/EDTA. 3 mL medium (DMEM, D6546 Sigma Aldrich) was added, cells resuspended and centrifuged at 200 x g for 5 min. The supernatant was aspirated and cells resuspended in medium to 1,000,000 cells/mL. 100 µL is added to each well so that a total of 100,000 cells have been seeded per well.

24 h after seeding the plate was aspirated and washed with 200 µL PBS/well. The cells were fixed with 100 µL/well 4% formaldehyde for 10 min. Then washed twice with 100 µL/well Tris-buffered saline (TBS). The plate was incubated with 100 µL/well blocking buffer (2% (w/v) BSA in TBST) for 30 minutes at 400 rpm. The blocking buffer was aspirated and the plate was incubated with 100 µL/well mouse anti-FLAG primary antibody (1 µg/mL, Sigma F3165) for 2 h at 400 rpm. The antibody was aspirated and after washing thrice with 200 µL/well TBST prior to addition of goat anti-mouse HRP-conjugated secondary antibody (1:10,000 dilution. Jackson ImmunoResearch Laboratories 115-035-003) and 1 h incubation at 400 rpm. The plate was aspirated and washed thrice with 200 µL/well TBS. The plate was incubated with 100 µL/well TMB in the dark for 10 min. until the reaction was quenched with 100 µL 1 M H_3PO_4. Absorbance was measured at 450 nm with the Wallac EnVisionTM (Perking Elmer).

Membrane Preparation

For membrane preparation, HEK293T cells were harvested 48 h after transfection. Cells were detached by scraping into 3 mL of phosphate-buffered saline (PBS) and subsequently centrifuged at 2000 x g for 5 min. Pellets were resuspended in ice-cold Tris buffer (50 mM Tris-HCl, pH 7.4) and homogenized with an Ultra Turrax homogenizer (IKA-Werke GmbH & Co. KG, Staufen, Germany). Cytosolic and membrane fractions were separated using a high-speed centrifugation step of 31,000 rpm in a Beckman Optima LE-80K ultracentrifuge with Ti70 Rotor for 20 min at 4 °C. After a second cycle of homogenization and centrifugation, the final pellets were resuspended in 50 mM Tris-HCl (pH 7.4), 5 mM $MgCl_2$ and stored in 100 µL aliquots at -80 °C until use. CHOK1_hCB_2R_bgal cells were harvested when reaching 90% confluence in 15 cm ø plates after one week subculture at a 1:6 ratio. Membrane preparation followed a similar procedure as described above. Final membrane pellets were resuspended in 50 mM Tris-HCl (pH 7.4) and stored in 100 µL aliquots at -80 °C until use. Membrane protein concentrations were determined using a BCA protein determination assay as described by the manufacturer (Smith et al., 1985).

[^{3}H]-RO6957022 Competition Association Assays

Prior to kinetic assessment of agonist binding, the affinity (IC_{50}) of the agonists at the hCB_2R was determined in [^{3}H]-RO6957022 displacement assays. CHOK1_hCB_2R_bgal was thawed, homogenized, and subsequently diluted to 1 µg protein per well. When studying endocannabinoids, membranes were preincubated with 50 µM PMSF for 30 minutes. Membranes were incubated with ~1.5 nM [^{3}H]-RO6957022 and six increasing concentrations of competing agonists in a total volume of 100 µL assay buffer (50 mM Tris-HCl (pH 7.4), 0.1% (w/v) BSA). Incubations were done for 2 h at 10 °C to reach equilibrium. Subsequently, in competition association assays, agonists were incubated at their IC_{50} concentration in the presence of ~1.5 nM [^{3}H]-RO6957022 in a total volume of 100 µL assay buffer at 10 °C. Competition was initiated by addition of membrane homogenates at different time points for 2 h. Non-specific binding was determined with 10 µM AM630. Organic solvent (DMSO or acetonitrile) concentrations were <1% in all samples. Incubations were terminated by rapid vacuum filtration with ice-cold 50 mM Tris-HCl (pH 7.4), 0.1% (w/v) BSA buffer through Whatman GF/C filters using a

Filtermate 96-well harvester (PerkinElmer). Filters were dried for at least 30 min at 55 °C and subsequently 25 µL MicroScint scintillation cocktail was added per well. Filter-bound radioactivity was measured by scintillation spectrometry using a Microbeta2 2450 counter (PerkinElmer).

[^{35}S]GTPγS Binding Assays

G protein activation was measured with agonists LEI-102, APD371, HU308, CP-55,940 AEA and 2-AG. Transient HEK293T membrane homogenates (10 µg/well) were diluted in assay buffer (50 mM Tris-HCl (pH 7.4), 5 mM $MgCl_2$, 150 mM NaCl, 1 mM EDTA, 0.05% BSA (w/v) and 1 mM DTT) and pretreated with 10 µg saponin and 1 µM GDP. For endocannabinoid samples, the membranes were additionally pretreated for 30 minutes with 50 µM phenylmethylsulfonyl fluoride (PMSF) before agonist addition. The membranes were incubated with 10 µM CP-55,940 (E_{max}) or six increasing concentrations of agonist (ranging from 0.01 nM to 1 µM) for 30 minutes at rt. Basal receptor activity was determined in the presence of vehicle only (0.2% DMSO/acetonitrile). [^{35}S]GTPγS (0.3 nM) was added for 100 µL final volume. The mixture was co-incubated for 90 minutes at 25 °C while shaking at 400 rpm. The plate was filtered with wash buffer (50 mM Tris-HCl (pH 7.4), 0.1% (w/v) BSA) through Whatman GF/C filters using a Filtermate 96-well harvester (PerkinElmer). Filters were dried for at least 30 min at 55 °C and subsequently 25 µL MicroScint scintillation cocktail was added per well. Filter-bound radioactivity was measured by scintillation spectrometry using a Microbeta2 2450 counter (PerkinElmer).

[^{3}H]-CP-55,940 Homologous and Heterologous Displacement Assays

To determine agonist affinity (K_i) on WT and mutant receptors. The amount of transient HEK293T membrane was 0.75 µg to 10 µg protein per well, chosen to reach a specific [^{3}H]-CP-55,940 binding window of 1200-1500 disintegrations per minute (dpm). Only the CB_2R-quadruple mutant was used with 20 µg/well for a window of ~500 dpm. Membranes were thawed and subsequently homogenized using an Ultra Turrax homogenizer. For AEA and 2-AG the membranes were preincubated for 30 minutes with 50 µM PMSF. Homologous displacement assays were performed with 1.5 nM final concentration [^{3}H]-CP-55,940 against six increasing concentrations (0.1 nM to 10 µM) of cold CP-55,940. Heterologous displacement assays were done with LEI-102, APD371, HU308, AEA and 2-AG using 1.5 nM final concentration [^{3}H]-CP-55,940 with one concentration (10 µM) or six increasing concentrations (ranging from 0.1 nM to 10 µM) in assay buffer. To a 96-well roundbottom plate was added 25 µL assay buffer, 25 uL agonist (or buffer for negative control), 25 uL 6 nM [^{3}H]-CP-55,940, and 25 uL membrane, in order. Incubation was for 2 h at 25 °C. Separation of bound from free radioligand was performed by rapid filtration through GF/C filters (Whatman, Clifton, NJ) using a Filtermate Harvester (Brandel Inc., Gaithersburg, MD). Filters were dried for at least 30 min at 55 °C and subsequently 25 µL MicroScint scintillation cocktail was added per well. Filter-bound radioactivity was measured by scintillation spectrometry using a Microbeta2 2450 counter (PerkinElmer).

References

1. Mechoulam R, Hanuš LO, Pertwee R, Howlett AC. Early phytocannabinoid chemistry to endocannabinoids and beyond. *Nat Rev Neurosci*. 2014;15(11):757-764. doi:10.1038/nrn3811

2. Pacher P, Bátkai S, Kunos G. The Endocannabinoid System as an Emerging Target of Pharmacotherapy. *Pharmacol Rev*. 2006;58(3):389-462. doi:10.1124/pr.58.3.2

3. Badowski M, Yanful PK. Dronabinol oral solution in the management of anorexia and weight loss in AIDS and cancer. *Ther Clin Risk Manag*. 2018;Volume 14:643-651. doi:10.2147/TCRM.S126849

4. Grimison P, Mersiades A, Kirby A, et al. Oral THC:CBD cannabis extract for refractory chemotherapy-induced nausea and vomiting: a randomised, placebo-controlled, phase II crossover trial. *Ann Oncol*. 2020;31(11):1553-1560. doi:10.1016/j.annonc.2020.07.020

5. Inglet S, Winter B, Yost SE, et al. Clinical Data for the Use of Cannabis-Based Treatments: A Comprehensive Review of the Literature. *Ann Pharmacother*. 2020;54(11):1109-1143. doi:10.1177/1060028020930189

6. Jones É, Vlachou S. A Critical Review of the Role of the Cannabinoid Compounds Δ9-Tetrahydrocannabinol (Δ9-THC) and Cannabidiol (CBD) and their Combination in Multiple Sclerosis Treatment. *Molecules*. 2020;25(21):4930. doi:10.3390/molecules25214930

7. Adams IB, Martin BR. Cannabis: pharmacology and toxicology in animals and humans. *Addiction*. 1996;91(11):1585-1614. http://www.ncbi.nlm.nih.gov/pubmed/8972919.

8. Lucas CJ, Galettis P, Schneider J. The pharmacokinetics and the pharmacodynamics of cannabinoids. *Br J Clin Pharmacol*. 2018;84(11):2477-2482. doi:10.1111/bcp.13710

9. Pacher P, Steffens S, Haskó G, Schindler TH, Kunos G. Cardiovascular effects of marijuana and synthetic cannabinoids: the good, the bad, and the ugly. *Nat Rev Cardiol*. 2018;15(3):151-166. doi:10.1038/nrcardio.2017.130

10. Riera R, Pacheco RL, Bagattini ÂM, Martimbianco ALC. Efficacy and safety of therapeutic use of cannabis derivatives and their synthetic analogs: Overview of systematic reviews. *Phyther Res*. 2022;36(1):5-21. doi:10.1002/ptr.7263

11. Munro S, Thomas KL, Abu-Shaar M. Molecular characterization of a peripheral receptor for cannabinoids. *Nature*. 1993;365(6441):61-65. doi:10.1038/365061a0

12. Howlett AC. International Union of Pharmacology. XXVII. Classification of Cannabinoid Receptors. *Pharmacol Rev*. 2002;54(2):161-202. doi:10.1124/pr.54.2.161

13. Pertwee RG, Howlett AC, Abood ME, et al. International Union of Basic and Clinical Pharmacology. LXXIX. Cannabinoid Receptors and Their Ligands: Beyond CB 1 and CB 2. *Pharmacol Rev*. 2010;62(4):588-631. doi:10.1124/pr.110.003004

14. Howlett AC, Abood ME. CB 1 and CB 2 Receptor Pharmacology. In: ; 2017:169-206. doi:10.1016/bs.apha.2017.03.007

15. Howlett A, Blume L, Dalton G. CB1 Cannabinoid Receptors and their Associated Proteins. *Curr Med Chem*. 2010;17(14):1382-1393. doi:10.2174/092986710790980023

16. Galiegue S, Mary S, Marchand J, et al. Expression of Central and Peripheral Cannabinoid Receptors in Human Immune Tissues and Leukocyte Subpopulations. *Eur J Biochem*. 1995;232(1):54-61. doi:10.1111/j.1432-1033.1995.tb20780.x

17. Pacher P, Mechoulam R. Is lipid signaling through cannabinoid 2 receptors part of a protective system? *Prog Lipid Res*. 2011;50(2):193-211. doi:10.1016/j.plipres.2011.01.001

18. Hanuš L, Breuer A, Tchilibon S, et al. HU-308: A specific agonist for CB 2 , a peripheral cannabinoid receptor. *Proc Natl Acad Sci*. 1999;96(25):14228-14233. doi:10.1073/pnas.96.25.14228

19. Guindon J, Hohmann AG. Cannabinoid CB 2 receptors: a therapeutic target for the treatment of inflammatory and neuropathic pain. *Br J Pharmacol*. 2008;153(2):319-334. doi:10.1038/sj.bjp.0707531

20. Hussain MT, Greaves DR, Iqbal AJ. The Impact of Cannabinoid Receptor 2 Deficiency on Neutrophil Recruitment and Inflammation. *DNA Cell Biol*. 2019;38(10):1025-1029. doi:10.1089/dna.2019.5024

21. Rizzo MD, Henriquez JE, Blevins LK, Bach A, Crawford RB, Kaminski NE. Targeting Cannabinoid Receptor 2 on Peripheral Leukocytes to Attenuate Inflammatory Mechanisms Implicated in HIV-Associated Neurocognitive Disorder. *J Neuroimmune Pharmacol*. 2020;15(4):780-793. doi:10.1007/s11481-020-09918-7

22. Liu Q-R, Aseer KR, Yao Q, et al. Anti-Inflammatory and Pro-Autophagy Effects of the Cannabinoid Receptor CB2R: Possibility of Modulation in Type 1 Diabetes. *Front Pharmacol*. 2021;12:809965. doi:10.3389/fphar.2021.809965

23. Brennecke B, Gazzi T, Atz K, et al. Cannabinoid receptor type 2 ligands: an analysis of granted patents since 2010. *Pharm Pat Anal*. 2021;10(3):111-163. doi:10.4155/ppa-2021-0002

24. Whiting ZM, Yin J, de la Harpe SM, Vernall AJ, Grimsey NL. Developing the Cannabinoid Receptor 2 (CB2) pharmacopoeia: past, present, and future. *Trends Pharmacol Sci*. 2022;43(9):754-771. doi:10.1016/j.tips.2022.06.010

25. Soethoudt M, Grether U, Fingerle J, et al. Cannabinoid CB2 receptor ligand profiling reveals biased signalling and off-target activity. *Nat Commun*. 2017;8(1):13958. doi:10.1038/ncomms13958

26. Han S, Thoresen L, Jung J-K, et al. Discovery of APD371: Identification of a Highly Potent and Selective CB 2 Agonist for the Treatment of Chronic Pain. *ACS Med Chem Lett*. 2017;8(12):1309-1313. doi:10.1021/acsmedchemlett.7b00396

27. Yacyshyn BR, Hanauer S, Klassen P, et al. Safety, Pharmacokinetics, and Efficacy of Olorinab, a Peripherally Acting, Highly Selective, Full Agonist of the Cannabinoid Receptor 2, in a Phase 2a Study of Patients With Chronic Abdominal Pain Associated With Crohn's Disease. *Crohn's Colitis 360*. 2021;3(1). doi:10.1093/crocol/otaa089

28. van der Stelt M, Cals J, Broeders-Josten S, et al. Discovery and Optimization of 1-(4-(Pyridin-2-yl)benzyl)imidazolidine-2,4-dione Derivatives As a Novel Class of Selective Cannabinoid CB2 Receptor Agonists. *J Med Chem*. 2011;54(20):7350-7362. doi:10.1021/jm200916p

29. Mukhopadhyay P, Baggelaar M, Erdelyi K, et al. The novel, orally available and peripherally restricted selective cannabinoid CB 2 receptor agonist LEI-101 prevents cisplatin-induced nephrotoxicity. *Br J Pharmacol*. 2016;173(3):446-458. doi:10.1111/bph.13338

30. Soethoudt M, Hoorens MWH, Doelman W, Martella A, van der Stelt M, Heitman LH. Structure-kinetic relationship studies of cannabinoid CB 2 receptor agonists reveal substituent-specific lipophilic effects on residence time. *Biochem Pharmacol*. 2018;152:129-142. doi:10.1016/j.bcp.2018.03.018

31. Hua T, Vemuri K, Pu M, et al. Crystal Structure of the Human Cannabinoid Receptor CB1. *Cell*. 2016;167(3):750-762.e14. doi:10.1016/j.cell.2016.10.004

32. Shao Z, Yin J, Chapman K, et al. High-resolution crystal structure of the human CB1 cannabinoid

receptor. *Nature*. 2016;540(7634):602-606. doi:10.1038/nature20613

33. Li X, Hua T, Vemuri K, et al. Crystal Structure of the Human Cannabinoid Receptor CB2. *Cell*. 2019;176(3):459-467.e13. doi:10.1016/j.cell.2018.12.011

34. Hua T, Li X, Wu L, et al. Activation and Signaling Mechanism Revealed by Cannabinoid Receptor-Gi Complex Structures. *Cell*. 2020;180(4):655-665.e18. doi:10.1016/j.cell.2020.01.008

35. Xing C, Zhuang Y, Xu T-H, et al. Cryo-EM Structure of the Human Cannabinoid Receptor CB2-Gi Signaling Complex. *Cell*. 2020;180(4):645-654.e13. doi:10.1016/j.cell.2020.01.007

36. Hua T, Vemuri K, Nikas SP, et al. Crystal structures of agonist-bound human cannabinoid receptor CB1. *Nature*. 2017;547(7664):468-471. doi:10.1038/nature23272

37. Shao Z, Yan W, Chapman K, et al. Structure of an allosteric modulator bound to the CB1 cannabinoid receptor. *Nat Chem Biol*. 2019;15(12):1199-1205. doi:10.1038/s41589-019-0387-2

38. Yang X, Wang X, Xu Z, et al. Molecular mechanism of allosteric modulation for the cannabinoid receptor CB1. *Nat Chem Biol*. 2022;18(8):831-840. doi:10.1038/s41589-022-01038-y

39. McAllister SD, Hurst DP, Barnett-Norris J, Lynch D, Reggio PH, Abood ME. Structural Mimicry in Class A G Protein-coupled Receptor Rotamer Toggle Switches. *J Biol Chem*. 2004;279(46):48024-48037. doi:10.1074/jbc.M406648200

40. Krishna Kumar K, Shalev-Benami M, Robertson MJ, et al. Structure of a Signaling Cannabinoid Receptor 1-G Protein Complex. *Cell*. 2019;176(3):448-458.e12. doi:10.1016/j.cell.2018.11.040

41. Díaz Ó, Dalton JAR, Giraldo J. Revealing the Mechanism of Agonist-Mediated Cannabinoid Receptor 1 (CB1) Activation and Phospholipid-Mediated Allosteric Modulation. *J Med Chem*. 2019;62(11):5638-5654. doi:10.1021/acs.jmedchem.9b00612

42. Bow EW, Rimoldi JM. The Structure–Function Relationships of Classical Cannabinoids: CB1/CB2 Modulation. *Perspect Medicin Chem*. 2016;8:PMC.S32171. doi:10.4137/PMC.S32171

43. Kapur A, Hurst DP, Fleischer D, et al. Mutation Studies of Ser7.39 and Ser2.60 in the Human CB 1 Cannabinoid Receptor: Evidence for a Serine-Induced Bend in CB 1 Transmembrane Helix 7. *Mol Pharmacol*. 2007;71(6):1512-1524. doi:10.1124/mol.107.034645

44. Wang X, Jespers W, Prieto-Díaz R, et al. Identification of V6.51L as a selectivity hotspot in stereoselective A2B adenosine receptor antagonist recognition. *Sci Rep*. 2021;11(1):14171. doi:10.1038/s41598-021-93419-x

45. Xu W, Li J, Chen C, et al. Comparison of the Amino Acid Residues in the Sixth Transmembrane Domains Accessible in the Binding-Site Crevices of μ, δ, and κ Opioid Receptors. *Biochemistry*. 2001;40(27):8018-8029. doi:10.1021/bi002490d

46. Javitch JA, Ballesteros JA, Weinstein H, Chen J. A Cluster of Aromatic Residues in the Sixth Membrane-Spanning Segment of the Dopamine D2 Receptor Is Accessible in the Binding-Site Crevice. *Biochemistry*. 1998;37(4):998-1006. doi:10.1021/bi972241y

47. Lin X, Li M, Wang N, et al. Structural basis of ligand recognition and self-activation of orphan GPR52. *Nature*. 2020;579(7797):152-157. doi:10.1038/s41586-020-2019-0

48. Hanson MA, Roth CB, Jo E, et al. Crystal Structure of a Lipid G Protein–Coupled Receptor. *Science (80-)*. 2012;335(6070):851-855. doi:10.1126/science.1215904

49. Jakowiecki J, Filipek S. Hydrophobic Ligand Entry and Exit Pathways of the CB1 Cannabinoid Receptor. *J Chem Inf Model*. 2016;56(12):2457-2466. doi:10.1021/acs.jcim.6b00499

50. Stanley N, Pardo L, Fabritiis G De. The pathway of ligand entry from the membrane bilayer to a lipid G protein-coupled receptor. *Sci Rep*. 2016;6(1):22639. doi:10.1038/srep22639

51. Szlenk CT, GC JB, Natesan S. Does the Lipid Bilayer Orchestrate Access and Binding of Ligands to Transmembrane Orthosteric/Allosteric Sites of G Protein-Coupled Receptors? *Mol Pharmacol*. 2019;96(5):527-541. doi:10.1124/mol.118.115113

52. Bokoch MP, Jo H, Valcourt JR, et al. Entry from the Lipid Bilayer: A Possible Pathway for Inhibition of a Peptide G Protein-Coupled Receptor by a Lipophilic Small Molecule. *Biochemistry*. 2018;57(39):5748-5758. doi:10.1021/acs.biochem.8b00577

53. Sykes DA, Parry C, Reilly J, Wright P, Fairhurst RA, Charlton SJ. Observed Drug-Receptor Association Rates Are Governed by Membrane Affinity: The Importance of Establishing "Micro-Pharmacokinetic/Pharmacodynamic Relationships" at the β 2 -Adrenoceptor. *Mol Pharmacol*. 2014;85(4):608-617. doi:10.1124/mol.113.090209

54. van der Velden WJC, Heitman LH, Rosenkilde MM. Perspective: Implications of Ligand–Receptor Binding Kinetics for Therapeutic Targeting of G Protein-Coupled Receptors. *ACS Pharmacol Transl Sci*. 2020;3(2):179-189. doi:10.1021/acsptsci.0c00012

55. Motulsky HJ, Mahan LC. The kinetics of competitive radioligand binding predicted by the law of mass action. *Mol Pharmacol*. 1984;25(1):1 LP - 9. http://molpharm.aspetjournals.org/content/25/1/1.abstract.

56. Copeland RA, Pompliano DL, Meek TD. Drug–target residence time and its implications for lead optimization. *Nat Rev Drug Discov*. 2006;5(9):730-739. doi:10.1038/nrd2082

57. Yung-Chi C, Prusoff WH. Relationship between the inhibition constant (KI) and the concentration of inhibitor which causes 50 per cent inhibition (I50) of an enzymatic reaction. *Biochem Pharmacol*. 1973;22(23):3099-3108. doi:10.1016/0006-2952(73)90196-2

58. Mastronarde DN. Automated electron microscope tomography using robust prediction of specimen movements. *J Struct Biol*. 2005;152(1):36-51. doi:10.1016/j.jsb.2005.07.007

59. Punjani A, Rubinstein JL, Fleet DJ, Brubaker MA. cryoSPARC: algorithms for rapid unsupervised cryo-EM structure determination. *Nat Methods*. 2017;14(3):290-296. doi:10.1038/nmeth.4169

60. Heymann JB. Single particle reconstruction and validation using Bsoft for the map challenge. *J Struct Biol*. 2018;204(1):90-95. doi:10.1016/j.jsb.2018.07.003

61. Pettersen EF, Goddard TD, Huang CC, et al. UCSF Chimera?A visualization system for exploratory research and analysis. *J Comput Chem*. 2004;25(13):1605-1612. doi:10.1002/jcc.20084

62. Emsley P, Lohkamp B, Scott WG, Cowtan K. Features and development of Coot. *Acta Crystallogr Sect D Biol Crystallogr*. 2010;66(4):486-501. doi:10.1107/S0907444910007493

63. Adams PD, Afonine P V., Bunkóczi G, et al. PHENIX : a comprehensive Python-based system for macromolecular structure solution. *Acta Crystallogr Sect D Biol Crystallogr*. 2010;66(2):213-221. doi:10.1107/S0907444909052925

64. Chen VB, Arendall WB, Headd JJ, et al. MolProbity : all-atom structure validation for macromolecular crystallography. *Acta Crystallogr Sect D Biol Crystallogr*. 2010;66(1):12-21. doi:10.1107/S0907444909042073

65. Chen C, Okayama H. High-efficiency transformation of mammalian cells by plasmid DNA. *Mol Cell Biol*. 1987;7(8):2745-2752. doi:10.1128/mcb.7.8.2745-2752.1987

Acknowledgements

This work was supported by the National Science Fund for Distinguished Young Scholars 32022038 (Tian Hua, T.H.), the National Natural Science Foundation of China grant 91953202 (Z.-J.L.), the CAS Strategic Priority Research Program XDB37030104 (Zhi-Jie Liu[a,b], Z.-J.L.), the National Natural Science Foundation of China grant 31870744 (T.H.), the National Key Research and Development Program of China grant 2018YFA0507000 (T.H.), the Shanghai Rising-Star Program 20QA1406500 (T.H.); the Dutch Research Council (NWO, Vidi #16573) (Laura H. Heitman[c], L.H.H) and (NWO, Navistroke #15851) (Mario van der Stelt[d], M.v.d.S.). and Intramural Research Program of National Institutes of Health/NIAAA (Pal Pacher, P.P.).

Author contributions: Conceptualization, T.H., Z.J.L., J.B. (Jara Bouma[c]), L.V.d.P. (Laura de Paus[d]), A.P.A.J. (Antonius P.A. Janssen[d]), M.v.d.S., L.H.H and P.P.; Conducting Experiments, X.T.L. (Xiaoting Li[a]), H.C. (Hao Chang[a,b]), J.B., L.V.d.P., C.v.d.H (Cas van der Horst[c]), S.S.K (Sanjay Sunil Kumar[c]), L.J.W. (Lijie Wu[a,b]), Y.N.Y. (Yanan Yu[a,b]), R.J.B.H.N.v.d.B (Richard J. B. H. N. van den Berg[d]), A.P.A.J., M.M. (Mohammed Mustafa[f]), P.M. (Partha Mukhopadhyay[e]) , J.P. (Janos Paloczi[e]); Writing-Original Draft, X.T.L., H.C., J.B., L.V.d.P., A.P.A.J., and P.P.; Writing Review & Editing, M.v.d.S., L.H.H., A.L. (Aron Lichtman[f]), P.P. T.H., and Z.J.L.; Visualization, X.T.L., H.C., J.B., A.P.A.J., P.M., L.J.W.; Supervision, M.v.d.S., L.H.H, P.P., T.H., and Z.J.L

[a]iHuman Institute, ShanghaiTech University, Shanghai 201210, China. [b]School of Life Science and Technology, ShanghaiTech University, Shanghai, China. [c]Division of Drug Discovery and Safety, Leiden Academic Center for Drug Research, Leiden University, Oncode Institute, Leiden, the Netherlands. [d]Department of Molecular Physiology, Leiden Institute of Chemistry, Leiden University, Oncode Institute, Leiden, the Netherlands. [e]Laboratory of Cardiovascular Physiology and Tissue Injury, National Institute of Health/National Institute on Alcohol Abuse and Alcoholism, Rockville, MD, USA. [f]Department of Pharmacology and Toxicology, Virginia Commonwealth University, Richmond, VA, USA.

Chapter 3

Discovery of a Photoaffinity Probe that Captures the Active Conformation of the Cannabinoid CB2 Receptor

Discovery of a Photoaffinity Probe that Captures the Active Conformation of the Cannabinoid CB_2 Receptor

Introduction

G protein-coupled receptors (GPCRs) constitute a valuable protein family for drug discovery. The cannabinoid receptor type 2 (CB_2R) is a GPCR expressed in cells of the immune system and is considered as a potential drug target due to its anti-inflammatory effects upon activation.[1] However, its low endogenous levels and inducible nature complicate the understanding of its cellular mechanism-of-action, which makes the drug discovery process more challenging. Chemical and biological tools can aid in the cellular characterization of CB_2R.[2] Antibodies are widely used to study GPCR localization and expression, but CB_2R antibodies suffer from poor quality, low selectivity and large batch to batch variability.[3] Therefore, the development of fluorescent chemical probes targeting CB_2R has become an attractive strategy to study its cellular localization, dynamics and occupancy by drugs.[4–6] For example, previously a probe with a silicon-rhodamine fluorophore was reported that was cell permeable and able to selectively label the CB_2 receptor in CB_2R overexpressing cells as well as in primary cultures of human macrophages.[1]

LEI-121 (**1**, Figure 3.1) was previously developed at Leiden University, a photoaffinity probe that is able to monitor endogenous CB_2R expression levels and their occupancy.[7] LEI-121 is a bifunctional CB_2R-selective probe based on the 5-fluoropyridin-2-yl-benzyl-imidazolidine-2,4-dione scaffold.[8] It includes a diazirine group that forms a covalent bond with CB_2R upon photoactivation. The alkyne click handle allows for ligand binding to the receptor prior to incorporation of a fluorescent tag. This This two-step photoaffinity-based protein profiling (ABPP) strategy prevents a decrease of the binding affinity and reduces non-specific binding due to the bulky fluorophore. LEI-121 was able to label CB_2R in gel-based ABPP using recombinant CB_2R, and detected endogenous CB_2R in primary human immune cells using flow cytometry.[7]

LEI-121 is an inverse agonist and reduces the constitutive activity of CB_2Rs.[7] To complete the toolbox and allow targeting of active CB_2Rs, a new probe that behaves as an agonist was developed. Here the structure-based design and synthesis of photo-affinity probes (**2**-**4**, Figure 3.1) is described, which were based on the recently published structure of LEI-102, a close analog of LEI-121, in complex with the CB_2R elucidated by cryogenic electron microscopy (cryo-EM) (Figure 3.2).[9] LEI-102 is a high-affinity CB_2R ligand (pK_i of 8.0 ± 0.1) with over 1000-fold selectivity over CB_1R. LEI-102 activates the CB_2 receptor as a partial agonist (pEC_{50} 6.9 ± 0.2, E_{max} 76 ± 1%).[9]

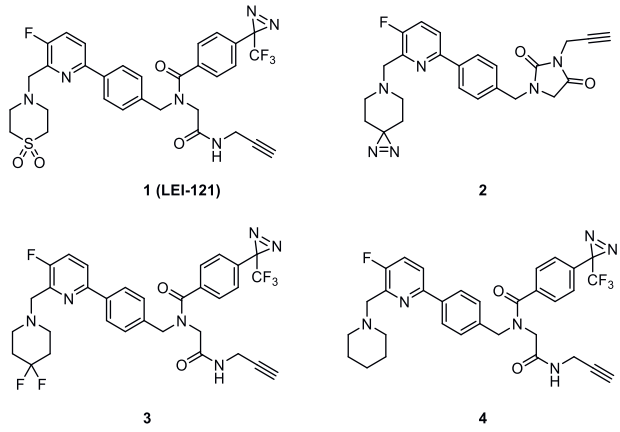

Figure 3.1 The chemical structures of LEI-121 (**1**) and the newly designed two-step photo affinity probes **2-4**.

Results and Discussion

Design

To design novel photoreactive probes, LEI-121 was docked into the recently published CB_2R cryo-EM structure (Figure 3.2B). The CB_2R-G_i structure was reported in complex with CB_2R selective agonist LEI-102 with a resolution 2.9 Å.[9] Considering previous structure activity relationship (SAR) reports[8], the thiomorpholine 1,1-dioxide (**1**) of LEI-121 was substituted for a diaziridine-piperidine (**2**), a difluoropiperidine (**3**) or a piperidine (**4**) to investigate their effect on the potency and functionality of the probe.[8] Furthermore, compound **2** was designed to more closely resemble the structure of LEI-102, in an attempt to create an agonist probe. The hypothesis is that the positioning of the propargylamide in LEI-121 is responsible for its inverse agonistic activity by occupying in a subpocket, which may stabilize the inactive receptor conformation. This resembles the change in functionality, we have previously reported with a lipophilic spacer on this scaffold.[10] In compound **2** the propargyl moiety was introduced on the imidazolidine moiety to act as a ligation handle and the diazirine was moved to the piperidine. Of note, compound **2** had a similar binding pose as LEI-102 in the CB_2R structure (Figure 3.2C).

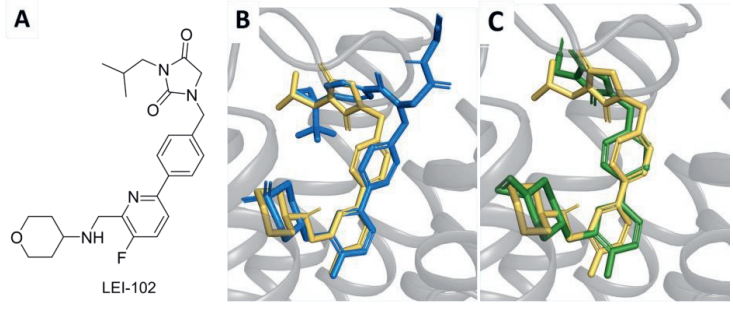

Figure 3.2 The chemical structure of LEI-102 (A), and the docked poses of LEI-121 (blue, B) and **2** (green, C) overlayed with the cryo-EM structure of LEI-102 (yellow). Docking was performed in the cryo-EM structure of CB_2R containing LEI-102 (PDB: 8GUT).

Synthesis

The synthesis of probes **1**,**3** and **4** started with oxidation of 6-bromo-3-fluoro-2-methylpyridine with *m*-CPBA followed by a Boekelheide rearrangement to yield **5**. Conjugation of **5** and (4-formylphenyl) boronic acid through a Suzuki coupling led to pyridyl benzaldehyde **6** (Scheme 3.1). Subsequent mesylation (**6** → **7**) and nucleophilic substitution with the desired piperidines gave the thiomorpholine 1,1-dioxide **8**, 4,4-difluoropiperidine **9** and piperidine **10** intermediates. The alkyne click handle was introduced via reductive amination of 2-amino-*N*-propargyl acetamide (**12**), obtained through HBTU mediated condensation of Boc-Gly-OH with propargylamine followed by Boc deprotection, and intermediates **8**-**10** to gain **13**-**15**. Finally, conjugation of 4-(3-(trifluoromethyl)-3*H*-diazirin-3-yl)benzoic acid to **13**-**15** afforded the probes **1**,**3** and **4**.

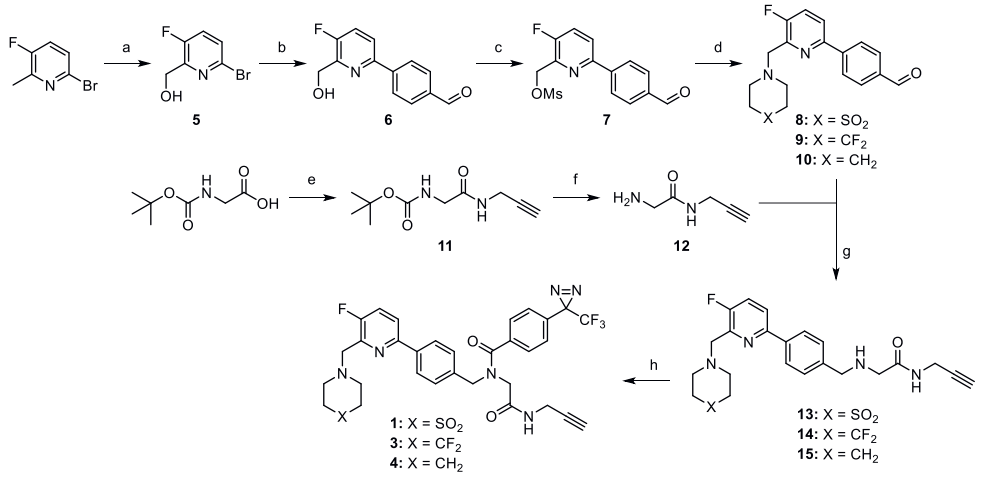

Scheme 3.1 The Synthesis of compounds **1**, **3** and **4**. Reagents and conditions: a) Step 1: *m*-CPBA (1.8 eq), 0 °C-RT, DCM (0.2 M), 4 days; Step 2: TFAA (2.2 eq), 0 °C-55 °C, 3 h; Step 3: K_2CO_3 (2.3 eq), THF:MeOH (20:1), 17 h, 35% (three steps); b) (4-formylphenyl) boronic acid (1.5 eq), $Pd(PPh_3)_4$ (0.1 eq), K_2CO_3 (6 eq), toluene : EtOH (0.4 M, 4 : 1 v/v), 80 °C, 96 h, 80%; c) DiPEA (2 eq), MsCl (1 eq), DCM (0.2 M), 0 °C, 1 h, 75%; d) **8**: Thiomorpholine 1,1-dioxide / **9**: 4,4 difluoropiperidine/ **10**: piperidine (1.2 eq), K_2CO_3 (3.6 eq), ACN (0.2 M), 60 °C, 3 h, 70-80%; e) propargylamine (1 eq), *N*-methylmorpholine (1.1 eq), HOBt (1.1 eq), EDC.HCl (1.1 eq), DCM (0.2 M), RT, 6 h, 74%; f) HCl (4 M, 1.6 eq) in dioxane, RT, 2.5 h, 46%; g) acetic acid (1 eq), $NaBH(OAc)_3$ (3.6 eq), THF (0.1 M), RT, 16 h, 43-54%; h) 4-(3-(trifluoromethyl)-3H-diazirin-3-yl)benzoic acid (1 eq), HBTU (1.5 eq), DiPEA (3 eq), DCM (0.1 M), RT, 1 h, 28-31%.

The construction of probe **2** was similar to the synthesis of LEI-102.[9] To start, reductive amination of 4-bromobenzaldehyde and 2-aminoacetamide led to compound **16**. After cyclization the formed imidazolidinedione **17** was alkylated with 3-bromo-1-(trimethylsilyl)-1-propyne (**18**) and subsequent borylation gave building block **19**. Simultaneously, previously synthesized (6-bromo-3-fluoropyridin-2-yl)methanol (**5**) was mesylated (**20**) followed by substituted of the mesyl with piperidin-4-one to gain ketone **21**. Suzuki coupling of **19** and **21** gave key intermediate **22**. The reaction conditions used for the conversion of the ketone in **22** to a diazirine led to simultaneous demasking of the alkyne function to give the photoaffinity probe **2**.

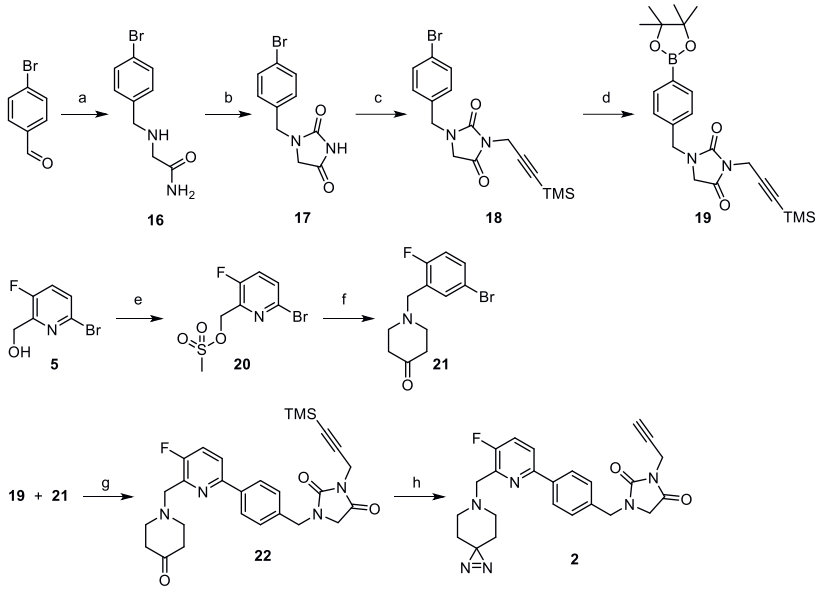

Scheme 3.2 The synthesis of the hydantoin probe **2**. Reagents and conditions: a) Step 1: 2-aminoacetamide hydrochloride (1.0 eq), NaOH (1.1 eq), MeOH:H_2O (0.3 M, 5:1 (v/v)), RT, 18 h; Step 2: $NaBH_4$ (2.1 eq), 18 h, 91% (two steps); b) CDI (2.1 eq), DMAP (2.1 eq), ACN (0.1 M), 60 °C, 70 h, 37%; c) 3-bromo-1-(trimethylsilyl)-1-propyne (1.2 eq), K_2CO_3 (1 eq), DMF (0.3 M), 50 °C, 16 h, 61%; d) bis(pinacol)diborane (1.5 eq), KOAc (4 eq), $Pd(dppf)Cl_2$ (0.5 eq), 1,4 dioxane (0.1 M), 80 °C, 16 h, used as crude; e) Et_3N (2.3 eq), MsCl (1.7 eq), THF (0.2 M), 0 °C-RT, 1 h, 75%; f) 4-piperidone hydrochloride (1.2 eq), K_2CO_3 (3 eq), ACN (0.2 M), 70 °C, 48 h, 78%; g) K_2CO_3 (1.8 eq), $Pd(PPh_3)_4$ (0.1 eq), toluene:EtOH (0.1 M, 4:1 (v/v)), 50 °C, 16 h, 29%; h) Step 1: NH_3 (g), MeOH (0.2 M), 0 °C, 5 h; Step 2: NH_2SO_3H (1.5 eq), MeOH (0.2 M), 16 h, RT, Step 3: I_2, MeOH, 0 °C 15 min., 27% (three steps).

Molecular Pharmacology

Next probes **1**-**4** were tested in a [^{3}H]CP-55,940 radioligand displacement assay to determine their affinity (pK_i or displacement %) for the CB_2R and CB_1R. Compounds with less than 50% displacement on CB_1R at 1 µM were considered inactive. Additionally, their potency (EC_{50}) and maximal efficacy (E_{max}) were measured in a [^{35}S]-GTPγS functional assay. The results are summarized in Table 3.1.

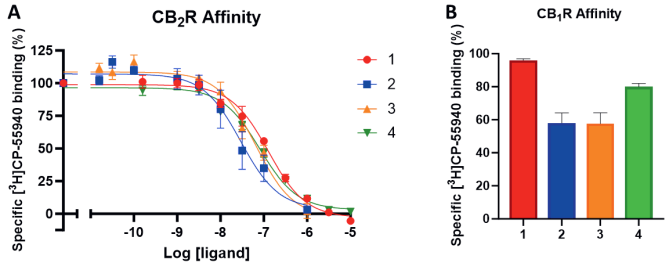

Figure 3.3 The affinity (pK_i or displacement) of compounds **1**-**4** on CB_2R (A) and CB_1R (B). Binding was normalized to binding of [^{3}H]CP-55,940 at 10 µM. Percentage displacement was determined with 1 µM compound. Data are presented as the mean ± SEM from three independent experiment performed in triplicate (CB_1R two experiments in duplicate).

Table 3.1 The Affinity and Potency of the two-step probes **1-4** on CB_1R and CB_2R.

Probe	CB_2R				CB_1R	
	pK_i ± SEM	pEC_{50} ± SEM	E_{max} (% ± SEM)	Displacement at 1 µM (%)	pEC_{50} ± SEM	E_{max} (% ± SEM)
LEI-102	8.6 ± 0.3	6.9 ± 0.2	76 ± 1	< 50	n.d.	n.d.
LEI-121[9]	7.2 ± 0.4	6.6 ± 0.2	-50 ± 7	<50	n.d.	n.d.
1 (LEI-121)	7.24 ± 0.06	7.06 ± 0.19	-35 ± 3	4 ± 1	6.08 ± 0.21	-26 ± 4
2	7.89 ± 0.13	8.56 ± 0.56	58 ± 4	42 ± 6	6.97 ± 0.13	35 ± 3
3	7.59 ± 0.09	7.75 ± 0.19	-26 ± 2	42 ± 7	7.00 ± 0.23	-16 ± 2
4	7.42 ± 0.05	7.10 ± 0.33	-28 ± 2	20 ± 2	5.98 ± 0.16	-19 ± 3

Binding affinities (pK_i or displacement %) and potency (pEC_{50}) were determined with a [^{3}H]CP-55,940 displacement assay and [^{35}S]GTPγS functional assay respectively on CBR overexpressing CHO membranes. Potency values (pEC_{50}) were obtained for compounds with displacement ≥ 35% using a [^{35}S]GTPγS assay. Efficacy (E_{max}) was normalized to the effect of 10 µM CP-55,940. Data are presented as the mean ± SEM from three independent experiments performed in triplicate.

All probes showed improved affinity for CB_2R compared to LEI-121 (Figure 3.3, Table 3.1), while retaining selectivity over CB_1R. This was accompanied by increased activity on hCB_2R by probes **2**-**4** compared to LEI-121 (Figure 3.4, Table 3.1). Probe **2** had the highest affinity (pK_i 7.89 ± 0.13) and activity (pEC_{50} 8.56 ± 0.56), which was 15-fold increased compared to LEI-102.

Compounds **3** and **4** behaved as inverse agonists with an E_{max} ≈ -30%, comparable to LEI-121 (**1**).[8] In contrast, probe **2** acted as a partial agonist (E_{max} 58% ± 4) (Figure 3.4). While probe **2** at 1 µM showed less than 50% radioligand displacement at the CB_1R, the compound did show some activity in the G protein activation assay. Of note, probe **2** was 77-fold selective over CB_1R and elicited 40-fold more potent receptor activation for CB_2R compared to CB_1R.

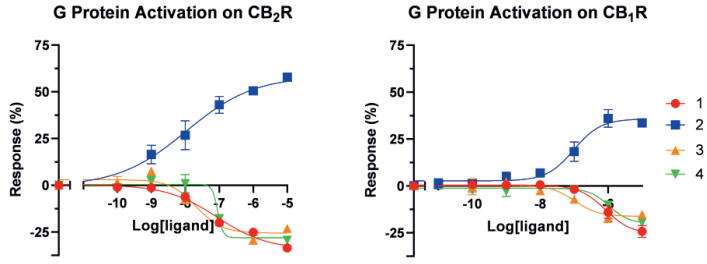

Figure 3.4 G protein activation of CB_2R and CB_1R by compounds **1**-**4** were measured with [^{35}S]GTPγS functional assays on CBR overexpressing CHO membranes. The results showed the switch of **2** from inverse agonist to partial agonist. Data points are presented as the mean ± SEM of at least three independent experiments performed in triplicate.

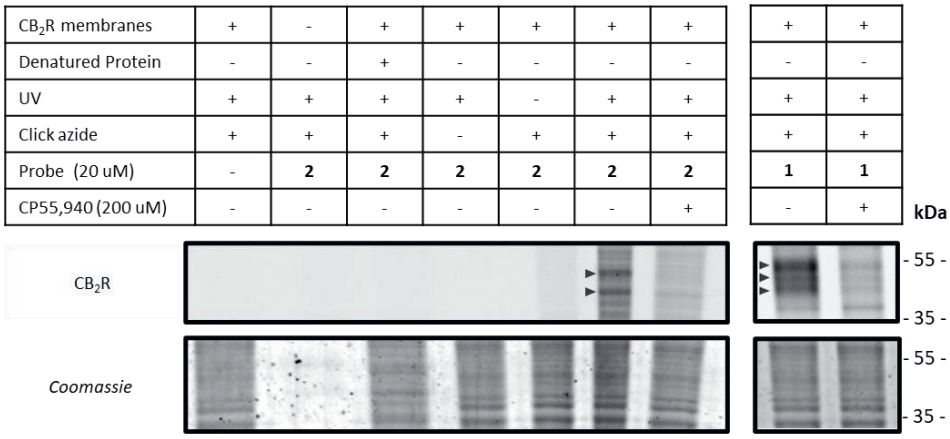

Figure 3.5 Probes **1** and **2** were able to label CB_2R (45-55 kDa) in CB_2R-overexpressing CHO membranes. Denaturation of the protein prior to probe incubation, or omitting the UV irradiation step prevented labelling of CB_2R by the probes. Additionally, no signal was detected in the absence of either click azide or probe. Labelling was outcompeted by CP-55,940. The gels are representative of two independent experiments.

Since probe **2** was the only compound that behaved as a partial agonist, its ability to visualize CB_2R was analysed by two-step pAfBPP. Probe **1** was used as a positive control. To this end, membrane preparations of hCB_2R-overexpressing CHO cells were incubated with probe **1** or **2**. Cross-linking was effected by UV-irradiation (λ = 350 nm, 5 min) using a CaproBox, a device used for controlled irradiation of biological samples with simultaneous cooling at 4 °C, to counteract the heat induced by the irradiation. Next, the membranes were subjected to copper(I)-catalysed click reaction conditions, utilizing Cy5-N_3 as the fluorescent azide to analyse the probe–protein complex by SDS-PAGE and in-gel fluorescence imaging. In this manner, two major bands with an apparent molecular weight of ~47 and ~41 kDa (Figure 3.5) were visualized for both probes, and these were absent in membranes from wild-type CHO cells. Heat-induced denaturation prior to probe incubation also resulted in a loss of fluorescent bands, indicating that the recognition is dependent on an intact three-dimensional protein conformation. The bands were also absent in non-UV treated samples, demonstrating that the probe does not covalently interact with CB_2Rs in the absence of irradiation. Furthermore, omission of the click-mixture showed that labelling was dependent on copper(I)-catalysed azide alkyne click ligation (Figure 3.5). Preincubation with CP-55,940 was able to prevent the CB_2R labelling by probes **1** and **2**. Of note, probe **2** did show two off-targets with a molecular weight around 30 kDa not present for the original LEI-121 and derivatives.[7] The identity of the off-targets is unknown, but one of the off-targets is also competed out by CP-55,940.

The labelling pattern of probes **1** and **2** is slightly different. Probe **2** labels two distinct bands, while labelling with probe **1** yields multiple intense bands. GPCRs including CB_2R can have a wide variety of post translational modifications such as N-glycosylation and phosphorylation.[11,12] Phosphorylation patterns change depending on receptor activity, thus a partial agonist probe may recognize a different receptor population than an inverse agonistic probe.[13]

Conclusion

A structure-based approach exploiting the recently published cryo-EM structure of the CB_2R in complex with LEI-102 was used to develop a new bifunctional photoaffinity probe that stabilized the active conformation of CB_2R. Probe **2** had high binding affinity (pK_i 7.89 ± 0.13), selective of CB_1R and behaved as a partial agonist (EC_{50} 8.56 ± 0.56 with, E_{max} 58% ± 4). Probe **2** labelled the CB_2R upon photoactivation

in a slightly different manner compared to LEI-121 (probe **1**), which is an inverse agonist. This may suggest that the stabilization of a different receptor conformations result in a different labelling pattern, which could be dependent on different post-translational modifications.[10,11] Probe **2** has potential to be used to isolate the CB_2R in the active state using a biotin-reporter and affinity enrichment from primary cells and tissues, which may facilitate the identification of post-translational modifications and potential protein interaction partners of the active receptor. To conclude, a novel photoaffinity probe was developed for the CB_2R that may hold promise to study different receptor conformations in relation to its cellular function.

Experimental Section

Chemistry

General Remarks

All reagents and solvents were purchased from commercial sources and were of analytical grade (Sigma-Aldrich, BroadPharm®[®]) and used without further purification. All moisture sensitive reactions were performed under inert atmosphere. Solvents were dried using 4 Å molecular sieves prior to use when anhydrous conditions were required. Water used in reactions was always demineralized. Analytical thin-layer chromatography (TLC) was routinely performed to monitor the progression of a reaction and was conducted on Merck Silica gel 60 F254 plates. Reaction compounds on the TLC plates were visualized by UV irradiation (λ_{254}) and/or spraying with potassium permanganate solution (K_2CO_3 (40 g), $KMnO_4$ (6 g), and H_2O (600 mL)), ninhydrin solution (ninhydrin (1.5 g), n-butanol (100 mL) and acetic acid (3.0 mL)) or molybdenum solution ($(NH_4)_6MO_7O_{24}{\cdot}4H_2O$ (25 g/L) and $(NH_4)_4Ce(SO_4)_4{\cdot}2H_2O$ (10 g/L) in sulfuric acid (10%)) followed by heating as appropriate. Purification by flash column chromatography was performed using Screening Devices B.V. silica gel 60 (40-63 µm, pore diameter of 60 Å). Solutions were concentrated using a Heidolph laborata W8 4000 efficient rotary evaporator with a Laboport vacuum pump. Analytical purity was determined with liquid chromatography-mass spectrometry (LC-MS) using a Finnigan LCQ Advantage MAX apparatus with electrospray ionization (ESI), equipped with a Phenomenex Gemini 3 µm NX-C18 110Å column (50x4.6mm), measuring absorbance at 254 nm using a Waters 2998 PDA UV detector and the m/z ratio by using an Acquity Single Quad (Q1) detector. Injection was with the Finnigan Surveyor Autosampler Plus and pumped through the column with the Finnigan Surveyor LC pump plus to be analysed with the Finnigan Surveyor PDA plus detector. Samples were analysed using eluent gradient 10% → 90% ACN in MilliQ water (+ 0.1% TFA (v/v)). For purification by mass guided preparative High-Performance Liquid Chromatography (Prep-HPLC) was performed on a Waters AutoPurification HPLC/MS apparatus with a Gemini prep column 5 µm 18C 110 Å (150x21.2mm), Waters 2767 Sample manager, Waters 2545 Binary gradient module, Waters SFO System fluidics organizer, Waters 515 HPLC pump M, Waters 515 HPLC pump L attached to a Waters SQ detector Acquity Ultra performance LC. A five column volume purification protocol was applied with the eluents A: 0.2% aq. TFA, B: ACN, flow 25 mL/min, with a minimum start gradients of 0% to maximum end gradient of 100% of B. All final compounds had a purity > 95%. ^1H and ^{13}C nuclear magnetic resonance (NMR) spectra were recorded on a Bruker AV 300 (300/75 MHz), AV 400 (400/100 MHz) or AV 500 (500/125 MHz) spectrometer at ambient temperature using $CDCl_3$ or MeOD as solvent. Chemical shifts (δ) are referenced in parts per million (ppm) with tetramethylsilane (TMS) or $CDCl_3$ resonance as the internal standard peak ($CDCl_3$/TMS, δ 0.00 for ^1H (TMS), δ 77.16 for ^{13}C ($CDCl_3$)). The internal standard peaks for MeOD solvent are δ 3.31 (^1H) and 49.00 (^{13}C). Multiplicity is reported as s = singlet, d = doublet, dd = doublet of doublet, dt = doublet of triplet, t = triplet, q = quartet, p = quintet, hept = heptet, m = multiplet. Coupling-constants (*J*) are reported in Hertz (Hz).

Synthesis of Probes 1, 3, and 4.

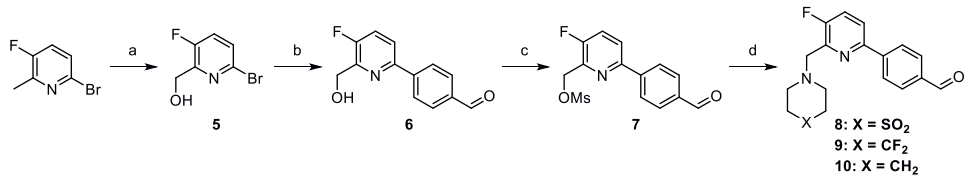

Scheme 3.3 Synthesis of Intermediates **8**-**10**. Reagents and conditions: a) Step 1: *m*-CPBA (1.8 eq), 0 °C-RT, DCM (0.2 M), 4 days; Step 2: TFAA (2.2 eq), 0 °C-55 °C, 3 h; Step 3: K_2CO_3 (2.3 eq), THF:MeOH (20:1), 17 h, 35% (three steps); b) (4-formylphenyl) boronic acid (1.5 eq), $Pd(PPh_3)_4$ (0.1 eq), K_2CO_3 (6 eq), toluene : EtOH (0.4 M, 4 : 1 v/v), 80 °C, 96 h, 80%; c) DiPEA (2 eq), MsCl (1 eq), DCM (0.2 M), 0 °C, 1 h, 75%; d) **8**: Thiomorpholine 1,1-dioxide / **9**: 4,4 difluoropiperidine/ **10**: piperidine (1.2 eq), K_2CO_3 (3.6 eq), ACN (0.2 M), 60 °C, 3 h, 70-80%.

(6-Bromo-3-fluoropyridin-2-yl)methanol (5): To a stirred and cooled (0 °C) mixture under inert atmosphere of 6-bromo-3-fluoro-2-methylpyridine (10.7 g, 56.3 mmol, 1 eq) in DCM (370 mL) was added portion-wise *m*-CPBA (23.6 g, 70-75%, 100 mmol, 1.8 eq). The reaction mixture was stirred at room temperature (RT) for 4 days. Sat. $NaHCO_3$ (aq) and sat. $Na_2S_2O_3$ (aq) was added (1:1, v/v) and the layers were separated. The aqueous layer was extracted thrice with DCM. The combination of organic layers was dried ($MgSO_4$), filtered, and concentrated under reduced pressure. To the residue was added TFAA (17 mL, 122 mmol, 2.2 eq) at 0 °C. After 15 minutes the temperature was increased to 55 °C for 3 h. The mixture was concentrated under reduced pressure, redissolved in DCM and sat. Na_2CO_3 (aq) was added. The layers were separated and the organic layer was washed with sat. $NaHCO_3$ (aq). The solvent was evaporated and the residue was dissolved in THF:MeOH (20:1, v/v) and K_2CO_3 (18.2 g, 132 mmol, 2.3 eq) was added. After 17 h H_2O was added and the layers were separated. The aqueous layer was extracted thrice with EtOAc. The combination of organic layers was dried ($MgSO_4$), filtered, and the solvent evaporated under reduced pressure. The crude product was purified with flash column chromatography (SiO_2, 10-20% EtOAc in pentane) to yield a white solid (5.79 g, 19.7 mmol, 35%). ^{1}H-NMR (500 MHz, $CDCl_3$) δ 7.42 (ddt, *J* = 8.5, 3.5, 0.7 Hz, 1H), 7.29 (t, *J* = 8.5 Hz, 1H), 4.80 (d, *J* = 3.3 Hz, 2H). ^{13}C-NMR (126 MHz, $CDCl_3$) δ 156.10 (d, *J* = 256.2 Hz), 148.74 (d, *J* = 19.1 Hz), 135.01 (d, *J* = 2.9 Hz), 128.17 (d, *J* = 4.2 Hz), 126.09 (d, *J* = 19.8 Hz), 59.07.

4-(5-Fluoro-6-(hydroxylmethyl) pyridine-2-yl) benzaldehyde (6): Under inert atmosphere of a degassed stirred mixture of **5** (1.90 g, 9.2 mmol, 1 eq), (4-formylphenyl) boronic acid (2.08 g, 13.8 mmol, 1.5 eq) and $Pd(PPh_3)_4$ (1.07 g, 0.9 mmol, 0.1 eq) in toluene:EtOH (22 mL, 4:1 (v/v)) was added aqueous K_2CO_3 (aq) (27.7 mL, 0.2 M, 55.3 mmol, 6 eq) and mixture was heated (80 °C) for 96 h. The mixture was filtered and diluted with H_2O (30 mL) and EtOAc (40 mL). The layers were separated and the aqueous layer extracted thrice with EtOAc. The combination of organic layers was washed with brine, dried ($MgSO_4$), filtered, and the solvent evaporated under reduced pressure. The crude product was purified with flash column chromatography (SiO_2, 30-80% EtOAc in pentane) to yield a yellow solid (1.71 g, 7.4 mmol, 80%). ^{1}H-NMR (500 MHz, $CDCl_3$) δ 10.08 (s, 1H), 8.14 (d, *J* = 8.2 Hz, 2H), 7.99 (d, *J* = 8.2 Hz, 2H), 7.77 (dd, *J* = 8.5, 3.6 Hz, 1H), 7.52 (t, *J* = 8.6 Hz, 1H), 4.87 (d, *J* = 1.8 Hz, 2H), 4.04 (s, 1H). ^{13}C NMR (126 MHz, $CDCl_3$) δ 191.89, 156.22 (d, *J* = 258.2 Hz), 150.62 (d, *J* = 4.7 Hz), 147.21 (d, *J* = 18.6 Hz), 143.23, 136.41, 130.20, 127.29, 123.83 (d, *J* = 18.4 Hz), 121.21 (d, *J* = 4.1 Hz), 59.20.

(3-Fluoro-6-(4-formylphenyl) pyridin-2-yl) methylmethanesulfonate (7): To a cooled (0 °C) and stirred mixture of **6** (1.41 g, 6.1 mmol, 1 eq) in DCM (30 mL) was added DiPEA (2.2 mL, 12.2 mmol, 2 eq) and methanesulfonyl chloride (0.5 mL, 6.1 mmol, 1 eq). After stirring at 0 °C for 1 h the reaction was diluted with H_2O (16 mL) and DCM (10 mL). The layers were separated and the aqueous layer was extracted thrice with DCM. The combination of organic layers was dried ($MgSO_4$), filtered and the solvent evaporated under reduced pressure. The crude product was purified with flash column

chromatography (SiO_2, 30-50% EtOAc in pentane) to yield a yellow solid (1.42 g, 4.6 mmol, 75%). ^{1}H-NMR (500 MHz, $CDCl_3$) δ 10.08 (s, 1H), 8.15 (d, *J* = 8.1 Hz, 2H), 7.98 (d, *J* = 8.3 Hz, 2H), 7.89 (dd, *J* = 8.5 Hz, 2.3 Hz, 1H), 7.61 (t, *J* = 8.7 Hz, 1H), 5.49 (d, *J* = 2.1 Hz, 2H), 3.14 (s, 3H). ^{13}C NMR (101 MHz, $CDCl_3$) δ 191.95, 159.43, 156.81, 143.09, 141.44 (d, *J* = 15.2 Hz), 136.72, 130.39, 127.54, 125.01 (d, *J* = 19.4 Hz), 123.60 (d, *J* = 4.5 Hz), 66.70 (d, *J* = 1.9 Hz), 38.32.

4-(6-((1,1-Dioxidothiomorpholino) methyl)-5-fluoropyridin-2-yl) benzaldehyde (8): A stirred mixture of **7** (0.66 g, 2.1 mmol, 1 eq), thiomorpholine 1,1-dioxane (0.35 g, 2.6 mmol, 1.2 eq) and K_2CO_3 (1.07 g, 7.7 mmol, 3.6 eq) in acetonitrile (12 mL) was heated (60 °C) for 3 h. The reaction mixture was diluted at RT with H_2O (15 mL) and DCM (15 mL), the layers were separated and the aqueous layer was extracted thrice with DCM. The combination of organic layers was washed with brine, dried ($MgSO_4$), filtered and the solvent evaporated under reduced pressure. The crude product was purified with flash column chromatography (SiO_2, 30-50% EtOAc in pentane) to yield a yellow solid (0.52 g, 1.5 mmol, 70%). ^{1}H-NMR (500 MHz, $CDCl_3$) δ 10.07 (s, 1H), 8,11 (d, *J* = 8.3 Hz, 2H), 7.99 (d, *J* = 8.4 Hz, 2H), 7.78 (dd, *J* = 8.6, 3.6 Hz, 1H), 7.52 (t, *J* = 8.8 Hz, 1H), 4.03 (d, *J* = 2.4 Hz, 2H), 3.21 (dd, *J* = 7.1, 3.6 Hz, 4H), 3.09 (dd, *J* = 7.5, 3.3 Hz, 4H). ^{13}C NMR (126 MHz, $CDCl_3$) δ 191.96, 158.22 (d, *J* = 260.0 Hz), 151.47 (d, *J* = 4.8 Hz), 144.93 (d, *J* = 15.1 Hz), 136.51, 130.33, 127.42, 124.33 (d, *J* = 20.2 Hz), 121.92 (d, *J* = 4.5 Hz), 56.68 (d, *J* = 2.8 Hz), 51.67, 50.61.

4-(6-((4,4-Difluoropiperidin-1-yl) methyl)-5-fluoropyridin-2-yl) benzaldehyde (9): A stirred mixture of **7** (0.66 g, 2.1 mmol, 1 eq) 4,4-difluoropiperidine hydrochloride (0.41 g, 2.6 mmol, 1.2 eq) and K_2CO_3 (1.07 g, 7.7 mmol, 3.6 eq) in acetonitrile (12 mL) was heated (60 °C) for 3 h. The reaction mixture was diluted at RT with H_2O (15 mL) and DCM (15 mL), the layers were separated and the aqueous layer was extracted thrice with DCM. The combination of organic layers was washed with brine, dried ($MgSO_4$), filtered and the solvent evaporated under reduced pressure. The crude product was purified with flash column chromatography (SiO_2, 70-100% EtOAc in pentane) to yield a yellow solid (0.57 g, 1.7 mmol, 80%). ^{1}H-NMR (500 MHz, $CDCl_3$) δ 10.06 (s, 1H), 8.13 (d, *J* = 8.3 Hz, 2H), 7.97 (d, *J* = 8.5 Hz, 2H), 7.74 (dd, *J* = 8.6, 3.6 Hz, 1H), 7.49 (t, *J* = 8.7 Hz, 1H), 3.90 (d, *J* = 2.5 Hz, 2H), 2.76 (t, *J* = 5.7 Hz, 4H), 2.02 (hept, *J* = 5.8 Hz, 4H). ^{13}C-NMR (126 MHz, $CDCl_3$) δ 192.03, 158.26 (d, *J* = 260.0 Hz), 151.18 (d, *J* = 4.9 Hz), 145.87 (d, *J* = 15.1 Hz), 143.91, 136.37, 130.28, 127.43, 124.02 (d, *J* = 20.3 Hz), 121.98 (t, *J* = 241.5 Hz), 121.50 (d, *J* = 4.4 Hz), 57.09, 49.96 (t, *J* = 5.3 Hz), 34.10 (t, *J* = 22.9 Hz).

4-(5-Fluoro-6-(piperidin-1-ylmethyl) pyridin-2-yl) benzaldehyde (10): A stirred mixture of **7** (0.66 g, 2.1 mmol, 1 eq), piperidine (0.22 g, 2.6 mmol, 1.2 eq) and K_2CO_3 (1.07 g, 7.7 mmol, 3.6 eq) in acetonitrile (12 mL) was heated (60 °C) for 3 h. The reaction mixture was diluted at RT with H_2O (15 mL) and DCM (15 mL), the layers were separated and the aqueous layer was extracted thrice with DCM. The combination of organic layers was washed with brine, dried ($MgSO_4$), filtered and the solvent evaporated under reduced pressure. The crude product was purified with flash column chromatography (SiO_2, 30% EtOAc in pentane) to yield a white solid (0.51 g, 1.7 mmol, 73%). ^{1}H-NMR (500 MHz, $CDCl_3$) δ 10.06 (s, 1H), 8.14 (d, *J* = 8.3 Hz, 2H), 7.96 (d, *J* = 8.4 Hz, 2H), 7.71 (dd, *J* = 8.6, 3.5 Hz, 1H), 7.46 (t, *J* = 8.7 Hz, 1H), 3.83 (d, *J* = 2.6 Hz, 2H), 2.59 (t, *J* = 5.4 Hz, 4H), 1.61 (p, *J* = 5.6 Hz, 4H), 1.46 – 1.37 (m, 2H). ^{13}C-NMR (126 MHz, $CDCl_3$) δ 192.07, 158.35 (d, *J* = 260.0 Hz), 150.95 (d, *J* = 4.8 Hz), 146.50 (d, *J* = 15.2 Hz), 144.19, 136.31, 130.25, 127.48, 123.77 (d, *J* = 20.3 Hz), 121.13 (d, *J* = 4.4 Hz), 58.64 (d, *J* = 3.0 Hz), 54.53, 26.08, 24.25.

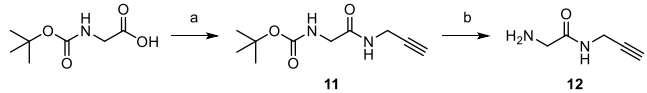

Scheme 3.4 Synthesis of intermediate **12**. Reagents and Conditions: e) propargylamine (1 eq), *N*-methylmorpholine (1.1 eq), HOBt (1.1 eq), EDC.HCl (1.1 eq), DCM (0.2 M), RT, 6 h, 74%; f) HCl (4 M, 1.6 eq) in dioxane, RT, 2.5 h, 46%.

***tert*-Butyl (2-oxo-2-(prop-2-yn-1-ylamino) ethyl) carbamate (11)**: A mixture of *N*-(*tert*-butoxycarbonyl) glycine (5.78 g, 33.0 mmol, 1.1 eq), propargylamine (1.9 mL, 30 mmol, 1 eq), *N*-methylmorpholine (3.6 mL, 33.0 mmol, 1.1 eq), HOBt (5.05 g, 33.0 mmol, 1.1 eq) and EDC.HCl (5.89 g, 33.0 mmol, 1.1 eq) in anhydrous DCM (125 mL) was stirred at RT for 6 h. The mixture was diluted with EtOAc and the combination of organic layers was washed with 0.4 M HCl, H_2O and brine, dried ($MgSO_4$), filtered and the solvent evaporated under reduced pressure. The crude product was purified with recrystallization in EtOAc and hexane to yield a white solid (4.70 g, 22.1 mmol, 74%). ^{1}H-NMR (500 MHz, $CDCl_3$) δ 6.75 (s, 1H), 5.36 (t, *J* = 5.9 Hz, 1H), 4.07 (dd, *J* = 5.4, 2.6 Hz, 2H), 3.84 (d, *J* = 5.7 Hz, 2H), 2.23 (t, *J* = 2.6 Hz, 1H), 1.46 (s, 9H). ^{13}C-NMR (101 MHz, $CDCl_3$) δ 183.38, 169.49, 80.60, 79.22, 71.92, 44.51, 29.27, 28.42.

2-Amino-*N*-(prop-2-yn-1-yl) acetamide. HCl (12): A mixture of 4 M HCl in dioxane (10 mL, 40 mmol, 1.6 eq) and **11** (4.70 g, 24.4 mmol, 1eq) was stirred at RT for 2.5 h. The solvent was evaporated under reduced pressure and the crude product was purified with recrystallization in MeOH to yield a white solid (1.67 g, 11.2 mmol, 46%). ^{1}H-NMR (500 MHz, MeOD) δ 4.05 (d, *J* = 2.6 Hz, 2H), 3.64 (s, 2H), 2.62 (t, *J* = 2.6 Hz, 1H). ^{13}C-NMR (101 MHz, MeOD) δ 171.91, 80.62, 72.72, 41.43, 29.55.

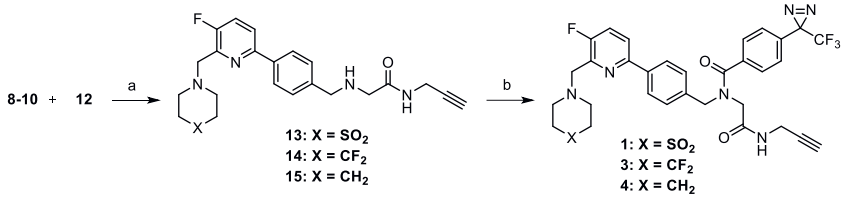

Scheme 3.5 Synthesis of Probes **1**,**3** and **4**. Reagents and Conditions: g) acetic acid (1 eq), $NaBH(OAc)_3$ (3.6 eq), THF (0.1 M), RT, 16 h, 43-54%; h) 4-(3-(trifluoromethyl)-3H-diazirin-3-yl)benzoic acid (1 eq), HBTU (1.5 eq), DiPEA (3 eq), DCM (0.1 M), RT, 1 h, 28-31%.

2-((4-(6-((1,1-Dioxidothiomorpholino) methyl)-5-fluoropyridin-2-yl) benzyl) amino)-*N*-(prop-2-yn-1-yl) acetamide (13): A mixture of **8** (0.24 g, 0.7 mmol, 1 eq), **12** (0.15 g, 1.4 mmol, 2 eq), acetic acid (0.04 mL, 0.7 mmol, 1 eq) and $NaBH(OAc)_3$ (0.53 g, 2.5 mmol, 3.6 eq) in THF (9 mL) was stirred at RT for 16 h. The reaction was diluted with sat. $NaHCO_3$ (aq, 8 mL) and DCM (10 mL). The layers were separated and the aqueous layer extracted thrice with DCM. The combination of organic layers was dried ($MgSO_4$), filtered and the solvent evaporated under reduced pressure. The crude product was purified with flash column chromatography (SiO_2, 5% MeOH (with 1% Et_3N) in DCM) to yield a yellow oil (0.13 g, 0.30 mmol, 43%). ^{1}H-NMR (500 MHz, $CDCl_3$) δ 7.91 (d, *J* = 8.3 Hz, 2H), 7.68 (dd, *J* = 8.6, 3.6 Hz, 1H), 7.47 (t, *J* = 8.8 Hz, 1H), 7.40 (app t, *J* = 8.5 Hz, 3H), 4.07 (dd, *J* = 5.5, 2.6 Hz, 2H), 4.01 (d, *J* = 2.4 Hz, 2H), 3.84 (s, 2H), 3.34 (s, 2H), 3.24 – 3.18 (m, 4H), 3.12 – 3.06 (m, 4H), 2.24 (t, *J* = 2.6 Hz, 1H), 1.84 (s, 1H).^{13}C-NMR (126 MHz, $CDCl_3$) δ 171.21, 157.73 (d, *J* = 257.9 Hz), 152.70 (d, *J* = 4.9 Hz), 144.31 (d, *J* = 14.8 Hz), 140.22, 137.53, 128.75, 127.16, 124.16 (d, *J* = 20.2 Hz), 121.04 (d, *J* = 4.1 Hz), 79.73, 71.60, 56.65 (d, *J* = 2.8 Hz), 53.67, 51.83, 51.72, 50.63, 28.81.

2-((4-(6-((4,4-Difluoropiperidin-1-yl) methyl)-5-fluoropyridin-2-yl) benzyl) amino)-*N*-(prop-2-yn-1-yl) acetamide (14): A mixture of **9** (0.23 g, 0.7 mmol, 1eq), **12** (0.15 g, 1.4 mmol, 2 eq), acetic acid (0.04 mL, 0.7 mmol, 1 eq) and $NaBH(OAc)_3$ (0.53 g, 2.5 mmol, 3.6 eq) in THF (9 mL) was stirred at RT for 16 h. The reaction was diluted with sat. $NaHCO_3$ (aq, 8 mL) and DCM (10 mL). The layers were separated and the aqueous layer extracted thrice with DCM. The combination of organic layers was dried ($MgSO_4$), filtered and the solvent evaporated under reduced pressure. The crude product was purified with flash column chromatography (SiO_2, 5% MeOH (with 1% Et_3N) in DCM) to yield a colourless oil (0.13 g, 0.30 mmol, 45%). ^{1}H-NMR (500 MHz, $CDCl_3$) δ 7.92 (d, *J* = 8.2 Hz, 2H), 7.64 (dd, *J* = 8.6, 3.6 Hz, 1H), 7.43 (t, *J* = 8.8 Hz, 2H), 7.38 (d, *J* = 8.3 Hz, 2H), 4.06 (dd, *J* = 5.5, 2.6 Hz, 2H), 3.88 (d,

J = 2.5 Hz, 2H), 3.82 (s, 2H), 3.32 (s, 2H), 2.75 (t, *J* = 5.7 Hz, 4H), 2.24 (t, *J* = 2.6 Hz, 1H), 2.01 (hept, *J* = 5.9 Hz, 4H), 1.95 (s, 1H). ^{13}C- NMR (126 MHz, $CDCl_3$) δ 171.27, 157.75 (d, *J* = 257.7 Hz), 152.39 (d, *J* = 4.9 Hz), 145.15 (d, *J* = 14.6 Hz), 139.99, 137.74, 128.63, 127.15, 123.86 (d, *J* = 20.2 Hz), 122.04 (d, *J* = 241.3 Hz), 120.62 (d, *J* = 4.2 Hz), 79.69, 71.56, 57.04, 53.64, 51.78, 49.91 (t, *J* = 5.3 Hz), 34.09 (t, *J* = 22.8 Hz), 28.76.

2-((4-(5-Fluoro-6-(piperidin-1-ylmethyl pyridin-2-yl) benzyl) amino)-*N*-(prop-2-yn-1-yl) acetamide (15): A mixture of **10** (0.20 g, 0.7 mmol, 1 eq), **12** (0.15 g, 1.4 mmol, 2 eq), acetic acid (0.04 mL, 0.7 mmol, 1 eq) and $NaBH(OAc)_3$ (0.53 g, 2.5 mmol, 3.6 eq) in THF (9 mL) was stirred at RT for 16 h. The reaction was diluted with sat. $NaHCO_3$ (aq, 8 mL) and DCM (10 mL). The layers were separated and the aqueous layer extracted thrice with DCM. The combination of organic layers was dried ($MgSO_4$), filtered and the solvent evaporated under reduced pressure. The crude product was purified with flash column chromatography (SiO_2, 10% EtOH (with 1% Et_3N) in DCM) to yield a colourless oil (0.14 g, 0.36 mmol, 54%). ^{1}H-NMR (500 MHz, $CDCl_3$) δ 7.93 (d, *J* = 8.2 Hz, 2H), 7.61 (dd, *J* = 8.5, 3.5 Hz, 1H), 7.40 (t, *J* = 8.8 Hz, 2H), 7.37 (d, *J* = 8.3 Hz, 2H), 4.06 (dd, *J* = 5.5, 2.6 Hz, 2H), 3.82 (d, *J* = 2.6 Hz, 2H), 3.81 (s, 2H), 3.32 (s, 2H), 2.59 (s, 4H), 2.23 (t, *J* = 2.6 Hz, 1H), 2.05 (s, 1H), 1.60 (p, *J* = 5.6 Hz, 4H), 1.41 (p, *J* = 6.3 Hz, 2H). ^{13}C-NMR (126 MHz, $CDCl_3$) δ 171.27, 157.83 (d, *J* = 257.7 Hz), 152.14 (d, *J* = 4.8 Hz), 145.62 (d, *J* = 14.1 Hz), 139.83, 137.94, 128.57, 127.18, 123.61 (d, *J* = 20.2 Hz), 120.27 (d, *J* = 4.1 Hz), 79.70, 71.53, 58.55 (d, *J* = 3.2 Hz), 54.40, 53.69, 51.82, 28.75, 26.04, 24.21.

***N*-(4-(6-((1,1-Dioxidothiomorpholino) methyl)-5-fluoropyridin-2-yl) benzyl)-*N*-(2-oxo-2-(prop-2-yn-1-ylamino) ethyl)-4-(3-(trifluoromethyl)-3*H*-diazirin-3-yl) benzamide (1)**: A mixture of HBTU (74.2 mg, 0.20 mmol, 1.5 eq), 4-(3(trifluoromethyl)-3*H*-diazirin-3-yl)) benzonic acid (30 mg, 0.13 mmol, 1 eq) and DiPEA (0.07 mL, 0.40 mmol, 3 eq) in anhydrous DCM (1 mL) was placed under inert atmosphere in a microwave vial. After stirring at RT for 1 h, **13** (63.6 mg, 0.14 mmol, 1.1 eq) dissolved in anhydrous DCM (1 mL) was added dropwise to the reaction mixture. After stirring at RT for 16 h the reaction was diluted with sat. $NaHCO_3$ (aq). The layers were separated and the aqueous layer was extracted thrice with DCM. The combination of organic layers was dried ($MgSO_4$), filtered and the solvent evaporated under reduced pressure. The crude product was purified with flash column chromatography (SiO_2, 70-90% EtOAc in pentane) followed by preparative HPLC and freeze drying to yield a white solid (36.3 mg, 0.06 mmol, 42%). ^{1}H-NMR (400 MHz, MeOD) δ 7.94 (d, *J* = 8.0 Hz, 2H), 7.68 (dd, *J* = 8.6, 3.5 Hz, 1H), 7.56 (d, *J* = 8.0 Hz, 2H), 7.49 (t, *J* = 8.8 Hz, 1H), 7.28 (d, *J* = 8.1 Hz, 2H), 7.22 (d, *J* = 8.1 Hz, 2H), 4.67 (s, 2H), 4.10 (s, 2H), 4.09 – 4.04 (m, 2H), 4.03 (d, *J* = 2.4 Hz, 2H), 3.25 – 3.19 (m, 4H), 3.13 – 3.08 (m, 4H), 2.26 (s, 1H). ^{13}C-NMR (126 MHz, $CDCl_3$) δ 171.93, 168.05, 158.90, 157.86 (d, *J* = 259.7 Hz), 152.29 (d, *J* = 7.5 Hz), 144.39 (d, *J* = 20.4 Hz), 124.29 (d, *J* = 20.1 Hz), 138.18, 136.40, 136.11, 131.56, 127.63, 127.62, 127.54, 126.92, 124.37, 124.21, 123.11, 121.16 (d, *J* = 4.1 Hz), 79.51, 71.99, 56.64, 53.93, 51.74, 50.61, 49.24, 29.38. HRMS $[C_{31}H_{28}F_4N_6O_4S + H]^+$: 657.19016 calculated, 657.18978 found.

***N*-(4-(6-((4,4-Difluoropiperidin-1-yl) methyl)-5-fluoropyridin-2-yl) benzyl)-*N*-(2-oxo-2-(prop-2-yn-1-ylamino) ethyl)-4-(3-(trifluoromethyl)-3*H*-diazirin-3-yl) benzamide (3)**: A mixture of HBTU (74.2 mg, 0.20 mmol, 1.5eq), 4-(3(trifluoromethyl)-3*H*-diazirin-3-yl)) benzonic acid (30 mg, 0.13 mmol, 1 eq) and DiPEA (0.07 mL, 0.40 mmol, 3 eq) in anhydrous DCM (1 mL) was placed under inert atmosphere in a microwave vial. After stirring at RT for 1 h, **14** (61.7 mg, 0.14 mmol, 1.1eq) dissolved in anhydrous DCM (1 mL) was added dropwise to the reaction mixture. After stirring at RT for 16 h the reaction was diluted with sat. $NaHCO_3$ (aq). The layers were separated and the aqueous layer was extracted thrice with DCM. The combination of organic layers was dried ($MgSO_4$), filtered and the solvent evaporated under reduced pressure. The crude product was purified with flash column chromatography (SiO_2, 70-100% EtOAc in pentane) followed by preparative HPLC and freeze drying to yield a white solid (36.6 mg, 0.06 mmol, 44%). ^{1}H-NMR (400 MHz, MeOD) δ 8.03 (t, *J* = 7.5 Hz, 2H), 7.86 (dt, *J* = 8.0, 3.8 Hz, 1H), 7.69

– 7.57 (m, 3H), 7.48 (d, *J* = 7.9 Hz, 1H), 7.38 – 7.28 (m, 3H), 4.82 (s, 1H), 4.62 (s, 1H), 4.14 (s, 1H), 3.97 (dd, *J* = 34.5, 2.5 Hz, 2H), 3.89 (s, 2H), 3.82 (s, 1H), 2.76 (s, 4H), 2.67 – 2.59 (m, 1H), 2.08 – 1.94 (m, 4H). ^{13}C-NMR (126 MHz, $CDCl_3$) δ 172.48, 163.97, 149.08, 148.53, 129.22, 126.92, 124.81, 77.41, 77.16, 76.91, 53.93, 49.61, 49.26, 29.39. HRMS $[C_{32}H_{28}F_6N_6O_2 + H]^+$: 643.22507 calculated, 643.22467 found.

***N*-(4-(5-Fluoro-6-(piperidin-1-ylmethyl) pyridin-2-yl) benzyl)-*N*-(2-oxo-2-(prop-2-yn-1-ylamino) ethyl)-4-(3-(trifluoromethyl)-3*H*-diazirin-3-yl) benzamide (4)**: A mixture of HBTU (74.2 mg, 0.20 mmol, 1.5eq), 4-(3(trifluoromethyl)-3*H*-diazirin-3-yl)) benzonic acid (30 mg, 0.13 mmol, 1 eq) and DiPEA (0.07 mL, 0.40 mmol, 3 eq) in anhydrous DCM (1 mL) was placed under inert atmosphere in a microwave vial. After stirring at RT for 1 h, **15** (56.6 mg, 0.14 mmol, 1.1 eq) dissolved in anhydrous DCM (1 mL) was added dropwise to the reaction mixture. After stirring at RT for 16 h the reaction was diluted with sat. $NaHCO_3$ (aq). The layers were separated and the aqueous layer was extracted thrice with DCM. The combination of organic layers was dried ($MgSO_4$), filtered and the solvent evaporated under reduced pressure. The crude product was purified with flash column chromatography (SiO_2, 90-100% EtOAc in pentane) followed by preparative HPLC and freeze drying to yield a white solid (36.6 mg, 0.06 mmol, 46%). ^{1}H-NMR (500 MHz, $CDCl_3$) δ 7.96 (d, *J* = 7.9 Hz, 2H), 7.61 (dd, *J* = 8.6, 3.5 Hz, 1H), 7.55 (d, *J* = 8.0 Hz, 2H), 7.48 – 7.38 (m, 3H), 7.21 (d, *J* = 8.1 Hz, 2H), 4.65 (s, 2H), 4.16 – 4.00 (m, 4H), 3.82 (d, *J* = 2.7 Hz, 2H), 2.58 (s, 4H), 1.87 (s, 1H), 1.60 (t, *J* = 5.8 Hz, 4H), 1.45 – 1.37 (m, 2H), 1.25 (t, *J* = 7.2 Hz, 1H). ^{13}C-NMR (126 MHz, $CDCl_3$) δ 171.96, 168.09, 162.36, 162.08, 138.81, 137.40, 127.67, 126.92, 125.06 (d, *J* = 20.0 Hz), 122.69, 117.83, 115.51, 73.94, 71.91, 54.50, 53.32, 49.13, 29.34, 22.88, 22.05. HRMS $[C_{32}H_{30}F_4N_6O_2 + H]^+$: 607.24391 calculated, 607.24317 found.

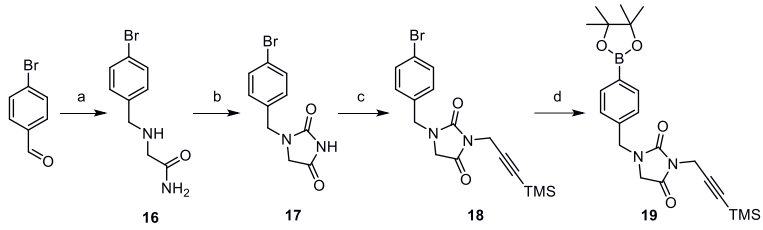

Scheme 3.6 Synthesis of Suzuki Coupling Reagent **19**. Reagents and conditions: a) Step 1: 2-aminoacetamide hydrochloride (1.0 eq), NaOH (1.1 eq), MeOH:H_2O (0.3 M, 5:1 (v/v)), RT, 18 h; Step 2: $NaBH_4$ (2.1 eq), 18 h, 91% (two steps); b) CDI (2.1 eq), DMAP (2.1 eq), ACN (0.1 M), 60 °C, 70 h, 37%; c) 3-bromo-1-(trimethylsilyl)-1-propyne (1.2 eq), K_2CO_3 (1 eq), DMF (0.3 M), 50 °C, 16 h, 61%; d) bis(pinacol)diborane (1.5 eq), KOAc (4 eq), Pd(dppf)Cl_2 (0.5 eq), 1,4 dioxane (0.1 M), 80 °C, 16 h, used as crude.

2-((4-Bromobenzyl)amino)acetamide (16): To a stirred mixture of 4-bromobenzaldehyde (9.2 g (49.7 mmol, 1.1 eq) and 2-aminoacetamide hydrochloride (5.06 g, 45.8 mmol, 1.0 eq) in MeOH:H_2O (170 mL, 5:1, v/v) was added NaOH (2.06 g, 51.5 mmol, 1.1 eq). After stirring at RT overnight, $NaBH_4$ (3.6 g, 95.2 mmol, 2.1 eq) was added and the solution was stirred overnight at RT. The solution was acidified to pH 3 with 2 M HCl, then neutralized with sat. $NaHCO_3$ (aq). Methanol was evaporated under reduced pressure and the resulting slurry was filtered to yield a white solid (11.0 g, 45.2 mmol, 91%). ^{1}H-NMR (300 MHz, MeOD) δ 7.69 – 7.59 (m, 2H), 7.47 – 7.38 (m, 2H), 4.22 (s, 2H), 3.81 (s, 2H).

1-(4-Bromobenzyl)imidazolidine-2,4-dione (17): To stirred suspension of **16** (10.0 g, 40.1 mmol, 1.0 eq) in acetonitrile (300 mL) were added CDI (13.86 g, 85.5 mmol, 2.1 eq) and DMAP (10.2 g, 83.5 mmol, 2.1 eq). The mixture was heated (60 °C) under inert atmosphere for 70 h. 1 M HCl (aq, 250 mL) was added and the aqueous layer extracted thrice with EtOAc. The combination of organic layers was washed with H_2O and brine, dried ($MgSO_4$), filtered, and the solvent evaporated under reduced pressure. The crude product was purified with flash column chromatography with dry loading over Celite (SiO_2, 5-10% acetone in DCM) to yield a yellow solid (3.95 g, 14.7 mmol, 37%). ^{1}H-NMR (300 MHz,

$CDCl_3$) δ 7.83 (bs, 1H), 7.56 – 7.45 (m, 2H), 7.20 – 7.10 (m, 2H), 4.49 (s, 2H), 3.79 (s, 2H). ^{13}C-NMR (75 MHz, $CDCl_3$) δ 132.41, 129.95, 77.58, 77.16, 76.74, 50.36, 46.01.

1-(4-Bromobenzyl)-3-(3-(trimethylsilyl) prop-2-yn-1-yl) imidazolidine-2,4-dione (18): To a stirred mixture of **17** (0.52 g, 1.9 mmol, 1 eq) in DMF (6 mL) under inert atmosphere were added K_2CO_3 (0.27 g, 1.9 mmol, 1 eq) and 3-bromo-1-(trimethylsilyl)-1-propyne (0.38 g, 2.3 mmol, 1.2 eq). The reaction mixture was heated (50 °C) for 16 h. and subsequently diluted with 0.4 M K_2CO_3 (aq) and EtOAc. The layers were separated and the aqueous layer was extracted thrice with EtOAc. The combination of organic layers was washed with brine, dried ($MgSO_4$), filtered and the solvent evaporated under reduced pressure. The crude product was purified with flash column chromatography (SiO_2, 40-80% EtOAc in pentane) to yield a yellow oil (0.44 g, 1.2 mmol, 61%). ^{1}H-NMR (500 MHz, $CDCl_3$) δ 7.48 (d, *J* = 8.3 Hz, 2H), 7.13 (d, *J* = 8.3 Hz, 2H), 4.52 (s, 2H), 4.29 (s, 2H), 3.74 (s, 2H), 0.14 (s, 9H).

1-(4-(4,4,5,5-Tetramethyl-1,3,2-dioxaborolan-2-yl) benzyl)-3-(3-(trimethylsilyl) prop-2-yn-1-yl) imidazolidine-2,4-dione (19): A stirred mixture of **18** (0.23 g, 0.61 mmol, 1 eq), bis(pinacolato)diboron (0.23 g, 0.91 mmol, 1.5 eq), Pd(dppf)Cl_2 (0.03 g, 0.03 mmol, 0.5 eq) and KOAc (0.24 g, 2.44 mmol, 4 eq) in 1,4-dioxane (5 mL) under inert atmosphere was heated (80 °C) for 16 h. The reaction mixture was concentrated under reduced pressure. The mixture was diluted with sat. $NaHCO_3$ (aq, 10 mL) and H_2O (15 mL) and the layers were separated. The aqueous layer was extracted thrice with EtOAc. The combination of organic layers was washed with brine, dried ($MgSO_4$), filtered and the solvent evaporated under reduced pressure. The crude product **19** was used directly in the next step to form **22**.

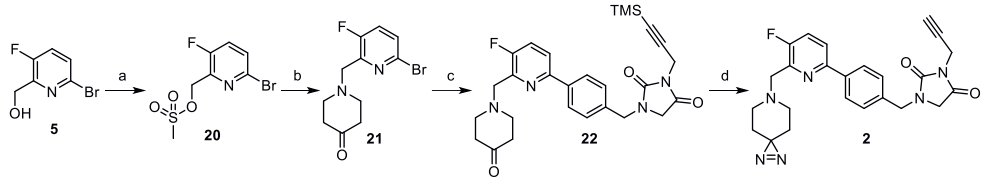

Scheme 3.7 Synthesis of Probe **2**. Reagents and Conditions: a) Et_3N (2.3 eq), MsCl (1.7 eq), THF (0.2 M), 0 °C-RT, 1 h, 75%; b) 4-piperidone hydrochloride (1.2 eq), K_2CO_3 (3 eq), ACN (0.2 M), 70 °C, 48 h, 78%; c) K2CO3 (1.8 eq), Pd(PPh3)4 (0.1 eq), toluene:EtOH (0.1 M, 4:1 (v/v)), 50 °C, 16 h, 29%; d) Step 1: NH3 (g), MeOH (0.2 M), 0 °C, 5 h; Step 2: NH2SO3H (1.5 eq), MeOH (0.2 M), 16 h, RT, Step 3: I2, MeOH, 0 °C 15 min., 27% (three steps).

(6-Bromo-3-fluoropyridin-2-yl)methyl methanesulfonate (20): To a cooled (0 °C) mixture of **5** (1.6 g, 7.8 mmol, 1 eq) and Et_3N (2.5 mL, 17.9 mmol, 2.3 eq) in dry THF (40 mL) was added dropwise MsCl (1.0 mL, 12.9 mmol, 1.7 eq). After stirring at RT for 1 h the solution was concentrated under reduced pressure. DCM and H_2O were added and the layers were separated. The aqueous layer was extracted thrice with DCM. The combination of organic layers was washed with brine, dried ($MgSO_4$), filtered, and the solvent evaporated under reduced pressure to yield a yellow solid (1.65 g, 5.8 mmol, 75%). ^{1}H-NMR (500 MHz, $CDCl_3$) δ 7.52 (dd, *J* = 8.6, 3.5 Hz, 1H), 7.37 (t, *J* = 8.5 Hz, 1H), 5.33 (d, *J* = 2.1 Hz, 2H), 3.13 (s, 3H). ^{13}C-NMR (126 MHz, $CDCl_3$) δ 157.82 (d, *J* = 261.3 Hz), 142.15 (d, *J* = 16.0 Hz), 130.74 (d, *J* = 4.4 Hz), 127.06 (d, *J* = 20.4 Hz), 65.50 (d, *J* = 1.6 Hz), 38.39.

1-((6-Bromo-3-fluoropyridin-2-yl) methyl) piperidin-4-one (21): A stirred degassed mixture of **20** (0.67 g, 2.4 mmol, 1 eq), 4-piperidone hydrochloride (0.39 g, 2.8 mmol, 1.2 eq) and K_2CO_3 (0.98 g, 7.1 mmol, 3 eq) in acetonitrile (12 mL) was heated (70 °C) for 48 h. The reaction mixture was diluted with H_2O (10 mL) and DCM (5 mL) and the layers were separated. The aqueous layer was extracted thrice with DCM. The combination of organic layers was dried ($MgSO_4$), filtered and the solvent evaporated under reduced pressure. The crude product was purified with flash column chromatography (SiO_2, 30-70% EtOAc in pentane) to yield a yellow solid (0.53 g, 1.9 mmol, 78%).

^{1}H-NMR (500 MHz, $CDCl_3$) δ 7.42 (dd, *J* = 8.5, 3.5 Hz, 1H), 7.30 (t, *J* = 8.5 Hz, 1H), 3.84 (d, *J* = 2.5 Hz, 2H), 2.87 (t, *J* = 6.1 Hz, 4H), 2.46 (t, *J* = 6.2 Hz, 4H). ^{13}C-NMR (126 MHz, $CDCl_3$) δ 208.82, 158.22 (d, *J* = 258.0 Hz), 146.93 (d, *J* = 15.8 Hz), 135.20, 128.69 (d, *J* = 4.4 Hz), 126.31 (d, *J* = 21.6 Hz), 56.40 (d, *J* = 2.8 Hz), 53.02, 41.34.

1-(4-(5-Fluoro-6-((4-oxopiperidin-1-yl) methyl) pyridin-2-yl) benzyl)-3-(3-(trimethylsilyl) prop-2-yn-1-yl) imidazolidine-2,4-dione (22): A stirred mixture of crude **19** (max. 0.61 mmol, 1.5 eq), **21** (0.12 g, 0.41 mmol, 1 eq), K_2CO_3 (0.10 g, 0.73 mmol, 1.8 eq) and $Pd(PPh_3)_4$ (0.07 g, 0.06 mmol, 0.1 eq) in degassed toluene:EtOH (4 mL, 4:1 (v/v)) was heated (50 °C) for 16 h. The mixture was filtered and the residue rinsed with EtOAc. H_2O (10 mL) was added and the layers were separated. The aqueous layer was extracted thrice with EtOAc. The combination of organic layers was washed with brine, dried ($MgSO_4$), filtered and the solvent evaporated under reduced pressure. The crude product was purified with flash column chromatography (SiO_2, 0-10% MeOH in EtOAc) to yield a yellow oil (60.0 mg, 0.12 mmol, 29%). ^{1}H-NMR (400 MHz, $CDCl_3$) δ 7.95 (d, *J* = 8.3 Hz, 2H), 7.66 (dd, *J* = 8.6, 3.6 Hz, 1H), 7.47 (t, *J* = 8.8 Hz, 1H), 7.36 (d, *J* = 8.2 Hz, 2H), 4.63 (s, 2H), 4.32 (s, 2H), 3.98 (d, *J* = 2.4 Hz, 2H), 3.78 (s, 2H), 2.96 (t, *J* = 6.1 Hz, 4H), 2.49 (t, *J* = 6.1 Hz, 4H), 1.23 (s, 9H). ^{13}C-NMR (101 MHz, $CDCl_3$) δ 206.47, 127.72, 126.86, 124.37 (d, *J* = 21.5 Hz), 121.96 (d, *J* = 5.5 Hz), 83.40, 72.26, 56.74, 51.74, 50.66, 43.65, 29.86, 29.56, 0.15.

1-(4-(6-((1,2,6-Triazaspiro [2.5] oct-1-en-6-yl) methyl)-5-fluoropyridin-2-yl) benzyl)-3-(prop-2-yn-1-yl) imidazolidine-2,4-dione (2): In a microwave vial a stirred and cooled (0 °C) solution of **22** (60 mg, 0.12 mmol, 1eq) in anhydrous MeOH (0.5 mL) for 1 h an NH_3 (g) gas flow was established. The reaction was stirred at RT for an additional 5 h. NH_2SO_3H (25 mg, 0.18 mmol, 1.5 eq) dissolved in anhydrous MeOH (0.2 mL) was added dropwise to the reaction mixture. After stirring at RT for 16 h the reaction was filtered over Celite and the solution concentrated under reduced pressure. To a cooled (0 °C) solution of the crude in MeOH (1 mL) was added dropwise sat. I_2 in anhydrous MeOH until a colour change to orange persisted for 15 minutes. The reaction was quenched with sat. $Na_2S_2O_3$ (aq) (2 mL) and diluted with EtOAc. The layers separated and the aqueous layer was extracted thrice with EtOAc. The combination of organic layers was washed with 2 M HCl and brine, dried ($MgSO_4$), filtered and the solvent evaporated under reduced pressure. The crude product was purified with flash column chromatography (SiO_2, 100% EtOAc). The compound was freeze dried to yield a white solid (14.2 mg, 0.03 mmol, 27%). ^{1}H-NMR (500 MHz, $CDCl_3$) δ 7.96 (d, *J* = 8.3 Hz, 2H), 7.65 (dd, *J* = 8.6, 3.5 Hz, 1H), 7.46 (t, *J* = 8.7 Hz, 1H), 7.38 – 7.33 (m, 2H), 4.63 (s, 2H), 4.32 (d, *J* = 2.5 Hz, 2H), 3.95 (d, *J* = 2.5 Hz, 2H), 3.79 (s, 2H), 2.81 (t, *J* = 5.8 Hz, 4H), 2.25 (t, *J* = 2.5 Hz, 1H), 1.33 (t, *J* = 5.7 Hz, 4H). ^{13}C-NMR (126 MHz, $CDCl_3$) δ 168.70, 158.00 (d, *J* = 258.2 Hz), 155.58, 152.02 (d, *J* = 4.9 Hz), 145.61, 138.77, 135.82, 128.79, 127.65, 123.93 (d, *J* = 20.4 Hz), 120.70 (d, *J* = 4.1 Hz), 71.86, 57.84 (d, *J* = 2.9 Hz), 51.99, 49.29, 46.70, 31.37, 28.30. HRMS $[C_{24}H_{23}FN_6O_2 + H]^+$: 447.19393 calculated, 447.19360 found.

Biology

"General Remarks", "Cell Culture", "Membrane Preparation", "[^{3}H]CP-55,940 Heterologous Displacement", "[^{35}S]GTPγS Binding Assay" and "Quantification and Statistical Analysis" have been previously described in **Chapter 2**.

SDS PAGE

CHO-K1 hCB_2R_bgal membranes were diluted to 0.78 ug/uL and homogenized for 15 seconds with an Ultra Turrax homogenizer (IKA-Werke GmbH & Co. KG, Staufen, Germany). Benzonase was added (1:10000 dilution from $2.5 \cdot 10^6$ U/mL). To each sample was added 16 µL membrane followed by 1 µL 360 µM CP-55,940 or DMSO. To the denatured sample was also added 2 µL 10% SDS. After incubation of 30 minutes at RT 1 µL 36 µM probe was added to the samples. After 30 minutes incubation at RT the samples (except the no UV samples) were irradiated with 350 nm light in a Caprobox™ for 5 minutes.

2 µL click mix (11 mM $CuSO_4$, 66 mM NaAsc, 2.2 mM THPTA, 10 µM Cy5-N_3 (not present in azide free mix)) was added to the samples. After incubation for 30 minutes at RT the samples were denatured with 5 µL 4* Laemmli buffer. After 30 minutes at RT the samples were loaded onto 12.5% 1.5 mm SDS gels (15 µL sample/well). Gels were run at 180V for 80-90 minutes. Gels were imaged with a ChemiDoc (Biorad, The Netherlands). After imaging all proteins loading of the wells was visualized by staining with Coomassie Brilliant Blue R-250 Dye and sequentially destaining with destaining fluid (50/40/10 H_2O/MeOH/AcOH). After leaving overnight in H_2O, pictures were made on the ChemiDoc (Biorad, The Netherlands).

Molecular Docking

The structure of CB_2R in complex with LEI-102 (8GUT) was retrieved from the Protein Data Bank using ICM Molsoft's inbuilt feature. This structure was converted to an ICM object, with 'optimize hydrogens' set to true, after which all but the R chain (the receptor) was removed. The probe LEI-121 was inserted as ICM objects via the 'New 3D Chemical' functionality. LEI-102 was extracted from the receptor object and a pocket box was defined around this molecule using default settings. Two probes were docked with the 'thoroughness' parameter set to 10, and the 10 best poses were retained. The resulting poses were manually inspected and visualised using the Open Source PyMOL application.

References

1 Gazzi T, Brennecke B, Atz K, et al. Detection of cannabinoid receptor type 2 in native cells and zebrafish with a highly potent, cell-permeable fluorescent probe. *Chem Sci*. 2022;13(19):5539-5545. doi:10.1039/D1SC06659E

2. Tyler DS, Vappiani J, Cañeque T, et al. Click chemistry enables preclinical evaluation of targeted epigenetic therapies. *Science (80-)*. 2017;356(6345):1397-1401. doi:10.1126/science.aal2066

3. Cécyre B, Thomas S, Ptito M, Casanova C, Bouchard J-F. Evaluation of the specificity of antibodies raised against cannabinoid receptor type 2 in the mouse retina. *Naunyn Schmiedebergs Arch Pharmacol*. 2014;387(2):175-184. doi:10.1007/s00210-013-0930-8

4. Sarott RC, Westphal M V., Pfaff P, et al. Development of High-Specificity Fluorescent Probes to Enable Cannabinoid Type 2 Receptor Studies in Living Cells. *J Am Chem Soc*. 2020;142(40):16953-16964. doi:10.1021/jacs.0c05587

5. Soethoudt M, Grether U, Fingerle J, et al. Cannabinoid CB2 receptor ligand profiling reveals biased signalling and off-target activity. *Nat Commun*. 2017;8(1):13958. doi:10.1038/ncomms13958

6. Basagni F, Rosini M, Decker M. Functionalized Cannabinoid Subtype 2 Receptor Ligands: Fluorescent, PET, Photochromic and Covalent Molecular Probes. *ChemMedChem*. 2020;15(15):1374-1389. doi:10.1002/cmdc.202000298

7. Soethoudt M, Stolze SC, Westphal M V., et al. Selective Photoaffinity Probe That Enables Assessment of Cannabinoid CB 2 Receptor Expression and Ligand Engagement in Human Cells. *J Am Chem Soc*. 2018;140(19):6067-6075. doi:10.1021/jacs.7b11281

8. Soethoudt M, Hoorens MWH, Doelman W, Martella A, van der Stelt M, Heitman LH. Structure-kinetic relationship studies of cannabinoid CB2 receptor agonists reveal substituent-specific lipophilic effects on residence time. *Biochem Pharmacol*. 2018;152(March):129-142. doi:10.1016/j.bcp.2018.03.018

9. Li X, Chang H, Bouma J, et al. Structural basis of selective cannabinoid CB2 receptor activation. *Nat Commun*. 2023;14(1):1447. doi:10.1038/s41467-023-37112-9

10. de Paus LV, Janssen APA, et al. Discovery of a Cannabinoid CB2 Receptor Fluorescent Probe Based on a Pyridin-2-yl-benzyl-imidazolidine-2,4-dione Scaffold. *Synlett* 2023;35 doi:10.1055/a-2230-1003

11. Rapino C, Castellucci A, Lizzi AR, et al. Modulation of Endocannabinoid-Binding Receptors in Human Neuroblastoma Cells by Tunicamycin. *Molecules*. 2019;24(7):1432. doi:10.3390/molecules24071432

12. Soto AG, Smith TH, Chen B, et al. N-linked glycosylation of protease-activated receptor-1 at extracellular loop 2 regulates G-protein signaling bias. *Proc Natl Acad Sci*. 2015;112(27). doi:10.1073/pnas.1508838112

13. Latorraca NR, Masureel M, et al. How GPCR Phosphorylation Patterns Orchestrate Arrestin-Mediated Signaling. *Cell* 2020, 183(7), 1813–1825. doi: 10.1016/j.cell.2020.11.014

Acknowledgements

Prof. dr. G.J.P. van Westen is kindly acknowledged for access to the computational resources needed for this work.

This work was supported by the Dutch Research Council (NWO, Navistroke #15851) (Mario van der Stelt[d], M.v.d.S.).

Author contributions: Conducting Experiments, A.Y. (Yu An), L.V.d.P. (Laura V. de Paus), A.P.A.J. (Antonius P.A. Janssen); Writing-Original Draft, L.V.d.P.; Writing Review & Editing, M.v.d.S., L.H.H. (Laura H. Heitman), R.J.B.H.N.v.d.B (Richard J. B. H. N. van den Berg); Supervision, M.v.d.S.

Chapter 4

Discovery of a Cannabinoid CB_2 Receptor Fluorescent Probe Based on a Pyridin-2-yl-benzyl-imidazolidine-2,4-dione Scaffold

Published as: de Paus LV, Janssen APA, Halimi A, van den Berg RJBHN, Heitman LH, van der Stelt M. Discovery of a cannabinoid CB2 receptor fluorescent probe based on a pyridin-2-yl-benzyl-imidazolidine-2,4-dione scaffold. Synlett. December 2023. doi:10.1055/a-2230-1003

Discovery of a Cannabinoid CB_2 Receptor Fluorescent Probe Based on a Pyridin-2-yl-benzyl-imidazolidine-2,4-dione Scaffold

Introduction

The cannabinoid receptor type 2 (CB_2R) is a class A G protein-coupled receptor (GPCR) with a role in inflammation and neurodegenerative diseases, making it an interesting target for drug discovery for multiple applications.[1] Confirming target engagement and understanding the biological cascades that lead to the therapeutic effect of a therapeutic agent are necessary for the successful translation of compounds into the clinic. At the moment no CB_2R-selective drugs have yet reached the market.[2] Fluorescent probes are ideal for detecting CB_2R in relevant cell types, target engagement studies and explore the roles of CB_2R in healthy and pathological systems.[3] To this end, several fluorescent probes have been reported.[2–14] Leiden university has also contributed to this field and reported the 5-fluoropyridin-2-yl-benzyl-imidazolidine-2,4-dione LEI-121 (Figure 4.1A) as a CB_2R selective bifunctional probe that captured the CB_2R upon photoactivation.[15] An incorporated alkyne served as a ligation handle for the introduction of fluorescent reporter groups. LEI-121 enabled target engagement studies and visualization of endogenously expressed CB_2R in HL-60 and primary human immune cells using flow cytometry.[15] However, LEI-121 is a two-step probe that requires copper-catalysed azide-alkyne cycloaddition (click-reaction) with a fluorophore to visualize the receptor. For live imaging purposes, it would be beneficial to avoid the copper-mediated click reaction, which is toxic to cells, and to have a one-step fluorescent probe in which the fluorophore is incorporated into the structure of the ligand.

Previously, Leiden university reported the three-dimensional structure of CB_2R in complex with the 5-fluoropyridin-2-yl-benzyl-imidazolidine-2,4-dione analogue LEI-102 using cryogenic electron microscopy (Figure 4.1).[16] This provided an excellent opportunity for the structure-based design of novel one-step fluorescent CB_2R probes. To validate this reasoning, novel one-step fluorescent CB_2R probes based on the 5-fluoropyridin-2-yl-benzyl-imidazolidine-2,4-dione series were designed, synthesized and characterized.

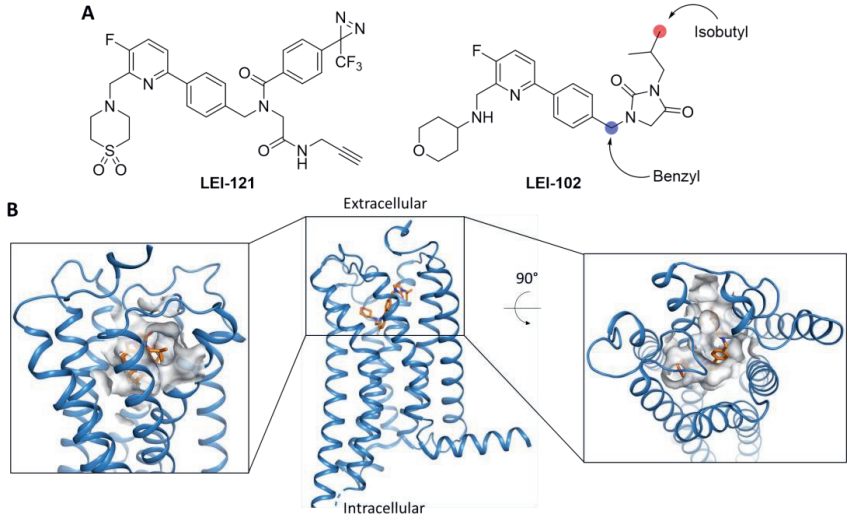

Figure 4.1 LEI-121 and LEI-102 and the resolved cryo-EM structure of hCB_2R with LEI-102. (A) The chemical structures of CB_2R probe LEI-121 and CB_2R agonist LEI-102. The optimal positions to attach a spacer have been marked in the structure of

LEI-102. (B) Cryo-EM structures of CB_2R (sky blue, PDB: 8GUT) in complex with LEI-102 (orange) at two different angles, with surface representation of receptor atoms within 4 Å. Figure generated with Open Source PyMOL Molecular Viewer v2.4.[16]

Results & Discussion

Design

The cryo-EM structure of the human CB_2R in complex with LEI-102 was inspected to find the best exit vector on the scaffold for the introduction of a spacer that could be coupled to various fluorophores. The isobutyl and benzylic position were positioned equally well to serve as an attachment point for spacer plus fluorophore. For synthetic reasons the isobutyl position was chosen to introduce an optionally methyl substituted ethylamine (compound **1**-**3**) as attachment point for various alkyl (compound **4**-**9**) or polyethylene glycol (PEG) (compound **10**-**18**) spacers. The most promising scaffold spacer compound (**5**) was coupled to four different fluorophores, *i.e.* BODIPY 493/503, BODIPY-TMR-X, DY480-XL and Cy-5, resulting in compound **19**-**22** (Scheme 4.1). BODIPY dyes have the advantages of high quantum yield, high molar extinction coefficients an brightness, as well as being relatively insensitive to the pH of their environment.[17,18] Cy5 is frequently used and emits in the near infrared range which is not affected by biological auto-fluorescence, shows high stability, moderate insensitivity to solvent polarity, is highly water soluble, and has one of the highest molar extinction coefficients.[19–21] DY 480XL has a large stokes shift which increases the signal to noise by lowering chance of self-quenching, self-absorption and excitation source cross-talk.[22]

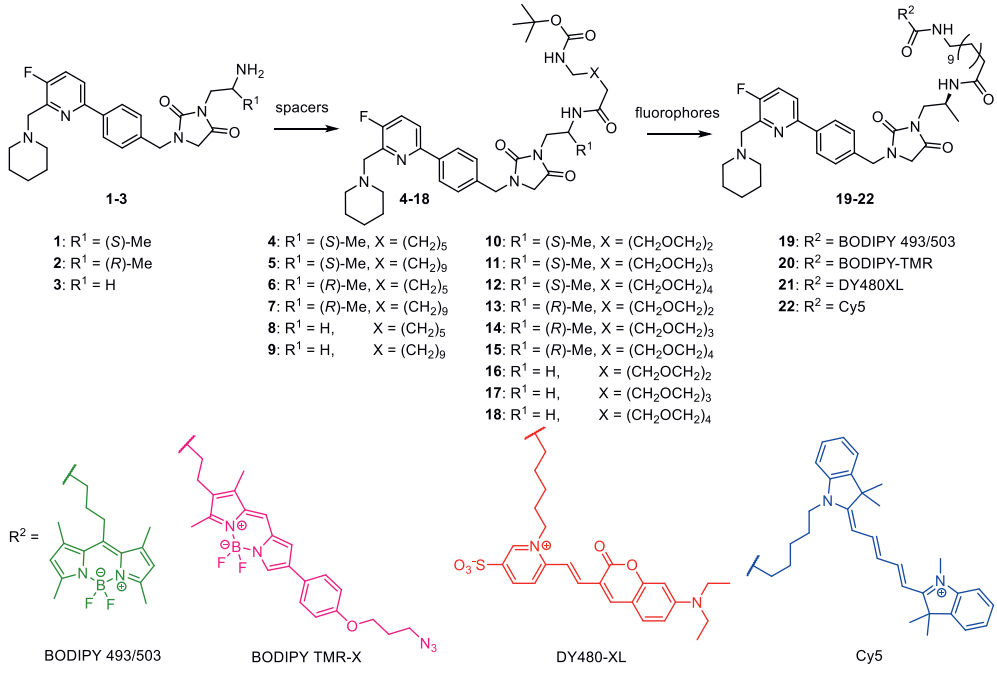

Scheme 4.1 The synthesis plan of the LEI-102-derived fluorescent probes. The scaffold contains an amine conjugation site which is either the (*S*)- or (*R*)- 2-aminopropyl enantiomer or achiral 2-aminoethyl moiety. To all three scaffolds a selection of five spacers was conjugated: C_8, C_{12}, PEG2, PEG3, or PEG4. **5** exhibited the highest CB_2R affinity and was conjugated to the four fluorophores. The Cy5 conjugate **22** showed the best biochemical properties.

Synthesis

The synthesis of the CB_2R selective fluorescent probes based on LEI-102 **19**-**22** started with the construction of the pyridinylbenzylimidazolidine-2,4-dione intermediates **1**-**18**. Commercially available

alaninol (D/L, Scheme 4.2) was carbamate protected (**23**, **24**), then subsequent iodination gave iodide derivatives **25** and **26**, respectively. Meanwhile reductive amination of 4-bromobenzaldehyde and aminoacetamide led to compound **27**. After cyclization the formed imidazolidinedione **28** was alkylated with tert-butyl-(2-bromoethyl)carbamate, **25**, or **26** which afforded compounds **29**-**31**. Next, oxidation of 6-bromo-3-fluoro-2-methylpyridine with *m*-CPBA followed by a Boekelheide rearrangement led to **32**. After mesylation of the primary alcohol, the mesyl **33** was substituted with piperidine (**34**). Subsequently, borylation of **29**-**31** with pinacolboronic ester and conjugation to **34** via a Suzuki coupling (**35**-**37**) and finally acidolysis gained pharmacophores **1**-**3** (Scheme 4.2).

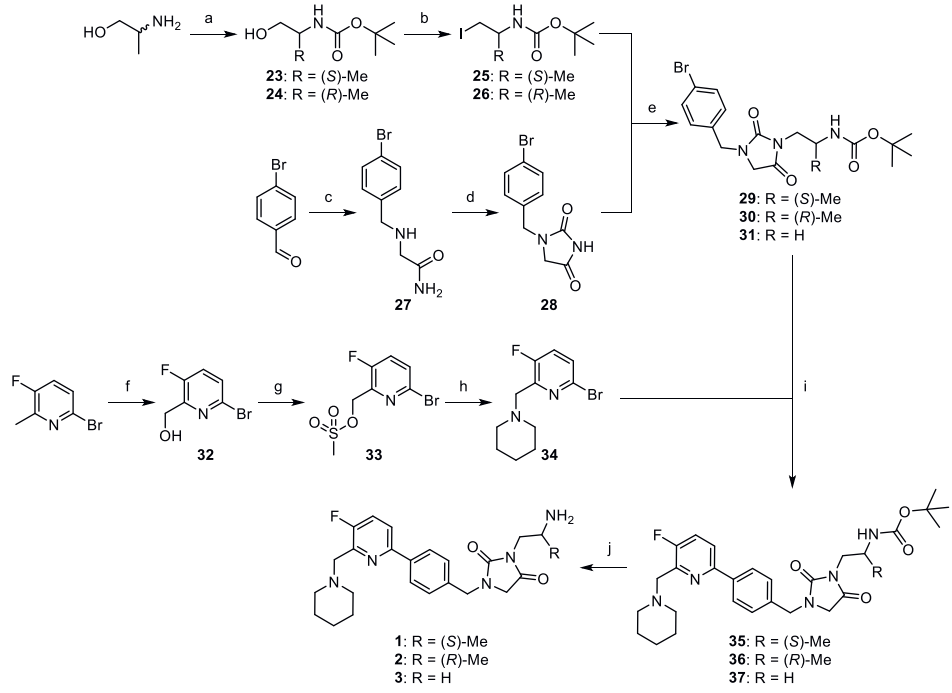

Scheme 4.2 The synthesis of the three scaffold intermediates **1**-**3**. Reagents and conditions: a) Boc_2O (1-2 eq), NaOH (1 M, 2 eq), 1,4 dioxane, RT, 3 h, 97-99%; b) PPh_3 (1.2-1.5 eq), imidazole (1.4-1.8 eq), iodine (1.3-1.7 eq), ACN:Et_2O (3:10, v/v), RT, 16 h, 53-62%; c) step 1: 2-aminoacetamide hydrochloride (1.0 eq), NaOH (1.1 eq), MeOH:H_2O (5:1), RT, 18 h; Step 2: $NaBH_4$ (2.1 eq), 18 h, 91% (two steps); d) CDI (2.1 eq), DMAP (2.1 eq), ACN, 60 °C, 70 h, 37%; e) *tert*-butyl-(2-bromoethyl)carbamate for **31**/ **25** for **29**/ **26** for **30** (2 eq), 1-(4-bromobenzyl)imidazolidine-2,4-dione (1 eq), K_2CO_3 (6 eq), 18-crown-6 (0.2 eq), DMF (0.2 M), 50 °C, 16 h, 62-88%; f) step 1: *m*-CPBA (1.8 eq), 0 °C-RT, DCM, 4 days; step 2: TFAA (2.2 eq), 55 °C, 3 h; step 3: K_2CO_3 (2.3 eq), THF:MeOH (20:1), 17 h, 35% (three steps); g) Et_3N (2.3 eq), MsCl (1.7 eq), THF, 0 °C-RT, 1 h, 75%; h) K_2CO_3 (2.2 eq), piperidine (1.2 eq), ACN (0.2 M), 50 °C, 1.5 h, 93%; i) step 1: KOAc (4-6 eq), bis(pinacolato)diboron (1.5-2.2 eq), $Pd(dppf)Cl_2$ (0.05-0.08 eq), DMF (degassed, 0.2 M), 75 °C, 16 h; step 2: 34 (1 eq), K_2CO_3 (4-8 eq), $Pd(PPh_3)_4$ (0.05-0.2 eq), toluene:EtOH (degassed, 4:1, v/v, 0.2 M), 75 °C, 16 h, 36-76% (two steps); j) 4 M HCl (1,4 dioxane, 4 eq), acetonitrile (0.5 M), 80 °C, 2 h, 62-86%.

The various alkyl and ethyleneglycol based spacers (**42**-**45**, **51**) were synthesized according to the generic synthesis depicted in Scheme 4.3A-B. Alkyl spacers C8 and C12 were synthesized from 8 aminooctanoic acid and 12 aminododeanoic acid respectively. The glycol spacers PEG2 and PEG3 were synthesized from 3-(2-(2-aminoethoxy)ethoxy)propanoic acid and 3-(2-(2-(2-aminoethoxy)ethoxy)ethoxy)propanoic acid respectively. The amino acids were *N*-Boc protected (**38**-**41**) and subsequently converted to the O-Su active esters **42**-**45**. The PEG4 glycol spacer required several additional steps (Scheme 4.3B). Tosylation of tetraethylene glycol (**46**) was followed by azide substitution (**47**) of the sulfonate ester. This allowed a Michael addition to tert-butyl acrylate under

TBAF conditions to give **48**. Acidolysis of the ester (**49**) was followed by reduction of the azide and simultaneous *N*-Boc protection gained acid **50**. The last step introduced the *N*-succinimide ester to give **51**.

The three pharmacophores (**1**-**3**) were under basic conditions conjugated to the five spacers (**42**-**45**, **51**) to yield the fifteen CB_2R probe precursors, **4**-**18** (Scheme 4.3C). The most potent of theses series, *i.e.* compound **5**, was *N*-Boc deprotected (**52**) and thereafter conjugated to the four fluorophores (Scheme 4.3D): affording the BODIPY 493/503 (**19**), BODIPY TMR X (**20**), DY480 XL (**21**) and Cy5 (**22**) LEI-102 based probes.

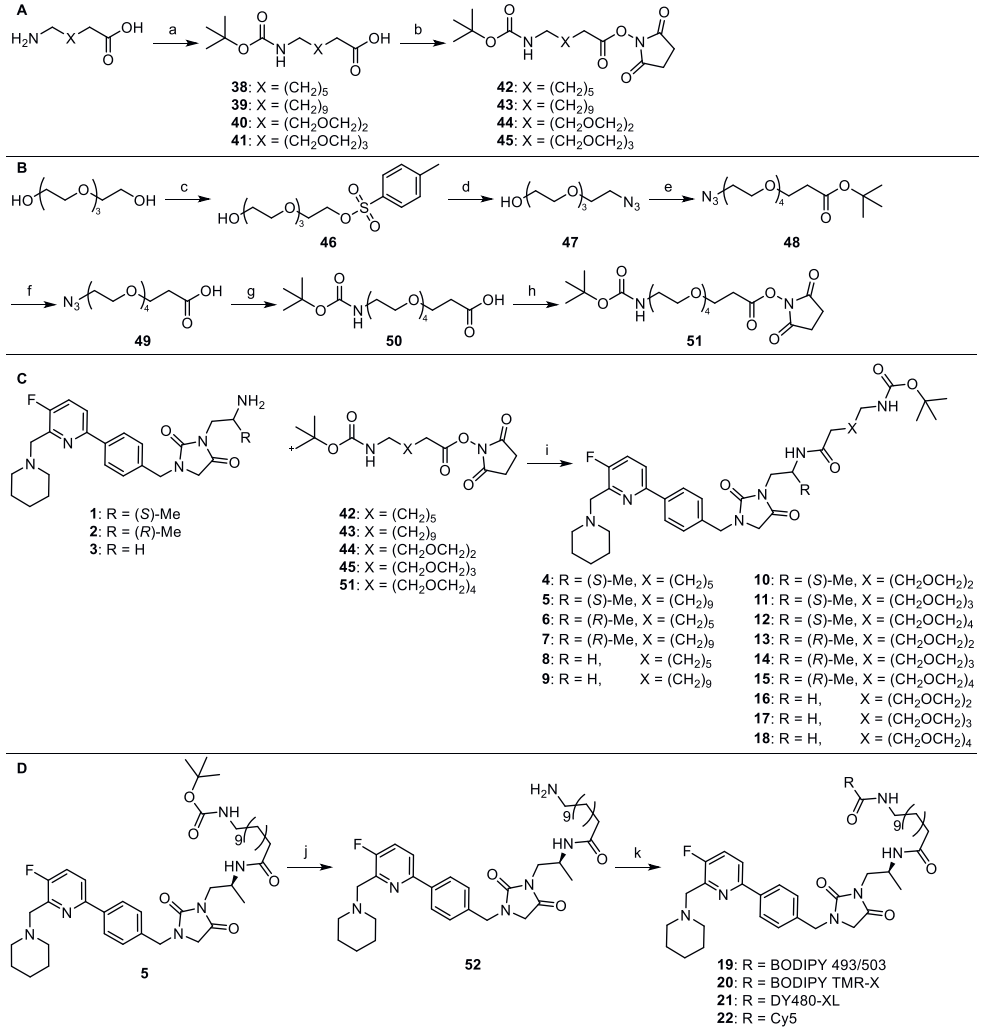

Scheme 4.3 The synthesis of the fifteen intermediates followed by the synthesis of the fluorescent probes. Reagents and conditions: a) *Alkyl*: Et_3N (2 eq), Boc_2O (1.1 eq), acetone:H_2O (1:1, v/v, 0.5 M), RT, 16 h, 95-99%; *PEG*: K_2CO_3 (3 eq), Boc_2O (1.3 eq), H_2O:THF (1:1, v/v, 0.1 M), RT, 16 h, 40-81%; b) *Alkyl*: EDC.HCl (0.8-0.9 eq), NHS (1.7-2.8 eq), DCM (0.3 M), RT, 16-72 h, 36-40%; *PEG*: EDC.HCl (3 eq), NHS (1.5 eq), Et_3N (3 eq), DCM (0.2 M), RT, 16 h, 46-58%; c) *p*-TsCl (1 eq), NaOH (2 M, 1.6 eq), THF (0.6 M), 0 °C, 4 h, 90%; d) NaN_3 (1.5 eq), ACN (0.4 M), 80 °C, 8 h, 94%; e) *tert*-butyl acrylate (1 eq), TBAF (0.4 eq), NaOH (25 wt% in H_2O, 2.6 eq), DCM, RT, 8 h, 75%; f) TFA (50 eq), DCM, RT, 4 h, 65%; g) step 1: 10% Pd/C (0.1 eq), H_2 (g), EtOH (0.3 M), RT, 16 h; step 2: K_2CO_3 (3 eq), Boc_2O (1.3 eq), H_2O:THF (1:1, v/v, 0.1 M), RT, 16 h, 55% (two steps); h) EDC.HCl (1.2 eq),

NHS (1.1 eq), DCM (0.2 M), RT, 16 h, 84% ; i) Et_3N (6 eq), DCM (0.3 M), RT, 1-3 h, 13-65%. j) TFA (110 eq), DCM, RT, 2 h, quant.; k) **19**-**21**: Et_3N (1 eq), fluorophore-NHS ester (1 eq), DCM (0.3 M), RT, 13 h, 64-100%; **22**: HOBt (1.2 eq), DIPEA (2.5 eq), EDC.HCl (1.3 eq), Cyanine 5 carboxylic acid (1.1 eq), DMF (0.007 M), RT, 16 h, quant.).

Molecular Pharmacology

Compounds **1**-**22** were tested at 1 μM in a [^{3}H]CP-55,940 radioligand displacement assay to determine their affinity for the CB_2R and CB_1R. Compounds with less than 50% displacement were considered inactive. The results are shown in Table 4.1.

Table 4.1 hCB_1R and hCB_2R binding affinity and potency of compounds **1**-**22**.

		CB_2R			CB_1R
Compound	**Displacement (% ± SEM)**	**pKi ± SEM**	**pEC_{50} ± SEM**	**E_{max} (% ± SEM)**	**Displacement (% ± SEM)**
LEI-102	84 ± 04	8.6 ± 0.3	7.3 ± 0.4	46 ± 17	-20 ± 08
1	35 ± 10	< 5	6.4 ± 0.1	28 ± 04	-20 ± 27
2	-4 ± 10	n.d.	n.d.	n.d.	-20 ± 17
3	0 ± 13	n.d.	n.d.	n.d.	-2 ± 18
4	25 ± 09	n.d.	n.d.	n.d.	28 ± 13
5	63 ± 05	6.5 ± 0.1	6.3 ± 0.2	-73 ± 04	36 ± 03
6	22 ± 07	n.d.	n.d.	n.d.	-16 ± 29
7	19 ± 08	n.d.	n.d.	n.d.	30 ± 02
8	27 ± 10	n.d.	n.d.	n.d.	-15 ± 28
9	43 ±4	n.d.	n.d.	n.d.	32 ± 20
10	-13 ± 22	n.d.	n.d.	n.d.	-17 ± 24
11	-4 ± 04	n.d.	n.d.	n.d.	-22 ± 14
12	11 ± 21	n.d.	n.d.	n.d.	1 ± 12
13	-12 ± 15	n.d.	n.d.	n.d.	5 ± 10
14	3 ± 01	n.d.	n.d.	n.d.	-3 ± 15
15	1 ± 19	n.d.	n.d.	n.d.	-2 ± 10
16	-7 ± 16	n.d.	n.d.	n.d.	0 ± 16
17	1 ±10	n.d.	n.d.	n.d.	5 ± 19
18	15 ± 14	n.d.	n.d.	n.d.	7 ± 16
19	31 ± 03	< 5	n.d.	n.d.	-12 ± 06
20	16 ± 04	< 5	n.d.	n.d.	-63 ± 37
21	17 ± 14	< 5	n.d.	n.d.	-16 ± 19
22	39 ± 05	6.2 ± 0.6	5.3 ± 0.1	-63 ± 06	10 ± 18

Binding affinities were determined either as displacement (%) or pK_i using a [^{3}H]CP-55,940 radioligand displacement assay on CHO cells stably over expressing either hCB_2R_bgal or hCB_1R_bgal. The displacement percentages represent the percentage of radioligand displaced from the receptor at 1 μM compound. Total binding at vehicle concentration was set at 0%, while non-specific binding was set at 100%. Potency values (pEC_{50}) were obtained for compounds with displacement ≥ 35% using a [^{35}S]GTPγS assay on CHO cells stably over expressing hCB_2R_bgal. The maximum effect (E_{max} in %) was normalized to reference full agonist CP-55,940. All values are presented as the mean ± SEM of at least two independent experiments performed in triplicate. N.d. not determined.

Compound **5** was the only scaffold that was active on hCB_2R (63% ± 5 at 1 μM), but not hCB_1R (pK_i < 5), therefore the four fluorophores were only conjugated to this scaffold. Subsequently, the binding affinity (pK_i), potency (pEC_{50}) and efficacy (E_{max}) of compounds **19**-**22** was determined in a functional [^{35}S]GTPγS assay (Table 4.1 and Figure 4.2). Compound **22** displayed a pK_i (CB_2R) of 6.2 ± 0.6 and was inactive on CB_1R. The other fluorescent probes were inactive at CB_2R. In contrast to LEI-102 and the parent compound **1**, compound **22** was an inverse agonist with a pEC_{50} of 5.3 ± 0.1 and E_{max} of -63% ± 6. Previous research on LEI-121 showed that very small structural changes in a compound may change the functional behaviour of the CB2R.[15] It is not clear from a structural point of view what is the cause of this switch in functionality. However, it could be presumed that the alkyl linker may prevent the

conformational change needed by one or more of the seven transmembrane helices in the binding site to activate the receptor.

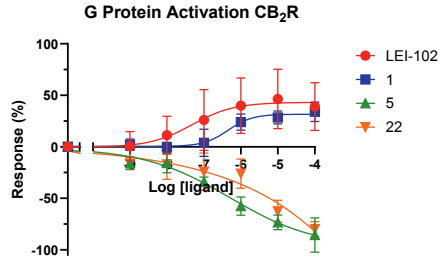

Figure 4.2 G protein activation levels on CB_2R were determined with a [^{35}S]GTPγS assay. Basal activity in presence of vehicle was set to 0%, whereas full G protein activation was determined using 10 µM of full agonist CP-55,940 and was set as 100%. Data are expressed as mean ± SEM from three experiments performed in triplicate.

Conclusion

A structure-based approach in combination with rational design was used to develop a one-step fluorescent probe for the cannabinoid CB_2 receptor based on a pyridin-2-yl-benzyl-imidazolidine-2,4-dione scaffold. Ultimately probe **22** was synthesized with an alkyl spacer and Cy5 fluorescent dye. Probe **22** demonstrated reasonable CB_2R affinity (pK_i 6.2 ± 0.6), was selective over CB_1R and behaved as an inverse agonist (EC_{50} 5.3 ± 0.1, E_{max} -63% ± 6). It is envisioned that probe **22** can be used to visualize CB_2R in cells without the need for copper-assisted click reactions.

Experimental

Chemistry

General Remarks

All reagents and solvents were purchased from commercial sources and were of analytical grade (Sigma-Aldrich, BroadPharm®). Reagents and solvents were not further purified before use. All moisture sensitive reactions were performed under inert atmosphere. Solvents were dried using 4 Å molecular sieves prior to use when anhydrous conditions were required. Water used in reactions was always demineralized. Analytical Thin-layer Chromatography (TLC) was routinely performed to monitor the progression of a reaction and was conducted on Merck Silica gel 60 F254 plates. Reaction compounds on the TLC plates were visualized by UV irradiation (λ254) and/or spraying with potassium permanganate solution (K_2CO_3 (40 g), $KMnO_4$ (6 g), and H_2O (600 mL)), ninhydrin solution (ninhydrin (1.5 g), n-butanol (100 mL) and acetic acid (3.0 mL)) or molybdenum solution ($(NH_4)_6MO_7O_{24}{\cdot}4H_2O$ (25 g/L) and $(NH_4)_4Ce(SO_4)_4{\cdot}2H_2O$ (10 g/L) in sulfuric acid (10%)) followed by heating as appropriate. Purification by flash column chromatography was performed using Screening Devices B.V. silica gel 60 (40-63 µm, pore diameter of 60 Å). Solutions were concentrated using a Heidolph laborata W8 4000 efficient rotary evaporator with a Laboport vacuum pump. Analytical purity was determined with Liquid Chromatography-Mass Spectrometry (LC-MS) using a Finnigan LCQ Advantage MAX apparatus with electrospray ionization (ESI), equipped with a Phenomenex Gemini 3 µm NX-C18 110Å column (50x4.6mm), measuring absorbance at 254 nm using a Waters 2998 PDA UV detector and the m/z ratio by using an Acquity Single Quad (Q1) detector. Injection was with the Finnigan Surveyor Autosampler Plus and pumped through the column with the Finnigan Surveyor LC pump plus to be analysed with the Finnigan Surveyor PDA plus detector. Samples were analysed using eluent gradient 10% → 90% ACN in MilliQ water (+ 0.1% TFA (v/v)). For purification by mass guided preparative High-Performance Liquid Chromatography (Prep-HPLC) was performed on a Waters AutoPurification HPLC/MS apparatus with a Gemini prep column 5 µm 18C 110 Å (150x21.2mm), Waters 2767 Sample manager, Waters 2545

Binary gradient module, Waters SFO System fluidics organizer, Waters 515 HPLC pump M, Waters 515 HPLC pump L attached to a Waters SQ detector Acquity Ultra performance LC. A five column volume purification protocol was applied with the eluents A: 0.2% aq. TFA, B: ACN, flow 25 mL/min, with a minimum start gradients of 0% to maximum end gradient of 100% of B. 1H, 13C, 1H-COSY and HSQC Nuclear Magnetic Resonance (NMR) spectra were recorded on a Bruker AV 300 (300/75 MHz), AV 400 (400/100 MHz), AV 500 (500/125 MHz) or AV 850 (850/214 MHz) spectrometer at ambient temperature using CDCl3 as solvent. Chemical shifts (δ) are referenced in parts per million (ppm) with tetramethylsilane (TMS) or CDCl3 resonance as the internal standard peak (CDCl3/TMS, δ 0.00 for 1H (TMS), δ 77.16 for 13C (CDCl3)). Multiplicity is reported as s = singlet, d = doublet, dd = doublet of doublet, t = triplet, q = quartet, p = quintet, hept = heptet, m = multiplet. Coupling-constants (*J*) are reported in Hertz (Hz).

Synthesis of the imidazolidine building block:

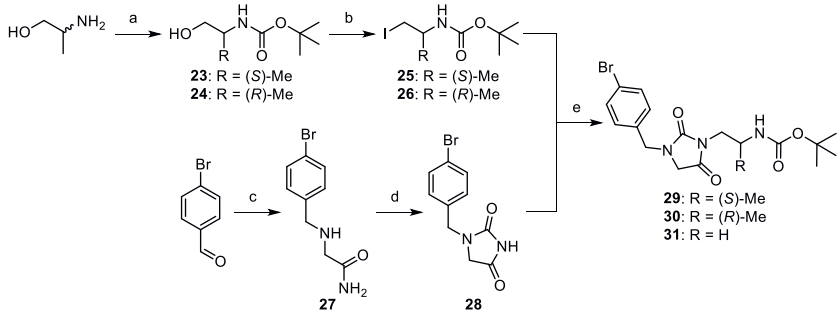

Scheme 4.4 Reagents and conditions: a) Boc_2O (1-2 eq), NaOH (1 M, 2 eq), 1,4-dioxane, RT, 3 h, 97-99%; b) PPh_3 (1.2-1.5 eq), imidazole (1.4-1.8 eq), iodine (1.3-1.7 eq), ACN:Et_2O (3:10, v/v), RT, 16 h, 53-62%; c) step 1: 2-aminoacetamide hydrochloride (1.0 eq), NaOH (1.1 eq), MeOH:H_2O (5:1), RT, 18 h; Step 2: $NaBH_4$ (2.1 eq), 18 h, 91% (two steps); d) CDI (2.1 eq), DMAP (2.1 eq), ACN, 60 °C, 70 h, 37%; e) tert-butyl-(2-bromoethyl)carbamate for **31**/ **25** for **29**/ **26** for **30** (2 eq), 1-(4-bromobenzyl)imidazolidine-2,4-dione (1 eq), K_2CO_3 (6 eq), 18-crown-6 (0.2 eq), DMF (0.2 M), 50 °C, 16 h, 62-88%.

***tert*-Butyl (*S*)-(1-hydroxypropan-2-yl)carbamate (23):** To a cooled (0 °C) and stirred mixture of L-alaninol (0.38 g, 5.0 mmol, 1 eq) in 1 M NaOH (10 mL) was added Boc_2O (2.20 g, 10.0 mmol, 2 eq) dissolved in 1,4-dioxane (10 mL). After stirring for 3 h at RT, the organic solvent was evaporated under reduced pressure and the aqueous layer was acidified to pH = 8 with sat. NH_4Cl (aq). The aqueous layer was extracted thrice with EtOAc. The combined organic layer was washed with H_2O and brine, dried ($MgSO_4$), filtered, and the solvent evaporated under reduced pressure. The crude product was purified with flash column chromatography (SiO_2, 33% EtOAc in pentane) to yield a colourless oil (0.87 g, 5.0 mmol, 99%). ^{1}H-NMR (400 MHz, $CDCl_3$) δ 4.79 (s, 1H), 3.74 (s, 1H), 3.64 – 3.56 (m, 1H), 3.52 – 3.43 (m, 1H), 3.10 (bs, 1H), 1.42 (s, 9H), 1.12 (d, *J* = 7.3 Hz, 3H). ^{13}C-NMR (101 MHz, $CDCl_3$) δ 156.48, 79.78, 67.35, 48.66, 29.61, 17.42. LC-MS (ESI, 10-90): t_R = 4.25 min; m/z = 175.60 $[M]^+$.

***tert*-Butyl (*R*)-(1-hydroxypropan-2-yl)carbamate (24):** To a cooled (0 °C) and stirred mixture of D-alaninol (0.38 g, 5.0 mmol, 1 eq) in 1 M NaOH (10 mL) was added Boc_2O (1.20 g, 5.5 mmol, 1.1 eq) dissolved in 1,4-dioxane (5.5 mL). After stirring for 3 h at RT, the organic solvent was evaporated under reduced pressure and the aqueous layer was acidified to pH = 8 with sat. NH_4Cl (aq). The aqueous layer was extracted thrice with EtOAc. The combined organic layer was washed with H_2O and brine, then dried ($MgSO_4$), filtered and the solvent evaporated under reduced pressure. The crude product was purified with flash column chromatography (SiO_2, 33% EtOAc in pentane) to yield a colourless oil (0.85 g, 4.9 mmol, 97%). ^{1}H-NMR (400 MHz, $CDCl_3$) δ 4.68 (s, 1H), 3.80 – 3.72 (m, 1H), 3.62 (dd, *J* = 10.9, 3.8 Hz, 1H), 3.49 (dd, *J* = 10.9, 6.2 Hz, 1H), 2.75 (bs, 1H) 1.44 (s, 9H), 1.13 (d, *J* = 6.8 Hz, 3H). ^{13}C-NMR

(101 MHz, $CDCl_3$) δ 79.85, 67.60, 48.74, 28.51, 17.44. LC-MS (ESI, 10-90): t_R = 4.20 min; m/z = 175.67 $[M]^+$.

(*S*)-2-((*tert*-Butoxycarbonyl)amino)propyl iodide (25): To a cooled (0 °C) and stirred mixture of **23** (2.00 g, 11.4 mmol, 1 eq), imidazole (1.09 g, 16.0 mmol, 1.4 eq) and PPh_3 (3.59 g, 13.7 mmol, 1.2 eq) in Et_2O:ACN (65 mL, 10:3 v/v) was added I_2 (3.77 g, 14.8 mmol, 1.3 eq). After stirring overnight at RT, the mixture was diluted with EtOAc and quenched with sat. $Na_2S_2O_3$ (aq). After stirring 0.5 h at RT the layers were separated and the aqueous layer extracted twice with EtOAc. The combined organic layer was washed with H_2O and brine, dried ($MgSO_4$), filtered, and the solvent evaporated under reduced pressure. The crude product was purified with flash column chromatography (SiO_2, 2-20% EtOAc in pentane) to yield a yellow oil (2.02 g, 7.1 mmol, 62%). ^{1}H-NMR (400 MHz, $CDCl_3$) δ 4.63 (s, 1H), 3.53 (s, 1H), 3.41 (s, 1H), 3.30 (dd, *J* = 9.8, 3.7 Hz, 1H), 1.45 (s, 9H), 1.20 (d, *J* = 6.6 Hz, 3H). ^{13}C-NMR (101 MHz, $CDCl_3$) δ 154.94, 79.83, 46.00, 28.50, 21.34, 16.21. LC-MS (ESI, 10-90): t_R = 3.77 min; m/z = 285.27 $[M+H]^+$.

(*R*)-2-((*tert*-Butoxycarbonyl)amino)propyl iodide (26): To a cooled (0 °C) and stirred mixture of **24** (7.25 g, 41.4 mmol, 1 eq), imidazole (5.07 g, 74.5 mmol, 1.8 eq) and 16.28 g PPh_3 (62.1 mmol, 1.5 eq) in Et_2O:ACN (250mL, 10:3, v/v) was added I_2 (17.85 g, 70.3 mmol, 1.7 eq). After stirring overnight at RT, the mixture was diluted with EtOAc and quenched with sat. $Na_2S_2O_3$ (aq). After stirring 0.5 h at RT the layers were separated and the aqueous layer extracted twice with EtOAc. The combined organic layer was washed with H_2O and brine, dried over $MgSO_4$, filtered, and the solvent evaporated under reduced pressure. The crude product was purified with flash column chromatography (SiO_2, 2-20% EtOAc in pentane) to yield a yellow oil (6.28 g, 21.9 mmol, 53%). ^{1}H-NMR (400 MHz, $CDCl_3$) δ 4.62 (s, 1H), 3.56 – 3.45 (m, 1H), 3.39 (dd, *J* = 9.9, 3.7 Hz, 1H), 3.27 (dd, *J* = 9.9, 3.7 Hz, 1H), 1.43 (s, 9H), 1.18 (d, *J* = 6.6 Hz, 3H). ^{13}C-NMR (101 MHz, $CDCl_3$) δ 154.91, 79.78, 46.41, 28.47, 20.94, 16.15.

2-((4-Bromobenzyl)amino)acetamide (27): To a stirred mixture of 4-bromobenzaldehyde (9.2 g (49.7 mmol, 1.1 eq) and 2-aminoacetamide hydrochloride (5.06 g, 45.8 mmol, 1.0 eq) in MeOH:H_2O (170 mL, 5:1, v/v) was added NaOH (2.06 g, 51.5 mmol, 1.1 eq). After stirring at RT overnight, $NaBH_4$ (3.6 g, 95.2 mmol, 2.1 eq) was added and the solution was stirred overnight at RT. The solution was acidified to pH 3 with 2 M HCl, then neutralized with sat. $NaHCO_3$ (aq). Methanol was evaporated under reduced pressure and the resulting slurry was filtered to yield a white solid (11.0 g, 45.2 mmol, 91%). ^{1}H-NMR (400 MHz, $CDCl_3$) δ 7.50 – 7.43 (m, 2H), 7.22 – 7.16 (m, 2H), 6.93 (s, 1H), 5.85 (s, 1H), 3.75 (s, 2H), 3.29 (s, 2H). ^{13}C-NMR (101 MHz, $CDCl_3$) δ 174.42, 138.40, 131.80, 129.89, 121.32, 53.29, 51.78.

1-(4-Bromobenzyl)imidazolidine-2,4-dione (28): To stirred suspension of **27** (10.0 g, 40.1 mmol, 1.0 eq) in acetonitrile (300 mL) were added CDI (13.86 g, 85.5 mmol, 2.1 eq) and DMAP (10.2 g, 83.5 mmol, 2.1 eq). The mixture was heated (60 °C) under inert atmosphere for 70 h. 1 M HCl (aq, 250 mL) was added and the aqueous layer extracted thrice with EtOAc. The combined organic layer was washed with H_2O and brine, dried ($MgSO_4$), filtered, and the solvent evaporated under reduced pressure. The crude product was purified with flash column chromatography with dry loading over Celite (5-10% acetone in DCM) to yield a yellow solid (3.95 g, 14.7 mmol, 37%). ^{1}H-NMR (400 MHz, $CDCl_3$) δ 7.90 (s, 1H), 7.51 (d, *J* = 8.4 Hz, 2H), 7.15 (d, *J* = 8.4 Hz, 2H), 4.49 (s, 2H), 3.79 (s, 2H). ^{13}C-NMR (101 MHz, $CDCl_3$) δ 174.26, 132.41, 129.37, 51.17, 46.78.

***tert*-Butyl (*S*)-(1-(3-(4-bromobenzyl)-2,5-dioxoimidazolidin-1-yl)propan-2-yl)carbamate (29):** A mixture of **28** (2.70 g, 10.0 mmol, 1 eq), **25** (5.72 g, 20.1 mmol, 2 eq), K_2CO_3 (8.32 g, 60.2 mmol, 6 eq) and 18-crown-6 (0.53 g, 2.0 mmol, 0.2 eq) in DMF (55 mL) was heated (50 °C) overnight. After cooling

to RT the mixture was diluted with H_2O (40 mL) and Et_2O (40 mL). The layers were separated and the aqueous layer extracted thrice with Et_2O. The combined organic layer was washed five times with H_2O and once with brine, dried ($MgSO_4$), filtered, and the solvent evaporated under reduced pressure. The crude product was purified with flash column chromatography (SiO_2, 20-50% EtOAc in pentane) to yield a yellow solid (2.67 g, 6.3 mmol, 62%). ^{1}H-NMR (850 MHz, $CDCl_3$) δ 7.48 (d, *J* = 8.4 Hz, 2H), 7.18 (d, *J* = 8.1 Hz, 2H), 4.71 – 4.67 (m, 2H), 4.34 (d, *J* = 15.3 Hz, 1H), 4.06 (hept, *J* = 6.5 Hz, 1H), 3.72 (d, *J* = 17.1 Hz, 1H), 3.66 (d, *J* = 17.2 Hz, 1H), 3.51 (d, *J* = 7.9 Hz, 2H), 1.37 (s, 9H), 1.17 (d, *J* = 6.8 Hz, 3H). ^{13}C-NMR (214 MHz, $CDCl_3$) δ 170.11, 157.03, 155.73, 134.58, 132.24, 129.93, 122.26, 79.32, 49.10, 46.16, 45.52, 44.97, 28.41, 18.63. LC-MS (ESI, 10-90): t_R = 7.64 min; m/z = 425.53 $[M + H]^+$.

***tert*-Butyl (*R*)-(1-(3-(4-bromobenzyl)-2,5-dioxoimidazolidin-1-yl)propan-2-yl)carbamate (30):** A mixture of **28** (2.58 g, 9.6 mmol, 1 eq), **26** (6.28 g, 22.0 mmol, 2.3 eq), K_2CO_3 (7.95 g, 57.5 mmol, 6 eq) and 18-crown-6 (0.51 g, 1.9 mmol, 0.2 eq) in DMF (55 mL) was heated (50 °C) overnight. After cooling to RT the mixture was diluted with H_2O (40 mL) and Et_2O (40 mL). The layers were separated and the aqueous layer extracted thrice with Et_2O. The combined organic layer was washed five times with H_2O and once with brine, dried ($MgSO_4$), filtered, and the solvent evaporated under reduced pressure. The crude product was purified with flash column chromatography (SiO_2, 20-50% EtOAc in pentane) to yield a yellow solid (2.69 g, 6.3 mmol, 66%). ^{1}H-NMR (300 MHz, $CDCl_3$) δ 7.48 (d, *J* = 8.4 Hz, 2H), 7.17 (d, *J* = 8.3 Hz, 2H), 4.75 – 4.64 (m, 2H), 4.35 (d, *J* = 15.3 Hz, 1H), 4.06 (hept, *J* = 7.1 Hz, 1H), 3.69 (d, *J* = 7.0 Hz, 2H), 3.51 (d, *J* = 7.1 Hz, 2H), 1.38 (s, 9H), 1.17 (d, *J* = 6.8 Hz, 3H). ^{13}C-NMR (101 MHz, $CDCl_3$) δ 170.10, 157.03, 155.74, 134.58, 132.25, 129.93, 122.23, 80.50, 49.11, 46.18, 45.52, 44.96, 28.41, 18.63. LC-MS (ESI, 10-90): t_R = 7.60 min; m/z = 425.67 $[M + H]^+$.

***tert*-Butyl (2-(3-(4-bromobenzyl)-2,5-dioxoimidazolidin-1-yl)ethyl)carbamate (31):** A mixture of **28** (1.74 g, 6.5 mmol, 1 eq), *tert*-butyl-(2-bromoethyl)carbamate (2.90 g, 12.9 mmol, 2 eq), K_2CO_3 (5.36 g, 38.8 mmol, 6 eq) and 18-crown-6 (0.34 g, 1.3 mmol, 0.2 eq) was heated (50 °C) overnight. After cooling to RT the mixture was diluted with H_2O (40 mL) and Et_2O (40 mL). The layers were separated and the aqueous layer extracted thrice with Et_2O. The combined organic layer was washed five times with H_2O and once with brine, dried ($MgSO_4$), filtered, and the solvent evaporated under reduced pressure. The crude product was purified with flash column chromatography (SiO_2, 20-50% EtOAc in pentane) to yield a yellow solid (2.35 g, 5.7 mmol, 88%). ^{1}H-NMR (400 MHz, $CDCl_3$) δ 7.47 (d, *J* = 8.4 Hz, 2H), 7.16 (d, *J* = 8.0 Hz, 2H), 4.94 (t, *J* = 6.2 Hz, 1H), 4.51 (s, 2H), 3.70 (s, 2H), 3.68 – 3.62 (m, 2H), 3.37 (q, *J* = 5.8 Hz, 2H), 1.38 (s, 9H). ^{13}C-NMR (101 MHz, $CDCl_3$) δ 13C NMR (101 MHz, CDCl3) δ 170.05, 156.89, 156.25, 134.53, 132.24, 129.91, 122.27, 79.46, 49.15, 46.17, 39.58, 39.33, 28.41. LC-MS (ESI, 10-90): t_R = 7.21 min; m/z = 413.47 $[M + H]^+$.

Synthesis of the pyridinylbenzyl building block:

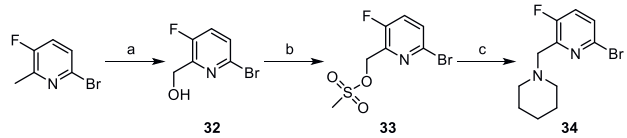

Scheme 4.5 Reagents and conditions: a) step 1: m-CPBA (1.8 eq), 0 °C-RT, DCM, 4 days; step 2: TFAA (2.2 eq), 55 °C, 3 h; step 3: K_2CO_3 (2.3 eq), THF:MeOH (20:1), 17 h, 35% (three steps); b) Et_3N (2.3 eq), MsCl (1.7 eq), THF, 0 °C-RT, 1 h, 75%; c) K_2CO_3 (2.2 eq), piperidine (1.2 eq), ACN (0.2 M), 50 °C, 1.5 h, 93%.

(6-Bromo-3-fluoropyridin-2-yl)methanol (32): To a stirred and cooled (0 °C) mixture under inert atmosphere of 6-bromo-3-fluoro-2-methylpyridine (10.7 g, 56.3 mmol, 1 eq) in DCM (370 mL) was added portion-wise *m*-CPBA (23.6 g, 70-75%, 100 mmol, 1.8 eq). The reaction mixture was stirred at room temperature (RT) for 4 days. Sat. $NaHCO_3$ (aq) and sat. $Na_2S_2O_3$ (aq) was added (1:1, v/v) and the

layers were separated. The aqueous layer was extracted thrice with DCM. The combined organic layer was dried ($MgSO_4$), filtered, and concentrated under reduced pressure. To the residue was added TFAA (17 mL, 122 mmol, 2.2 eq) at 0 °C. After 15 minutes the temperature was increased to 55 °C for 3 h. The mixture was concentrated under reduced pressure, redissolved in DCM and sat. Na_2CO_3 (aq) was added. The layers were separated and the organic layer was washed with sat. $NaHCO_3$ (aq). The solvent was evaporated and the residue was dissolved in THF:MeOH (20:1, v/v) and K_2CO_3 (18.2 g, 132 mmol, 2.3 eq) was added. After 17 h H_2O was added and the layers were separated. The aqueous layer was extracted thrice with EtOAc. The combined organic layer was dried ($MgSO_4$), filtered, and the solvent evaporated under reduced pressure. The crude product was purified with flash column chromatography (10-20% EtOAc in pentane) to yield a white solid (5.79 g, 19.7 mmol, 35%). ^{1}H-NMR (400 MHz, $CDCl_3$) δ 7.42 (dd, *J* = 8.3, 3.5 Hz, 1H), 7.29 (t, *J* = 8.5 Hz, 1H), 4.80 (d, *J* = 2.0 Hz, 2H), 3.36 (s, 1H). ^{13}C-NMR (101 MHz, $CDCl_3$) δ 156.10 (d, *J* = 256.6 Hz), 148.84, 135.01 (d, *J* = 2.8 Hz), 128.17 (d, *J* = 4.1 Hz), 126.09 (d, *J* = 20.0 Hz), 59.08.

(6-Bromo-3-fluoropyridin-2-yl)methyl methanesulfonate (33): To a cooled (0 °C) mixture of **32** (1.6 g, 7.8 mmol, 1 eq) and Et_3N (2.5 mL, 17.9 mmol, 2.3 eq) in dry THF (40 mL) was added dropwise MsCl (1.0 mL, 12.9 mmol, 1.7 eq). After stirring at RT for 1 h the solution was concentrated under reduced pressure. DCM and H_2O were added and the layers were separated. The aqueous layer was extracted thrice with DCM. The combined organic layer was washed with brine, dried ($MgSO_4$), filtered, and the solvent evaporated under reduced pressure to yield a yellow solid (1.65 g, 5.8 mmol, 75%). ^{1}H-NMR (400 MHz, $CDCl_3$) δ 7.53 (dd, *J* = 8.6, 3.5 Hz, 1H), 7.38 (t, *J* = 8.5 Hz, 1H), 5.34 (d, *J* = 2.1 Hz, 2H), 3.14 (s, 3H). ^{13}C-NMR (101 MHz, $CDCl_3$) δ 157.85 (d, *J* = 261.4 Hz), 142.22 (d, *J* = 16.4 Hz), 135.64 (d, *J* = 3.1 Hz), 130.75 (d, *J* = 4.6 Hz), 127.06 (d, *J* = 20.5 Hz), 65.50, 38.46.

6-Bromo-3-fluoro-2-(piperidin-1-ylmethyl)pyridine (34): A mixture of **33** (4.68 g, 16.5 mmol, 1 eq), K_2CO_3 (4.98 g, 36.2 mmol, 2.2 eq) and piperidine (1.95 mL, 19.8 mmol, 1.2 eq) in ACN (80 mL) was heated (50 °C) for 1.5 h. After adding H_2O (100 mL) and DCM (100 mL) the layers were separated and the aqueous layer extracted thrice with DCM. The combined organic layer was washed with brine, dried ($MgSO_4$), filtered, and the solvent evaporated under reduced pressure. The crude product was purified with flash column chromatography (SiO_2, 20-50% EtOAc in pentane) to yield a yellow solid (4.18 g, 15.3 mmol, 93%). ^{1}H-NMR (400 MHz, $CDCl_3$) δ 7.36 (dd, *J* = 8.5, 3.5 Hz, 1H), 7.24 (t, *J* = 8.5 Hz, 1H), 3.67 (d, *J* = 2.7 Hz, 2H), 2.48 (t, *J* = 5.3 Hz, 4H), 1.56 (p, *J* = 5.8 Hz, 4H), 1.44 – 1.35 (m, 2H). ^{13}C-NMR (101 MHz, $CDCl_3$) δ 158.24 (d, *J* = 257.9 Hz), 147.66 (d, *J* = 16.7 Hz), 134.85 (d, *J* = 4.1 Hz), 128.16 (d, *J* = 4.3 Hz), 126.02 (d, *J* = 21.8 Hz), 58.19 (d, *J* = 3.1 Hz), 54.45, 25.97, 24.16. LC-MS (ESI, 10-90): t_R = 1.32 min; m/z = 273.07 $[M + H]^+$.

Synthesis of the pyridinylbenzylimidazolidine-2,4-dione scaffolds:

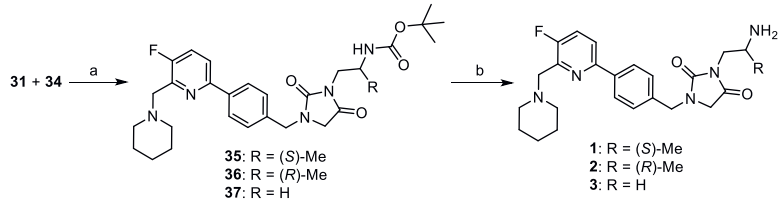

Scheme 4.6 Reagents and conditions: a) step 1: KOAc (4-6 eq), bis(pinacolato)diboron (1.5-2.2 eq), $Pd(dppf)Cl_2$ (0.05-0.08 eq), DMF (degassed, 0.2 M), 75 °C, 16 h; step 2: 34 (1 eq), K_2CO_3 (4-8 eq), $Pd(PPh_3)_4$ (0.05-0.2 eq), toluene:EtOH (degassed, 4:1, v/v, 0.2 M), 75 °C, 16 h, 36-76% (two steps); b) 4 M HCl (1,4-dioxane, 4 eq), acetonitrile (0.5 M), 80 °C, 2 h, 62-86%.

***tert*-Butyl (*S*)-(1-(3-(4-(5-fluoro-6-(piperidin-1-ylmethyl)pyridin-2-yl)benzyl)-2,5-dioxoimidazolidin-1-yl)propan-2-yl)carbamate (35):** A stirred and degassed mixture of **29** (2.67 g, 6.3 mmol, 1.1 eq), $Pd(dppf)Cl_2$ (0.24 g, 0.3 mmol, 0.05 eq), bis(pinacolato)diboron (2.40 g, 9.5 mmol, 1.5 eq) and KOAc (2.70 g, 27.5 mmol, 4.4 eq) in DMF (30 mL) was heated (75 °C) overnight. The reaction was diluted at RT with H_2O and EtOAc. The layers were separated and the aqueous layer extracted thrice with EtOAc. The combined organic layer was washed with sat. $NaHCO_3$ (aq), H_2O, and brine, dried ($MgSO_4$), filtered and the solvent evaporated under reduced pressure. The crude residue was used without further purification. The crude residue was co-evaporated thrice with chloroform and re-dissolved in degassed toluene:EtOH (30 mL, 4:1, v/v). To the stirred mixture was added **34** (1.64 g, 6.0 mmol, 1 eq), K_2CO_3 (3.46 g, 25.0 mmol, 4 eq) and $Pd(PPh_3)_4$ (0.50 g, 0.4 mmol, 0.06 eq). After heating (75 °C) overnight the reaction was diluted at RT with H_2O and EtOAc. The layers were separated and the aqueous layer extracted thrice with EtOAc. The combined organic layer was washed with H_2O and brine, dried ($MgsO_4$), filtered and the solvent evaporated under reduced pressure. The crude product was purified with flash column chromatography (SiO_2, 0-4% MeOH in DCM) to yield a brown oil (1.40 g, 2.6 mmol, 42%). ^{1}H-NMR (400 MHz, $CDCl_3$) δ 7.94 (d, *J* = 8.3 Hz, 2H), 7.60 (dd, *J* = 8.6, 3.5 Hz, 1H), 7.41 (t, *J* = 8.8 Hz, 1H), 7.35 (d, *J* = 7.9 Hz, 2H), 4.82 – 4.68 (m, 2H), 4.47 (d, *J* = 15.2 Hz, 1H), 4.05 (p, *J* = 7.1 Hz, 1H), 3.82 (d, *J* = 2.7 Hz, 2H), 3.72 (d, *J* = 8.8 Hz, 2H), 3.52 (d, *J* = 6.6 Hz, 2H), 2.62 – 2.55 (m, 4H), 1.59 (p, *J* = 5.7 Hz, 4H), 1.38 (s, 11H), 1.17 (d, *J* = 6.7 Hz, 3H). ^{13}C-NMR (101 MHz, $CDCl_3$) δ 170.27, 157.94 (d, *J* = 258.1 Hz), 157.06, 155.71, 151.88 (d, *J* = 4.9 Hz), 145.63 (d, *J* = 15.1 Hz), 138.62, 135.95, 128.59, 127.61, 127.55, 123.70 (d, *J* = 20.4 Hz), 120.39 (d, *J* = 4.1 Hz), 79.26, 58.44 (d, *J* = 3.0 Hz), 54.36, 49.10, 46.49, 45.60, 44.80, 28.43, 25.98, 24.18, 18.62. LC-MS (ESI, 10-90): t_R = 5.47 min; m/z = 540.20 $[M + H]^+$.

***tert*-Butyl (*R*)-(1-(3-(4-(5-fluoro-6-(piperidin-1-ylmethyl)pyridin-2-yl)benzyl)-2,5-dioxoimidazolidin-1-yl)propan-2-yl)carbamate (36):** A stirred and degassed mixture of **30** (2.69 g, 6.3 mmol, 1 eq), $Pd(dppf)Cl_2$ (0.26 g, 0.4 mmol, 0.06 eq), bis(pinacolato)diboron (2.40 g, 9.5 mmol, 1.5 eq) and KOAc (2.72 g, 27.8 mmol, 4.4 eq) in DMF (30 mL) was heated (75 °C) overnight. The reaction was diluted at RT with H_2O and EtOAc. The layers were separated and the aqueous layer extracted thrice with EtOAc. The combined organic layer was washed with sat. $NaHCO_3$ (aq), H_2O, and brine, dried ($MgSO_4$), filtered and the solvent evaporated under reduced pressure. The crude residue was used without further purification. The crude residue was co-evaporated thrice with chloroform and re-dissolved in degassed toluene:EtOH (30 mL, 4:1, v/v). To the stirred mixture was added **34** (1.67 g, 6.1 mmol, 1 eq), K_2CO_3 (5.05 g, 36.5 mmol, 5.8 eq) and $Pd(PPh_3)_4$ (0.73 g, 0.6 mmol, 0.1 eq). After heating (75 °C) overnight the reaction was diluted at RT with H_2O and EtOAc. The layers were separated and the aqueous layer extracted thrice with EtOAc. The combined organic layer was washed with H_2O and brine, dried ($MgsO_4$), filtered and the solvent evaporated under reduced pressure. The crude product was purified with flash column chromatography (SiO_2, 0-4% MeOH in DCM) to yield an orange oil (2.57 g, 4.8 mmol, 76%). ^{1}H-NMR (300 MHz, $CDCl_3$) δ 7.95 (d, *J* = 8.3 Hz, 2H), 7.60 (dd, *J* = 8.6, 3.6 Hz, 1H), 7.41 (t, *J* = 8.8 Hz, 1H), 7.36 (d, *J* = 8.2 Hz, 2H), 4.81 – 4.69 (m, 1H), 4.48 (d, *J* = 15.2 Hz, 1H), 4.06 (p, *J* = 7.0 Hz, 1H), 3.81 (d, *J* = 2.6 Hz, 2H), 3.72 (d, *J* = 5.0 Hz, 2H), 3.53 (d, *J* = 6.6 Hz, 2H), 2.58 (t, *J* = 5.4 Hz, 4H), 1.66 – 1.52 (m, 4H), 1.39 (s, 11H), 1.17 (d, *J* = 6.7 Hz, 3H). ^{13}C-NMR (75 MHz, $CDCl_3$) δ 170.24, 158.36 (d, *J* = 195.0 Hz), 156.24, 155.69, 151.84 (d, *J* = 4.9 Hz), 145.94 (d, *J* = 16.0 Hz), 138.71, 135.94, 128.60, 127.57, 123.66 (d, *J* = 20.4 Hz), 120.31 (d, *J* = 4.2 Hz), 79.27, 58.64 (d, *J* = 3.2 Hz), 54.47, 53.56, 49.12, 46.53, 45.65, 44.80, 28.45, 26.13, 24.28, 18.65.LC-MS (ESI, 10-90): t_R = 5.51 min; m/z = 540.20 $[M + H]^+$.

***tert*-Butyl (2-(3-(4-(5-fluoro-6-(piperidin-1-ylmethyl)pyridin-2-yl)benzyl)-2,5-dioxoimidazolidin-1-yl)ethyl)carbamate (37)**: A stirred and degassed mixture of **31** (2.35 g, 5.5 mmol, 1.4 eq), $Pd(dppf)Cl_2$ (0.23 g, 0.3 mmol, 0.08 eq), bis(pinacolato)diboron (2.10 g, 8.3 mmol, 2.2 eq) and KOAc (2.38 g, 24.3 mmol, 6.4 eq) in DMF (30 mL) was heated (75 °C) overnight. The reaction was diluted at RT with

H_2O and EtOAc. The layers were separated and the aqueous layer extracted thrice with EtOAc. The combined organic layer was washed with sat. $NaHCO_3$ (aq), H_2O, and brine, dried ($MgSO_4$), filtered and the solvent evaporated under reduced pressure. The crude residue was used without further purification. The crude residue was co-evaporated thrice with chloroform and re-dissolved in degassed toluene:EtOH (30 mL, 4:1, v/v). To the stirred mixture was added **34** (1.04 g, 3.8 mmol, 1 eq), K_2CO_3 (4.57 g, 33.1 mmol, 8.7 eq) and $Pd(PPh_3)_4$ (0.64 g, 0.6 mmol, 0.2 eq). After heating (75 °C) overnight the reaction was diluted at RT with H_2O and EtOAc. The layers were separated and the aqueous layer extracted thrice with EtOAc. The combined organic layer was washed with H_2O and brine, dried ($MgsO_4$), filtered and the solvent evaporated under reduced pressure. The crude product was purified with flash column chromatography (SiO_2, 0-4% MeOH in DCM) to yield an orange oil (1.04 g, 2.0 mmol, 36%). ^{1}H-NMR (400 MHz, $CDCl_3$) δ 7.95 (d, *J* = 8.3 Hz, 2H), 7.61 (dd, *J* = 8.6, 3.6 Hz, 1H), 7.41 (t, *J* = 8.8 Hz, 1H), 7.35 (d, *J* = 7.9 Hz, 2H), 4.98 (t, *J* = 6.2 Hz, 1H), 4.60 (s, 2H), 3.82 (d, *J* = 2.6 Hz, 2H), 3.73 (s, 2H), 3.71 – 3.64 (m, 2H), 3.39 (q, *J* = 5.7 Hz, 2H), 2.58 (t, *J* = 5.4 Hz, 4H), 1.59 (p, *J* = 5.6 Hz, 4H), 1.41 (s, 11H). ^{13}C-NMR (101 MHz, $CDCl_3$) δ 170.11, 157.84 (d, *J* = 258.0 Hz), 156.84, 156.13, 151.75 (d, *J* = 4.8 Hz), 138.62, 135.78, 128.53, 127.49, 123.60 (d, *J* = 20.5 Hz), 120.27 (d, *J* = 4.2 Hz), 79.38, 58.48 (d, *J* = 3.0 Hz), 54.35, 49.06, 46.42, 39.37, 28.35, 27.43, 25.98, 24.15. LC-MS (ESI, 10-90): t_R = 5.33 min; m/z = 526.13 $[M + H]^+$.

(*S*)-3-(2-Aminopropyl)-1-(4-(5-fluoro-6-(piperidin-1-ylmethyl)pyridin-2-yl)benzyl)imidazolidine-2,4-dione (1): To a solution of **35** (1.40 g, 2.6 mmol, 1 eq) in ACN (5 mL) was added 4 M HCl in 1,4-dioxane (2.7 mL, 10.8 mmol, 4.1 eq). After the reaction was heated (80 °C) for 2 h, the ACN was evaporated under reduced pressure. The mixture was basified with 1M NaOH (aq) until pH = 10. The aqueous layer was extracted with $CHCl_3$:MeOH (7:1, v/v). NaCl was added for increased separation. The combined organic layer was dried ($MgSO_4$), filtered, and the solvent evaporated under reduced pressure. The crude product was purified with flash column chromatography (SiO_2, 0-4% MeOH in DCM with 2% Et_3N (v/v)) to yield an orange oil (0.98 g, 2.2 mmol, 86%). ^{1}H-NMR (400 MHz, $CDCl_3$) δ 7.96 (d, *J* = 8.2 Hz, 2H), 7.62 (dd, *J* = 8.6, 3.5 Hz, 1H), 7.42 (t, *J* = 8.8 Hz, 1H), 7.34 (d, *J* = 8.3 Hz, 2H), 4.61 (s, 2H), 3.83 (d, *J* = 2.7 Hz, 2H), 3.78 (s, 2H), 3.54 – 3.38 (m, 2H), 3.32 – 3.19 (m, 1H), 2.59 (s, 4H), 1.60 (p, *J* = 5.6 Hz, 6H), 1.46 – 1.36 (m, 2H), 1.13 (d, *J* = 6.4 Hz, 3H). ^{13}C-NMR (101 MHz, $CDCl_3$) δ 170.35, 157.98 (d, *J* = 258.1 Hz), 157.25, 151.84 (d, *J* = 4.9 Hz), 145.80 (d, *J* = 15.0 Hz), 138.79, 135.92, 128.66, 127.63, 123.73 (d, *J* = 20.4 Hz), 120.43 (d, *J* = 4.2 Hz), 58.55 (d, *J* = 3.2 Hz), 54.45, 49.15, 47.19, 46.61, 46.21, 26.06, 24.23, 22.10. LC-MS (ESI, 10-90): t_R = 3.74 min; m/z = 440.33 $[M + H]^+$. HRMS $[C_{24}H_{30}FN_5O_2 + H]^+$: 440.24563 calculated, 440.24533 found.

(*R*)-3-(2-Aminopropyl)-1-(4-(5-fluoro-6-(piperidin-1-ylmethyl)pyridin-2-yl)benzyl)imidazolidine-2,4-dione (2): To a solution of **36** (2.57 g, 4.8 mmol, 1 eq) in ACN (10 mL) was added 4 M HCl in 1,4-dioxane (4.9 mL, 19.8 mmol, 4.1 eq). After the reaction was heated (80 °C) for 2 h, the ACN was evaporated under reduced pressure. The mixture was basified with 1 M NaOH (aq) until pH = 10. The aqueous layer was extracted with $CHCl_3$:MeOH (7:1, v/v). NaCl was added for increased separation. The combined organic layer was dried ($MgSO_4$), filtered, and the solvent evaporated under reduced pressure. The crude product was purified with flash column chromatography (SiO_2, 0-4% MeOH in DCM with 2% Et_3N (v/v)) to yield an orange oil (1.70 g, 3.8 mmol, 81%). ^{1}H-NMR (400 MHz, $CDCl_3$) δ 7.94 (d, *J* = 8.3 Hz, 2H), 7.60 (dd, *J* = 8.6, 3.6 Hz, 1H), 7.40 (t, *J* = 8.7 Hz, 1H), 7.33 (d, *J* = 8.3 Hz, 2H), 4.60 (s, 2H), 3.80 (d, *J* = 2.6 Hz, 2H), 3.76 (s, 2H), 3.52 – 3.36 (m, 2H), 3.24 (h, *J* = 6.5 Hz, 1H), 2.57 (t, *J* = 5.4 Hz, 4H), 1.58 (p, *J* = 5.6 Hz, 4H), 1.52 – 1.46 (m, 2H), 1.44 – 1.34 (m, 2H), 1.11 (d, *J* = 6.4 Hz, 3H). ^{13}C-NMR (101 MHz, $CDCl_3$) δ 170.29, 157.92 (d, *J* = 258.2 Hz), 157.20, 151.76 (d, *J* = 4.9 Hz), 145.90 (d, *J* = 15.0 Hz), 138.75, 135.87, 128.61, 127.58, 123.66 (d, *J* = 20.4 Hz), 120.33 (d, *J* = 4.1 Hz), 58.59 (d, *J* = 3.1 Hz), 54.43, 49.09,

47.18, 46.55, 46.15, 26.07, 24.23, 22.08. LC-MS (ESI, 10-90): t_R = 3.72 min; m/z = 440.20 $[M + H]^+$. HRMS $[C_{24}H_{30}FN_5O_2 + H]^+$: 440.24563 calculated, 440.24530 found.

3-(2-Aminoethyl)-1-(4-(5-fluoro-6-(piperidin-1-ylmethyl)pyridin-2-yl)benzyl)imidazolidine-2,4-dione (3): To a solution of **37** (1.04 g, 2.0 mmol, 1 eq) in ACN (4 mL) was added 4 M HCl in 1,4-dioxane (2.1 mL, 8.2 mmol, 4.1 eq). After the reaction was heated (80 °C) for 2 h, the ACN was evaporated under reduced pressure. The mixture was basified with 1 M NaOH (aq) until pH = 10. The aqueous layer was extracted with $CHCl_3$:MeOH (7:1, v/v). NaCl was added for increased separation. The combined organic layer was dried ($MgSO_4$), filtered, and the solvent evaporated under reduced pressure. The crude product was purified with flash column chromatography (SiO_2, 0-4% MeOH in DCM with 2% Et_3N (v/v)) to yield an orange oil (0.52 g, 1.2 mmol, 62%). ^{1}H-NMR (400 MHz, $CDCl_3$) δ 7.95 (d, *J* = 8.3 Hz, 2H), 7.61 (dd, *J* = 8.6, 3.6 Hz, 1H), 7.42 (t, *J* = 8.8 Hz, 1H), 7.34 (d, *J* = 8.3 Hz, 2H), 4.61 (s, 2H), 3.82 (d, *J* = 2.7 Hz, 2H), 3.77 (s, 2H), 3.61 (t, *J* = 6.3 Hz, 2H), 2.95 (t, *J* = 6.3 Hz, 2H), 2.65 – 2.54 (m, 4H), 1.59 (p, *J* = 5.6 Hz, 4H), 1.45 – 1.35 (m, 2H), 1.07 (t, *J* = 7.2 Hz, 2H). ^{13}C-NMR (101 MHz, $CDCl_3$) δ 170.24, 157.97 (d, *J* = 257.9 Hz), 157.11, 151.79 (d, *J* = 5.0 Hz), 146.00 (d, *J* = 15.1 Hz), 138.83, 135.87, 128.66, 127.63, 123.69 (d, *J* = 20.4 Hz), 120.36 (d, *J* = 4.2 Hz), 58.65 (d, *J* = 3.1 Hz), 54.48, 49.17, 46.59, 42.25, 40.53, 26.14, 24.29. LC-MS (ESI, 10-90): t_R = 3.70 min; m/z = 426.07 $[M + H]^+$. HRMS $[C_{23}H_{28}FN_5O_2 + H]^+$: 426.22998 calculated, 426.23010 found.

Synthesis of the alkyl and glycol (PEG2/3) spacers:

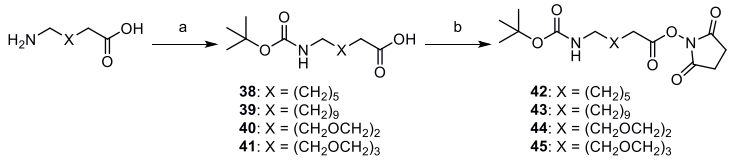

Scheme 4.7 Reagents and conditions: a) Alkyl: Et_3N (2 eq), Boc_2O (1.1 eq), acetone:H_2O (1:1, v/v, 0.5 M), RT, 16 h, 95-99%; PEG: K_2CO_3 (3 eq), Boc_2O (1.3 eq), H_2O:THF (1:1, v/v, 0.1 M), RT, 16 h, 40-81%; b) Alkyl: EDC.HCl (0.8-0.9 eq), NHS (1.7-2.8 eq), DCM (0.3 M), RT, 16-72 h, 36-40%; PEG: EDC.HCl (3 eq), NHS (1.5 eq), Et_3N (3 eq), DCM (0.2 M), RT, 16 h, 46-58%.

8-((*tert*-Butoxycarbonyl)amino)octanoic acid (38): To a cooled (0 °C) and stirred mixture of 8-aminooctanoic acid (2.00 g, 12.6 mmol, 1 eq) and Et_3N (3.5 mL, 25.1 mmol, 2 eq) in acetone:H_2O (25 mL, 1:1, v/v) was added dropwise Boc_2O (3.02 g, 13.8 mmol, 1.1 eq) in acetone (6 mL). After stirring at RT overnight the acetone was evaporated under reduced pressure. The aqueous layer was acidified with 1 M HCl to pH = 4 before being extracted thrice with EtOAc. The combined organic layer was washed with brine, dried ($MgSO_4$), and filtered. The solvent was evaporated under reduced pressure to yield a white solid (3.23 g, 12.5 mmol, 99%). ^{1}H-NMR (400 MHz, $CDCl_3$) δ 4.54 (s, 1H), 3.10 (q, *J* = 6.8 Hz, 2H), 2.34 (t, *J* = 7.5 Hz, 2H), 1.62 (q, *J* = 7.2 Hz, 2H), 1.53 – 1.39 (m, 11H), 1.38 – 1.26 (m, 6H). ^{13}C-NMR (101 MHz, $CDCl_3$) δ 179.34, 156.21, 79.27, 40.68, 34.12, 30.08, 29.08, 29.01, 28.56, 26.69, 24.73. LC-MS (ESI, 10-90): t_R = 6.48 min; m/z = 259.73 $[M]^+$.

12-((*tert*-Butoxycarbonyl)amino)dodecanoic acid (39): To a cooled (0 °C) and stirred mixture of 12-aminododecanoic acid (1.50 g, 7.0 mmol, 1 eq) and Et_3N (1.9 mL, 13.9 mmol, 2 eq) in acetone:H_2O (14 mL, 1:1, v/v) was added dropwise Boc_2O (1.67 g, 7.7 mmol, 1.1 eq) in acetone (4 mL). After stirring at RT overnight the acetone was evaporated under reduced pressure. The aqueous layer was acidified with 1 M HCl to pH = 4 before being extracted thrice with EtOAc. The combined organic layer was washed with brine, dried ($MgSO_4$), and filtered. The solvent was evaporated under reduced pressure to yield a white solid (2.09 g, 6.6 mmol, 95%). ^{1}H-NMR (400 MHz, $CDCl_3$) δ 4.54 (s, 1H), 3.10 (m, 2H), 2.34 (t, *J* = 7.4 Hz, 2H), 1.63 (p, *J* = 7.4 Hz, 2H), 1.51 – 1.40 (m, 11H), 1.38 – 1.21 (m, 14H). ^{13}C-NMR (101

MHz, $CDCl_3$) δ 179.28, 156.27, 79.12, 40.64, 33.98, 30.02, 29.44, 29.42, 29.34, 29.24, 29.18, 29.02, 28.44, 26.78, 24.69. LC-MS (ESI, 10-90): t_R = 8.44 min; m/z = 315.60 $[M + H]^+$.

3-(2-(*tert*-butoxycarbonyl-2-aminoethoxy)ethoxy)propanoic acid (40): To a cooled (0 °C) and stirred mixture of 3-(2-(2-aminoethoxy)ethoxy)propanoic acid (0.50 g, 2.8 mmol, 1 eq) and K_2CO_3 (1.17 g, 8.5 mmol, 3 eq) in H_2O (15 mL) was added dropwise Boc_2O (0.74 g, 3.4 mmol, 1.2 eq) in THF (10 mL). After stirring at RT overnight the solution was acidified with 1 M HCl to pH = 4. The layers were separated and the aqueous layer extracted thrice with DCM. The combined organic layer was washed twice with H_2O and once with brine, dried ($MgSO_4$), and filtered. The solvent was evaporated under reduced pressure to yield a colourless oil (0.31 g, 1.1 mmol, 40%). ^{1}H-NMR (400 MHz, $CDCl_3$) δ 5.11 (s, 1H), 3.78 (t, *J* = 6.2 Hz, 2H), 3.67 – 3.56 (m, 4H), 3.54 (t, *J* = 5.4 Hz, 2H), 3.30 (q, *J* = 5.4 Hz, 2H), 2.63 (t, *J* = 6.2 Hz, 2H), 1.45 (s, 9H). ^{13}C-NMR (101 MHz, $CDCl_3$) δ 175.89, 156.23, 79.54, 70.43, 70.32, 70.07, 66.50, 40.44, 34.89, 28.51. LC-MS (ESI, 10-90): t_R = 4.75 min; m/z = 277.84 $[M]^+$.

2,2-Dimethyl-4-oxo-3,8,11,14-tetraoxa-5-azaheptadecan-17-oic acid (41): To a cooled (0 °C) and stirred solution of 3-(2-(2-(2-aminoethoxy)ethoxy)ethoxy)propanoic acid (1.00 g, 4.5 mmol, 1 eq) and K_2CO_3 (1.87 g, 13.6 mmol, 3 eq) in H_2O (20 mL) was added dropwise Boc_2O (1.28 g, 5.9 mmol, 1.3 eq) in THF (20 mL). After stirring at RT overnight the solution was acidified with 1 M HCl to pH = 4. The layers were separated and the aqueous layer extracted thrice with DCM. The combined organic layer was washed twice with H_2O and once with brine, dried ($MgSO_4$), and filtered. The solvent was evaporated under reduced pressure to yield a colourless oil (1.18 g, 3.7 mmol, 81%). ^{1}H-NMR (400 MHz, $CDCl_3$) δ 5.19 (s, 1H), 3.78 (t, *J* = 6.5 Hz, 2H), 3.69 – 3.58 (m, 8H), 3.59 – 3.46 (m, 2H), 3.39 – 3.20 (m, 2H), 2.62 (d, *J* = 6.4 Hz, 2H), 1.45 (s, 9H). ^{13}C-NMR (101 MHz, $CDCl_3$) δ 175.44, 156.23, 79.35, 70.59, 70.54, 70.47, 70.42, 70.21, 66.46, 40.38, 34.84, 27.42. LC-MS (ESI, 10-90): t_R = 4.84 min; m/z = 321.80 $[M]^+$.

8-((*tert*-Butoxycarbonyl)amino)octanoic acid *N*-succinimidyl ester (42): To a stirred solution of **38** (3.23 g, 12.5 mmol, 1.1 eq) in DCM (40 mL) was added EDC.HCl (2.15 g, 11.2 mmol, 1 eq) and *N*-hydoxysuccinimide (2.15 g, 18.7 mmol, 1.7 eq). After stirring at RT for 3 days the reaction was quenched with sat. NH_4Cl (aq). The layers were separated and the aqueous layer was extracted once with DCM. The combined organic layer was dried ($MgSO_4$), filtered, and the solvent evaporated under reduced pressure. The crude product was purified with flash column chromatography (SiO_2, 10-40% EtOAc in pentane) to yield a white solid (1.40 g, 4.0 mmol, 36%). ^{1}H-NMR (400 MHz, $CDCl_3$) δ 4.54 (s, 1H), 3.10 (q, *J* = 6.7 Hz, 2H), 2.84 (d, *J* = 4.2 Hz, 4H), 2.60 (t, *J* = 7.4 Hz, 2H), 1.74 (p, *J* = 7.4 Hz, 2H), 1.47 – 1.43 (m, 11H), 1.41 – 1.25 (m, 6H). ^{13}C-NMR (101 MHz, $CDCl_3$) δ 169.33, 168.76, 79.15, 40.64, 31.02, 30.03, 28.83, 28.74, 28.55, 26.61, 25.72, 24.60. LC-MS (ESI, 10-90): t_R = 7.28 min; m/z = 356.67 $[M]^+$.

12-((*tert*-Butoxycarbonyl)amino)dodecanoic acid *N*-succinimidyl ester (43): To a stirred solution of **39** (2.09 g, 6.6 mmol, 1.3 eq) in DCM (35 mL) was added EDC.HCl (0.99 g, 5.2 mmol, 1 eq) and *N*-hydroxysuccinimide (1.66 g, 14.4 mmol, 2.8 eq). After stirring at RT for 3 days the reaction was quenched with sat. NH_4Cl (aq). The layers were separated and the aqueous layer was extracted once with DCM. The combined organic layer was dried ($MgSO_4$), filtered, and the solvent evaporated under reduced pressure. The crude product was purified with flash column chromatography (SiO_2, 10-40% EtOAc in pentane) to yield a white solid (0.88 g, 2.1 mmol, 40%). ^{1}H-NMR (400 MHz, $CDCl_3$) δ 4.54 (s, 1H), 3.12 (q, *J* = 6.8 Hz, 2H), 2.86 (d, *J* = 4.3 Hz, 4H), 2.62 (t, *J* = 7.5 Hz, 2H), 1.76 (p, *J* = 7.4 Hz, 2H), 1.50 – 1.42 (m, 11H), 1.35 – 1.25 (m, 14H). ^{13}C-NMR (101 MHz, $CDCl_3$) δ 169.34, 168.83, 165.27, 156.11, 79.12, 40.76, 31.07, 30.18, 29.61, 29.54, 29.41, 29.39, 29.17, 28.88, 28.56, 26.92, 25.72, 24.69. LC-MS (ESI, 10-90): t_R = 8.87 min; m/z = 412.60 $[M]^+$.

2,5-Dioxopyrrolidin-1-yl 2,2-dimethyl-4-oxo-3,8,11-trioxa-5-azatetradecan-14-oate (44): To a stirred mixture of **40** (1.53 g, 5.5 mmol, 1 eq), Et_3N (2.3 mL, 16.6 mmol, 3 eq) and *N*-hydroxysuccinimide (0.95 g, 8.3 mmol, 1.5 eq) in DCM (30 mL) was added dropwise EDC.HCl (3.17 g, 16.6 mmol, 3 eq) in DCM (15 mL). After stirring at RT overnight the reaction was quenched with H_2O and DCM. The layers were separated and the aqueous layer extracted thrice with DCM. The combined organic layer was washed thrice with H_2O and once with brine, dried ($MgSO_4$), filtered, and the solvent evaporated under reduced pressure. The crude product was purified with flash column chromatography (SiO_2, 50-70% EtOAc in pentane) to yield a yellow oil (1.19 g, 3.2 mmol, 58%). ^{1}H-NMR (400 MHz, $CDCl_3$) δ 5.11 (s, 1H), 3.86 (t, *J* = 6.3 Hz, 2H), 3.69 – 3.59 (m, 4H), 3.55 (t, *J* = 5.2 Hz, 2H), 3.31 (q, *J* = 5.4 Hz, 2H), 2.91 (t, *J* = 6.3 Hz, 2H), 2.85 (d, *J* = 3.4 Hz, 4H), 1.44 (s, 9H). ^{13}C-NMR (101 MHz, $CDCl_3$) δ 171.97, 169.16, 166.84, 156.24, 79.32, 70.72, 70.31, 70.18, 65.83, 40.42, 32.26, 28.49, 25.66, 25.46. LC-MS (ESI, 10-90): t_R = 5.66 min; m/z = 374.80 $[M]^+$.

2,5-Dioxopyrrolidin-1-yl 2,2-dimethyl-4-oxo-3,8,11,14-tetraoxa-5-azaheptadecan-17-oate (45): To a stirred mixture of **41** (1.18 g, 3.7 mmol, 1 eq), Et_3N (1.5 mL, 11.0 mmol, 3 eq) and *N*-hydroxysuccinimide (0.63 g, 5.5 mmol, 1.5 eq) in DCM (18 mL) was added dropwise EDC.HCl (2.11 g, 11.0 mmol, 3 eq) in DCM (10 mL). After stirring at RT overnight the reaction was quenched with H_2O and DCM. The layers were separated and the aqueous layer extracted thrice with DCM. The combined organic layer was washed thrice with H_2O and once with brine, dried ($MgSO_4$), filtered, and the solvent evaporated under reduced pressure. The crude product was purified with flash column chromatography (SiO_2, 50-70% EtOAc in pentane) to yield a yellow oil (0.70 g, 1.7 mmol, 46%). ^{1}H-NMR (400 MHz, $CDCl_3$) δ 5.09 (s, 1H), 3.86 (t, *J* = 6.4 Hz, 2H), 3.69 – 3.58 (m, 8H), 3.54 (t, *J* = 5.1 Hz, 2H), 3.31 (q, *J* = 5.4 Hz, 2H), 2.91 (t, *J* = 6.4 Hz, 2H), 2.84 (d, *J* = 3.0 Hz, 4H), 1.44 (s, 9H). ^{13}C-NMR (101 MHz, $CDCl_3$) δ 169.10, 166.84, 156.14, 79.24, 70.82, 70.64, 70.56, 70.30, 70.25, 65.80, 40.42, 32.22, 28.50, 25.65, 25.47. LC-MS (ESI, 10-90): t_R = 5.63 min; m/z = 418.80 $[M]^+$.

Synthesis of the PEG4 spacer:

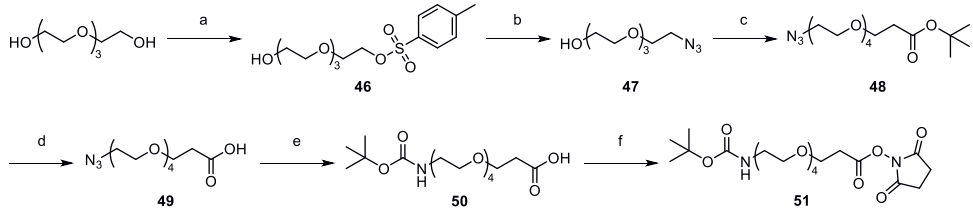

Scheme 4.8 Reagents and conditions: a) *p*-TsCl (1 eq), NaOH (2 M, 1.6 eq), THF (0.6 M), 0 °C, 4 h, 90%; b) NaN_3 (1.5 eq), ACN (0.4 M), 80 °C, 8 h, 94%; c) tert-butyl acrylate (1 eq), TBAF (0.4 eq), NaOH (25 wt% in H_2O, 2.6 eq), DCM, RT, 8 h, 75%; d) TFA (50 eq), DCM, RT, 4 h, 65%; e) step 1: 10% Pd/C (0.1 eq), H_2 (g), EtOH (0.3 M), RT, 16 h; step 2: K_2CO_3 (3 eq), Boc_2O (1.3 eq), H_2O:THF (1:1, v/v, 0.1 M), RT, 16 h, 55% (two steps); f) EDC.HCl (1.2 eq), NHS (1.1 eq), DCM (0.2 M), RT, 16 h, 84%.

2-(2-(2-(2-Hydroxyethoxy)ethoxy)ethoxy)ethyl 4-methylbenzenesulfonate (46): To a stirred and cooled (0 °C) solution of tetraethylene glycol (23.00 g, 118.0 mmol, 8 eq) in THF (26 mL) was added 2 M NaOH (12 mL). After 15 minutes additionally *p*-TsCl (2.81 g, 14.7 mmol, 1 eq) was added. After stirring at 0 °C for 4 h the reaction was quenched with ice cold H_2O (200 mL) and stirred 15 minutes at RT. The layers were separated and the aqueous layer extracted thrice with DCM. The combined organic layer was washed thrice with H_2O and once with brine, dried ($MgSO_4$), filtered, and the solvent evaporated under reduced pressure to yield a colourless oil (4.63 g, 13.3 mmol, 90%). ^{1}H-NMR (400 MHz, $CDCl_3$) δ 7.75 (d, *J* = 8.3 Hz, 2H), 7.31 (d, *J* = 7.8 Hz, 2H), 4.12 (t, *J* = 4.8 Hz, 2H), 3.68 – 3.63 (m, 4H), 3.63 – 3.57 (m, 4H), 3.57 – 3.53 (m, 6H), 2.40 (s, 3H). ^{13}C-NMR (101 MHz, $CDCl_3$) δ 144.87, 132.89, 129.86, 128.92,

72.47, 70.69, 70.62, 70.51, 70.43, 70.29, 69.30, 68.66, 61.66, 21.64. LC-MS (ESI, 10-90): t_R = 5.40 min; m/z = 348.41 $[M]^+$.

2-(2-(2-(2-Azidoethoxy)ethoxy)ethoxy)ethan-1-ol (47): A stirred mixture of **46** (5.40 g, 15.5 mmol, 1 eq) and NaN_3 (1.51 g, 23.2 mmol, 1.5 eq) in acetonitrile (43 mL) was refluxed for 8 h. After cooling down the reaction was diluted with H_2O (40 mL). The aqueous layer was extracted thrice with DCM. The combined organic layer was dried ($MgSO_4$), filtered, and the solvent evaporated under reduced pressure to yield a yellow oil (3.09 g. 14.5 mmol, 94%). ^{1}H-NMR (400 MHz, $CDCl_3$) δ 3.73 – 3.68 (m, 2H), 3.68 – 3.64 (m, 10H), 3.61 – 3.57 (m, 2H), 3.38 (t, *J* = 5.3 Hz, 2H), 2.61 (t, *J* = 6.2 Hz, 1H). ^{13}C-NMR (101 MHz, $CDCl_3$) δ 72.55, 70.78, 70.74, 70.68, 70.43, 70.14, 61.81, 50.73. LC-MS (ESI, 10-90): t_R = 1.35 min; m/z = 219.87 $[M]^+$.

***tert*-Butyl 1-azido-3,6,9,12-tetraoxapentadecan-15-oate (48):** A stirred mixture of **47** (2.70 g, 12.3 mmol, 1 eq), *tert*-butyl acrylate (1.78 mL, 12.2 mmol, 1 eq), TBAF (1.29 g, 4.9 mmol, 0.4 eq) and NaOH (5 mL, 25 wt% in H_2O) in DCM (30 mL) was stirred at RT for 8 h. The mixture was diluted with H_2O (40 mL) and the layers separated. The aqueous layer was extracted thrice with DCM. The combined organic layer was wased twice with H_2O and once with brine, dried ($MgSO_4$), filtered, and the solvent evaporated under reduced pressure. The crude product was purified with flash column chromatography (0-100% EtOAc in pentane) to yield a colourless oil (3.22 g, 9.3 mmol, 75%). ^{1}H-NMR (400 MHz, $CDCl_3$) δ 3.71 (t, *J* = 6.6 Hz, 2H), 3.66 (d, *J* = 3.6 Hz, 10H), 3.64 – 3.60 (m, 4H), 3.39 (t, *J* = 5.0 Hz, 2H), 2.51 (t, *J* = 6.6 Hz, 2H), 1.45 (s, 9H). ^{13}C-NMR (101 MHz, $CDCl_3$) δ 171.01, 80.60, 70.80, 70.78, 70.74, 70.71, 70.60, 70.47, 70.14, 67.00, 50.78, 36.36, 28.19. LC-MS (ESI, 10-90): t_R = 7.01 min; m/z = 347.67 $[M]^+$.

1-Azido-3,6,9,12-tetraoxapentadecan-15-oic acid (49): A mixture of **48** (3.72 g, 10.7 mmol, 1 eq) and TFA (42 mL, 0.55 mol, 51 eq) in DCM (86 mL) was stirred at RT for 4 h. The volatile compounds were removed under reduced pressure. The crude product was co-evaporated four times with Et_2O and twice with MeOH to yield a colourless oil (2.04 g, 7.0 mmol, 65%). ^{1}H-NMR (400 MHz, $CDCl_3$) δ 3.77 (t, *J* = 6.3 Hz, 2H), 3.70 – 3.64 (m, 14H), 3.40 (t, *J* = 5.1 Hz, 2H), 2.64 (t, *J* = 6.2 Hz, 2H). ^{13}C-NMR (101 MHz, $CDCl_3$) δ 176.15, 70.78, 70.72, 70.67, 70.64, 70.52, 70.37, 70.10, 66.50, 50.76, 34.98. LC-MS (ESI, 10-90): t_R = 4.14 min; m/z = 291.80 $[M]^+$.

2,2-Dimethyl-4-oxo-3,8,11,14,17-pentaoxa-5-azaicosan-20-oic acid (50): A stirred mixture of **49** (1.55 g, 5.3 mmol, 1 eq) and 10% Pd/C (0.06 g, 0.4 mmol, 0.1 mmol) in absolute EtOH (20 mL) was purged with H_2 (g) for 15 minutes and kept under H_2 (g) atmosphere for an additional 16 h at RT. The mixture was filtered through a celite pad and the solvent evaporated under reduced pressure. The crude residue was used without further purification. To a cooled (0 °C) mixture of the crude residue re-dissolved in H_2O (25 mL) with K_2CO_3 (2.20 g, 15.9 mmol, 3 eq) was added dropwise Boc_2O (1.51 g, 6.9 mmol, 1.3 eq) in THF (25 mL). After stirring overnight at RT the reaction mixture was acidified with 1 M HCl to pH 4. The layers were separated and the aqueous layer extracted thrice with DCM. The combined organic layer was washed twice with H_2O and once with brine, dried ($MgSO_4$), filtered, and the solvent evaporated under reduced pressure. The crude product was purified with flash column chromatography (2-4% MeOH in DCM with 3% AcOH) to yield a colourless oil (1.07 g, 2.9 mmol, 55%). ^{1}H-NMR (400 MHz, $CDCl_3$) δ 5.19 (s, 1H), 3.74 (t, *J* = 6.2 Hz, 2H), 3.67 – 3.58 (m, 14H), 3.53 (t, *J* = 5.2 Hz, 2H), 2.59 (t, *J* = 6.3 Hz, 2H), 1.42 (d, *J* = 3.5 Hz, 9H). ^{13}C-NMR (101 MHz, $CDCl_3$) δ 175.41, 156.28, 79.52, 70.66, 70.64, 70.56, 70.50, 70.39, 70.38, 70.26, 66.61, 40.30, 35.06, 28.50. LC-MS (ESI, 10-90): t_R = 5.14 min; m/z = 365.93 $[M]^+$.

2,5-Dioxopyrrolidin-1-yl 2,2-dimethyl-4-oxo-3,8,11,14,17-pentaoxa-5-azaicosan-20-oate (51): A mixture of **50** (1.04 g, 2.9 mmol, 1 eq), EDC.HCl (0.66 g, 3.4 mmol, 1.2 eq) and *N*-hydroxysuccinimide (0.36 g, 3.1 mmol, 1.1 eq) in DCM (14 mL) was stirred at RT overnight. The reaction mixture was diluted with DCM (15 mL). The organic layer was washed thrice with H_2O, dried ($MgSO_4$), filtered, and the solvent evaporated under reduced pressure. The crude product was purified with flash column chromatography (50-70% EtOAc in pentane) to yield a colourless oil (1.10 g, 2.4 mmol, 84%). ^{1}H-NMR (400 MHz, $CDCl_3$) δ 5.08 (s, 1H), 3.82 (t, *J* = 6.4 Hz, 2H), 3.65 – 3.57 (m, 12H), 3.51 (t, *J* = 5.2 Hz, 2H), 3.28 (q, *J* = 5.4 Hz, 2H), 2.88 (t, *J* = 6.4 Hz, 2H), 2.81 (m, 4H), 1.41 (s, 9H). ^{13}C-NMR (101 MHz, $CDCl_3$) δ 171.94, 169.11, 166.81, 156.16, 70.77, 70.68, 70.62, 70.54, 70.25, 65.77, 40.41, 32.19, 28.49, 25.64. LC-MS (ESI, 10-90): t_R = 5.81 min; m/z = 426.73 $[M]^+$.

Synthesis of key intermediates:

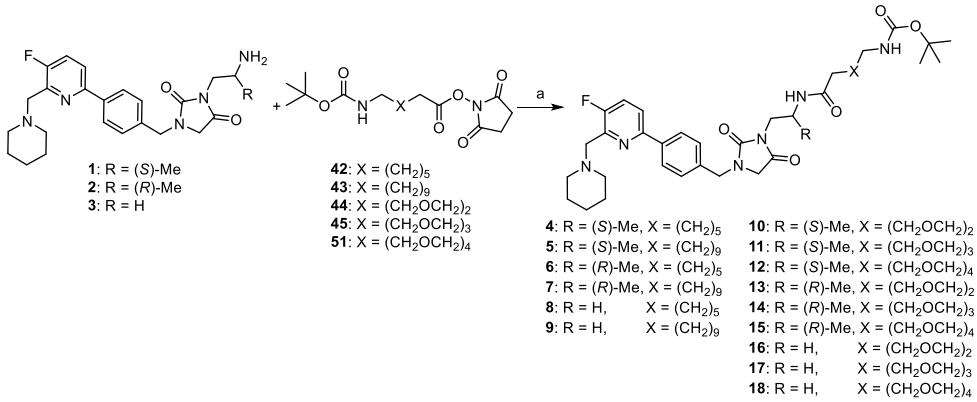

Scheme 4.9 Reagents and conditions: a) Et_3N (6 eq), DCM (0.3 M), RT, 1-3 h, 13-65%.

General procedure for the synthesis of key intermediates (4-18)

A mixture of **1**, **2 or 3** (1 eq), Et_3N (6 eq) and *O*-Su ester (**42**, **43**, **44**, **45** or **51,** 1 eq) in DCM (0.3 M) was stirred at RT for 1-3 h. The reaction mixture was diluted with H_2O and DCM. The layers were separated and the aqueous layer was extracted thrice with DCM. The combined organic layer was washed with H_2O and brine, dried ($MgSO_4$), filtered, and the solvent evaporated under reduced pressure. The crude product was purified using preparative HPLC and freeze dried twice.

***tert*-Butyl (*S*)-(8-((1-(3-(4-(5-fluoro-6-(piperidin-1-ylmethyl)pyridin-2-yl)benzyl)-2,5-dioxoimidazolidin-1-yl)propan-2-yl)amino)-8-oxooctyl)carbamate (4):** The title compound was synthesized according to general procedure using **1** (29.0 mg, 66.1 µmol, 1 eq) and **42** (23.5 mg, 66.1 µmol, 1 eq). The product was obtained as a white solid (28.8 mg, 42.4 µmol, 64%). ^{1}H-NMR (500 MHz, $CDCl_3$) δ 7.96 (d, *J* = 8.3 Hz, 2H), 7.62 (dd, *J* = 8.6, 3.5 Hz, 1H), 7.43 (t, *J* = 8.8 Hz, 1H), 7.34 (d, *J* = 8.3 Hz, 2H), 5.99 (d, *J* = 8.1 Hz, 1H), 4.61 (s, 2H), 4.38 – 4.25 (m, 1H), 3.84 – 3.80 (m, 2H), 3.69 – 3.66 (m, 2H), 3.63 – 3.53 (m, 2H), 3.40 (q, *J* = 4.7 Hz, 1H), 3.06 (d, *J* = 6.8 Hz, 2H), 2.59 (s, 4H), 2.10 (t, *J* = 7.7 Hz, 2H), 1.63 – 1.52 (m, 6H), 1.43 (s, 10H), 1.29 – 1.24 (m, 9H), 1.18 (d, *J* = 6.7 Hz, 3H). ^{13}C-NMR (126 MHz, $CDCl_3$) δ 173.10, 170.42, 158.00 (d, *J* = 258.0 Hz), 157.26, 138.82, 135.78, 128.57, 127.66, 123.74 (d, *J* = 20.3 Hz), 120.40, 70.87, 54.50, 49.23, 46.61, 45.12, 44.25, 36.92, 30.12, 29.85, 29.25, 29.10, 28.58, 26.75, 26.12, 25.55, 24.29, 18.45. LC-MS (ESI, 10-90): t_R = 5.99 min; m/z = 681.33 $[M + H]^+$. HRMS $[C_{37}H_{53}FN_6O_5 + H]^+$: 681.41342 calculated, 681.41326 found.

***tert*-Butyl (*S*)-(12-((1-(3-(4-(5-fluoro-6-(piperidin-1-ylmethyl)pyridin-2-yl)benzyl)-2,5-dioxoimidazolidin-1-yl)propan-2-yl)amino)-12-oxododecyl)carbamate (5):** The title compound was synthesized according to general procedure using **1** (92.0 mg, 21.0 µmol, 1 eq) and **43** (87.0 mg, 21.0 µmol, 1 eq). The product was obtained as a white solid (75.2 mg, 0.10 mmol, 49%). ^{1}H-NMR (400 MHz, $CDCl_3$) δ 7.97 (d, *J* = 8.0 Hz, 2H), 7.63 (dd, *J* = 8.6, 3.5 Hz, 1H), 7.43 (t, *J* = 8.8 Hz, 1H), 7.34 (d, *J* = 8.0 Hz, 2H), 6.00 (d, *J* = 8.1 Hz, 1H), 4.62 (s, 2H), 4.54 (s, 1H), 4.39 – 4.24 (m, 1H), 3.86 (d, *J* = 2.5 Hz, 2H), 3.76 (q, *J* = 17.3 Hz, 2H), 3.64 – 3.51 (m, 2H), 3.09 (q, *J* = 6.7 Hz, 2H), 2.62 (s, 4H), 2.11 (t, *J* = 7.6 Hz, 2H), 1.66 – 1.54 (m, 6H), 1.44 (s, 13H), 1.34 – 1.23 (m, 14H), 1.19 (d, *J* = 6.7 Hz, 3H). ^{13}C-NMR (101 MHz, $CDCl_3$) δ 173.25, 170.39, 158.01 (d, *J* = 258.3 Hz), 157.26, 151.82, 138.76, 135.80, 128.55, 127.65, 123.75 (d, *J* = 20.2 Hz), 120.46, 77.48, 77.16, 76.84, 58.34, 54.31, 49.22, 46.60, 45.07, 44.23, 40.77, 37.03, 30.19, 29.64, 29.58, 29.47, 29.41, 28.57, 26.93, 25.95, 25.70, 24.19, 18.45. LC-MS (ESI, 10-90): t_R = 7.10 min; m/z = 737.33 $[M + H]^+$. HRMS $[C_{41}H_{61}FN_6O_5 + H]^+$: 737.47602 calculated, 737.47562 found.

***tert*-Butyl (*R*)-(8-((1-(3-(4-(5-fluoro-6-(piperidin-1-ylmethyl)pyridin-2-yl)benzyl)-2,5-dioxoimidazolidin-1-yl)propan-2-yl)amino)-8-oxooctyl)carbamate (6):** The title compound was synthesized according to general procedure using **2** (38.2 mg, 87.0 µmol, 1.1 eq) and **42** (29.2 mg, 81.9 µmol, 1 eq). The product was obtained as a white solid (18.2 mg, 26.8 µmol, 31%). ^{1}H-NMR (500 MHz, $CDCl_3$) δ 7.96 (d, *J* = 8.3 Hz, 2H), 7.61 (dd, *J* = 8.6, 3.5 Hz, 1H), 7.42 (t, *J* = 8.8 Hz, 1H), 7.34 (d, *J* = 8.3 Hz, 2H), 5.99 (d, *J* = 7.8 Hz, 1H), 4.61 (s, 2H), 4.38 – 4.26 (m, 1H), 3.82 (d, *J* = 2.6 Hz, 2H), 3.75 (d, *J* = 17.7 Hz, 2H), 3.71 – 3.67 (m, 1H), 3.60 – 3.57 (m, 2H), 3.06 (q, *J* = 6.7 Hz, 2H), 2.58 (s, 4H), 2.10 (t, *J* = 7.7 Hz, 2H), 1.59 (dt, *J* = 17.0, 8.5 Hz, 6H), 1.43 (s, 10H), 1.32 – 1.23 (m, 9H), 1.18 (d, *J* = 6.7 Hz, 3H). ^{13}C-NMR (126 MHz, $CDCl_3$) δ 173.09, 170.41, 157.99 (d, *J* = 258.0 Hz), 157.26, 151.83, 151.80, 138.82, 135.77, 128.56, 127.66, 123.72 (d, *J* = 20.6 Hz), 120.38 (d, *J* = 4.2 Hz), 58.64, 54.50, 49.22, 46.60, 45.11, 44.25, 40.68, 36.91, 30.11, 29.84, 29.25, 29.09, 28.58, 26.13, 25.54, 24.29, 18.44. LC-MS (ESI, 10-90): t_R = 6.03 min; m/z = 681.27 $[M + H]^+$. HRMS $[C_{37}H_{53}FN_6O_5 + H]^+$: 681.41342 calculated, 681.41308 found.

***tert*-Butyl (*R*)-(12-((1-(3-(4-(5-fluoro-6-(piperidin-1-ylmethyl)pyridin-2-yl)benzyl)-2,5-dioxoimidazolidin-1-yl)propan-2-yl)amino)-12-oxododecyl)carbamate (7):** The title compound was synthesized according to general procedure using **2** (105.1 mg, 0.24 mmol, 1 eq) and **43** (98.5 mg, 0.24 mmol, 1 eq). The product was obtained as a white solid (85.6 mg, 0.12 mmol, 49%). ^{1}H-NMR (400 MHz, $CDCl_3$) δ 7.96 (d, *J* = 8.3 Hz, 2H), 7.62 (dd, *J* = 8.6, 3.6 Hz, 1H), 7.42 (t, *J* = 8.8 Hz, 1H), 7.34 (d, *J* = 8.3 Hz, 2H), 5.98 (d, *J* = 8.1 Hz, 1H), 4.61 (s, 2H), 4.53 (s, 1H), 4.32 (m, 1H), 3.84 (d, *J* = 2.6 Hz, 2H), 3.82 – 3.68 (m, 2H), 3.64 – 3.50 (m, 2H), 3.08 (q, *J* = 6.7 Hz, 2H), 2.60 (s, 4H), 2.10 (t, *J* = 7.7 Hz, 2H), 1.59 (1.66 – 1.53, 6H), 1.43 (s, 9H), 1.32 – 1.20 (m, 18H), 1.18 (d, *J* = 6.7 Hz, 3H). ^{13}C-NMR (101 MHz, $CDCl_3$) δ 173.24, 170.39, 158.00 (d, *J* = 258.9 Hz), 157.25, 151.87, 138.76, 135.79, 128.55, 127.64, 123.74 (d, *J* = 20.3 Hz), 120.44 (d, *J* = 4.2 Hz), 69.36, 58.39, 54.33, 49.21, 46.59, 45.06, 44.22, 40.75, 37.02, 30.18, 29.63, 29.58, 29.46, 29.40, 28.57, 26.93, 25.97, 25.69, 24.20, 18.45. LC-MS (ESI, 10-90): t_R = 7.10 min; m/z = 737.27 $[M + H]^+$. HRMS $[C_{41}H_{61}FN_6O_5 + H]^+$: 737.47602 calculated, 737.47552 found.

***tert*-Butyl (8-((2-(3-(4-(5-fluoro-6-(piperidin-1-ylmethyl)pyridin-2-yl)benzyl)-2,5-dioxoimidazolidin-1-yl)ethyl)amino)-8-oxooctyl)carbamate (8):** The title compound was synthesized according to general procedure using **3** (22.5 mg, 53.0 µmol, 1 eq) and **42** (18.9 mg, 53.0 µmol, 1 eq). The product was obtained as a white solid (21.7 mg, 33.0 µmol, 61%). ^{1}H-NMR (500 MHz, $CDCl_3$) δ 7.96 (d, *J* = 8.3 Hz, 2H), 7.62 (dd, *J* = 8.6, 3.5 Hz, 1H), 7.42 (t, *J* = 8.7 Hz, 1H), 7.35 (d, *J* = 8.3 Hz, 2H), 6.13 (s, 1H), 4.61 (s, 2H), 3.82 (d, *J* = 2.6 Hz, 2H), 3.77 (s, 2H), 3.75 – 3.70 (m, 2H), 3.55 – 3.46 (m, 2H), 3.25 – 3.18 (m, 1H), 3.14 – 3.02 (m, 4H), 2.59 (s, 4H), 2.14 (t, *J* = 7.6 Hz, 2H), 1.60 (p, *J* = 5.7 Hz, 6H), 1.43 (s, 9H), 1.32 – 1.26

(m, 8H). ^{13}C-NMR (126 MHz, $CDCl_3$) δ 173.71, 170.33, 158.00 (d, *J* = 258.2 Hz), 157.14, 151.84, 138.86, 136.40, 135.75, 128.64, 128.25, 127.67, 123.74 (d, *J* = 20.6 Hz), 120.40 (d, *J* = 4.1 Hz), 58.61 (d, *J* = 1.7 Hz), 54.50, 51.75, 50.63, 49.29, 46.64, 46.58, 39.19, 39.05, 36.72, 30.10, 29.85, 29.24, 29.05, 26.72, 26.12, 25.53, 24.29. LC-MS (ESI, 10-90): t_R = 5.90 min; m/z = 667.33 $[M + H]^+$. HRMS $[C_{36}H_{51}FN_6O_5 + H]^+$: 667.39777 calculated, 667.39749 found.

***tert*-Butyl (12-((2-(3-(4-(5-fluoro-6-(piperidin-1-ylmethyl)pyridin-2-yl)benzyl)-2,5-dioxoimidazolidin-1-yl)ethyl)amino)-12-oxododecyl)carbamate (9):** The title compound was synthesized according to general procedure using **3** (21.6 mg, 51.0 µmol, 1 eq) and **43** (21.0 mg, 51.0 µmol, 1 eq). The product was obtained as a white solid (22.0 mg, 30.0 µmol, 60%). ^{1}H-NMR (500 MHz, $CDCl_3$) δ 7.96 (d, *J* = 8.2 Hz, 2H), 7.61 (dd, *J* = 8.6, 3.5 Hz, 1H), 7.42 (t, *J* = 8.8 Hz, 1H), 7.34 (d, *J* = 8.3 Hz, 2H), 6.11 (s, 1H), 4.61 (s, 2H), 4.52 (s, 1H), 3.82 (d, *J* = 2.6 Hz, 2H), 3.76 (s, 2H), 3.75 – 3.69 (m, 2H), 3.54 – 3.47 (m, 2H), 3.08 (q, *J* = 7.2, 6.6 Hz, 2H), 2.58 (d, *J* = 5.6 Hz, 4H), 2.18 – 2.11 (m, 2H), 1.79 – 1.75 (m, 2H), 1.60 (p, *J* = 5.6 Hz, 6H), 1.43 (s, 9H), 1.32 – 1.21 (m, 16H). ^{13}C-NMR (126 MHz, $CDCl_3$) δ 173.81, 170.30, 158.00 (d, *J* = 258.2 Hz), 157.14, 151.81 (d, *J* = 5.0 Hz), 145.99 (d, *J* = 15.4 Hz), 138.87, 135.73, 128.62, 127.67, 123.71 (d, *J* = 20.5 Hz), 120.38 (d, *J* = 4.2 Hz), 58.64 (d, *J* = 3.0 Hz), 54.49, 49.28, 46.64, 40.77, 39.17, 39.02, 36.84, 30.30, 30.19, 29.84, 29.62, 29.56, 29.45, 29.43, 29.39, 28.58, 26.12, 25.68, 24.29. LC-MS (ESI, 10-90): t_R = 6.93 min; m/z = 723.33 $[M + H]^+$. HRMS $[C_{40}H_{59}FN_6O_5 + H]^+$: 723.46037 calculated, 723.46000 found.

***tert*-Butyl (*S*)-(2-(2-(3-((1-(3-(4-(5-fluoro-6-(piperidin-1-ylmethyl)pyridin-2-yl)benzyl)-2,5-dioxoimidazolidin-1-yl)propan-2-yl)amino)-3-oxopropoxy)ethoxy)ethyl)carbamate (10):** The title compound was synthesized according to general procedure using **1** (27.0 mg, 62 µmol, 1 eq) and **44** (23.1 mg, 62.0 µmol, 1 eq). The product was obtained as a white solid (6.9 mg, 9.9 µmol, 16%). ^{1}H-NMR (500 MHz, $CDCl_3$) δ 7.95 (d, *J* = 8.3 Hz, 2H), 7.61 (dd, *J* = 8.6, 3.5 Hz, 1H), 7.42 (t, *J* = 8.8 Hz, 1H), 7.34 (d, *J* = 7.1 Hz, 2H), 4.61 (q, *J* = 15.1 Hz, 2H), 4.41 – 4.31 (m, 1H), 3.81 (d, *J* = 2.6 Hz, 2H), 3.80 – 3.71 (m, 2H), 3.71 – 3.67 (m, 2H), 3.67 – 3.58 (m, 6H), 3.58 – 3.54 (m, 2H), 3.55 – 3.49 (m, 2H), 3.30 (q, *J* = 5.7 Hz, 1H), 2.87 (t, *J* = 5.1 Hz, 1H), 2.57 (s, 4H), 2.48 – 2.33 (m, 2H), 1.82 (s, 2H), 1.59 (p, *J* = 5.6 Hz, 4H), 1.43 (s, 9H), 1.19 (dd, *J* = 6.8, 2.5 Hz, 3H). ^{13}C-NMR (126 MHz, $CDCl_3$) δ 171.45, 170.42, 157.97 (d, *J* = 258.1 Hz), 157.18, 151.86 (d, *J* = 4.9 Hz), 145.99 (d, *J* = 15.1 Hz), 138.73, 135.96, 128.52, 127.61, 123.69 (d, *J* = 20.4 Hz), 120.37 (d, *J* = 4.1 Hz), 73.30, 70.61, 70.52, 70.35, 67.17, 58.67 (d, *J* = 3.1 Hz), 54.49, 49.22, 46.57, 44.53, 44.42, 41.81, 37.09, 28.56, 26.15, 24.30, 18.31. LC-MS (ESI, 10-90): t_R = 5.35 min; m/z = 699.13 $[M + H]^+$. HRMS $[C_{36}H_{51}FN_6O_7 + H]^+$: 699.38760 calculated, 699.38718 found.

***tert*-Butyl (*S*)-(15-(3-(4-(5-fluoro-6-(piperidin-1-ylmethyl)pyridin-2-yl)benzyl)-2,5-dioxoimidazolidin-1-yl)-14-methyl-12-oxo-3,6,9-trioxa-13-azapentadecyl)carbamate (11):** The title compound was synthesized according to general procedure using **1** (25.7 mg, 59.0 µmol, 1 eq) and **45** (24.5 mg, 59.0 µmol, 1 eq). The product was obtained as a white solid (5.8 mg, 7.8 µmol, 13%). ^{1}H-NMR (500 MHz, $CDCl_3$) δ 7.95 (d, *J* = 8.3 Hz, 2H), 7.61 (dd, *J* = 8.6, 3.5 Hz, 1H), 7.42 (t, *J* = 8.8 Hz, 1H), 7.34 (d, *J* = 7.2 Hz, 2H), 4.67 – 4.55 (m, 2H), 4.42 – 4.31 (m, 1H), 3.82 (d, *J* = 2.6 Hz, 2H), 3.80 – 3.72 (m, 2H), 3.71 – 3.67 (m, 2H), 3.67 – 3.58 (m, 10H), 3.58 – 3.55 (m, 2H), 3.55 – 3.50 (m, 2H), 3.30 (d, *J* = 5.6 Hz, 1H), 2.87 (t, *J* = 5.4 Hz, 1H), 2.58 (s, 4H), 2.49 – 2.34 (m, 2H), 1.79 (s, 2H), 1.60 (p, *J* = 5.6 Hz, 4H), 1.43 (s, 9H), 1.19 (dd, *J* = 6.8, 2.8 Hz, 3H). ^{13}C-NMR (126 MHz, $CDCl_3$) δ 171.46, 171.40, 170.40, 157.97 (d, *J* = 258.1 Hz), 157.18, 151.87 (d, *J* = 4.7 Hz), 145.99 (d, *J* = 15.1 Hz), 138.74, 135.96, 128.53, 127.61, 123.69 (d, *J* = 20.4 Hz), 120.37 (d, *J* = 4.2 Hz), 73.28, 70.61, 70.59, 70.52, 70.50, 70.35, 67.17, 58.66 (d, *J* = 3.1 Hz), 54.50, 49.23, 46.57, 44.53, 44.49, 41.80, 37.10, 28.57, 26.15, 24.30, 18.31. LC-MS (ESI, 10-90): t_R = 5.35 min; m/z = 743.27 $[M + H]^+$. HRMS $[C_{38}H_{55}FN_6O_8 + H]^+$: 743.41382 calculated, 743.41351 found.

***tert*-Butyl (*S*)-(18-(3-(4-(5-fluoro-6-(piperidin-1-ylmethyl)pyridin-2-yl)benzyl)-2,5-dioxoimidazolidin-1-yl)-17-methyl-15-oxo-3,6,9,12-tetraoxa-16-azaoctadecyl)carbamate (12):** The title compound was synthesized according to general procedure using **1** (32.5 mg, 74.0 µmol, 1 eq) and **51** (34.2 mg, 74.0 µmol, 1 eq). The product was obtained as a white solid (38.0 mg, 48.0 µmol, 65%). ^{1}H-NMR (500 MHz, $CDCl_3$) δ 7.95 (d, *J* = 8.3 Hz, 2H), 7.61 (dd, *J* = 8.6, 3.5 Hz, 1H), 7.42 (t, *J* = 8.8 Hz, 1H), 7.34 (d, *J* = 8.3 Hz, 2H), 4.67 – 4.55 (m, 2H), 4.41 – 4.31 (m, 1H), 3.81 (d, *J* = 2.6 Hz, 2H), 3.74 (d, *J* = 13.5 Hz, 2H), 3.68 (t, *J* = 5.6 Hz, 2H), 3.66 – 3.58 (m, 14H), 3.58 – 3.54 (m, 2H), 3.54 – 3.51 (m, 2H), 3.30 (q, *J* = 5.4 Hz, 1H), 2.93 (td, *J* = 5.0, 1.9 Hz, 1H), 2.58 (s, 4H), 2.41 (t, *J* = 6.9 Hz, 2H), 1.98 (bs, 2H), 1.60 (p, *J* = 5.6 Hz, 4H), 1.43 (s, 9H), 1.18 (d, *J* = 6.8 Hz, 3H). ^{13}C-NMR (126 MHz, $CDCl_3$) δ 171.44, 170.52, 170.41, 157.98 (d, *J* = 257.9 Hz), 157.17, 151.89 (d, *J* = 4.7 Hz), 145.94 (d, *J* = 14.9 Hz), 138.72, 136.03, 135.98, 128.53, 127.61, 123.70 (d, *J* = 20.4 Hz), 120.40 (d, *J* = 4.2 Hz), 70.73, 70.64, 70.59, 70.52, 70.42, 70.40, 70.34, 70.31, 67.15, 58.63 (d, *J* = 3.0 Hz), 54.49, 49.23, 46.57, 44.55, 44.44, 37.08, 28.57, 26.12, 24.29, 18.31. LC-MS (ESI, 10-90): t_R = 5.41 min; m/z = 787.27 $[M + H]^+$. HRMS $[C_{40}H_{59}FN_6O_9 + H]^+$: 787.44003 calculated, 787.43948 found.

***tert*-Butyl (*R*)-(2-(2-(3-((1-(3-(4-(5-fluoro-6-(piperidin-1-ylmethyl)pyridin-2-yl)benzyl)-2,5-dioxoimidazolidin-1-yl)propan-2-yl)amino)-3-oxopropoxy)ethoxy)ethyl)carbamate (13):** The title compound was synthesized according to general procedure using **2** (27.4 mg, 62.5 µmol, 1 eq) and **44** (23.3 mg, 62.2 µmol, 1 eq). The product was obtained as a white solid (5.8 mg, 8.3 µmol, 13%). ^{1}H-NMR (500 MHz, $CDCl_3$) δ 7.95 (d, *J* = 8.3 Hz, 2H), 7.61 (dd, *J* = 8.6, 3.5 Hz, 1H), 7.41 (t, *J* = 8.8 Hz, 1H), 7.34 (d, *J* = 8.2 Hz, 2H), 6.53 (d, *J* = 8.5 Hz, 1H), 5.16 (s, 1H), 4.60 (q, *J* = 14.9 Hz, 2H), 4.41 – 4.31 (m, 1H), 3.81 (d, *J* = 2.6 Hz, 2H), 3.74 (q, *J* = 14.4 Hz, 2H), 3.70 – 3.66 (m, 2H), 3.64 – 3.57 (m, 4H), 3.58 – 3.49 (m, 4H), 3.31 (q, *J* = 5.5 Hz, 1H), 2.86 (t, *J* = 4.9 Hz, 1H), 2.58 (t, *J* = 5.5 Hz, 4H), 2.47 – 2.35 (m, 2H), 1.73 (s, 2H), 1.59 (p, *J* = 5.6 Hz, 4H), 1.42 (s, 9H), 1.18 (dd, *J* = 6.8, 2.9 Hz, 3H). ^{13}C-NMR (126 MHz, $CDCl_3$) δ 171.38, 170.38, 157.97 (d, *J* = 258.1 Hz), 157.16, 156.15, 151.85 (d, *J* = 5.0 Hz), 145.99 (d, *J* = 15.0 Hz), 138.74, 135.93, 128.52, 127.61, 123.69 (d, *J* = 20.5 Hz), 120.36 (d, *J* = 4.2 Hz), 73.51, 70.37, 70.31, 70.22, 67.15, 58.66 (d, *J* = 3.0 Hz), 54.49, 49.22, 46.56, 44.56, 44.40, 41.84, 37.09, 28.56, 26.14, 24.30, 18.34. LC-MS (ESI, 10-90): t_R = 5.34. min; m/z = 699.27 $[M + H]^+$. HRMS $[C_{36}H_{51}FN_6O_7 + H]^+$: 699.38760 calculated, 699.38720 found.

***tert*-Butyl (*R*)-(15-(3-(4-(5-fluoro-6-(piperidin-1-ylmethyl)pyridin-2-yl)benzyl)-2,5-dioxoimidazolidin-1-yl)-14-methyl-12-oxo-3,6,9-trioxa-13-azapentadecyl)carbamate (14):** The title compound was synthesized according to general procedure using **2** (25.3 mg, 58.0 µmol, 1 eq) and **45** (24.1 mg, 58.0 µmol, 1 eq). The product was obtained as a white solid (7.2 mg, 9.7 µmol, 17%). ^{1}H-NMR (500 MHz, $CDCl_3$) δ 7.96 (d, *J* = 8.3 Hz, 2H), 7.62 (dd, *J* = 8.6, 3.5 Hz, 1H), 7.42 (t, *J* = 8.8 Hz, 1H), 7.35 (d, *J* = 8.2 Hz, 2H), 6.52 (d, *J* = 8.5 Hz, 1H), 5.17 (s, 1H), 4.67 – 4.55 (m, 2H), 4.42 – 4.31 (m, 1H), 3.82 (d, *J* = 2.6 Hz, 2H), 3.75 (d, *J* = 17.6 Hz, 2H), 3.70 – 3.59 (m, 6H), 3.58 – 3.52 (m, 8H), 3.32 (d, *J* = 5.7 Hz, 2H), 2.59 (s, 4H), 2.42 (q, *J* = 6.2 Hz, 2H), 1.64 – 1.57 (m, 6H), 1.43 (s, 9H), 1.19 (d, *J* = 6.7 Hz, 3H). ^{13}C-NMR (126 MHz, $CDCl_3$) δ 171.46, 171.40, 170.42, 157.98 (d, *J* = 259.6 Hz), 157.18, 151.89, 146.06, 145.94, 138.75, 135.97, 128.53, 127.61, 123.70 (d, *J* = 21.4 Hz), 120.37 (d, *J* = 5.0 Hz), 73.31, 70.62, 70.60, 70.53, 70.51, 70.37, 67.17, 58.67 (d, *J* = 3.8 Hz), 54.50, 49.23, 46.58, 44.54, 44.43, 37.10, 28.57, 26.16, 24.31, 18.32. LC-MS (ESI, 10-90): t_R = 5.35 min; m/z = 743.27 $[M + H]^+$. HRMS $[C_{38}H_{55}FN_6O_8 + H]^+$: 743.41382 calculated, 743.41333 found.

***tert*-Butyl (*R*)-(18-(3-(4-(5-fluoro-6-(piperidin-1-ylmethyl)pyridin-2-yl)benzyl)-2,5-dioxoimidazolidin-1-yl)-17-methyl-15-oxo-3,6,9,12-tetraoxa-16-azaoctadecyl)carbamate (15):** The title compound was synthesized according to general procedure using **2** (31.0 mg, 71.0 µmol, 1.1 eq) and **51** (30.0 mg, 65.0 µmol, 1 eq). The product was obtained as a white solid (35.1 mg, 45.0 µmol, 63%). ^{1}H-NMR (500

MHz, $CDCl_3$) δ 7.95 (d, *J* = 8.2 Hz, 2H), 7.61 (dd, *J* = 8.6, 3.5 Hz, 1H), 7.42 (t, *J* = 8.8 Hz, 1H), 7.35 (dd, *J* = 8.3, 3.0 Hz, 2H), 6.57 (d, *J* = 8.4 Hz, 1H), 5.12 (s, 1H), 4.61 (q, *J* = 15.3 Hz, 2H), 4.41 – 4.31 (m, 1H), 3.81 (d, *J* = 2.6 Hz, 2H), 3.76 – 3.69 (m, 2H), 3.66 – 3.58 (m, 14H), 3.58 – 3.51 (m, 4H), 3.30 (q, *J* = 5.5 Hz, 2H), 2.58 (s, 2H), 2.48 – 2.35 (m, 2H), 1.97 (s, 2H), 1.60 (p, *J* = 5.6 Hz, 6H), 1.43 (s, 9H), 1.19 (t, *J* = 6.4 Hz, 3H). ^{13}C-NMR (126 MHz, $CDCl_3$) δ 171.46, 170.41, 157.98 (d, *J* = 257.9 Hz), 157.17, 151.90 (d, *J* = 5.0 Hz), 145.93 (d, *J* = 14.9 Hz), 138.70, 135.99, 128.54, 127.60, 123.71 (d, *J* = 20.4 Hz), 120.41 (d, *J* = 3.9 Hz), 72.57, 70.73, 70.65, 70.64, 70.51, 70.41, 70.33, 67.15, 58.62 (d, *J* = 3.0 Hz), 54.49, 49.23, 46.56, 44.53, 44.44, 41.62, 36.98, 29.84, 28.57, 26.12, 24.29, 18.30. LC-MS (ESI, 10-90): t_R = 5.41 min; m/z = 787.27 $[M + H]^+$. HRMS $[C_{40}H_{59}FN_6O_9 + H]^+$: 787.44003 calculated, 787.43971 found.

***tert*-Butyl (2-(2-(3-((2-(3-(4-(5-fluoro-6-(piperidin-1-ylmethyl)pyridin-2-yl)benzyl)-2,5-dioxoimidazolidin-1-yl)ethyl)amino)-3-oxopropoxy)ethoxy)ethyl)carbamate (16):** The title compound was synthesized according to general procedure using **3** (29.3 mg, 69.0 µmol, 1 eq) and **44** (25.8 mg, 69.0 µmol, 1 eq). The product was obtained as a white solid (12.9 mg, 19 µmol, 27%). ^{1}H-NMR (500 MHz, $CDCl_3$) δ 7.98 (d, *J* = 8.2 Hz, 2H), 7.65 (dd, *J* = 8.6, 3.4 Hz, 1H), 7.45 (t, *J* = 8.7 Hz, 1H), 7.37 (d, *J* = 8.2 Hz, 2H), 6.89 (s, 1H), 5.12 (s, 1H), 4.63 (s, 2H), 3.87 (t, J = 6.4 Hz, 2H), 3.77 (s, 2H), 3.73 (t, *J* = 5.7 Hz, 2H), 3.69 – 3.59 (m, 6H), 3.58 – 3.49 (m, 4H), 3.32 (d, *J* = 5.0 Hz, 4H), 2.63 (s, 2H), 2.47 (t, *J* = 5.8 Hz, 2H), 1.64 (s, 6H), 1.45 (s, 9H). ^{13}C-NMR (126 MHz, $CDCl_3$) δ 172.20, 170.32, 158.02 (d, *J* = 258.2 Hz), 157.06, 128.63, 127.63, 70.55, 70.38, 70.34, 70.22, 67.10, 54.38, 49.30, 46.60, 39.17, 38.39, 36.92, 28.57. LC-MS (ESI, 10-90): t_R = 5.16 min; m/z = 685.13 $[M + H]^+$. HRMS $[C_{35}H_{49}FN_6O_7 + H]^+$: 685.37195 calculated, 685.37165 found.

***tert*-Butyl (15-(3-(4-(5-fluoro-6-(piperidin-1-ylmethyl)pyridin-2-yl)benzyl)-2,5-dioxoimidazolidin-1-yl)-12-oxo-3,6,9-trioxa-13-azapentadecyl)carbamate (17):** The title compound was synthesized according to general procedure using **3** (28.8 mg, 68.0 µmol, 1 eq) and **45** (28.3 mg, 67.6 µmol, 1 eq). The product obtained as a white solid (6.3 mg, 8.7 µmol, 13%). ^{1}H-NMR (500 MHz, $CDCl_3$) δ 7.96 (d, *J* = 8.3 Hz, 2H), 7.61 (dd, *J* = 8.6, 3.5 Hz, 1H), 7.42 (t, *J* = 8.8 Hz, 1H), 7.35 (d, *J* = 8.3 Hz, 2H), 6.81 (s, 1H), 5.16 (s, 1H), 4.61 (s, 2H), 3.82 (d, *J* = 2.6 Hz, 2H), 3.75 (s, 2H), 3.74 – 3.67 (m, 4H), 3.60 (s, 6H), 3.57 – 3.48 (m, 4H), 3.31 (d, *J* = 5.8 Hz, 2H), 2.58 (s, 4H), 2.45 (t, *J* = 5.8 Hz, 2H), 1.82 (s, 2H), 1.60 (p, *J* = 5.6 Hz, 6H), 1.42 (s, 9H). ^{13}C-NMR (126 MHz, $CDCl_3$) δ 172.08, 170.30, 157.98 (d, *J* = 258.1 Hz), 157.03, 156.18, 151.83 (d, *J* = 4.5 Hz), 146.00 (d, *J* = 14.9 Hz), 138.81, 135.86, 128.62, 127.63, 123.71 (d, *J* = 20.3 Hz), 120.37 (d, *J* = 4.1 Hz), 73.32, 70.34, 70.29, 70.22, 70.14, 70.02, 67.12, 58.65 (d, *J* = 3.1 Hz), 54.50, 49.27, 46.60, 41.79, 40.42, 39.17, 38.42, 36.93, 28.56, 26.14, 24.30. LC-MS (ESI, 10-90): t_R = 5.21 min; m/z = 729.27 $[M + H]^+$. HRMS $[C_{37}H_{53}FN_6O_8 + H]^+$: 729.39817 calculated, 729.39767 found.

***tert*-Butyl (18-(3-(4-(5-fluoro-6-(piperidin-1-ylmethyl)pyridin-2-yl)benzyl)-2,5-dioxoimidazolidin-1-yl)-15-oxo-3,6,9,12-tetraoxa-16-azaoctadecyl)carbamate (18):** The title compound was synthesized according to general procedure using **3** (28.5 mg, 65.0 µmol, 1 eq) and **51** (32.8 mg, 70.9 µmol, 1.1 eq). The product obtained as a white solid (22.6 mg, 28.8 µmol, 44%). ^{1}H-NMR (500 MHz, $CDCl_3$) δ 7.96 (d, *J* = 8.2 Hz, 2H), 7.61 (dd, *J* = 8.6, 3.5 Hz, 1H), 7.42 (t, *J* = 8.8 Hz, 1H), 7.35 (d, *J* = 8.3 Hz, 2H), 6.91 (s, 1H), 5.11 (s, 1H), 4.61 (s, 2H), 3.82 (d, *J* = 2.7 Hz, 2H), 3.76 (d, *J* = 5.0 Hz, 2H), 3.70 (t, *J* = 5.4 Hz, 2H), 3.67 – 3.58 (m, 12H), 3.56 – 3.48 (m, 4H), 3.30 (q, *J* = 5.2 Hz, 2H), 2.58 (s, 2H), 2.45 (t, *J* = 6.0 Hz, 2H), 1.84 (s, 4H), 1.60 (p, *J* = 5.6 Hz, 6H), 1.43 (s, 9H). ^{13}C-NMR (126 MHz, $CDCl_3$) δ 172.22, 170.33, 157.99 (d, *J* = 258.1 Hz), 157.13, 157.07, 151.87 (d, *J* = 4.8 Hz), 145.94 (d, *J* = 15.5 Hz), 138.77, 135.96, 128.60, 127.62, 123.71 (d, *J* = 20.4 Hz), 120.38 (d, *J* = 4.1 Hz), 70.72, 70.67, 70.63, 70.55, 70.41, 70.37, 70.32, 70.23, 67.24, 67.10, 58.66 (d, *J* = 3.0 Hz), 54.51, 49.29, 46.60, 39.22, 36.92, 29.84, 28.58, 26.15, 24.31. LC-MS (ESI, 10-90): t_R = 5.28 min; m/z = 773.27 $[M + H]^+$. HRMS $[C_{39}H_{57}FN_6O_9 + H]^+$: 773.42438 calculated, 773.42407 found.

Synthesis of the fluorescent probes:

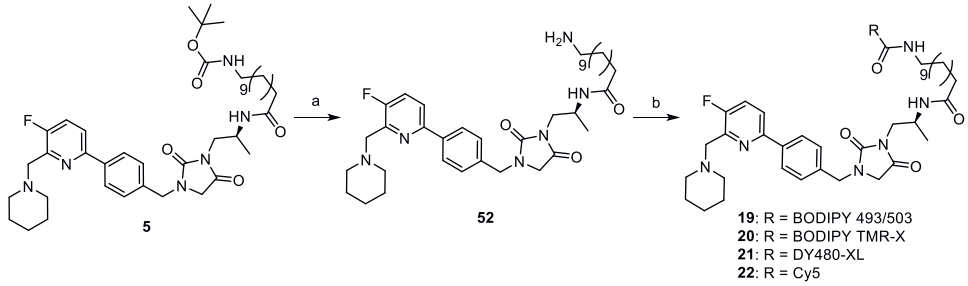

Scheme 4.10 Reagent and conditions: a) TFA (110 eq), DCM, RT, 2 h, quant.; b) **19-21**: Et_3N (1 eq), fluorophore-NHS ester (1 eq), DCM (0.3 M), RT, 1-3 h, 64-100%; **22**: HOBt (1.2 eq), DiPEA (2.5 eq), EDC.HCl (1.3 eq), Cyanine 5 carboxylic acid (1.1 eq), DMF (0.007 M), RT, 16 h, quant.).

(*S*)-12-Amino-*N*-(1-(3-(4-(5-fluoro-6-(piperidin-1-ylmethyl)pyridin-2-yl)benzyl)-2,5-dioxoimidazolidin-1-yl)propan-2-yl)dodecanamide (52): A mixture of **5** (435 mg, 0.6 mmol, 1 eq) and TFA (5 mL, 64.9 mmol, 110 eq) in DCM (10 mL) was stirred at RT for 2 h. The volatile compounds were evaporated under reduced pressure. The crude was re-dissolved in DCM and 1 M (aq) NaOH was added until pH 10. The layers were separated and the aqueous layer extracted thrice with chloroform. The combined organic layer was dried ($MgSO_4$), filtered and the solvent evaporated under reduced pressure to yield a yellow oil (376 mg, 0.59 mmol, quant.). ^{1}H-NMR (500 MHz, $CDCl_3$) δ 7.94 (d, *J* = 8.3 Hz, 2H), 7.60 (dd, *J* = 8.6, 3.5 Hz, 1H), 7.41 (t, *J* = 8.8 Hz, 1H), 7.33 (d, *J* = 8.3 Hz, 2H), 6.09 (d, *J* = 8.1 Hz, 1H), 4.60 (s, 2H), 4.35 – 4.25 (m, 1H), 3.81 (d, *J* = 2.6 Hz, 2H), 3.75 (q, *J* = 17.5 Hz, 2H), 3.62 – 3.49 (m, 2H), 2.74 (t, *J* = 7.5 Hz, 2H), 2.58 (s, 4H), 2.10 (t, *J* = 7.5 Hz, 2H), 1.59 (p, *J* = 5.6 Hz, 4H), 1.56 – 1.46 (m, 2H), 1.44 – 1.37 (m, 2H), 1.29 – 1.18 (m, 16H), 1.17 (d, *J* = 6.7 Hz, 3H). ^{13}C-NMR (126 MHz, $CDCl_3$) δ 173.48, 170.46, 162.32, 162.05, 157.93 (d, *J* = 258.3 Hz), 157.21, 156.90, 151.95 (d, *J* = 5.0 Hz), 145.52 (d, *J* = 15.1 Hz), 138.63, 135.82, 128.52, 127.58, 123.78 (d, *J* = 20.2 Hz), 120.56 (d, *J* = 5.0 Hz), 58.29 (d, *J* = 2.5 Hz), 54.37, 53.54, 50.57, 49.19, 46.49, 44.78, 44.18, 40.98, 36.86, 30.40, 29.40, 29.36, 29.27, 29.24, 29.18, 28.92, 28.82, 26.63, 25.88, 25.60, 24.13, 18.27. LC-MS (ESI, 10-90): t_R = 4.84 min; m/z = 637.53 $[M + H]^+$.

General procedure for the synthesis of final compounds (19-21)

A mixture of **52** (1 eq) Et_3N, (1 eq) and fluorophore-NHS-ester (1 eq) in DCM (0.3 M) was stirred at RT for 1-3 h. The reaction mixture was diluted with H_2O and DCM. The layers were separated and the aqueous layer extracted thrice with DCM. The combined organic layer was washed with H_2O and brine, dried ($MgSO_4$), filtered, and the solvent evaporated under reduced pressure. The crude product was purified with preparative HPLC and freeze-dried twice.

(*S*)-12-(4-(5,5-Difluoro-1,3,7,9-tetramethyl-5H-4l4,5l4-dipyrrolo[1,2-c:2',1'-f][1,3,2]diazaborinin-10-yl)butanamido)-*N*-(1-(3-(4-(5-fluoro-6-(piperidin-1-ylmethyl)pyridin-2-yl)benzyl)-2,5-dioxoimidazolidin-1-yl)propan-2-yl)dodecanamide (19): The title compound was synthesized according to general final compound procedure using **52** (5.52 mg, 8.7 µmol, 1 eq) and BODIPY 493/503-NHS-ester (3.74 mg, 8.7 µmol, 1 eq). The product was obtained as orange solid (5.3 mg, 5.6 µmol, 64%). ^{1}H-NMR (500 MHz, $CDCl_3$) δ 7.96 (d, *J* = 8.3 Hz, 2H), 7.62 (dd, *J* = 8.6, 3.5 Hz, 1H), 7.42 (t, *J* = 8.7 Hz, 1H), 7.33 (d, *J* = 8.3 Hz, 2H), 5.98 (d, *J* = 8.1 Hz, 1H), 5.53 (s, 1H), 5.37 – 5.32 (m, 1H), 4.60 (s, 2H), 4.36 – 4.27 (m, 1H), 3.84 (s, 2H), 3.75 (q, *J* = 17.4 Hz, 2H), 3.64 – 3.51 (m, 2H), 3.22 (q, *J* = 6.8 Hz, 2H), 3.04 – 2.97 (m, 2H), 2.60 (s, 4H), 2.51 (s, 3H), 2.42 (s, 6H), 2.31 (t, *J* = 7.1 Hz, 2H), 2.10 (t, *J* =

7.7 Hz, 2H), 2.04 – 1.92 (m, 2H), 1.65 – 1.53 (m, 6H), 1.50 – 1.39 (m, 2H), 1.34 – 1.20 (m, 18H), 1.18 (d, *J* = 6.7 Hz, 3H), 0.88 (t, *J* = 6.9 Hz, 2H). ^{13}C-NMR (126 MHz, $CDCl_3$) δ 173.23, 171.56, 170.38, 158.01 (d, *J* = 258.2 Hz), 157.27, 154.20, 145.53, 140.66, 138.74, 138.44, 138.10, 138.08, 135.83, 130.12 (d, *J* = 12.7 Hz), 129.96 (d, *J* = 19.0 Hz), 128.56, 127.65, 123.78 (d, *J* = 19.5 Hz), 121.90, 120.48, 115.27, 54.42, 49.23, 46.60, 45.07, 44.23, 39.83, 37.00, 36.50, 29.84, 29.74, 29.57, 29.55, 29.51, 29.46, 29.41, 29.36, 27.70, 27.62, 27.36, 27.03, 25.66, 22.83, 18.45, 16.57, 14.61, 14.26. LC-MS (ESI, 10-90): t_R = 7.47 min; m/z = 953.33 $[M + H]^+$. HRMS $[C_{53}H_{72}BF_3N_8O_4 + H]^+$: 953.57964 calculated, 953.57929 found.

(*S*)-12-(3-(8-(4-(3-azidopropoxy)phenyl)-5,5-difluoro-1,3-dimethyl-5*H*-4λ4,5λ4-dipyrrolo[1,2-c:2',1'-f][1,3,2]diazaborinin-2-yl)propanamido)-*N*-(1-(3-(4-(5-fluoro-6-(piperidin-1-ylmethyl)pyridin-2-yl)benzyl)-2,5-dioxoimidazolidin-1-yl)propan-2-yl)dodecanamide (20): The title compound was synthesized according to general final compound procedure using **52** (10.0 mg, 15.7 µmol, 1 eq) and BODIPY TMR-X-NHS-ester (8.6 mg, 15.8 µmol, 1 eq). The product was obtained as orange solid (12.4 mg, 11.6 µmol, 74%). ^{1}H-NMR (500 MHz, $CDCl_3$) δ 7.95 (d, *J* = 8.3 Hz, 2H), 7.86 (d, *J* = 8.9 Hz, 2H), 7.61 (dd, *J* = 8.6, 3.5 Hz, 1H), 7.41 (t, *J* = 8.8 Hz, 1H), 7.33 (d, *J* = 8.3 Hz, 2H), 7.08 (s, 1H), 6.97 (d, *J* = 2.1 Hz, 1H), 6.97 – 6.92 (m, 2H), 6.53 (d, *J* = 4.1 Hz, 1H), 5.98 (d, *J* = 8.1 Hz, 1H), 5.42 (t, *J* = 5.8 Hz, 1H), 4.60 (s, 2H), 4.35 – 4.27 (m, 1H), 4.10 (t, *J* = 5.9 Hz, 2H), 3.82 (d, *J* = 2.6 Hz, 2H), 3.74 (d, *J* = 17.5 Hz, 2H), 3.61 – 3.50 (m, 2H), 2.75 (d, *J* = 7.7 Hz, 2H), 2.59 (s, 4H), 2.52 (s, 3H), 2.25 (d, *J* = 7.2 Hz, 2H), 2.20 (s, 3H), 2.13 – 2.02 (m, 4H), 1.75 (s, 6H), 1.63 – 1.53 (m, 4H), 1.41 (q, *J* = 7.0, 6.3 Hz, 2H), 1.27 – 1.19 (m, 16H), 1.18 (d, *J* = 6.7 Hz, 3H). ^{13}C-NMR (126 MHz, $CDCl_3$) δ 173.22, 171.59, 170.39, 159.60, 159.55, 158.00 (d, *J* = 258.2 Hz), 157.27, 155.65, 151.83, 139.96, 138.78, 135.81, 135.10, 134.54, 130.86 (t, *J* = 4.2 Hz), 130.77, 128.56, 127.99, 127.65, 125.90, 123.74 (d, *J* = 20.4 Hz), 122.97, 120.44 (d, *J* = 5.6 Hz), 118.43, 114.34, 64.60, 58.56, 54.47, 49.22, 48.39, 46.59, 45.07, 44.23, 39.85, 37.01, 36.65, 29.84, 29.67, 29.56, 29.52, 29.50, 29.39, 29.35, 28.92, 26.98, 26.07, 25.66, 24.25, 20.19, 18.45, 13.31, 9.76. LC-MS (ESI, 10-90): t_R = 7.91 min; m/z = 1086.40 $[M + H]^+$. HRMS $[C_{59}H_{75}BF_3N_{11}O_5 + H]^+$: 1086.60803 calculated, 1086.60667 found.

(*S,E*)-6-(2-(7-(diethylamino)-2-oxo-2*H*-chromen-3-yl)vinyl)-1-(6-((12-((1-(3-(4-(5-fluoro-6-(piperidin-1-ylmethyl)pyridin-2-yl)benzyl)-2,5-dioxoimidazolidin-1-yl)propan-2-yl)amino)-12-oxododecyl)amino)-6-oxohexyl)pyridin-1-ium-3-sulfonate (21): The title compound was synthesized according to general final compound procedure using **52** (1.04 mg, 1.41 µmol, 1 eq) and DY-480XL-NHS-ester (1.0 mg, 1.9 µmol, 1.4 eq). After Prep-HPLC, two product with the correct mass were obtained as red solids (1.8 mg, 1.6 µmol, quant.) and (0.9 mg, 0.8 µmol, 50%). *No NMR-data available*. LC-MS (ESI, 10-90): t_R = 6.41 min; m/z = 1133.60 $[M + H]^+$. HRMS $[C_{62}H_{83}FN_8O_9S + H]^+$: 1133.59040 calculated, 1133.59028 found.

2-((1*E*,3*E*)-5-((*E*)-1-(6-((12-(((*S*)-1-(3-(4-(5-Fluoro-6-(piperidin-1-ylmethyl)pyridin-2-yl)benzyl)-2,5-dioxoimidazolidin-1-yl)propan-2-yl)amino)-12-oxododecyl)amino)-6-oxohexyl)-3,3-dimethylindolin-2-ylidene)penta-1,3-dien-1-yl)-1,3,3-trimethyl-3*H*-indol-1-ium (22): To a stirred and cooled (0 °C) mixture of Cyanine5 carboxylic acid (23.4 g, 48.4 µmol, 1.1 eq) in DMF (7 mL) was added HOBt (8.09 mg, 52.8 µmol, 1.2 eq), **52** (26.94 mg, 42.4 µmol, 1 eq), DiPEA (18.4 µL, 105.6 µmol, 2.5 eq) and EDC.HCl (9.69 mg, 50.5 µmol, 1.2 eq). After stirring overnight at RT, H_2O (7 mL) and EtOAc (7 mL) was added. The layers were separated and the aqueous layer extracted thrice with EtOAc. The combined organic layer was washed with sat. (aq) $NaHCO_3$, five times with H_2O, and once with brine, dried ($MgSO_4$), filtered, and the solvent evaporated under reduced pressure. The crude product was purified with preparative HPLC and freeze-dried twice to yield a blue solid (50.4 mg, 45.8 µmol, quant.). ^{1}H-NMR (400 MHz, $CDCl_3$) δ 8.02 – 7.88 (m, 3H), 7.67 (t, *J* = 5.7 Hz, 1H), 7.61 (dd, *J* = 8.6, 3.5 Hz, 1H), 7.41 (t, *J* = 8.8 Hz, 1H), 7.38 – 7.29 (m, 6H), 7.20 (dt, *J* = 11.9, 7.4 Hz, 2H), 7.08 (dd, *J* = 17.4, 7.9 Hz, 2H), 6.91 (t, *J*

= 12.5 Hz, 1H), 6.56 (d, *J* = 13.7 Hz, 1H), 6.27 (d, *J* = 13.5 Hz, 1H), 6.12 (d, *J* = 8.0 Hz, 1H), 4.60 (s, 2H), 4.35 – 4.23 (m, 1H), 4.07 (t, *J* = 7.7 Hz, 2H), 3.81 (d, *J* = 2.6 Hz, 2H), 3.73 (q, *J* = 17.4 Hz, 2H), 3.64 – 3.50 (m, 4H), 3.19 (q, *J* = 6.4 Hz, 2H), 2.57 (s, 4H), 2.35 (t, *J* = 7.2 Hz, 2H), 2.09 (t, *J* = 7.8 Hz, 2H), 1.88 – 1.73 (m, 2H), 1.70 (s, 6H), 1.69 (s, 6H), 1.61 – 1.48 (m, 10H), 1.39 (q, *J* = 6.2 Hz, 2H), 1.29 – 1.19 (m, 18H), 1.16 (d, *J* = 6.7 Hz, 3H). ^{13}C-NMR (101 MHz, $CDCl_3$) δ 173.51, 173.48, 173.25, 172.57, 170.39, 157.93 (d, *J* = 258.0 Hz), 157.22, 154.02, 152.97, 151.77 (d, *J* = 4.9 Hz), 145.79 (d, *J* = 15.0 Hz), 142.94, 142.03, 141.33, 140.76, 138.70, 135.81, 128.88, 128.73, 128.53, 127.59, 126.90, 125.49, 124.94, 123.69 (d, *J* = 20.4 Hz), 122.28, 122.20, 120.38 (d, *J* = 4.2 Hz), 111.03, 110.22, 104.93, 103.65, 58.55 (d, *J* = 3.1 Hz), 54.36, 49.50, 49.20, 49.05, 46.53, 45.01, 44.71, 44.16, 39.67, 36.96, 36.21, 29.80, 29.70, 29.65, 29.62, 29.54, 29.45, 29.40, 29.35, 28.16, 27.23, 27.10, 26.51, 26.06, 25.67, 25.34, 24.22, 18.39. LC-MS (ESI, 10-90): t_R = 7.36 min; m/z = 1101.73 $[M]^+$. HRMS $[C_{68}H_{90}FN_8O_4 + H]^+$: 1101.70636 calculated, 1101.70696 found.

Biology

All biologic assays have been previously described. “General remarks”, “Quantification and statistical analysis”, “Cell culture”, “Membrane preparation”, “[^{3}H]CP-55,940 Heterologous Displacement Assays” and “[^{35}S]GTPγS Binding Assays” can be referenced in **Chapter 2.**

References

1. Mallipeddi S, Janero DR, Zvonok N, Makriyannis A. Functional selectivity at G-protein coupled receptors: Advancing cannabinoid receptors as drug targets. *Biochem Pharmacol*. 2017;128:1-11. doi:10.1016/j.bcp.2016.11.014

2. Basagni F, Rosini M, Decker M. Functionalized Cannabinoid Subtype 2 Receptor Ligands: Fluorescent, PET, Photochromic and Covalent Molecular Probes. *ChemMedChem*. 2020;15(15):1374-1389. doi:10.1002/cmdc.202000298

3. Hamilton AJ, Payne AD, Mocerino M, Gunosewoyo H. Imaging Cannabinoid Receptors: A Brief Collection of Covalent and Fluorescent Probes for CB. *Aust J Chem*. 2021;74(6):416-432. doi:10.1071/CH21007

4. Spinelli F, Giampietro R, Stefanachi A, et al. Design and synthesis of fluorescent ligands for the detection of cannabinoid type 2 receptor (CB2R). *Eur J Med Chem*. 2020;188:112037. doi:10.1016/j.ejmech.2020.112037

5. Ling X, Zhang S, Liu Y, Bai M. Light-activatable cannabinoid prodrug for combined and target-specific photodynamic and cannabinoid therapy. *J Biomed Opt*. 2018;23(10):1. doi:10.1117/1.JBO.23.10.108001

6. Zhang S, Shao P, Bai M. In Vivo Type 2 Cannabinoid Receptor-Targeted Tumor Optical Imaging Using a Near Infrared Fluorescent Probe. *Bioconjug Chem*. 2013;24(11):1907-1916. doi:10.1021/bc400328m

7. Singh S, Oyagawa CRMM, Macdonald C, Grimsey NL, Glass M, Vernall AJ. Chromenopyrazole-based High Affinity, Selective Fluorescent Ligands for Cannabinoid Type 2 Receptor. *ACS Med Chem Lett*. 2019;10(2):209-214. doi:10.1021/acsmedchemlett.8b00597

8. Martín-Couce L, Martín-Fontecha M, Palomares Ó, et al. Chemical Probes for the Recognition of Cannabinoid Receptors in Native Systems. *Angewandte Chemie International Edition*. 2012;51(28):6896-6899. doi:10.1002/anie.201200467

9. Martín-Fontecha M, Angelina A, Rückert B, et al. A Fluorescent Probe to Unravel Functional Features of Cannabinoid Receptor CB 1 in Human Blood and Tonsil Immune System Cells. *Bioconjug Chem*. 2018;29(2):382-389. doi:10.1021/acs.bioconjchem.7b00680

10. Sarott RC, Viray AEG, Pfaff P, et al. Optical Control of Cannabinoid Receptor 2-Mediated Ca 2+ Release Enabled by Synthesis of Photoswitchable Probes. *J Am Chem Soc*. 2021;143(2):736-743. doi:10.1021/jacs.0c08926

11. Cooper AG, Oyagawa CRM, Manning JJ, et al. Development of selective, fluorescent cannabinoid type 2 receptor ligands based on a 1,8-naphthyridin-2-(1 H)-one-3-carboxamide scaffold. *Medchemcomm*. 2018;9(12):2055-2067. doi:10.1039/C8MD00448J

12. Sarott RC, Westphal M V, Pfaff P, et al. Highly Specific, Fluorescent Cannabinoid Type 2 Receptor Probes Enable Applications in Microscopy, Flow Cytometry and FRET-based Binding Assays. *ChemRxiv*. Published online 2019. doi:https://doi.org/10.26434/chemrxiv.10288547.v1

13. Sarott RC, Westphal M V., Pfaff P, et al. Development of High-Specificity Fluorescent Probes to Enable Cannabinoid Type 2 Receptor Studies in Living Cells. *J Am Chem Soc*. 2020;142(40):16953-16964. doi:10.1021/jacs.0c05587

14. Gazzi T, Brennecke B, Atz K, et al. Detection of cannabinoid receptor type 2 in native cells and zebrafish with a highly potent, cell-permeable fluorescent probe. *Chem Sci*. 2022;13(19):5539-5545. doi:10.1039/D1SC06659E

15. Soethoudt M, Stolze SC, Westphal M V., et al. Selective Photoaffinity Probe That Enables Assessment of Cannabinoid CB 2 Receptor Expression and Ligand Engagement in Human Cells. *J Am Chem Soc*. 2018;140(19):6067-6075. doi:10.1021/jacs.7b11281

16. Li X, Chang H, Bouma J, et al. Structural basis of selective cannabinoid CB2 receptor activation. *Nat Commun*. 2023;14(1):1447. doi:10.1038/s41467-023-37112-9

17. Loudet A, Burgess K. BODIPY Dyes and Their Derivatives: Syntheses and Spectroscopic Properties. *Chem Rev*. 2007;107(11):4891-4932. doi:10.1021/cr078381n

18. Deng Y, Cheng Y yuan, Liu H, Mack J, Lu H, Zhu L guan. Asymmetrical aza-boron-dipyridomethene derivatives with large Stokes shifts: synthesis and spectroscopic properties. *Tetrahedron Lett*. 2014;55(28):3792-3796. doi:10.1016/j.tetlet.2014.05.066

19. Widengren J, Schwille P. Characterization of Photoinduced Isomerization and Back-Isomerization of the Cyanine Dye Cy5 by Fluorescence Correlation Spectroscopy. *J Phys Chem A*. 2000;104(27):6416-6428. doi:10.1021/jp000059s

20. Buschmann V, Weston KD, Sauer M. Spectroscopic Study and Evaluation of Red-Absorbing Fluorescent Dyes. *Bioconjug Chem*. 2003;14(1):195-204. doi:10.1021/bc025600x

21. Olympus Life Sciences. Fluorophores for Confocal Microscopy. Accessed April 15, 2020. https://www.olympus-lifescience.com/en/microscope-resource/primer/techniques/confocal/fluorophoresintro/

22. Gao Z, Hao Y, Zheng M, Chen Y. A fluorescent dye with large Stokes shift and high stability: synthesis and application to live cell imaging. *RSC Adv*. 2017;7(13):7604-7609. doi:10.1039/C6RA27547H

Acknowledgment

This work was supported by the Dutch Research Council (NWO, Navistroke #15851) (Mario van der Stelt[d], M.v.d.S.).

Author contributions: Design: A.P.A.J. (Antonius P.A. Janssen), A.H. (Asad Halimi), L.V.d.P. (Laura V. de Paus); Conducting Experiments, A.H., L.V.d.P.; Writing-Original Draft, L.V.d.P.; Writing Review & Editing, M.v.d.S., L.H.H. (Laura H. Heitman), R.J.B.H.N.v.d.B (Richard J. B. H. N. van den Berg).

Chapter 5

Ligand-Directed Targeting of Mitochondrial CB_1 Receptors

Ligand-Directed Targeting of Mitochondrial CB_1 Receptors

Introduction

Cannabinoid Receptor 1 (CB_1R) was cloned in 1990, which proved that Δ^9-tetrahydrocannabinol (THC), the psychoactive cannabinoid in marijuana, acts by interaction with a specific receptor to elicit central nervous system (CNS) effects, rather than through membrane disruption.[1] CB_1R is a $G_{i/o}$ protein-coupled receptor that suppresses transmitter release at synapses in neurons.[2] During both short- and long-term plasticity the G protein-dependent pathway inhibits Ca^{2+} influx by acting on voltage-gated Ca^{2+} channels. Additionally CB_1R engagement leads to inhibition of adenyl cyclase and downregulation of the cAMP/PKA pathway.[3] CB_1R is implied in many brain functions, including mood, nociception, appetite, and motor function.[4] Furthermore, dysfunction of the CB_1R has been linked to epilepsy[5], depression[3] and several neurological disorders including Alzheimer's, Parkinson's and Huntington's.[6]

A link between cannabinoids and mitochondria was established in the 1970's, prior to the discovery of CB_1R.[1,7–10] It was shown that THC and other cannabinoids can inhibit monoamine oxidase (MAO) and affect mitochondrial respiration.[11,12] This effect was later shown to be CB_1R-dependent, as inhibition of mitochondria respiration by cannabinoids could be reversed by antagonist AM251.[13] Additionally, fatty-acid amide hydrolase 1 (FAAH) and monoacylglycerol lipase (MAGL), enzymes which are responsible for the metabolism of the endogenous cannabinoids, were also found present in mitochondria.[14] In 2012 it was demonstrated that approximately 15% of CB_1R is located on mitochondria using electron immune-gold detection assays.[14] Recently, the presence of mitochondrial CB_1R ($mtCB_1R$) has been detected in spermatozoa[15], skeletal muscles[16] and several brain cell types including astrocytes.[17] $MtCB_1R$-induced ATP reduction affects learning and memory by modulating synaptic plasticity as well as feeding behavior.[18–22]

Most studies on $mtCB_1R$ utilize agonists that act both on the CB_1R in the plasma membrane and mitochondria. Differentiation between CB_1R subgroups is done by using membrane (im)permeable CB_1R ligands, manipulation of membrane permeability, or $mtCB_1R$ KO cells to enable or disable $mtCB_1R$ signalling. Another potential way to study the $mtCB_1R$ is to target ligands directly to mitochondria, such as lipophilic, cationic small molecules or peptides, nanocarriers.[23] The most common mitochondrial carrier is triphenyl phosphonium (TPP^+). TPP^+ easily passes through hydrophobic membranes due to the large, diffuse surface area of the cation, limiting its polarizing ability.[24,25] The negative membrane potential of mitochondria allows lipophilic cations to migrate towards the mitochondria.[25] While TPP^+ is commonly used, it has been shown to uncouple the oxidative phosphorylation (OXPHOS) system. *Para*-trifluoromethyl phenyl in tris(4-trifluormethyl)phenyl phosphonium ($TFPP^+$) has a decreased electron density of the phosphonium cation and consequently a reduced effect on mitochondrial membrane potential and uncoupling.[26]

The aim of this chapter is to design and synthesize mitochondria-targeted CB_1R agonists. To this end, TPP^+ and $TFPP^+$ were introduced into the scaffold of the non-selective CBR agonist ORG28611, which is a water-soluble, potent, high-efficacy CB_1R agonist (pK_i = 8.9, pEC_{50} = 7.6), which was evaluated in clinical trials as an intravenous analgesic agent.[27–29] Compounds (**1**-**4**) were designed as CB_1R agonists with an alkyl (**1**,**2**) or poly-glycol (**3**,**4**) spacer conjugated TPP^+ (**1**,**3**) or $TFPP^+$ (**2**,**4**) (Figure 5.1). Their binding activity and functional effect on CB_1R was tested. While these compounds represent the first $T(F)PP^+$-ligands capable of binding the CB_1R, further optimization of their potency and efficacy is required to study the biological role of $mtCB_1R$.

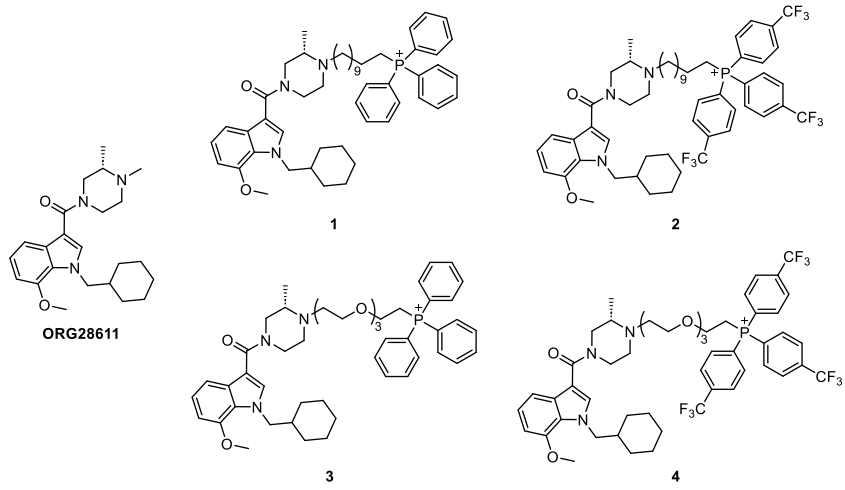

Figure 5.1 ORG28611 and the four mitochondrial-directed agonists **1**-**4** based on the indole-3-carboxamide scaffold of ORG28611. In **1** the scaffold is connected to TPP^+ with a C_{11} alkyl spacer. **2** has the C_{11} alkyl spacer and $TFPP^+$. In **3** the scaffold is connected to TPP^+ with a PEG3 spacer. **4** has the PEG3 spacer and $TFPP^+$.

Results & Discussion

Synthesis

The synthesis of the mitochondrial directing ORG28611-derived ligands commenced with the individual construction of the alkyl- and glycol-spacers and the indole-3-carboximide scaffold prior to conjugation and completed with the attachment of the phosphonium group. Thus, the glycol spacer (Scheme 5.1A) 2-(2-(2-(2-hydroxyethoxy)ethoxy)ethoxy)ethyl benzenesulfonate (**Chapter 4**) was substituted with lithium bromide (**5**) and the alcohol subsequently oxidized to an aldehyde (**6**). For the alkyl spacer (Scheme 6.1B) only an oxidation of 11-bromoundecanol (**7**) was required.

Synthesis of the indole-3-carboximide scaffold (**14**) (Scheme 5.1C) started with a reaction of iodine with the *in-situ* generated C6 lithium species of *tert*-butyl(2-methyloxyphenyl)carbamate (**8**) followed by a Sonogashira coupling with TMS-acetylene to give **9**. Basic induced indole formation (**9** → **10**) followed by TFAA mediated trifluoroketone introduction (**10** → **11**), and subsequent nucleophilic acyl substitution by hydroxide gained acid **12**. *N*-Alkylation with bromo-methylcyclohexane followed by HATU mediated peptide coupling introduced (*S*)-2-methylpiperazine in an region selective manner to give **14**. The glycol spacer **6** and alkyl spacer **7** were introduced (**15** and **16** respectively), directly followed by the conjugation to either TPP^+ and $TFPP^+$ to complete synthesis of the four ligands **1**-**4**.

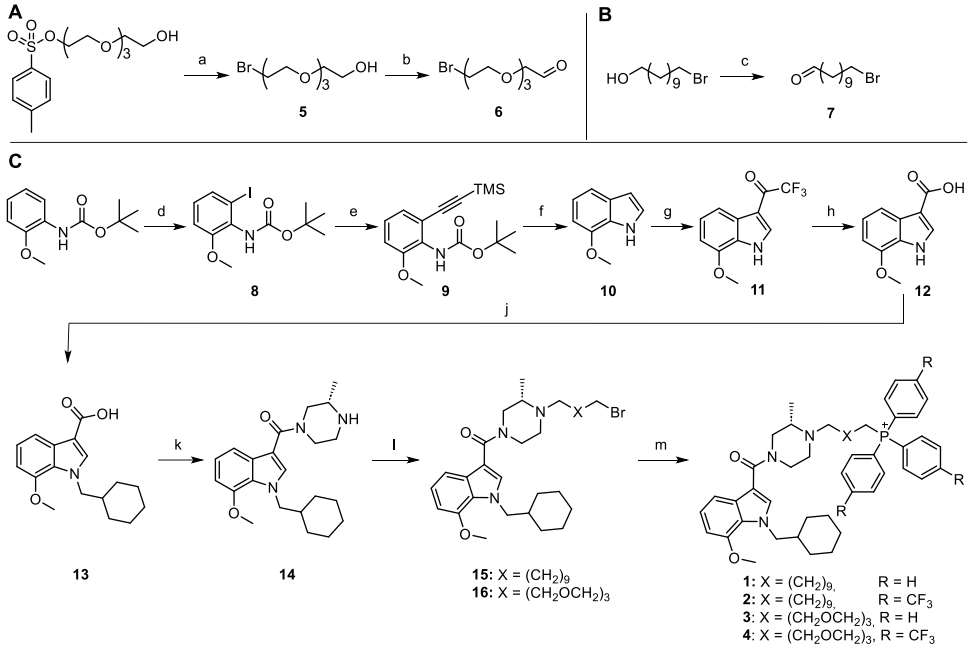

Scheme 5.1 Total synthesis of the four mitochondrial directing agonists. Reagents and conditions: a) LiBr, acetone, RT, 16 h, 93%; b) PCC, DCM, RT, 17 h, 36%; c) PCC, DCM, RT, 17 h, 43%; d) Step 1: *tert*-BuLi, Et_2O, -20 °C, 2 h; Step 2: I_2, -100 °C-RT, 17 h, 48%; e) Et_3N, $Pd(PPh_3)_4$, TMS-acetylene, 65 °C, 17 h, 57%; f) potassium *tert*-butoxide, *tert*-butanol, 85 °C, 4 h, 86%; g) TFAA, DMF, RT, 1 h, 96%; h) NaOH, H_2O, 100 °C, 2 h, 63%; j) NaH, bromo-methylcyclohexane, DMF, 60 °C, 2 h, 78%; k) Step 1: HATU, DiPEA, DMF, 0 °C, 1 h; Step 2: (*S*)-2-methylpiperazine, RT, 17 h, quant.; l) **6**/**7**, sodium triacetoxyborohydride. DCM, RT, 17 h, 19-77%; m) Step 1: PPh_3 (**1**/**3**) or tris(4-trifluoromethylphenyl)phosphine (**2**/**4**), ACN, 85 °C, 96 h, Step 2: 120-180 °C microwave, 0-14 h, 8-46%.

Molecular Pharmacology

After the synthesis of compounds **1**-**4** was completed, the ligands were evaluated for affinity (pK_i) in a [^{3}H]CP-55,940 radioligand displacement assay on membranes derived from CHO cells overexpressing hCB_1R or hCB_2R and compared to the parent compound ORG28611. Moreover, the potency (pEC_{50}) and maximal efficacy (E_{max}) were evaluated in a GTPγS assay (relative to CP-55,940, E_{max} = 100%) using the same membranes. The results are summarized in Table 5.1.

Table 5.1 The Pharmacochemical properties of the four ORG28611-based mitochondrial directing ligands **1**-**4**.

	CB_1R			CB_2R		
Compound	**Affinity pK_i ± SEM**	**Potency pEC_{50} ± SEM**	**E_{max} ± SEM**	**Affinity pK_i ± SEM**	**Potency pEC_{50} ± SEM**	**E_{max} ± SEM**
1	5.90 ± 0.17	< 5	-17 ± 1.13	6.33 ± 0.16	< 5	-22 ± 1.19
2	5.59 ± 0.23	< 5	-18 ± 0.52	6.13 ± 0.16	< 5	-16 ± 4.98
3	5.80 ± 0.26	5.90 ± 0.30	25 ± 1.56	6.19 ±0.18	< 5	9 ± 2.08
4	5.16 ± 0.57	5.70 ± 0.20	63 ± 2.28	5.79 ± 0.20	< 5	24 ± 1.55
ORG28611	8.61 ± 0.11	7.6[27]	77[27]	8.83 ± 0.11	-	-
CP-55,940	-	8.38 ± 0.06	105 ± 1.9	-	8.40 ± 0.09	96 ± 3.02

Binding affinities (pK_i) and potency (pEC_{50}) were determined as described previously (Chapter 2) on CBR-overexpressing CHO membranes. Efficacy (E_{max}) was normalized to the effect of 10 μM CP-55,940. Data are presented as the mean ± SEM from at least three (two for pEC_{50} of CB_2R) independent experiments performed in triplicate.

All compounds **1**-**4** have significantly decreased binding affinity (500- and 2800-fold) on both CB_1R and CB_2R compared to ORG28611. TPP^+ containing ligands **1** and **3** are slightly more potent than the $TFPP^+$ derivatives **2** and **4**.

Next, the potencies in the G protein activation assay for the CB_1R and CB_2R (Figure 5.2) were determined. Compounds **1** and **2** do not show any G protein activation at 1 µM, while compounds **3** and **4** activated CB_1R with potencies in a similar range as their binding affinities. This suggests that a PEG3 spacer is somewhat better tolerated than an alkyl spacer. While all compounds have moderate affinity for CB_2R, none showed significant G protein activation via CB_2R.

Interestingly, it seems that the functionality of compounds with a C_{11} spacer is switched from an agonist to an inverse agonist in both CB_1R and CB_2R, i.e. compare **3** and **4** to **1** and **2**, respectively. Compounds **1** and **2** have a negative maximal efficacy at 10 µM, signifying a decrease of basal receptor activity. This observation is in line with the hypothesis introduced in Chapter 4, that some hydrophobic interaction will stabilize the inactive state of the receptor. However, further investigation in this phenomenon was outside the scope of this chapter.

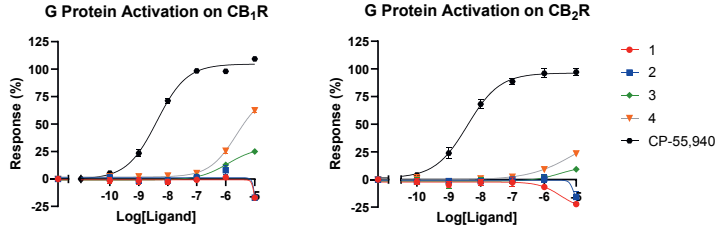

Figure 5.2 G protein activation levels were determined with a [^{35}S]GTPγS functionality assay. Basal receptor activity was set to 0%. G protein activation with 10 µM concentration of full agonist CP-55,940 was set as 100%. Data are expressed as mean ± SEM from at least three (two for CB_2R) independent experiments performed in triplicate.

Conclusion

Compounds **1**-**4** were successfully synthesized and profiled in molecular pharmacology assays. They represent the first representatives of $T(F)PP^+$-ligands that bind the CB_1R. Unfortunately, the compounds displayed weak affinity for the CB_1R and no selectivity over CB_2R. Additionally, compounds **1** and **2** behaved as inverse agonists, as opposed to parent compound ORG28611. Of note, the assays described in this chapter do not distinguish between plasmalemmal CB_1R and mitochondrial CB_1R. Hence, new compounds have to be designed and additional assays will need to be developed to assure the efficacy of the mitochondrial directing capability of the phosphine group.

Experimental Section

Chemistry

General Remarks

All reagents and solvents were purchased from commercial sources and were of analytical grade (Sigma-Aldrich, BroadPharm®). Reagents and solvents were not further purified before use. All moisture sensitive reactions were performed under inert atmosphere. Solvents were dried using 4 Å molecular sieves prior to use when anhydrous conditions were required. Water used in reactions was always demineralized. Analytical Thin-layer Chromatography (TLC) was routinely performed to monitor the progression of a reaction and was conducted on Merck Silica gel 60 F254 plates. Reaction compounds on the TLC plates were visualized by UV irradiation (λ_{254}) and/or spraying with potassium permanganate solution (K_2CO_3 (40 g), $KMnO_4$ (6 g), and H_2O (600 mL)), ninhydrin solution (ninhydrin (1.5 g), n-butanol

(100 mL) and acetic acid (3.0 mL)) or molybdenum solution ($(NH_4)_6MO_7O_{24}\cdot 4H_2O$ (25 g/L) and $(NH_4)_4Ce(SO_4)_4\cdot H_2O$ (10 g/L) in sulfuric acid (10%)) followed by heating as appropriate. Purification by flash column chromatography was performed using Screening Devices B.V. silica gel 60 (40-63 µm, pore diameter of 60 Å). Solutions were concentrated using a Heidolph laborata W8 4000 efficient rotary evaporator with a Laboport vacuum pump. Analytical purity was determined with Liquid Chromatography-Mass Spectrometry (LC-MS) using a Finnigan LCQ Advantage MAX apparatus with electrospray ionization (ESI), equipped with a Phenomenex Gemini 3 µm NX-C18 110Å column (50x4.6mm), measuring absorbance at 254 nm using a Waters 2998 PDA UV detector and the m/z ratio by using an Acquity Single Quad (Q1) detector. Injection was with the Finnigan Surveyor Autosampler Plus and pumped through the column with the Finnigan Surveyor LC pump plus to be analysed with the Finnigan Surveyor PDA plus detector. Samples were analysed using eluent gradient 10% → 90% ACN in MilliQ water (+ 0.1% TFA (v/v)). For purification by mass guided preparative High-Performance Liquid Chromatography (Prep-HPLC) was performed on a Waters AutoPurification HPLC/MS apparatus with a Gemini prep column 5 µm 18C 110 Å (150x21.2mm), Waters 2767 Sample manager, Waters 2545 Binary gradient module, Waters SFO System fluidics organizer, Waters 515 HPLC pump M, Waters 515 HPLC pump L attached to a Waters SQ detector Acquity Ultra performance LC. A five column volume purification protocol was applied with the eluents A: 0.2% aq. TFA, B: ACN, flow 25 mL/min, with a minimum start gradients of 0% to maximum end gradient of 100% of B. ^1H, ^{13}C, ^1H-COSY and HSQC Nuclear Magnetic Resonance (NMR) spectra were recorded on a Bruker AV 300 (300/75 MHz), AV 400 (400/100 MHz or AV850 (850/216 MHz) spectrometer at ambient temperature using $CDCl_3$ or MeOD as solvent. Chemical shifts (δ) are referenced in parts per million (ppm) with tetramethylsilane (TMS) or $CDCl_3$ resonance as the internal standard peak ($CDCl_3$/TMS, δ 0.00/7.26 for ^1H (TMS/$CDCl_3$), δ 77.16 for ^{13}C ($CDCl_3$)) or MeOD resonance internal standard peak (δ 3.31 (^1H) and δ 49.00 (^{13}C)). Multiplicity is reported as bs = broad singlet, s = singlet, d = doublet, dd = doublet of doublet, t = triplet, q = quartet, qd = quartet of doublets, p = quintet, hept = heptet, m = multiplet. Coupling-constants (*J*) are reported in Hertz (Hz).

Synthesis of the spacers:

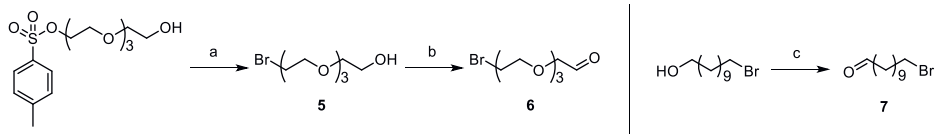

Scheme 5.2 Synthesis of the glycol (PEG3) and alkyl (C_{11}) spacers. Reagents and conditions: a) LiBr, acetone, RT, 16 h, 93%; b) PCC, DCM, RT, 17 h, 36%; c) PCC, DCM, RT, 17 h, 43%;

2-(2-(2-(2-Bromoethoxy)ethoxy)ethoxy)ethan-1-ol (5): To a stirred solution of 2-(2-(2-(2-hydroxyethoxy)ethoxy)ethoxy)ethyl 4-methylbenzenesulfonate (2.00 g, 5.8 mmol, 1 eq) in acetone (50 mL) was added LiBr (1.33 g, 11.5 mmol, 2 eq). After stirring at RT for 16 h the solvent was evaporated under reduced pressure. The crude product was redissolved in $CHCl_3$ (50 mL) and the organic layer was washed four times with brine, dried ($MgSO_4$), filtered and the solvent evaporated under reduced pressure to yield a colourless oil (1.38 g, 5.4 mmol, 93%). ^1H-NMR (400 MHz, $CDCl_3$) δ 3.49 (t, *J* = 5.5 Hz, 2H), 3.40 (t, *J* = 6.2 Hz, 2H), 3.31 – 3.20 (m, 8H), 3.18 – 3.15 (m, 2H), 3.11 (t, *J* = 6.2 Hz, 2H). *No C-NMR Available*.

2-(2-(2-(2-Bromoethoxy)ethoxy)ethoxy)acetaldehyde (6): A mixture of **5** (1.05 g, 4.1 mmol, 1 eq) and PCC (0.88 g, 4.1 mmol, 1 eq) in DCM (15 mL) was stirred at RT for 17 h. The solvent was evaporated under reduced pressure and the crude product re-dissolved in $CHCl_3$ (35 mL). The organic layer was washed twice with 2 M HCl (aq) and once with sat. $NaHCO_3$ (aq), dried ($MgSO_4$), filtered and the solved

evaporated under reduced pressure. The crude product was purified with flash column chromatography (SiO_2, 0-2% MeOH in DCM) to yield a colourless oil (0.37 g, 1.5 mmol, 36%). ^{1}H-NMR (400 MHz, $CDCl_3$) δ 9.64 (s, 1H), 3.72 (t, *J* = 6.3 Hz, 2H), 3.65 – 3.61 (m, 2H), 3.58 (s, 6H), 3.51 (t, *J* = 4.3 Hz, 2H), 3.39 (t, *J* = 6.2 Hz, 2H). *No C-NMR Available*.

11-Bromoundecanal (7): A mixture of 11-bromoundecanol (0.61 g, 2.4 mmol, 1 eq) and PCC (0.53 g. 2.4 mmol, 1 eq) in DCM (10 mL) was stirred at RT for 17 h. The solvent was evaporated under reduced pressure and the crude re-dissolved in Et_2O (20 mL). The organic layer was washed thrice with 2 M HCl (aq), four times with sat. $NaHCO_3$ (aq) and once with brine, dried ($MgSO_4$), filtered and the solvent evaporated under reduced pressure. The crude product was purified with flash column chromatography (SiO_2, 5-15% EtOAc in pentane) to yield a colourless oil (0.26 g, 1.04 mmol, 43%). ^{1}H-NMR (400 MHz, $CDCl_3$) δ 9.76 (t, *J* = 1.8 Hz, 1H), 3.40 (t, *J* = 6.9 Hz, 2H), 2.43 (td, *J* = 7.3, 1.8 Hz, 2H), 1.85 (p, *J* = 7.0 Hz, 2H), 1.62 (p, *J* = 7.3 Hz, 2H), 1.42 (p, *J* = 6.9 Hz, 2H), 1.30 (s, 10H). ^{13}C-NMR (101 MHz, $CDCl_3$) δ 202.63, 43.78, 33.90, 32.72, 29.26, 29.21, 29.12, 29.03, 28.63, 28.05, 21.96.

Synthesis of mitochondrial directing ligands 1-4

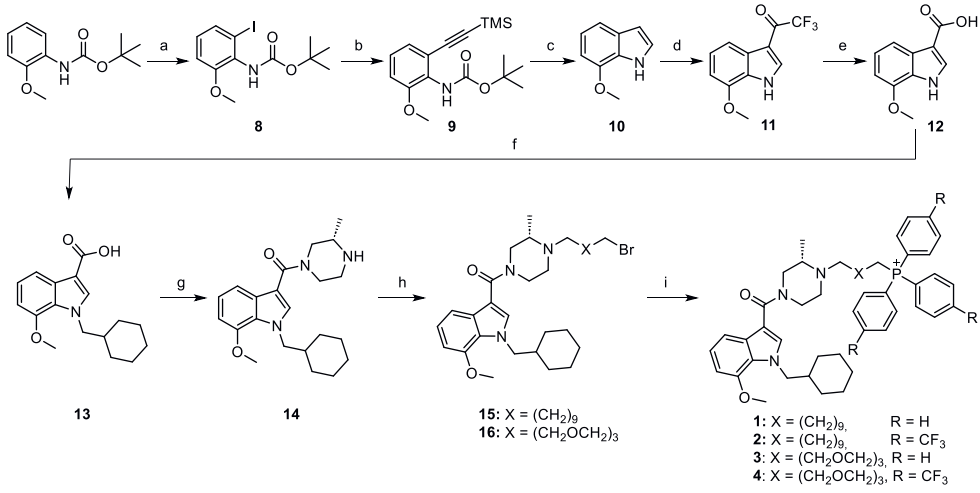

Scheme 5.3 Synthesis of the scaffold and the mitochondrial directing ligands **1-4**. Reagents and conditions: a) Step 1: *tert*-BuLi, Et_2O, -20 °C, 2 h; Step 2: I_2, -100 °C-RT, 17 h, 48%; b) Et_3N, $Pd(PPh_3)_4$, TMS-acetylene, 65 °C, 17 h, 57%; c) potassium *tert*-butoxide, *tert*-butanol, 85 °C, 4 h, 86%; d) TFAA, DMF, RT, 1 h, 96%; e) NaOH, H_2O, 100 °C, 2 h, 63%; f) NaH, bromomethylcyclohexane, DMF, 60 °C, 2 h, 78%; g) Step 1: HATU, DiPEA, DMF, 0 °C, 1 h; Step 2: (*S*)-2-methylpiperazine, RT, 17 h, quant.; h) **6**/**7**, sodium triacetoxyborohydride. DCM, RT, 17 h, 19-77%; j) Step 1: PPh_3 (**1**/**3**) or tris(4-trifluoromethylphenyl)phosphine (**2**/**4**), ACN, 85 °C, 96 h, ii) 120-180 °C microwave, 0-14 h, 8-46%.

tert-Butyl(2-iodo-6-methoxyphenyl)carbamate (8): To a cooled (-20 °C) and stirred mixture of *tert*-butyl(2-methyloxyphenyl)carbamate (2.00 g, 9.0 mmol, 1 eq) in anhydrous Et_2O (10 mL) under inert atmosphere was added dropwise *tert*-butyllithium (12 mL, 1.7 M in pentane, 20.4 mmol, 2.3 eq). After 2 h the mixture was cooled (-100 °C) further and iodine (2.73 g. 10.8 mmol, 1.2 eq) was added dropwise. The mixture was stirred at RT for 17 h. The reaction was quenched with sat. $Na_2S_2O_3$ (aq) (120 mL) and stirred for 45 minutes. After addition of Et_2O the layers were separated and the organic layer washed five times with sat. $Na_2S_2O_3$ (aq) and thrice with brine, dried ($MgSO_4$), filtered, and the solvent evaporated under reduced pressure. The crude product was purified with flash column chromatography (SiO_2, 2-20% EtOAc in pentane) to yield a yellow solid (1.55 g, 4.4 mmol, 48%). ^{1}H-NMR (300 MHz, $CDCl_3$) δ 7.37 (dd, *J* = 7.6, 1.3 Hz, 1H), 6.92 – 6.77 (m, 2H), 6.29 (s, 1H), 3.72 (s, 3H),

1.47 (s, 9H). ^{13}C-NMR (75 MHz, $CDCl_3$) δ 155.14, 153.12, 130.28, 128.71, 128.26, 111.17, 100.27, 79.77, 55.65, 28.04.[30]

tert-Butyl(2-methoxy-6-((trimethylsilyl)ethynyl)phenyl)carbamate (9): To a stirred mixture of **8** (1.55 g, 4.4 mmol, 1 eq), Et_3N (0.72 mL, 0.2 mmol, 0.05 eq) in THF (20 mL) under inert atmosphere was added $Pd(PPh_3)_4$ (0.10 g, 0.1 mmol, 0.02 eq) and trimethylsilylacetylene (0.75 mL, 5.4 mmol, 1.3 eq). After heating (70 °C) for 17 h H_2O and Et_2O were added and the mixture filtered over a Celite™ pad. The layers were separated and the organic layer was washed thrice with brine, dried ($MgSO_4$), filtered and the solvent evaporated under reduced pressure. The crude product was purified with flash column chromatography (SiO_2, 3-15% EtOAc in pentane) to yield a yellow oil (0.79 g, 2.5 mmol, 57%). ^{1}H-NMR (400 MHz, $CDCl_3$) δ 7.00 – 6.95 (m, 2H), 6.81 – 6.72 (m, 1H), 6.12 (s, 1H), 3.72 (s, 3H), 1.41 (s, 9H), 0.15 (s, 9H). ^{13}C-NMR (101 MHz, $CDCl_3$) δ 153.85, 153.28, 128.01, 126.31, 124.79, 121.37, 111.87, 101.78, 99.09, 80.04, 55.87, 28.33, 0.04.

7-Methoxyindole (10): To a stirred solution of **9** (0.20 g, 0.6 mmol, 1 eq) in *tert*-butanol (5 mL) under inert atmosphere was added potassium *tert*-butoxide (0.34 g, 3.0 mmol, 4.9 eq) in several portions. After heating (85 °C) for 4 h the mixture was diluted with H_2O and DCM. The layers were separated and the aqueous layer was extracted thrice with DCM. The combination of organic layers was washed thrice with brine, dried ($MgSO_4$), filtered and the solvent evaporated under reduced pressure. The crude product was purified with flash column chromatography (SiO_2, 2.5-5% EtOAc in pentane) to yield a brown oil (0.08 g, 0.54 mmol, 86%). ^{1}H-NMR (400 MHz, $CDCl_3$) δ 8.36 (s, 1H), 7.25 (d, *J* = 8.0 Hz, 1H), 7.11 (t, *J* = 2.8 Hz, 1H), 7.03 (t, *J* = 7.8 Hz, 1H), 6.63 (d, *J* = 7.0 Hz, 1H), 6.52 (dd, *J* = 3.1, 2.2 Hz, 1H), 3.93 (s, 3H). ^{13}C-NMR (101 MHz, $CDCl_3$) δ 146.26, 129.28, 126.53, 123.80, 120.23, 113.53, 102.93, 101.80, 55.39.[30]

2,2,2-Trifluoro-1-(7-methoxy-1*H*-indol-3-yl)ethan-1-one (11): To a cooled (0 °C) and stirred mixture of **10** (0.82 g, 5.6 mmol, 1 eq) in DMF (10 mL) was added dropwise trifluoroacetic anhydride (1.3 mL, 8.8 mmol, 1.3 eq). After stirring at RT for 1 h the reaction was quenched with H_2O (100 mL) and the precipitate filtered. The precipitate was dissolved in EtOAc and the organic layer was washed twice with sat. $NaHCO_3$ (aq) and twice with brine, dried ($MgSO_4$), filtered and the solvent evaporated under reduced pressure to yield a beige solid (1.31 g, 5.4 mmol, 96%). ^{1}H-NMR (400 MHz, MeOD) δ 8.03 (q, *J* = 1.9 Hz, 1H), 7.82 (d, *J* = 7.3 Hz, 1H), 7.21 (t, *J* = 8.0 Hz, 1H), 6.78 (d, *J* = 7.1 Hz, 1H), 3.96 (s, 3H). ^{13}C-NMR (101 MHz, MeOD) δ 174.96 (q, *J* = 34.4 Hz), 146.32, 134.85 (q, *J* = 4.8 Hz), 127.29, 126.60, 123.87, 116.79 (q, *J* = 290.5 Hz), 113.56, 109.96, 104.09, 54.63. LCMS (10-90%): t_r = 7.31 min, 244.0 m/z $[C_{11}H_8F_3NO_2+H]^+$.

7-Methoxy-1*H*-indole-3-carboxylic acid (12): A stirred solution of **11** (1.32 g, 5.4 mmol, 1 eq) in 4 M NaOH (aq) (50 mL) was heated (100 °C) for 2 h. The solution was diluted with Et_2O and the layers separated. The aqueous layer was washed once with Et_2O, then acidified to pH ~1 with 3 M HCl (aq). The formed precipitate was filtered to yield a beige solid (0.64 g, 3.4 mmol, 63%). ^{1}H-NMR (400 MHz, DMSO) δ 11.98 (s, 1H), 11.93 (s, 1H), 7.82 (d, *J* = 3.0 Hz, 1H), 7.57 (d, *J* = 7.9 Hz, 1H), 7.07 (t, *J* = 7.9 Hz, 1H), 6.75 (d, *J* = 6.9 Hz, 1H), 3.92 (s, 3H). ^{13}C-NMR (101 MHz, DMSO) δ 165.93, 146.33, 131.40, 127.56, 126.46, 121.71, 113.21, 107.96, 102.70, 55.25 LCMS (10→90%): t_r = 4.86 min, 192.07 m/z $[C_{10}H_9NO_3+H]^+$.[31]

1-(Cyclohexylmethyl)-7-methoxy-1*H*-indole-3-carboxylic acid (13): To a stirred (1 h) mixture of **12** (1.82 g, 9.5 mmol, 1 eq) and NaH (60% in mineral oil, 1.04 g, 23.8 mmol, 2.5 eq) in DMF (40 mL) under inert atmosphere was added dropwise bromo-methylcyclohexane (2.7 mL, 19.0 mmol, 2 eq). After heating (60 °C) for 2 h H_2O (120 mL) acidified to pH 1 with 3 M HCl and EtOAc (50 mL) were added. The layers were separated and the aqueous layer was extracted twice with EtOAc and twice with Et_2O. The

combination of organic layers was dried ($MgSO_4$), filtered and the solvent evaporated under reduced pressure. The crude product was purified with flash column chromatography (SiO_2, 2.5-10% MeOH in DCM) to yield a white solid (2.13 g, 7.4 mmol, 78%). ^{1}H-NMR (400 MHz, MeOD:$CDCl_3$ 1:1) δ 7.73 – 7.64 (m, 2H), 7.09 (t, *J* = 7.9 Hz, 1H), 6.68 (d, *J* = 7.9 Hz, 1H), 4.17 (d, *J* = 7.3 Hz, 2H), 3.91 (s, 3H), 1.79 (hept, *J* = 3.5 Hz, 1H), 1.73 – 1.59 (m, 3H), 1.55 (d, *J* = 12.7 Hz, 2H), 1.15 (s, 3H), 0.96 (q, *J* = 11.5 Hz, 2H). ^{13}C-NMR (101 MHz, MeOD:$CDCl_3$ 1:1) δ 167.30, 147.19, 136.04, 128.90, 125.88, 121.76, 113.41, 105.63, 103.04, 55.89, 54.51, 39.32, 29.95, 25.76, 25.19; LCMS (10-90%): t_r = 8.30 min, 288.07 m/z $[C_{17}H_{21}NO_3+H]^+$.

(*S*)-(1-(Cyclohexylmethyl)-7-methoxy-1*H*-indol-3-yl)(3-methylpiperazin-1-yl)methanone (14): To a cooled (0 °C) and stirred (1 h) mixture of **13** (0.50 g, 1.7 mmol, 1 eq), HATU (1.02 g, 2.7 mmol, 1.5 eq) and DiPEA (1.2 mL, 7.0 mmol, 4 eq) in DMF (20 mL) was added (*S*)-2-methylpiperazine (0.35 g, 3.5 mmol, 2 eq). After stirring at RT for 17 h the mixture was diluted with EtOAc. The organic layer was washed thrice with 4 M NaOH (aq). The combination of aqueous layers was extracted twice with EtOAc. The combination of organic layers was dried ($MgSO_4$), filtered and the solvent evaporated under reduced pressure. The crude product was purified with flash column chromatography (SiO_2, 1-15% MeOH in DCM) to yield a white solid (0.64 g, 1.7 mmol, quant.). ^{1}H-NMR (400 MHz, MeOD) δ 7.24 (s, 1H), 7.03 (d, *J* = 8.0 Hz, 1H), 6.82 (t, *J* = 8.0 Hz, 1H), 6.44 (d, *J* = 7.9 Hz, 1H), 4.11 (d, *J* = 13.6 Hz, 2H), 3.94 (d, *J* = 7.1 Hz, 2H), 3.61 (s, 3H), 3.11 – 2.93 (m, 3H), 2.87 – 2.77 (m, 2H), 1.51 (hept, *J* = 3.5 Hz, 1H), 1.41 – 1.26 (m, 3H), 1.22 (d, *J* = 11.6 Hz, 2H), 0.95 (d, *J* = 6.6 Hz, 3H), 0.90 – 0.66 (m, 5H). ^{13}C-NMR (101 MHz, MeOD) δ 168.60, 148.89, 133.66, 129.91, 126.89, 122.99, 113.51, 107.93, 104.62, 56.56, 55.80, 52.17, 44.13, 43.46, 40.89, 31.12, 27.14, 26.55, 15.94. LCMS (10-90%): t_r = 5.99 min, 370.0 m/z $[C_{22}H_{31}N_3O_2+H]^+$.

(*S*)-(4-(11-Bromoundecyl)-3-methylpiperazin-1-yl)(1-(cyclohexylmethyl)-7-methoxy-1Hindol-3-yl)methanone (15): A mixture of **14** (0.17 g, 0.5 mmol, 1 eq), **7** (0.26 g, 1.0 mmol, 2.3 eq) and $NaHB(OAc)_3$ (0.15 g, 0.7 mmol, 1.6 eq) in DCM (5 mL) under inert atmosphere was stirred at RT for 17 h. The reaction was quenched with sat. $NaHCO_3$ (aq) (20 mL), and the layers separated. The organic layer was washed twice with sat. $NaHCO_3$ (aq) and twice with brine. The aqueous layer was extracted twice with DCM. The combination of organic layers was dried ($MgSO_4$), filtered and the solvent evaporated under reduced pressure. The crude product was purified with flash column chromatography (SiO_2, 0-30% acetone in DCM) to yield a white solid (0.21 g, 0.4 mmol, 77%). ^{1}H-NMR (400 MHz, $CDCl_3$) δ 7.30 – 7.27 (m, 2H), 7.06 (t, *J* = 7.9 Hz, 1H), 6.64 (d, *J* = 7.5 Hz, 1H), 4.17 (dd, *J* = 7.0, 1.5 Hz, 2H), 3.91 (s, 3H), 3.39 (t, *J* = 6.9 Hz, 2H), 3.05 (dd, *J* = 12.7, 9.3 Hz, 2H), 2.86 (d, *J* = 11.6 Hz, 1H), 2.77 – 2.65 (m, 1H), 2.55 – 2.47 (m, 2H), 2.39 – 2.29 (m, 3H), 1.83 (p, *J* = 6.9 Hz, 2H), 1.72 – 1.56 (m, 7H), 1.49 – 1.37 (m, 4H), 1.27 (s, 12H), 1.16 (t, *J* = 7.3 Hz, 2H), 1.05 (d, J = 5.5 Hz, 3H), 0.97 (qd, *J* = 11.5, 2.5 Hz, 2H). ^{13}C-NMR (101 MHz, $CDCl_3$) δ 166.43, 147.52, 132.02, 128.50, 125.52, 121.10, 113.22, 109.63, 102.91, 56.06, 55.26, 54.97, 53.36, 50.65, 39.89, 33.97, 32.73, 30.59, 29.45, 29.43, 29.38, 29.33, 28.67, 28.07, 27.50, 26.30, 25.70, 25.28, 15.19. LCMS (10-90%): t_r = 8.72 min, 602.2 m/z. HRMS $[C_{33}H_{52}BrN_3O_2+H]^+$: 602.32429 calculated, 602.33133 found.

(*S*)-(4-(2-(2-(2-(2-Bromoethoxy)ethoxy)ethoxy)ethyl)-3-methylpiperazin-1-yl)(1- (cyclohexylmethyl)-7-methoxy-1*H*-indol-3-yl)methanone (16): A mixture of **14** (0.16 g, 0.4 mmol, 1eq), **6** (0.22 g, 0.9 mmol, 2 eq) and $NaHB(OAc)_3$ (0.16 g, 0.8 mmol, 1.8 eq) was stirred at RT for 17 h. The reaction was quenched with sat. $NaHCO_3$ (aq) (20 mL), and the layers separated. The organic layer was washed twice with sat. $NaHCO_3$ (aq) and twice with brine. The aqueous layer was extracted twice with DCM. The combination of organic layers was dried ($MgSO_4$), filtered and the solvent evaporated under reduced pressure. The crude product was purified with flash column chromatography (SiO_2, 0-20% 2-propanol in DCM) to yield a white solid (48.4 mg, 0.1 mmol, 19%). ^{1}H-NMR (400 MHz, $CDCl_3$) δ 7.26 (dd, *J* = 8.1,

0.9 Hz, 1H), 7.23 (s, 1H), 7.05 (t, *J* = 7.9 Hz, 1H), 6.63 (d, *J* = 7.0 Hz, 1H), 4.16 (dd, *J* = 7.0, 1.7 Hz, 2H), 4.07 (bs, 2H), 3.91 (s, 3H), 3.77 (t, *J* = 6.3 Hz, 2H), 3.69 – 3.54 (m, 10H), 3.44 (t, *J* = 6.3 Hz, 2H), 3.39 – 3.28 (m, 1H), 3.04 – 2.84 (m, 3H), 2.59 – 2.36 (m, 3H), 1.79 (hept, *J* = 3.8 Hz, 1H), 1.72 – 1.53 (m, 5H), 1.20 – 1.09 (m, 4H), 1.04 (d, *J* = 6.1 Hz, 3H), 0.95 (q, *J* = 10.6, 9.1 Hz, 1H). ^{13}C-NMR (101 MHz, CDCl3) δ 166.56, 147.66, 132.13, 128.60, 125.65, 121.20, 113.34, 109.82, 103.03, 71.23, 70.74, 70.65, 70.58, 70.49, 68.95, 61.76, 56.21, 55.52, 55.39, 53.53, 51.88, 40.03, 30.73, 30.39, 26.42, 25.82, 15.74. LCMS (10-90%): t_r = 6.87 min, 610.0 m/z. HRMS $[C_{30}H_{46}BrN_3O_5+H]^+$: 608.26208 calculated, 608.26922 found.

(*S*)-(11-(4-(1-(Cyclohexylmethyl)-7-methoxy-1H-indole-3-carbonyl)-2-methylpiperazin-1-yl)undecyl)triphenylphosphonium TFA-salt (1): A stirred mixture of **15** (62.8 mg, 0.10 mmol, 1 eq) and PPh_3 (27.3 mg, 0.10 mmol, 1eq) in ACN (2.5 mL) was heated (85 °C) for 96 h. The crude product was purified with preparative HPLC to yield a white solid (37.5 mg, 0.05 mmol, 46%). ^{1}H-NMR (300 MHz, MeOD) δ 7.95 – 7.82 (m, 3H), 7.86 – 7.68 (m, 12H), 7.55 (s, 1H), 7.27 (d, *J* = 8.0 Hz, 1H), 7.10 (t, *J* = 7.9 Hz, 1H), 6.76 (d, *J* = 7.9 Hz, 1H), 4.47 (s, 2H), 4.26 (d, *J* = 7.0 Hz, 2H), 3.95 (s, 3H), 3.46 – 3.32 (m, 3H), 3.11 (t, *J* = 8.4 Hz, 2H), 1.83 (hept, *J* = 3.5 Hz, 1H), 1.75 – 1.59 (m, 6H), 1.60 – 1.46 (m, 4H), 1.36 (s, 11H), 1.29 (s, 10H), 1.19 (t, *J* = 7.0 Hz, 2H), 1.03 (q, *J* = 11.6 Hz, 2H). ^{13}C-NMR (75 MHz, MeOD) δ 169.29, 149.22, 136.29, 136.25, 134.84, 134.71, 131.59, 131.43, 129.99, 123.17, 120.56, 119.41, 113.84, 108.46, 104.82, 57.03, 55.95, 54.00, 41.35, 31.76, 31.58, 31.55, 30.46, 30.43, 30.41, 30.19, 29.94, 27.60, 27.47, 26.90, 23.59, 23.54, 23.00, 22.32. LCMS (10-90%): t_r = 7.40 min, 784.6 m/z. HRMS $[C_{51}H_{67}N_3O_2P]^+$: 784.49654 calculated, 784.49600 found.

(*S*)-(11-(4-(1-(Cyclohexylmethyl)-7-methoxy-1*H*-indole-3-carbonyl)-2-methylpiperazin-1-yl)undecyl)tris(4-(trifluoromethyl)phenyl)phosphonium TFA-salt (2): A stirred mixture of **15** (103.0 mg, 0.13 mmol, 1 eq) and tris(4-trifluoromethylphenyl)phosphine (186.0 mg, 0.40 mmol, 3eq) in ACN (0.5 mL) was heated (85 °C) for 96 h. The mixture was transferred to the microwave and heated (180 °C) for an additional 4 h. The crude product was purified with preparative HPLC to yield a white solid (39.2 mg, 0.04 mmol, 31%). ^{1}H-NMR (400 MHz, MeOD) δ 8.13 – 8.04 (m, 12H), 7.55 (s, 1H), 7.26 (d, *J* = 8.0 Hz, 1H), 7.10 (t, *J* = 7.9 Hz, 1H), 6.77 (d, *J* = 7.0 Hz, 1H), 4.48 (bs, 2H), 4.26 (d, *J* = 7.1 Hz, 2H), 3.95 (s, 3H), 3.68 – 3.56 (m, 4H), 3.41 (s, 1H), 3.16 – 3.03 (m, 2H), 1.83 (hept, *J* = 3.7 Hz, 1H), 1.75 – 1.63 (m, 6H), 1.63 – 1.52 (m, 4H), 1.43 – 1.25 (m, 19H), 1.20 (t, *J* = 5.8 Hz, 2H), 1.03 (q, *J* = 10.5 Hz, 2H). ^{13}C-NMR (101 MHz, MeOD) δ 170.69, 149.22, 137.76 (dd, *J* = 33.3, 3.2 Hz), 136.18 (d, J = 10.8 Hz), 134.40, 129.99, 128.44 (dq, *J* = 13.1, 3.8 Hz), 127.22, 125.90 (d, *J* = 1.4 Hz), 123.57 (d, *J* = 85.0 Hz), 123.18, 113.83, 108.44, 104.80, 60.62, 57.05, 55.93, 54.29, 52.03, 51.56, 47.34, 41.35, 31.78, 31.59, 30.49, 30.46, 30.22, 29.87, 27.61, 27.47, 26.91, 23.36, 23.32, 22.28, 21.80, 14.68. LCMS (10-90%): t_r = 8.10 min, 988.5 m/z. HRMS $[C_{54}H_{64}F_9N_3O_2P]^+$: 988.45870 calculated, 988.45810 found.

(*S*)-(2-(2-(2-(2-(4-(1-(Cyclohexylmethyl)-7-methoxy-1*H*-indole-3-carbonyl)-2-methylpiperazin-1-yl)ethoxy)ethoxy)ethoxy)ethyl)triphenylphosphonium TFA-salt (3): A stirred mixture of **16** (24.0 mg, 0.04 mmol, 1 eq) and PPh_3 (33.0 mg, 0.12 mmol, 3 eq) in ACN (0.5 mL) was heated (85 °C) for 96 h. The mixture was transferred to the microwave and heated (180 °C) for an additional 2 h. The crude product was purified with preparative HPLC to yield a white solid (8.9 mg, 0.01 mmol, 28%). ^{1}H-NMR (400 MHz, MeOD) δ 7.90 – 7.75 (m, 9H), 7.76 – 7.67 (m, 6H), 7.55 (s, 1H), 7.26 (d, *J* = 8.0 Hz, 1H), 7.09 (t, *J* = 8.0 Hz, 1H), 6.77 (d, *J* = 7.6 Hz, 1H), 4.26 (d, *J* = 7.1 Hz, 2H), 3.95 (s, 3H), 3.84 (d, *J* = 3.3 Hz, 2H), 3.83 – 3.76 (m, 2H), 3.77 – 3.68 (m, 5H), 3.62 – 3.56 (m, 3H), 3.49 – 3.42 (m, 3H), 3.39 – 3.30 (m, 8H), 1.82 (hept, *J* = 3.6 Hz, 1H), 1.74 – 1.63 (m, 2H), 1.55 (d, *J* = 11.8 Hz, 2H), 1.37 (s, 2H), 1.18 (t, *J* = 8.9 Hz, 3H), 1.10 (s, 3H), 1.03 (q, *J* = 11.8 Hz, 1H). ^{13}C-NMR (101 MHz, MeOD) δ 168.40, 149.25, 136.09, 136.06, 135.09 (d, *J* = 10.3 Hz), 131.23 (d, *J* = 12.8 Hz), 129.99, 127.23, 123.24, 120.85, 119.98, 113.83, 104.84, 71.56, 71.34, 71.17, 71.08, 64.79, 64.72, 57.06, 55.97, 41.37, 31.59, 27.47, 26.92, 26.67. LCMS (10-90%): t_r = 6.60 min, 790.4 m/z. HRMS $[C_{48}H_{61}N_3O_5P]^+$: 790.43434 calculated, 790.43427 found.

(*S*)-(2-(2-(2-(2-(4-(1-(Cyclohexylmethyl)-7-methoxy-1*H*-indole-3-carbonyl)-2-methylpiperazin-1-yl)ethoxy)ethoxy)ethoxy)ethyl)tris(4-(trifluoromethyl)phenyl)phosphonium TFA-salt (4): A stirred mixture of **16** (24.0mg, 0.04 mmol, 1 eq) and tris(4-trifluoromethylphenyl)phosphine (114.0mg, 0.24mmol, 6 eq) in ACN (0.5 mL) was heated (85 °C) for 96 h. The mixture was transferred to the microwave and heated (120 °C) for an additional 14 h. The crude product was purified with preparative HPLC to yield a white solid (3.2mg, 3.0 µmol, 8%). ^{1}H-NMR (850 MHz, MeOD) δ 8.14 – 8.03 (m, 12H), 7.54 (s, 1H), 7.25 (d, *J* = 8.0 Hz, 1H), 7.09 (t, *J* = 7.9 Hz, 1H), 6.77 (d, *J* = 7.7 Hz, 1H), 4.43 (br, 1H), 4.26 (d, *J* = 7.1 Hz, 2H), 4.03 – 3.98 (m, 2H), 3.95 (s, 3H), 3.87 – 3.79 (m, 4H), 3.65 (m, 2H), 3.60 – 3.56 (m, 2H), 3.48 (m, 1H), 3.44 – 3.41 (m, 2H), 3.37 – 3.33 (m, 5H), 1.82 (m, 1H), 1.70-1.65 (m, 3H), 1.54 (m, 2H), 1.37 (m, 3H), 1.31 (m, 3H), 1.19 (m, 3H), 1.10 (s, 1H), 1.03 (m, 2H). ^{13}C-NMR (214 MHz, MeOD) δ 163.08, 149.27, 137.51 (qd, *J* = 32.8, 32.3, 2.8 Hz), 136.40 (d, *J* = 11.2 Hz), 134.32, 130.00, 128.12 (dd, *J* = 13.4, 3.6 Hz), 127.26, 124.40, 123.99, 123.22, 113.80, 108.45, 104.86, 71.63, 71.31, 71.05, 71.03, 64.43, 64.39, 57.06, 55.96, 55.95, 49.38, 47.93, 36.95, 31.59, 27.46, 26.90, 24.92, 24.68, 9.20. LCMS (10-90%): t_r = 9.45 min, 994.4 m/z. HRMS $[C_{51}H_{58}F_9N_3O_5P]^+$: 994.39649 calculated, 994.39586 found.

Biology

All biologic assays have been previously described. “General remarks”, “Quantification and statistical analysis”, “Cell culture”, “Membrane preparation”, “[^{3}H]CP-55,940 Heterologous Displacement Assays” and “[^{35}S]GTPγS Binding Assays” can be referenced in **Chapter 2.**

References

1. Matsuda LA, Lolait SJ, Brownstein MJ, Young AC, Bonner TI. Structure of a cannabinoid receptor and functional expression of the cloned cDNA. *Nature*. 1990;346(6284):561-564. doi:10.1038/346561a0

2. Katona I, Freund TF. Multiple functions of endocannabinoid signaling in the brain. *Annu Rev Neurosci*. 2012;35:529-558. doi:10.1146/annurev-neuro-062111-150420

3. Castillo PE, Younts TJ, Chávez AE, Hashimotodani Y. Endocannabinoid Signaling and Synaptic Function. *Neuron*. 2012;76(1):70-81. doi:10.1016/j.neuron.2012.09.020

4. Mechoulam R, Parker LA. The endocannabinoid system and the brain. *Annu Rev Psychol*. 2013;64:21-47. doi:10.1146/annurev-psych-113011-143739

5. Kendall DA, Yudowski GA. Cannabinoid Receptors in the Central Nervous System: Their Signaling and Roles in Disease. *Front Cell Neurosci*. 2017;10. doi:10.3389/fncel.2016.00294

6. Pérez-Olives C, Rivas-Santisteban R, Lillo J, Navarro G, Franco R. Recent Advances in the Potential of Cannabinoids for Neuroprotection in Alzheimer's, Parkinson's, and Huntington's Diseases. *Adv Exp Med Biol*. 2021;1264:81-92. doi:10.1007/978-3-030-57369-0_6

7. Melis M. *Endocannabinoids and Lipid Mediators in Brain Functions*. (Melis M, ed.). Cham: Springer International Publishing; 2017. doi:10.1007/978-3-319-57371-7

8. Schurr A, Livne A. Differential inhibition of mitochondrial monoamine oxidase from brain by hashish components. *Biochem Pharmacol*. 1976;25(10):1201-1203. doi:10.1016/0006-2952(76)90369-5

9. Chari-Bitron A, Bino T. Effect of Δ l-tetrahydrocannabinol on ATPase activity of rat liver mitochondria. *Biochem Pharmacol*. 1971;20(2):473-475. doi:10.1016/0006-2952(71)90084-0

10. Sarafian TA, Kouyoumjian S, Khoshaghideh F, Tashkin DP, Roth MD. Δ 9 -Tetrahydrocannabinol disrupts mitochondrial function and cell energetics. *Am J Physiol Cell Mol Physiol*. 2003;284(2):L298-L306. doi:10.1152/ajplung.00157.2002

11. Cohen G, Kesler N. Monoamine oxidase and mitochondrial respiration. *J Neurochem*. 1999;73(6):2310-2315. doi:10.1046/j.1471-4159.1999.0732310.x

12. Shih JC, Chen K, Ridd MJ. MONOAMINE OXIDASE: From Genes to Behavior. *Annu Rev Neurosci*. 1999;22(1):197-217. doi:10.1146/annurev.neuro.22.1.197

13. Fišar Z, Singh N, Hroudová J. Cannabinoid-induced changes in respiration of brain mitochondria. *Toxicol Lett*. 2014;231(1):62-71. doi:10.1016/j.toxlet.2014.09.002

14. Bénard G, Massa F, Puente N, et al. Mitochondrial CB 1 receptors regulate neuronal energy metabolism. *Nat Neurosci*. 2012;15(4):558-564. doi:10.1038/nn.3053

15. Aquila S, Guido C, Santoro A, et al. Rimonabant (SR141716) induces metabolism and acquisition of fertilizing ability in human sperm. *Br J Pharmacol*. 2010;159(4):831-841. doi:10.1111/j.1476-5381.2009.00570.x

16. Arrabal S, Lucena MA, Canduela MJ, et al. Pharmacological Blockade of Cannabinoid CB1 Receptors in Diet-Induced Obesity Regulates Mitochondrial Dihydrolipoamide Dehydrogenase in Muscle. Appanna VD, ed. *PLoS One*. 2015;10(12):e0145244. doi:10.1371/journal.pone.0145244

17. Serrat R, Covelo A, Kouskoff V, et al. Astroglial ER-mitochondria calcium transfer mediates endocannabinoid-dependent synaptic integration. *Cell Rep*. 2021;37(12):110133. doi:10.1016/j.celrep.2021.110133

18. Koch M, Varela L, Kim JG, et al. Hypothalamic POMC neurons promote cannabinoid-induced feeding. *Nature*. 2015;519(7541):45-50. doi:10.1038/nature14260

19. Hebert-Chatelain E, Desprez T, Serrat R, et al. A cannabinoid link between mitochondria and memory. *Nature*. 2016;539(7630):555-559. doi:10.1038/nature20127

20. Yin A, Wang F, Zhang X. Integrating endocannabinoid signaling in the regulation of anxiety and depression. *Acta Pharmacol Sin*. 2019;40(3):336-341. doi:10.1038/s41401-018-0051-5

21. Djeungoue-Petga M-A, Hebert-Chatelain E. Linking Mitochondria and Synaptic Transmission: The CB1 Receptor. *BioEssays*. 2017;39(12):1700126. doi:10.1002/bies.201700126

22. Pankratov Y V., Lalo U V., Krishtal OA. Role for P2X Receptors in Long-Term Potentiation. *J Neurosci*. 2002;22(19):8363-8369. doi:10.1523/JNEUROSCI.22-19-08363.2002

23. Jiménez-Uribe AP, Pedraza-Chaverri J. Promising Therapeutic Strategies Targeting Mitochondria in Kidney Diseases: From Small Molecules to Whole Mitochondria. *Futur Pharmacol*. 2022;2(3):256-275. doi:10.3390/futurepharmacol2030017

24. Ross MF, Kelso GF, Blaikie FH, et al. Lipophilic triphenylphosphonium cations as tools in mitochondrial bioenergetics and free radical biology. *Biochem*. 2005;70(2):222-230. doi:10.1007/s10541-005-0104-5

25. Murphy MP, Smith RAJ. Targeting Antioxidants to Mitochondria by Conjugation to Lipophilic Cations. *Annu Rev Pharmacol Toxicol*. 2007;47(1):629-656. doi:10.1146/annurev.pharmtox.47.120505.105110

26. Kulkarni CA, Fink BD, Gibbs BE, et al. A Novel Triphenylphosphonium Carrier to Target Mitochondria without Uncoupling Oxidative Phosphorylation. *J Med Chem*. 2021;64(1):662-676. doi:10.1021/acs.jmedchem.0c01671

27. Adam JM, Cairns J, Caulfield W, et al. Design, synthesis, and structure–activity relationships of indole-3-carboxamides as novel water soluble cannabinoid CB1 receptor agonists. *Medchemcomm*. 2010;1(1):54. doi:10.1039/c0md00022a

28. Kevin RC, Mirlohi S, Manning JJ, et al. Putative Synthetic Cannabinoids MEPIRAPIM, 5F-BEPIRAPIM (NNL-2), and Their Analogues Are T-Type Calcium Channel (Ca V 3) Inhibitors. *ACS Chem Neurosci*. 2022;13(9):1395-1409. doi:10.1021/acschemneuro.1c00822

29. Zuurman L, Passier P, de Kam M, Kleijn H, Cohen A, van Gerven J. Pharmacodynamic and pharmacokinetic effects of the intravenously administered CB1 receptor agonist Org 28611 in healthy male volunteers. *J Psychopharmacol*. 2009;23(6):633-644. doi:10.1177/0269881108091551

30. Kondo Y, Kojima S, Sakamoto T. General and Facile Synthesis of Indoles with Oxygen-Bearing Substituents at the Benzene Moiety. *J Org Chem*. 1997;62(19):6507-6511. doi:10.1021/jo970377w

31. Thakur G, Nikas S, Makriyannis A. CB1 Cannabinoid Receptor Ligands. *Mini-Reviews Med Chem*. 2005;5(7):631-640. doi:10.2174/1389557054368772

Acknowledgements

This work was supported by the Dutch Research Council (NWO, Navistroke #15851) (Mario van der Stelt[d], M.v.d.S.).

Author contributions: Conducting Experiments, L.d.B (Lorenzo de Bie), L.V.d.P. (Laura V. de Paus); Writing-Original Draft, L.V.d.P.; Writing Review & Editing, M.v.d.S., L.H.H. (Laura H. Heitman), R.J.B.H.N.v.d.B (Richard J. B. H. N. van den Berg); Supervision, R.J.B.H.N.v.d.B., M.v.d.S.

Chapter 6

Discussion & Future Prospects

Discussion & Future Prospects

The use of *Cannabis sativa* reaches as far back as 2700 B.C. when it's use as a therapeutical drug was discovered by Emperor Sheng Nun[1–5] and later written down in his pharmacopoeia.[1] The *Cannabis* preparations were prescribed a wide array of uses, including for arthritis, enhancement of appetite, depression, inflammation, pain[3], disorders of the female reproductive system, constipation and more.[1] Δ^9-tetrahydrocannabinol (THC) was discovered as the main psychoactive ingredient in *cannabis sativa* in 1942, though it's structure wasn't elucidated until 1964[6]. THC has since been approved for use against chemotherapy-induced nausea[7], enhancement of appetite in AIDS-patients and treatment of symptoms of multiple sclerosis patients[6,8]. CB_1R and CB_2R are the main receptors that bind THC, and over the last several decades research has been devoted to understanding their role in pathologies and developing improved therapeutics for many different diseases. Nonetheless, our understanding of the molecular mode-of-action CBRs is still limited. Information about cellular expression and distribution dynamics; target engagement and the activation mechanism is required to aid in therapeutic development. To this end novel chemical tools are required to investigate these properties of the cannabinoid receptors.

This thesis describes the development of several chemical tools for the study of CB_2R to further understand how the CB_2 receptor accomplices its effect and how selectivity over CB_1R can be retained when designing new ligands (**Chapter 2**-**4**). In the last chapter a new method to avoid the psychoactive effects of CB_1R engagement is proposed by selectively targeting a specific subset of the CB_1 receptors (**Chapter 5**).

The selectivity of ligands

Three-dimensional protein structures may reveal information on the mechanics of the protein, how they malfunction in disease and how to optimally target them with drugs. Despite the advances in modelling software, any *in silico* data generated should be validated with mutational data.[9] Furthermore, design of new therapeutics may benefit from information about the binding mode.

CB_2R agonists are being investigated as therapeutic agents in the clinic. However, their molecular mode-of-action is not fully understood. **Chapter 2** describes the discovery of LEI-102, a CB_2R agonist, used in conjunction with three other CBR ligands (APD371, HU308, and CP-55,940) to investigate the selective CB_2R activation by investigating their binding kinetics, and employing site-directed mutagenesis and cryo-EM studies. During this study it was found that the amino acid $V261^{5.61}$ in CB_2R (CB_2R-$V261^{5.61}$) and its extracellular loop 2 (ECL2) played an important role in selectivity. Furthermore, CB_2R-$F117^{3.36}$ has a role in receptor activation quite unlike the activity suppression role of CB_1R-$F200^{3.36}$. A quadruple mutation in TM1 and TM7 showed that highly lipophilic HU308 and the endocannabinoids, but not the more polar LEI-102, APD371, and CP-55,940, reach the binding pocket through a membrane channel in TM1-TM7.

In **Chapter 2** the molecular origin of signalling bias was not investigated, as the cryoEM structures were obtained in presence of a G protein only. However, it might be the case that different CB_2R agonists lead to different cellular responses depending on their ability to activate β-arrestin and/or G protein pathways.[10] Biased therapeutics that focus on only one of the two pathways may decrease on-target adverse effects. Three-dimensional ligand-receptor models combined with pharmacological data about functional activity could help in determining what drives signalling bias in order to design new drugs with bias in mind. To evaluate the viability of biased therapeutics further research is required. Among others, the bias of existing drugs should be mapped against their therapeutic uses and side effects. For

example, it was found that G protein-biased JWH133 exhibited prolonged analgesic effects in rodent mono-iodoacetate models, while the analgesic efficacy of β-arrestin biased GW833972A was hampered by rapid internalization of the CB_2 receptor.[11] Thus a biased CB_2R agonist with minimal β-arrestin could have potential as a longer-lasting analgesic. More generally, the determined bias of new drugs could help determine the appropriate use and possibly decrease detrimental side effects.

Development of a toolset for the research on the CB_2 receptor

The CB_2R has therapeutic potential for the treatment of inflammatory disorders. Small molecule probes are desirable to study the pharmacodynamics of the CB_2R. Two-step probes do not yet contain a reporter tag. Only after engagement with the target an *in situ* reaction is used to attach a reporter tag. This allows for smaller probes that are less lipophilic, have improved cell-permeability, higher binding affinity and less non-specific binding than ready-use probes. Furthermore, a diverse selection of reporter tags allows use over a wide array of assays. **Chapter 3** describes the structure-based design of several bifunctional probes based on photoaffinity probe LEI-121. While LEI-121 captures the inactive conformation of CB_2R, one of the new probes captures the active conformation of CB_2R upon irradiation with light. They exhibited good CB_2R affinity, selectivity over CB_1R and could successfully label the receptor in a gel-based ABPP assay. Compound **1** (Figure 6.1) was a partial agonist with good potency (pEC_{50} = 8.56 ± 0.56), while compound **2** (Figure 6.1) was the inverse agonist with the highest potency (pEC_{50} = 7.75 ± 0.19). The two different probes revealed different band patterns in gel-based ABPP, capturing the different states of CB_2R.

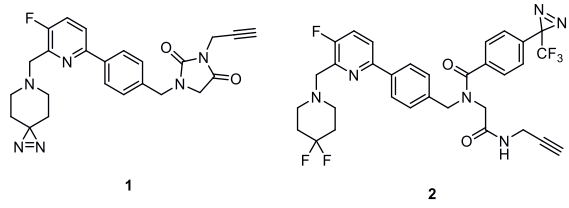

Figure 6.1 The chemical structures of partial CB_2R agonist **1** (nr. **2** in chapter 3) and inverse CB_2R agonist **2** (nr. **3** in chapter 3) from **Chapter 3**.

The covalent probes in **Chapter 3** have a photoreactive that can be activated by UV light. This diminishes off-target activity compared to normal warheads such as Michael acceptors; and the small size of the diazirine minimally affects potency of the compound. The bifunctional, photoreactive probe provides new options for studying proteins, such as with electrophoresis and proteomics.[12] In combination with an alkyne group to introduce different tags to the probe, a multi-purpose probe was created. A fluorophore can be used for visualization, biotin or similar for protein enrichment[13], or even radio-tags for radiopharmacology.[14] The efficacy of the probe should be evaluated over the different applications including electrophoreses, ABPP and flow cytometry, to determine the reach of this new two-step photoaffinity probe.[15]

While two-step probes can be applied over many different applications, they are incompatible with assays that require immediate read-out, or do not tolerate the copper-click conditions required to attach a recognizable tag. One-step probes are particularly useful for live-imaging.[16] Thus a complete toolbox to research CB_2R includes more than one probe to cover a plethora of applications and receptor states of activity. Fluorescent probes enable the detection of CB_2R in relevant cell types and serve as a chemical tool in cellular target engagement studies. In **Chapter 4**, the structure-based design and synthesis of a new CB_2R selective fluorescent probe was reported. Based on the cryo-EM structure of LEI-102 in complex with the CB_2R, 5-fluoropyridin-2-yl-benzyl-imidazolidine-2,4-dione analogues were synthesized in which a variety of linkers and fluorophores were introduced. Molecular pharmacological

characterization showed that probe **3** (Figure 6.2) containing a Cy5-fluorophore with an alkyl-spacer was the most potent probe with a pK_i of 6.2 ± 0.6. It was selective over the CB_1R and behaved as an inverse agonist (EC_{50} 5.3 ± 0.1, E_{max} -63% ± 6). Probe **3** may serve as a chemical tool in target and lead validation studies for the CB_2R, and its capability to selectively image CB_2R *in situ* should be evaluated next.

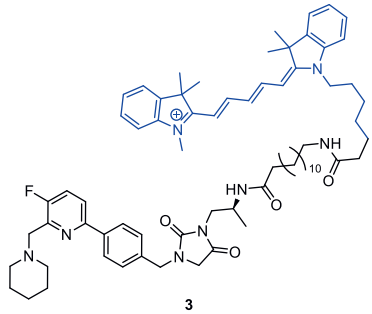

3
pK_i = 6.2 ± 0.6
pEC_{50} = 5.3 ± 0.1

Figure 6.2 The chemical structure of one-step probe **3** (nr. **22** in chapter 4) from **Chapter 4**.

An alternative approach to avoid CB_1R psychoactive effects

Recent developments have shown distinct roles for plasma and mitochondrial CB_1R receptors.[17,18] This could have a profound impact on future therapeutic application of cannabinoids, as several diseases have been linked to dysfunction of just one CB_1R subset.[19,20] For example, congestive heart failure, cardiac ischemic reperfusion injury, diabetes, Alzheimer's and Parkinson's have been linked to dysfunctional mitochondria and changes in OXPHOS respiration.[21] Specific targeting of either plasmalemmal (pl)CB_1R or $mtCB_1R$ may diminish side-effects resulting from activation of the other subgroup. For example, the rewarding feature of Δ^9-THC is a result of disinhibition of dopamine neurons as a result of decreased GABA release.[22] It was recently shown that depolarization-induced suppression of inhibition (DSI) is mediated by $mtCB_1R$, as cell permeable HU210 was able to completely occlude DSI, while HU-biotin only partially occluded DSI.[23] While neither $plCB_1R$ nor $mtCB_1R$ is solely responsible for GABA release inhibition, the rewarding effect on dopamine neurons may be weakened when one subgroup is excluded.

Currently the role of mitochondrial CB_1R ($mtCB_1R$) is determined by comparing effects when inhibiting the CB_1R activity with either a cell- permeable or impermeable antagonist[18], since a $mtCB_1R$ selective agonist is not available. This indirect method relies on absence of activity rather than directly showing effect of activity. A $mtCB_1R$-selective agonist would simplify $mtCB_1R$ role validation by yielding less convoluted results. Additionally, a selective $mtCB_1R$ therapeutic agent could be a possibility to limit undesired side-effects; *i.e.* there would be no $plCB_1R$ activation to dysregulate healthy systems when the pathology only affects $mtCB_1R$ dependent systems. (That is, if such a separation between $plCB_1R$ and $mtCB_1R$ really does exist.) **Chapter 5** described the design and synthesis of several compounds to specifically target $mtCB_1R$. The cationic phosphonium group directs the compound to the negative potential of the mitochondrial membrane.[24,25] CB_1R agonist **4** (Figure 6.3) was designed based on the ORG28611 scaffold with a polyglycerol spacer and tris(4-trifluormethyl)phenyl phosphonium ($TFTPP^+$). Compound **4** showed moderate potency (pEC_{50} = 5.70 ± 0.20) on CB_1R as a partial agonist, and despite affinity for CB_2R did not show significant G protein activity. The $TFTPP^+$ diminished OXPHOS interference compared to TPP^+ while the glycol spacer retained the partial agonist behaviour.

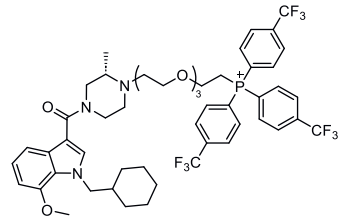

4
pEC_{50} = 5.70 ± 0.20

Figure 6.3 Compound **4** (nr. **4** in chapter 5) from **Chapter 5.**

While compound **4** had moderate activity on CB_1R, it showed a 40-fold decrease in affinity compared to parent structure ORG28611. Adjustments must be made in the structure to diminish the loss of affinity from the $TFTPP^+$ introduction. Only then can the compounds preference for $mtCB_1R$ over $plCB_1R$ be explored. The next step will require an adaptation of previously utilized *in situ* assays. A membrane impermeable antagonist could be used to compete with the agonist compound to determine the origin of its CB_1R activity.[23,26] As an alternative CB_1R activity could be compared in cells with either wild type or mutant DN22-CB_1R (the 22 amino acid deletion limits mitochondrial distribution of the CB_1R).[27] $MtCB_1R$ research is still in its budding stages and much is as of yet unknown.[28–30] However, if future endeavours reveal that there is indeed a distinction between the roles of $plCB_1R$ and $mtCB_1R$, perhaps organelle-specific therapeutics could be a new drug targeting concept.

Manipulating the functional behaviour of ligands

A change in internal efficacy was seen in several chapters after a modification of the parent chemical structure. In **Chapter 3** ring-opening of the imidazolidine in LEI-102 led to a new side chain in the photoaffinity probes that changed efficacy from partial agonist to inverse agonist in a functional [^{35}S]GTPγS assay at CB_2R. Then in **Chapter 4** showed introduction of the lipophilic spacer, but not the hydrophilic polyglycol spacer, changed intrinsic efficacy of the CB_2R partial agonist to inverse agonist. A similar trend was seen with the spacers from the CB_1R agonists in **Chapter 5**, albeit their affinity was low. Despite the large amount of research on the CB receptors, the molecular understanding how ligands assert different intrinsic efficacies is still lacking. In the basic two-state drug receptor interaction model it is assumed there is an equilibrium of the receptor between an active state and quiescent (inactive) state. Agonists stabilize the active state, leading to increased activity, while inverse agonists stabilize the quiescent state and thus decrease activity.[31] However, what interactions make a ligand prefer one state or the other? The recurring observation in **Chapters 3**-**5** is that intrinsic efficacy of a compound can switch by a lipophilic addition. If the newly created protein-ligand interactions can be mapped with for example in cryo-EM structures, perhaps one of the key interactions for (inverse) agonism can be identified. With a molecular understanding of the mechanism for intrinsic efficacy, the design of new ligands could be guided towards a desired functional effect. Additionally, while the type of efficacy is not always relevant for probes, antagonists and inverse agonists have the advantage that they do not affect receptor internalization like agonists do.[10,32,33]

Reducing Off-target Toxicity through Targeted Delivery of Prodrugs

Off-target toxicity and localization are two of the largest bottlenecks in drug discovery. Off-target toxicity may occur when high doses are required to obtain sufficient concentrations at the target location. New research is rekindling a 40 year old idea: High-Density Lipid (HDL) particles can be used to create localized concentration spots.[34] HDL particles occur naturally in the body to transport excess cholesterol to the liver. They are ideal for transport of lipophilic compounds, including drugs, in a stabilizing, biocompatible environment.[35] When an HDL particle arrives at the target destination, it

releases its payload intracellularly by fusing with the plasma membrane. Thereby, an HDL particle can increase a drugs half-life, increase its absorption and facilitate improved targeting depending on lipid composition.[36]

The wide distribution of CB_2R and role in many systems make it both a promising therapeutic target. However, translation to the clinic has proven difficult, with many candidates showing no efficacy. By locally restricting the distribution of ligand the effective concentration of ligand is improved and the therapeutic window is widened by avoiding any potential site that induces side-effects (including off-targets such as CB_1R when not selective enough). For example, CB_2R regulates macrophage differentiation and HDL particles that can specifically target myeloid cells could be useful for drug delivery.[37,38]

Acyloxymethyl Prodrug 5

For this reason the design of LEI-102 was altered to facilitate incorporation of the compound in HDL particles. This requires a lipophilic prodrug that can be incorporated in the lipid formulation of the HDL particle. LEI-102 contains a secondary nitrogen; however, prodrug **5** (Figure 6.4) was designed with a primary alcohol to accommodate a C_{16} alkyl chain in case the secondary nitrogen proved too sterically hindered. With the replacement of isobutyl from LEI-102 with 2-methylpropanol and introduction of the C_{16} alkyl chain the cLogP would increase from 3.3 (LEI-102) to 8.8 (**5**, Chemdraw22). *In vivo* the ester bond should hydrolyse to release compound **10** (Scheme 6.1).

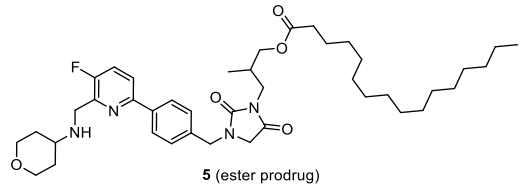

5 (ester prodrug)

Figure 6.4 The Design of the LEI-102-based prodrug **5** where the isobutyl is replaced by 2-methylpropanol to accommodate a C_{16} alkyl chain.

The synthesis of compound **10** (Scheme 6.1) closely followed the synthesis of LEI-102 (Chapter 2). In the first steps 2-methylpropane-1,3-diol was monoprotected with a TBDPS group (**6**) followed by tosylation of the remaining alcohol to give **7**. Next, **7** was coupled with 1-(4-bromobenzyl)imidazolidine-2,4-dione (Chapter 2) to give **8**, which after borylation was directly linked to *N*-((6-bromo-3-fluoropyridin-2-yl)methyl)tetrahydro-2*H*-pyran-4-amine (Chapter 2) to gain **9**. Deprotection with TBAF in the last step led to compound **10** for evaluation of the hydrolysis product.

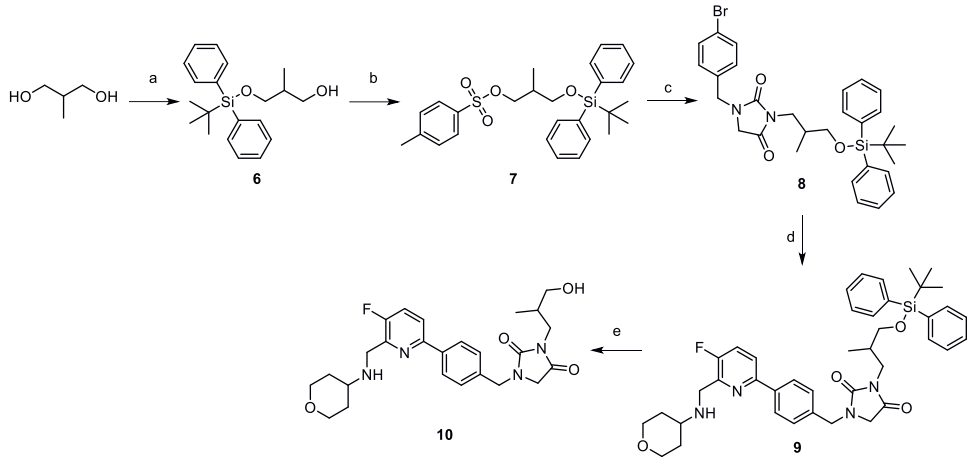

Scheme 6.1 The synthesis of the prodrug precursor. Reagents and conditions: a) *tert*-butylchlorodiphenylsilane, NaH, THF, RT, 24 h, 63%; b) 4-methylbenzenesulfonyl chloride, pyridine, DCM, RT, 144 h, 88%; c) 1-(4-bromobenzyl)imidazolidine-2,4-dione, K_2CO_3, 18-crown-6, DMF, 60 °C, 21 h, 84%; d) i) bis(pinacolato)diboron, Pd(dppf)Cl_2, KOAc, DMF, 75 °C, 23 h, ii) *N*-((6-bromo-3-fluoropyridin-2-yl)methyl)tetrahydro-2*H*-pyran-4-amine, Pd(PPh_3)$_4$, K_2CO_3, toluene:EtOH 4:1 (v/v), 75 °C, 19 h, 34% (two steps); e) TBAF (1 M in THF), RT, 2 h, 23%.

After the synthesis of compound **10**, it was evaluated for affinity (pK_i) on CB_2R in a [^{3}H]CP-55,940 radioligand displacement assay on membranes derived from CHO cells overexpressing hCB_2R_bgal, and compared to the parent compound LEI-102. The results are shown in Figure 6.5B-C.

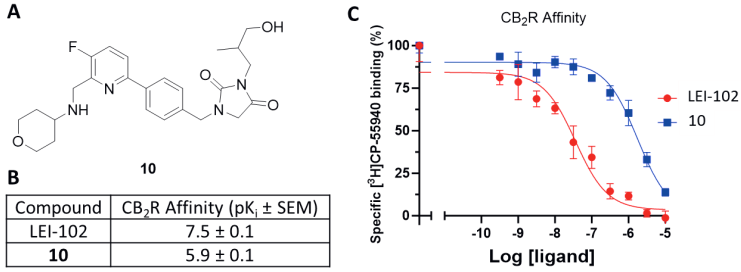

Compound	CB_2R Affinity (pK_i ± SEM)
LEI-102	7.5 ± 0.1
10	5.9 ± 0.1

Figure 6.5 (A) The chemical structure of compound **10**. (B) The affinity (pK_i) of compound **10** compared to LEI-102 determined with a [^{3}H]CP-55,940 radioligand displacement assay on CHO-K1 CB_2R_bgal membranes. (C) Same data displayed as displacement curve data. Binding was normalized to binding of [^{3}H]CP-55,940 at 10 µM. Data are presented as the mean ± SEM from one independent experiment performed in triplicate.

While compound **10** (pK_i 5.9 ± 0.1) shows a decrease in affinity compared to LEI-102, it is still moderately active on CB_2R.

Acyloxyethyloxycarbonyl prodrug 12

As it was observed during synthesis of compound **10** that the secondary nitrogen is sufficiently reactive, an alternative prodrug was designed where a C_{14} alkyl chain was introduced through an acyloxyethyloxycarbonyl (**12**, Scheme 6.2). The resulting prodrug has a high cLogP 9.4 (Chemdraw22) and would hydrolyse *in vivo* to LEI-102.[39] The synthesis of **12** is shown in Scheme 6.2.

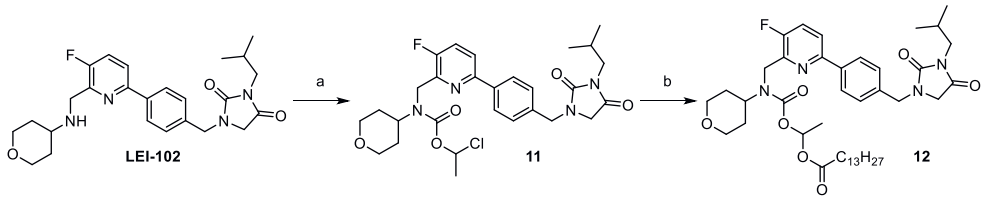

Scheme 6.2 The synthesis of the acyloxyethyloxycarbonyl prodrug of LEI-102 **8**. Reagents and Conditions: a) chloroethylchroloformate, Et_3N, DCM, RT, 2 h, 96%; b) myristic acid, Et_3N, DCM, 100 °C (microwave), 2 h, 30%.

The synthesis of acyloxyethyloxycarbonyl prodrug **12** (Scheme 6.2) started from LEI-102, for which the synthesis is described in **Chapter 2**. Introduction of chloroethyl chloroformate led to **11** in quantitative yield. In the second step myristic acid (C_{14}) was introduced under basic conditions heated in a microwave tube to successfully give prodrug **12**.

With the synthesis complete prodrug **12** has recently been successfully incorporated in HDL particles by Eindhoven university and is currently being tested in murine stroke models to compare the efficacy of HDL-LEI-102 to LEI-102 at Utrecht University (unpublished).

Additionally prodrug **5** synthesis could be completed to compare its performance to prodrug **12**. To finish the synthesis of prodrug **5**, compound **9** should be *N*-bocylated followed by silyl deprotection with TBAF. Acylation of the alcohol can then introduce the lipophilic chain, after which the nitrogen can be deprotected to yield prodrug **5**. After successful synthesis the *in vivo* pharmacodynamics can evaluated.

Final Note

To summarize, this thesis describes the design and synthesis of several new tools that can be used in a wide array of assays to improve our understanding of CB_2R and its function in different systems. It further shows the importance of three-dimensional protein-ligand complexes in understanding selectivity, activity and bias in receptors, and the value of having a receptor-ligand structure in guiding design of new probes and drug candidates. Only when we understand the molecular mode of action of CB_2R, can we learn how to successfully translate *in vitro* activity to clinical efficacy. This could be complemented by an approach to improve pharmacodynamics, such as nanocarriers that improve drug half-life and increase local drug concentration. It is anticipated that the tools presented in this thesis can be used to aid in the endeavour to uncover more about the pharmacological roles of CB_2R and how to successfully develop therapeutic agents targeting CB_2R.

Experimental Section

Chemistry

General Remarks

All reagents and solvents were purchased from commercial sources and were of analytical grade (Sigma-Aldrich, BroadPharm®). Reagents and solvents were not further purified before use. All moisture sensitive reactions were performed under inert atmosphere. Solvents were dried using 4 Å molecular sieves prior to use when anhydrous conditions were required. Water used in reactions was always demineralized. Analytical thin-layer chromatography (TLC) was routinely performed to monitor the progression of a reaction and was conducted on Merck Silica gel 60 F254 plates. Reaction compounds on the TLC plates were visualized by UV irradiation (λ_{254}) and/or spraying with potassium permanganate solution (K_2CO_3 (40 g), $KMnO_4$ (6 g), and H_2O (600 mL)), ninhydrin solution (ninhydrin (1.5 g), *n*-butanol (100 mL) and acetic acid (3.0 mL)) or molybdenum solution ($(NH_4)_6Mo_7O_{24}{\cdot}4H_2O$ (25 g/L) and $(NH_4)_4Ce(SO_4)_4{\cdot}H_2O$ (10 g/L) in sulfuric acid (10%)) followed by heating as appropriate. Purification by

flash column chromatography was performed using Screening Devices B.V. silica gel 60 (40-63 µm, pore diameter of 60 Å). Solutions were concentrated using a Heidolph laborata W8 4000 efficient rotary evaporator with a Laboport vacuum pump. Analytical purity was determined with liquid chromatography-mass spectrometry (LC-MS) using a Finnigan LCQ Advantage MAX apparatus with electrospray ionization (ESI), equipped with a Phenomenex Gemini 3 µm NX-C18 110Å column (50x4.6mm), measuring absorbance at 254 nm using a Waters 2998 PDA UV detector and the m/z ratio by using an Acquity Single Quad (Q1) detector. Injection was with the Finnigan Surveyor Autosampler Plus and pumped through the column with the Finnigan Surveyor LC pump plus to be analysed with the Finnigan Surveyor PDA plus detector. Samples were analysed using eluent gradient 10% → 90% ACN in MilliQ water (+ 0.1% TFA (v/v)). For purification by mass guided preparative high-performance liquid chromatography (Prep-HPLC) the Waters AutoPurification HPLC/MS apparatus was used with a Gemini prep column 5 µm 18C 110 Å (150x21.2mm), Waters 2767 Sample manager, Waters 2545 Binary gradient module, Waters SFO System fluidics organizer, Waters 515 HPLC pump M, Waters 515 HPLC pump L attached to a Waters SQ detector Acquity Ultra performance LC. ^{1}H, ^{13}C, ^{1}H-COSY and HSQC Nuclear Magnetic Resonance (NMR) spectra were recorded on a Bruker AV 300 (300/75 MHz), AV 400 (400/100 MHz) or AV 500 (500/125 MHz) spectrometer at ambient temperature using $CDCl_3$ or DMSO as solvent. Chemical shifts (δ) are referenced in parts per million (ppm) with tetramethylsilane (TMS) or $CDCl_3$ resonance as the internal standard peak ($CDCl_3$/TMS, δ 0.00 for ^{1}H (TMS), δ 77.16 for ^{13}C ($CDCl_3$)). DMSO internal standard peak is ^{1}H: δ 2.50 and ^{13}C: δ 39.52. Multiplicity is reported as s = singlet, d = doublet, dd = doublet of doublet, ddd = doublet of doublet of doublet, dt = doublet of triplet, dq = doublet of quartet, t = triplet, tt = triplet of triplet, q = quartet, p = quintet, hept = heptet, oct = octet, m = multiplet. Coupling-constants (*J*) are reported in Hertz (Hz).

Synthesis of alternative LEI-102 prodrug 5

3-((*tert*-Butyldiphenylsilyl)oxy)-2-methylpropan-1-ol (6): To a cooled (0 °C) and stirred solution of NaH (0.16 g, 60% in mineral oil, 4.0 mmol, 1.2 eq) in anhydrous THF (20 mL) under inert atmosphere was added dropwise 2-methyl-1,3-propanediol (0.3 mL, 3.4 mmol, 1 eq). After 35 minutes TBDPSCl (0.9 mL, 3.5 mmol, 1 eq) was dropwise added at RT. After stirring 24 h at RT the reaction was cooled (0 °C) and quenched with H_2O (20 mL). The layers were separated and the aqueous layer was extracted twice with EtOAc. The combination of organic layers was dried ($MgSO_4$), filtered and the solvent evaporated under reduced pressure. The crude product was purified with flash column chromatography (SiO_2, 10% EtOAc in pentane) to yield a colourless oil (0.70 g, 2.1 mmol, 63%). ^{1}H-NMR (400 MHz, $CDCl_3$) 7.72 – 7.65 (m, 4H), 7.46 – 7.38 (m, 6H), 3.74 (dd, *J* = 10.0, 4.5 Hz, 1H), 3.68 (t, *J* = 5.1 Hz, 2H), 3.60 (dd, *J* = 10.0, 7.7 Hz, 1H), 2.61 (t, *J* = 5.4 Hz, 1H), 2.01 (octet, *J* = 5.8 Hz, 1H), 1.07 (s, 9H), 0.84 (d, *J* = 7.0 Hz, 3H). ^{13}C-NMR (101 MHz, CDCl3) δ 135.72, 135.70, 133.25, 129.93, 127.90, 68.90, 67.84, 37.40, 26.96, 19.27, 13.29.

3-((*tert*-Butyldiphenylsilyl)oxy)-2-methylpropyl 4-methylbenzenesulfonate (7): To a cooled (0 °C) and stirred solution of **2** (0.70 g, 2.1 mmol, 1 eq) in anhydrous DCM (15 mL) under inert atmosphere was added pyridine (1.7 mL, 21.0 mmol, 10 eq) and 4-methylbenzenesulfonyl chloride (0.92 g, 4.8 mmol, 2.3 eq) dissolved in DCM (5 mL). After stirring 144 h at RT the reaction was diluted with NH_4Cl (15 mL) and the layers separated. The aqueous layer was extracted once with DCM. The combination of organic layers was dried ($MgSO_4$), filtered and the solvent evaporated under reduced pressure. The crude product was purified with flash column chromatography (SiO_2, 10% EtOAc in pentane) to yield a colourless oil (0.91 g, 1.9 mmol, 88%). ^{1}H-NMR (500 MHz, $CDCl_3$) δ 7.79 (d, *J* = 8.3 Hz, 2H), 7.59 (dt, *J* = 8.1, 1.7 Hz, 4H), 7.43 (tt, *J* = 7.4, 2.2 Hz, 2H), 7.37 (t, *J* = 7.7 Hz, 4H), 7.31 (d, *J* = 8.0 Hz, 2H), 4.17 – 4.09 (m, 1H), 4.01 (dd, *J* = 9.3, 6.1 Hz, 1H), 3.56 (dd, *J* = 10.2, 4.8 Hz, 1H), 3.47 (dd, *J* = 10.2, 6.6 Hz, 1H), 2.42 (s, 3H), 2.00 (oct, *J* = 6.2 Hz, 1H), 0.98 (s, 9H), 0.89 (d, *J* = 6.9 Hz, 3H).^{13}C-NMR (126 MHz, $CDCl_3$) δ 144.72,

135.64, 135.62, 133.47, 133.44, 133.16, 129.92, 129.82, 128.05, 127.81, 72.23, 64.61, 60.51, 35.75, 26.87, 21.74, 19.32, 14.32, 13.41.

1-(4-Bromobenzyl)-3-(3-((*tert*-butyldiphenylsilyl)oxy)-2-methylpropyl)imidazolidine-2,4-dione (8): A stirred solution of **3** (4.10 g, 8.5 mmol, 2 eq), 1-(4-bromobenzyl)imidazolidine-2,4-dione (1.15 g, 4.3 mmol, 1 eq), K_2CO_3 (3.30 g, 23.9 mmol, 5.6 eq), and 18-crown-6 (0.09 g, 0.3 mmol, 0.1 eq) in anhydrous DMF (80 mL) under inert atmosphere was heated (60 °C) for 21 h. The solution was diluted with brine (80 mL), H_2O (40 mL) and EtOAc (300 mL) and the layers separated. The organic layer was washed twice with brine, dried ($MgSO_4$), filtered and the solvent evaporated under reduced pressure. The crude product was purified with flash column chromatography (SiO_2, 5-15% EtOAc in pentane) to yield a yellow oil (2.09 g, 3.6 mmol, 84%). ^{1}H-NMR (300 MHz, $CDCl_3$) δ 7.68 (tt, *J* = 5.7, 1.7 Hz, 4H), 7.50 – 7.32 (m, 8H), 7.10 (d, *J* = 8.4 Hz, 2H), 4.47 (d, *J* = 2.3 Hz, 2H), 3.65 (dd, *J* = 13.6, 6.7 Hz, 1H), 3.65 (s, 2H), 3.57 (d, *J* = 5.7 Hz, 2H), 3.44 (dd, *J* = 13.6, 8.0 Hz, 1H), 2.24 (oct, *J* = 6.6 Hz, 1H), 1.07 (s, 9H), 0.94 (d, *J* = 6.8 Hz, 3H). ^{13}C-NMR (75 MHz, $CDCl_3$) δ 169.80, 157.06, 135.69, 135.67, 134.64, 133.69, 133.63, 132.22, 129.83, 129.70, 129.67, 127.74, 127.71, 122.24, 66.98, 48.93, 46.13, 42.61, 34.99, 26.92, 19.34, 14.84. LCMS (ESI, 50-90): t_R = 9.91 min; m/z: 579.0 (^{79}Br) + 580.83 (^{81}Br) $[M+H]^+$.

3-(3-((*tert*-Butyldiphenylsilyl)oxy)-2-methylpropyl)-1-(4-(5-fluoro-6-(((tetrahydro-2*H*-pyran-4-yl)amino)methyl)pyridin-2-yl)benzyl)imidazolidine-2,4-dione (9): To a solution of **4** (2.50 g, 4.3 mmol, 1.6 eq) in anhydrous and degassed DMF (75 mL) was added bis(pinacolato)diboron (1.73 g, 6.8 mmol, 2.5 eq), KOAc (1.90 g, 19.4 mmol, 7.2 eq) and a spatula tip Pd(dppf)Cl_2. After heating (75 °C) for 23 h the solution was diluted with H_2O (250 mL) and EtOAc (250 mL) and the layers separated. The aqueous layer was extracted thrice with EtOAc. The combination of organic layers was washed with sat. $NaHCO_3$ (aq), H_2O, and brine, dried ($MgSO_4$), filtered and the solvent evaporated under reduced pressure. To the crude redissolved in toluene:EtOH (75 mL, 4:1, v/v) under inert atmosphere was added *N*-((6-bromo-3-fluoropyridin-2-yl)methyl)tetrahydro-2*H*-pyran-4-amine (0.79 g, 2.7 mmol, 1 eq), K_2CO_3 (2.30 g, 16.6 mmol, 6.2 eq) and a spatula tip $Pd(PPh_3)_4$. After heating (75 °C) for 19 h the mixture was cooled to RT and filtered over a Celite™ pad and diluted with H_2O (120 mL), brine (20 mL), and EtOAc (120 mL). The layers were separated and the aqueous layer was extracted thrice with EtOAc. The combination of organic layers was washed with H_2O and brine, dried ($MgSO_4$), filtered and the solvent evaporated under reduced pressure. The crude product was purified with flash column chromatography (SiO_2, 100% EtOAc) to yield a yellow oil (0.68 g, 0.96 mmol, 36%). ^{1}H-NMR (500 MHz, $CDCl_3$) δ 7.93 (dd, *J* = 8.1, 2.1 Hz, 2H), 7.66 (t, *J* = 7.5 Hz, 4H), 7.60 (d, *J* = 8.6 Hz, 1H), 7.46 – 7.33 (m, 8H), 7.32 (d, *J* = 6.2 Hz, 1H), 4.58 (s, 2H), 4.08 (s, 2H), 4.00 (d, *J* = 11.5 Hz, 2H), 3.69 (s, 2H), 3.65 (dd, *J* = 14.6, 7.6 Hz, 1H), 3.56 (d, *J* = 4.0 Hz, 2H), 3.45 (dd, *J* = 13.4, 8.2 Hz, 1H), 3.39 (t, *J* = 11.5 Hz, 2H), 2.82 – 2.74 (m, 1H), 2.24 (oct, *J* = 6.4 Hz, 1H), 1.90 (d, *J* = 12.1 Hz, 2H), 1.54 (dq, *J* = 10.4, 3.5 Hz, 2H), 1.06 (s, 9H), 0.93 (d, *J* = 4.9 Hz, 3H). ^{13}C-NMR (126 MHz, $CDCl_3$) δ 170.04, 157.17, 156.92 (d, *J* = 256.4 Hz), 152.16 (d, *J* = 4.8 Hz), 147.26 (d, *J* = 16.3 Hz), 138.51, 136.27, 135.76, 135.74, 133.74 (d, *J* = 7.7 Hz), 129.74, 129.71, 128.64, 127.78, 127.76, 127.50, 123.64 (d, *J* = 19.8 Hz), 120.16 (d, *J* = 4.0 Hz), 67.06, 66.83, 53.74, 49.04, 46.49, 45.26, 42.67, 35.07, 33.71, 26.97, 19.40, 14.87.

1-(4-(5-Fluoro-6-(((tetrahydro-2H-pyran-4-yl)amino)methyl)pyridin-2-yl)benzyl)-3-(3-hydroxy-2-methylpropyl)imidazolidine-2,4-dione (10): A solution of **5** (0.20 g, 0.29 mmol, 1 eq) and TBAF (0.34 mL, 1 M in THF, 0.34 mmol, 1.2 eq) in anhydrous THF (10 mL) under inert atmosphere was stirred (RT) for 2 h. The reaction was diluted with H_2O (5 mL) and the aqueous layer was extracted thrice with EtOAc. The combination of organic layers was washed with H_2O and brine, dried ($MgSO_4$), filtered and the solvent evaporated under reduced pressure. The crude product was purified with flash column chromatography (SiO_2, 2-10% MeOH in DCM) to yield a colourless amorphous solid (31 mg, 0.07 mmol, 23%). ^{1}H-NMR (400 MHz, $CDCl_3$) δ 7.94 (d, *J* = 8.3 Hz, 2H), 7.60 (dd, *J* = 8.6, 3.6 Hz, 1H), 7.42 (t, *J* = 8.7

Hz, 1H), 7.33 (d, *J* = 8.3 Hz, 2H), 4.61 (dt, *J* = 15.0, 9.1 Hz, 2H), 4.07 (d, *J* = 2.0 Hz, 2H), 3.98 (ddd, *J* = 11.8, 4.3, 2.4 Hz, 2H), 3.80 (s, 2H), 3.76 – 3.69 (m, 1H), 3.56 (dd, *J* = 6.3, 2.6 Hz, 2H), 3.50 (dd, *J* = 12.0, 4.1 Hz, 1H), 3.44 – 3.30 (m, 3H), 2.78 (tt, *J* = 10.5, 4.1 Hz, 1H), 2.47 (bs, 1H), 2.05 – 1.94 (m, 1H), 1.90 (ddd, *J* = 12.6, 4.3, 2.1 Hz, 2H), 1.54 (ddd, *J* = 23.6, 12.3, 4.4 Hz, 2H), 0.94 (d, *J* = 7.0 Hz, 3H). ^{13}C-NMR (101 MHz, $CDCl_3$) δ 170.66, 157.75, 156.89 (d, *J* = 256.7 Hz), 152.04 (d, *J* = 4.9 Hz), 147.06 (d, *J* = 16.4 Hz), 138.60, 135.91, 128.65, 127.56, 123.67 (d, *J* = 19.7 Hz), 120.20 (d, *J* = 4.1 Hz), 66.79, 64.11, 53.73, 49.16, 46.56, 45.12, 40.99, 35.33, 33.58, 14.73. LCMS (ESI, 10-90): t_R = 4.1 min; m/z: 471.27 $[M+H]^+$. HRMS $[C_{25}H_{31}FN_4O_4]^+$: 471.24021 calculated, 471.24009 found.

Synthesis of LEI-102 prodrug 12**.**

1-Chloroethyl ((3-fluoro-6-(4-((3-isobutyl-2,4-dioxoimidazolidin-1-yl)methyl)phenyl)pyridin-2-yl)methyl)(tetrahydro-2*H*-pyran-4-yl)carbamate (11): To a cooled (°0C) and stirred solution of LEI102 (250 mg, 0.55 mmol, 1 eq) and Et_3N (0.31 mL, 2.20 mmol, 4 eq) in DCM (8 mL) under inert atmosphere (Ar) was added dropwise 1-chloroethyl chloroformate (0.12 mL, 1.10 mmol, 2 eq) in DCM (10 mL). After stirring at 0 °C for 2 h the reaction was quenched with H_2O (20 mL). The layers were separated and the aqueous layer was extracted twice with DCM. The combination of organic layers was dried (Na_2SO_4), filtered, and the solvent evaporated under reduced pressure to yield a brown oil as crude. The crude was used without purification in the next step.

1-((((3-Fluoro-6-(4-((3-isobutyl-2,4-dioxoimidazolidin-1-yl)methyl)phenyl)pyridin-2-yl)methyl)(tetrahydro-2*H*-pyran-4-yl)carbamoyl)oxy)ethyl tetradecanoate (12): A stirred mixture of crude **8** (309 mg, 0.55 mmol, 1 eq), Et_3N (0.31 mL, 2.2 mmol, 4 eq) and myristic acid (503 mg, 2.2 mmol, 4 eq) in DCM (4 mL) in a sealed microwave vial was heated (110 °C) for 2 h in the microwave. The reaction mixture was diluted with H_2O (20 mL) and DCM (20 mL). The layers were separated and the aqueous layer extracted twice with DCM. The combination of organic layers was dried (Na_2SO_4), filtered, and the solvent evaporated under reduced pressure. The crude product was purified with flash column chromatography (SiO_2, 50% acetone/toluene (1:1 v/v) in pentane) to yield a white solid (218 mg, 0.29 mmol, 53%). ^{1}H-NMR (500 MHz, DMSO) δ 8.02 (d, *J* = 8.0 Hz, 2H), 7.93 (d, *J* = 3.4 Hz, 1H), 7.75 (t, *J* = 9.1 Hz, 1H), 7.37 (d, *J* = 8.4 Hz, 2H), 6.62 (d, *J* = 5.4 Hz, 1H), 4.68 – 4.58 (m, 2H), 4.54 (s, 2H), 4.17 (d, *J* = 11.8 Hz, 1H), 3.93 (s, 2H), 3.85 (bs, 2H), 3.32 (s, 2H), 3.22 (d, *J* = 7.3 Hz, 2H), 2.08 – 1.99 (m, 2H), 1.95 (hept, *J* = 6.8 Hz, 1H), 1.82 – 1.67 (m, 2H), 1.64 (t, *J* = 11.8 Hz, 2H), 1.47 (d, *J* = 6.1 Hz, 2H), 1.28 – 1.08 (m, 23H), 0.86 (s, 3H), 0.85 (s, 6H). ^{13}C-NMR (126 MHz, DMSO) δ 170.90, 170.29, 156.82, 154.95, 153.29, 150.84, 145.12, 137.33, 136.87, 127.95, 126.51, 123.96 (d, J = 19.1 Hz), 120.11 – 120.01 (m), 88.73, 66.54, 53.78, 53.46, 49.33, 45.49, 45.48, 42.24, 33.22, 31.26, 30.43, 29.01, 28.98, 28.91, 28.79, 28.68, 28.56, 28.52, 28.12, 26.96, 24.47, 24.03, 22.06, 19.85, 19.34, 13.92. LC-MS (ESI, 10-90): t_R = 15.02 min; m/z = 753.17 $[M+H]^+$. HRMS $[C_{42}H_{61}FN_4O_7 + H]^+$: 753.45970 calculated, 753.45937 found.

Biology

All biologic assays have been previously described. “General remarks”, “Quantification and statistical analysis”, “Cell culture”, “Membrane preparation”, and “[^{3}H]CP-55,940 Heterologous Displacement Assays” can be referenced in **Chapter 2.**

References

1 Zuardi AW. History of cannabis as a medicine: a review. *Rev Bras Psiquiatr*. 2006;28(2):153-157. doi:10.1590/S1516-44462006000200015

2. THC Museum. The History of Cannabis Museum. https://thcmuseum.org/the-history/. Accessed June 1, 2022.

3. The University of Sydney. History of Cannabis. https://www.sydney.edu.au/lambert/medicinal-cannabis/history-of-cannabis.html. Accessed June 1, 2022.

4. Unschuld PU. *Medicine in China: A History of Pharmaceutics*. 1st ed. University of California Press; 1986. https://books.google.nl/books?id=WUgsy0yLEfoC&pg=PA17&lpg=PA17&dq=Pen-ts%27ao+Ching&source=bl&ots=ieyOAa1MV4&sig=ACfU3U2dxbRUqZWdZLVKOom7ZlvwZSv9yQ&hl=nl&sa=X&ved=2ahUKEwi76ZOk44v4AhUVg_0HHYBwA74Q6AF6BAgXEAM#v=onepage&q=Pen-ts'ao Ching&f=false.

5. Adams IB, Martin BR. Cannabis: pharmacology and toxicology in animals and humans. *Addiction*. 1996;91(11):1585-1614. http://www.ncbi.nlm.nih.gov/pubmed/8972919.

6. Pertwee RG. Cannabinoid pharmacology: the first 66 years. *Br J Pharmacol*. 2006;147(S1):S163-S171. doi:10.1038/sj.bjp.0706406

7. Laszlo J, Lucas VS, Hanson DC, Cronin CM, Sallan SE. Levonantradol for chemotherapy-induced emesis: phase I-II oral administration. *J Clin Pharmacol*. 1981;21(S1):51S-56S. doi:10.1002/j.1552-4604.1981.tb02573.x

8. Robson P. Human Studies of Cannabinoids and Medicinal Cannabis. In: *Cannabinoids*. Berlin/Heidelberg: Springer-Verlag; 2005:719-756. doi:10.1007/3-540-26573-2_25

9. Alhumaydhi FA, Aljasir MA, Aljohani ASM, et al. Probing the interaction of memantine, an important Alzheimer's drug, with human serum albumin: In silico and in vitro approach. *J Mol Liq*. 2021;340:116888. doi:10.1016/j.molliq.2021.116888

10. Ibsen MS, Connor M, Glass M. Cannabinoid CB 1 and CB 2 Receptor Signaling and Bias. *Cannabis Cannabinoid Res*. 2017;2(1):48-60. doi:10.1089/can.2016.0037

11. Mlost J, Kostrzewa M, Borczyk M, et al. CB2 agonism controls pain and subchondral bone degeneration induced by mono-iodoacetate: Implications GPCR functional bias and tolerance development. *Biomed Pharmacother*. 2021;136:111283. doi:10.1016/j.biopha.2021.111283

12. Soethoudt M, Stolze SC, Westphal M V., et al. Selective Photoaffinity Probe That Enables Assessment of Cannabinoid CB 2 Receptor Expression and Ligand Engagement in Human Cells. *J Am Chem Soc*. 2018;140(19):6067-6075. doi:10.1021/jacs.7b11281

13. Speers AE, Cravatt BF. Activity-Based Protein Profiling (ABPP) and Click Chemistry (CC)-ABPP by MudPIT Mass Spectrometry. *Curr Protoc Chem Biol*. 2009;1:29-41. doi:10.1002/9780470559277.ch090138

14. Chaturvedi S, Mishra AK. Small Molecule Radiopharmaceuticals – A Review of Current Approaches. *Front Med*. 2016;3. doi:10.3389/fmed.2016.00005

15. Sarott RC, Westphal M V., Pfaff P, et al. Development of High-Specificity Fluorescent Probes to Enable Cannabinoid Type 2 Receptor Studies in Living Cells. *J Am Chem Soc*. 2020;142(40):16953-16964. doi:10.1021/jacs.0c05587

16. Punt JM, van der Vliet D, van der Stelt M. Chemical Probes to Control and Visualize Lipid Metabolism in the Brain. *Acc Chem Res*. 2022;55(22):3205-3217.

doi:10.1021/acs.accounts.2c00521

17. Singlár Z, Ganbat N, Szentesi P, et al. Genetic Manipulation of CB1 Cannabinoid Receptors Reveals a Role in Maintaining Proper Skeletal Muscle Morphology and Function in Mice. *Int J Mol Sci*. 2022;23(24):15653. doi:10.3390/ijms232415653

18. Ma L, Jia J, Niu W, et al. Mitochondrial CB1 receptor is involved in ACEA-induced protective effects on neurons and mitochondrial functions. *Sci Rep*. 2015;5(1):12440. doi:10.1038/srep12440

19. Morales P, Jagerovic N. Novel approaches and current challenges with targeting the endocannabinoidsystem. *Expert Opin Drug Discov*. 2020;15(8):917-930. doi:https://doi.org/10.1080/17460441.2020.1752178

20. Wu Y, Chen M, Jiang J. Mitochondrial dysfunction in neurodegenerative diseases and drug targets via apoptotic signaling. *Mitochondrion*. 2019;49:35-45. doi:10.1016/j.mito.2019.07.003

21. Kulkarni CA, Fink BD, Gibbs BE, et al. A Novel Triphenylphosphonium Carrier to Target Mitochondria without Uncoupling Oxidative Phosphorylation. *J Med Chem*. 2021;64(1):662-676. doi:10.1021/acs.jmedchem.0c01671

22. Friend L, Weed J, Sandoval P, Nufer T, Ostlund I, Edwards JG. CB1-Dependent Long-Term Depression in Ventral Tegmental Area GABA Neurons: A Novel Target for Marijuana. *J Neurosci*. 2017;37(45):10943-10954. doi:10.1523/JNEUROSCI.0190-17.2017

23. Bénard G, Massa F, Puente N, et al. Mitochondrial CB 1 receptors regulate neuronal energy metabolism. *Nat Neurosci*. 2012;15(4):558-564. doi:10.1038/nn.3053

24. Ross MF, Kelso GF, Blaikie FH, et al. Lipophilic triphenylphosphonium cations as tools in mitochondrial bioenergetics and free radical biology. *Biochem*. 2005;70(2):222-230. doi:10.1007/s10541-005-0104-5

25. Murphy MP, Smith RAJ. Targeting Antioxidants to Mitochondria by Conjugation to Lipophilic Cations. *Annu Rev Pharmacol Toxicol*. 2007;47(1):629-656. doi:10.1146/annurev.pharmtox.47.120505.105110

26. Heimann AS, Gomes I, Dale CS, et al. Hemopressin is an inverse agonist of CB 1 cannabinoid receptors. *Proc Natl Acad Sci*. 2007;104(51):20588-20593. doi:10.1073/pnas.0706980105

27. Djeungoue-Petga M-A, Hebert-Chatelain E. Linking Mitochondria and Synaptic Transmission: The CB1 Receptor. *BioEssays*. 2017;39(12):1700126. doi:10.1002/bies.201700126

28. Castaneda JT, Harui A, Roth MD. Regulation of Cell Surface CB2 Receptor during Human B Cell Activation and Differentiation. *J Neuroimmune Pharmacol*. 2017;12(3):544-554. doi:10.1007/s11481-017-9744-7

29. Brailoiu GC, Deliu E, Marcu J, et al. Differential activation of intracellular versus plasmalemmal CB2 Cannabinoid receptors. *Biochemistry*. 2014;53(30):4990-4999. doi:10.1021/bi500632a

30. Schuchman EH, Ledesma MD, Simonaro CM. New paradigms for the treatment of lysosomal storage diseases: targeting the endocannabinoid system as a therapeutic strategy. *Orphanet J Rare Dis*. 2021;16(1):151. doi:10.1186/s13023-021-01779-4

31. Khilnani G, Khilnani A. Inverse agonism and its therapeutic significance. *Indian J Pharmacol*. 2011;43(5):492. doi:10.4103/0253-7613.84947

32. Chen X, Zheng C, Qian J, et al. Involvement of β-arrestin-2 and Clathrin in Agonist-Mediated Internalization of the Human Cannabinoid CB2 Receptor. *Curr Mol Pharmacol*.

2015;7(1):67-80. doi:10.2174/1874467207666140714115824

33. Grimsey NL, Goodfellow CE, Dragunow M, Glass M. Cannabinoid receptor 2 undergoes Rab5-mediated internalization and recycles via a Rab11-dependent pathway. *Biochim Biophys Acta - Mol Cell Res*. 2011;1813(8):1554-1560. doi:10.1016/j.bbamcr.2011.05.010

34. Counsell RE, Pohland RC. Lipoproteins as potential site-specific delivery systems for diagnostic and therapeutic agents. *J Med Chem*. 1982;25(10):1115-1120. doi:10.1021/jm00352a001

35. Lacko AG, Sabnis NA, Nagarajan B, McConathy WJ. HDL as a drug and nucleic acid delivery vehicle. *Front Pharmacol*. 2015;6. doi:10.3389/fphar.2015.00247

36. Zaro JL. Lipid-based drug carriers for prodrugs to enhance drug delivery. *AAPS J*. 2015;17(1):83-92. doi:10.1208/s12248-014-9670-z

37. Javed H, Azimullah S, Haque ME, Ojha SK. Cannabinoid Type 2 (CB2) Receptors Activation Protects against Oxidative Stress and Neuroinflammation Associated Dopaminergic Neurodegeneration in Rotenone Model of Parkinson's Disease. *Front Neurosci*. 2016;10. doi:10.3389/fnins.2016.00321

38. Mulder WJM, van Leent MMT, Lameijer M, Fisher EA, Fayad ZA, Pérez-Medina C. High-Density Lipoprotein Nanobiologics for Precision Medicine. *Acc Chem Res*. 2018;51(1):127-137. doi:10.1021/acs.accounts.7b00339

39. Hilaire JR, Bade AN, Sillman B, et al. Creation of a long-acting rilpivirine prodrug nanoformulation. *J Control Release*. 2019;311-312:201-211. doi:10.1016/j.jconrel.2019.09.001

Acknowledgements

This work was supported by the Dutch Research Council (NWO, Navistroke #15851) (Mario van der Stelt[d], M.v.d.S.).

Author contributions: Conducting Experiments, L.V.d.P. (Laura V. de Paus), R.J.B.H.N.v.d.B (Richard J. B. H. N. van den Berg), J.R. (Joel Rüegger); Writing-Original Draft, L.V.d.P.; Writing Review & Editing, M.v.d.S., L.H.H. (Laura H. Heitman), R.J.B.H.N.v.d.B; Supervision, R.J.B.H.N.v.d.B., M.v.d.S.

Nederlandse samenvatting

Het gebruik van cannabis voor therapeutische doeleinden werd al in 2700 v.Chr. gedocumenteerd door keizer Sheng Nun in zijn farmacopee. Het werd beschreven als een hulpmiddel bij artritis, het opwekken van eetlust, depressie, ontstekingen, pijn, constipatie en meer. Het belangrijkste actieve ingrediënt in cannabis dat zorgt voor de psychoactieve effecten is Δ^9-tetrahydrocannabinol (THC), dat in 1942 is ontdekt, hoewel de structuur pas sinds 1964 bekend is. Sindsdien is THC geaccepteerd als medicijn tegen door chemotherapie veroorzaakte misselijkheid, verbetering van de eetlust bij aids-patiënten en behandeling van symptomen bij patiënten met multiple sclerose (MS). De receptoren waarmee THC bindt, zijn de cannabinoïde receptor type 1 (CB_1R) en de cannabinoïde receptor type 2 (CB_2R). Deze receptoren maken deel uit van de familie van G-eiwit-gekoppelde receptoren en bevinden zich aan de buitenkant van cellen als onderdeel van het endocannabinoïde systeem (ECS). Dit systeem bestaat verder uit lipide-transmitters die kunnen binden aan de receptoren en enzymen die helpen bij de synthese en afbraak van endocannabinoïden. Het ECS-systeem speelt een belangrijke rol in meerdere fysiologische processen, waaronder cognitieve functie, immuunreacties en ook de psychoactieve effecten van cannabis.

CB_1R is de meest voorkomende G eiwit-gekoppelde receptor in de hersenen en speelt een rol in eetlust, leren, geheugen, angst, depressie en verslaving. Daarnaast speelt het een rol in neurologische aandoeningen zoals beroerte, MS, epilepsie en neurodegeneratieve ziekten. Buiten het zenuwstelsel is CB_1R betrokken bij pijnperceptie, ontsteking, energiemetabolisme, het maagdarmkanaal, het bewegingsapparaat, oogdruk, het hart- en vaatstelsel, klieren, reproductie en kanker. CB_2R bevindt zich voornamelijk in het immuunsysteem, inclusief de milt, amandelen, thymus en lymfocyten, en speelt een rol in ontstekingen en zou een rol kunnen spelen in verschillende auto-immuun- en neurodegeneratieve ziekten zoals Alzheimer en Parkinson.

THC maakt geen onderscheid tussen de type 1- en type 2-cannabinoïde receptoren en veroorzaakt als medicijn dus ook bijwerkingen, met name de psychoactieve effecten, door binding aan CB_1R. De afgelopen decennia is er veel onderzoek gedaan naar het begrijpen van de rol van CB_1R en CB_2R in verschillende ziekten en de ontwikkeling van therapeutische moleculen tegen deze ziekten. Desalniettemin hebben we nog maar beperkte kennis over de werking van de receptoren op moleculair niveau. Meer informatie is nodig om te helpen bij het ontwikkelen van werkzame medicijnen met minder bijwerkingen. Dit proefschrift beschrijft het ontwerp en de synthese van verschillende chemische moleculen die als 'tools' (letterlijk: gereedschappen) kunnen fungeren om de cannabinoïde receptoren te bestuderen.

In **Hoofdstuk 1** worden de twee receptoren waarmee THC bindt geïntroduceerd: cannabinoïde receptor type 1 (CB_1R) en cannabinoïde receptor type 2 (CB_2R). Er wordt uitgelegd hoe de receptoren werken en hoe ze zijn opgebouwd. De 3D-structuren van de CBR's, die zijn bepaald met behulp van kristallografie en cryogene elektronenmicroscopie, worden vergeleken. De momenteel beschikbare synthetische medicijnen worden besproken, evenals mogelijke methoden om problemen te omzeilen waar huidige CBR-medicijnen mee te maken hebben. Een aantal methoden worden besproken die receptoren zichtbaar kunnen maken, waaronder het gebruik van radio-isotopen of fluorescente moleculen; elektrofiele en fotoreactieve groepen kunnen het molecuul onomkeerbaar aan het eiwit binden. LEI-101 wordt geïntroduceerd, een CB_2R-selectief molecuul met een chemische structuur waarop verschillende moleculen in dit proefschrift zijn gebaseerd.

In **Hoofdstuk 2** wordt LEI-102 geïntroduceerd, gebaseerd op het LEI-101 molecuul. Dit nieuw gesynthetiseerde molecuul wordt, net als CP-55,940, APD371 en HU308, in complex gezet met CB_2R en wordt de 3D-structuur bepaald met behulp van een elektronenmicroscoop onder cryogene condities. Hiermee wordt de ligging van de moleculen in CB_2R bekeken. Een aantal aminozuren die zich op of bij de interface van de moleculen en het eiwit bevinden, zijn gekozen om te veranderen. Zo kon worden onderzocht wat de invloed was van die aminozuren op het binden van de moleculen en de activiteit van de receptor. Deze resultaten leidden tot een aantal observaties, bijvoorbeeld dat lipofiele moleculen een eigen "zij-ingang" naar de binnenkant van CB_2R en CB_1R lijken te hebben. Verder was er een verschil tussen de moleculen en hoe belangrijk bepaalde aminozuren waren voor de activatie van de receptor. Zo was histidine 2.65 (Ballesteros-Weinstein-nummering) belangrijk voor CB_2R-activatie met LEI-102, CP-55,940 en APD371, echter gaf het molecuul HU308 geen verandering in receptoractiviteit als de histidine 2.65 was gemuteerd. Fenylalanine 3.36 is belangrijk in CB_1R om activiteit te voorkomen, en een mutatie naar alanine zorgt voor constitutieve activatie. Dit gebeurt echter niet in CB_2R, waar een mutatie in fenylalanine 3.36 ervoor zorgt dat geen enkele molecuul meer in staat is CB_2R te activeren. De kleinste homologie tussen de receptoren zit in de lengte van extracellulaire lus 2 (ECL2), deze lus is groter en telt meer aminozuren in CB_1R dan in CB_2R. Moleculen die normaal selectief werken op alleen CB_2R kregen een kleine affiniteit voor CB_1R als een aminozuur in de lus wordt vervangen door een ander aminozuur dat daar aanwezig is in CB_2R. Het lijkt dus dat deze lus belangrijk is voor selectiviteit.

In **Hoofdstuk 3** wordt LEI-121 geïntroduceerd, een chemische ‘probe’ (letterlijk: sonde) die als gereedschap kan worden gebruikt om CB_2R te bestuderen. Het molecuul heeft een diazirine, een kleine groep die uiteenvalt in een zeer reactieve groep als deze wordt beschenen met ultraviolet licht. De zeer reactieve groep reageert snel met een andere groep in de buurt om een onomkeerbare binding te maken. Als dit gebeurt wanneer het molecuul in de CB_2 receptor zit, dan bindt de groep aan het eiwit vast. Daarnaast bevat LEI-121 een driedubbele koolstofbinding, een alkyn. Dit is een aanknopingspunt om iets anders aan te bouwen. Zo kan LEI-121 eerst met CB_2R binden, en dan pas wordt er bijvoorbeeld een fluorescerende groep op gezet zodat de receptor zichtbaar wordt. Twee variaties op LEI-121 worden gesynthetiseerd en vergeleken met LEI-121. Deze zorgen er, net zoals LEI-121, voor dat de receptoractiviteit omlaag gaat (inverse agonist) als het molecuul is gebonden. Een nieuwe ‘probe’ wordt ook geïntroduceerd waarvan de structuur meer lijkt op LEI-102, maar waarbij de diazirine en alkyn nog steeds aanwezig zijn. Deze nieuwe ‘probe’ zorgde juist voor verhoging van receptoractiviteit (agonist) na binden, vergelijkbaar met LEI-102. Met deze nieuwe ‘probe’ kunnen nieuwe receptorconformaties worden bestudeerd.

Hoofdstuk 4 gebruikt de structuur van het LEI-102-CB_2R-complex om nieuwe ‘probes’ te maken die geen alkyn bevatten, maar waarbij de fluorescerende probe al in het molecuul is gebouwd. Opnieuw werd de LEI-102 structuur als beginpunt gebruikt met een kleine aanpassing om het inbouwen van de fluorescerende groep mogelijk te maken. Er werd gevonden dat het molecuul met de hoogste affiniteit voor CB_2R nu een inverse agonist was. Het voordeel van de fluorescerende groep die al aan het molecuul is vastgemaakt, is dat nu geen extra stap nodig is tijdens het experiment. Een reactie kost tijd, en tijdens bepaalde experimenten heb je dat niet. Daarnaast voorkom je dat er koper (d.w.z. een katalysator die nodig is voor de reactie) bij je cellen komt, wat toxisch is en de experimentele uitkomst zou kunnen beïnvloeden. Deze nieuwe ‘probe’ is dus een aanvulling op de ‘probes’ uit hoofdstuk 3.

Ondanks de psychoactieve effecten van CB_1R is er nog veel medicijnonderzoek naar moleculen die aan CB_1R binden. Er zijn namelijk ook veel positieve effecten die we zien bij onder andere THC die te herleiden zijn tot de type 1 receptor. Met de ontdekking dat CB_1R zich niet alleen op het celmembraan, maar ook op mitochondriën bevindt, is er de vraag of er een verschil zit in de signalen van de twee

subgroepen. Er is al gevonden dat mitochondriaal CB_1R effect heeft op leren en geheugen, en eetgedrag. **Hoofdstuk 5** bespreekt de synthese van CB_1R-bindende moleculen op basis van de ORG28611-structuur die specifiek naar de mitochondriën kunnen bewegen vanwege hun negatieve lading. Het doel is om op den duur te onderzoeken of de psychoactieve en medicinale effecten worden veroorzaakt door een of beide subgroepen, en of deze hetzelfde of verschillend zijn. De moleculen die zijn ontworpen en gesynthetiseerd waren maar matig actief en optimalisatie zal nodig zijn voordat verdere proeven kunnen worden uitgevoerd.

Hoofdstuk 6 vat de resultaten van de voorgaande hoofdstukken samen en bespreekt wat de volgende stappen van het onderzoek zullen inhouden. Daarnaast wordt de synthese van een prodrug op basis van LEI-102 beschreven. Een prodrug is een molecuul dat is aangepast om een bepaalde eigenschap te verbeteren, zoals bijvoorbeeld oplosbaarheid of de tijd dat het stabiel blijft in het lichaam. Wanneer het molecuul op de juiste plek is aangekomen, zullen lichaamseigen enzymen de prodrug deels afbreken zodat het actieve molecuul achterblijft. Die kan dan met het 'doelwit' (letterlijk: target) binden en zijn werking uitvoeren. De prodrug besproken in hoofdstuk 6 heeft een lipofiele 'staart' aan LEI-102 gekoppeld zodat deze in een capsule van lipiden kan worden geplaatst. In deze lipide capsule kan LEI-102 beschermd naar de CB_2 receptor worden vervoerd, waar de staart er door enzymen wordt afgehaald en LEI-102 met hoge affiniteit kan binden. De synthese van de prodrug is afgerond en de volgende stap zou het vergelijken van de prodrug + capsule zijn met LEI-102 in vivo.

Dit proefschrift laat het ontwerp en de synthese van verschillende nieuwe 'tools' zien die gebruikt kunnen worden voor het verder bestuderen van CB_1R en CB_2R. Verder wordt het belang van 3D structuren van eiwitten in complex met bindende moleculen laten zien voor het begrijpen van hoe selectiviteit, activiteit en signaalvoorkeur door de moleculen worden gestuurd. Daarnaast kunnen 3D structuren worden gebruikt voor het ontwerp van nieuwe 'probes' en potentiële medicijnen. Pas als we begrijpen hoe de cannabinoïde receptoren werken kunnen we effectief *in vitro* resultaten van moleculen veranderen in effectiviteit in de kliniek. Dit zou gecombineerd kunnen worden met een methode om moleculen langer stabiel te houden, bijvoorbeeld door middel van een capsule. De 'tools' ontworpen in dit proefschrift kunnen in de toekomst helpen met uitzoeken hoe CB_2R zich gedraagt in ziektes en hoe we daar medicijnen voor zouden kunnen ontwikkelen.

List of Publications

de Paus,L. V.; An, Y.; Janssen, A. P. A.; van den Berg, R. J. B. H. N.; Heitman, L. H.; van der Stelt, M. Discovery of a Photoaffinity Probe that Captures the Active Conformation of the Cannabinoid CB2 Receptor. ChemBioChem 2024. https://doi.org/10.1002/cbic.202300785

de Paus, L. V.; Janssen, A. P. A.; Halimi, A.; van den Berg, R. J. B. H. N.; Heitman, L. H.; van der Stelt, M. Discovery of a Cannabinoid CB2 Receptor Fluorescent Probe Based on a Pyridin-2-Yl-Benzyl-Imidazolidine-2,4-Dione Scaffold. Synlett 2023. https://doi.org/10.1055/a-2230-1003.

Li, X.; Chang, H.; Bouma, J.; **de Paus, L. V.**; Mukhopadhyay, P.; Paloczi, J.; Mustafa, M.; van der Horst, C.; Kumar, S. S.; Wu, L.; Yu, Y.; van den Berg, R. J. B. H. N.; Janssen, A. P. A.; Lichtman, A.; Liu, Z.-J.; Pacher, P.; van der Stelt, M.; Heitman, L. H.; Hua, T. Structural Basis of Selective Cannabinoid CB2 Receptor Activation. Nat. Commun. 2023, 14 (1), 1447. https://doi.org/10.1038/s41467-023-37112-9.

Curriculum Vitae

Laura de Paus obtained her secondary school diploma (gymnasium) at Scala College in Alphen aan den Rijn in 2012. She subsequently joined the Bachelor program for Chemistry at Utrecht University, from which she graduated in 2015. For her masters she moved to Leiden to join the Master program for Chemistry at Leiden University. As part of the master program she performed a 10-month research project at the Biosynthesis department under supervision of Prof. Dr. Mario van der Stelt. The project encompassed designing and synthesizing compounds targeting FLT3 for study of its role in acute myeloid leukaemia. After three years she graduated in 2018 and obtained her Master's degree of Science in Chemistry *cum laude* and her Master's degree of Science in Life, Science and Technology.

In October 2018 she started as a PhD candidate at Leiden University at the Molecular Physiology department under supervision of Prof. Dr. Mario van der Stelt, Prof. Dr. Laura Heitman (Division of Drug Discovery and Safety of the LACDR) and Dr. Richard van den Berg. The research led to the publication of three papers and this thesis.